UTS UNIVERSITY OF TECHNOLOGY SYDNEY

Effects of Dynamic Soil-Structure Interaction on Seismic Behaviour of High-rise Buildings

by Xiaofeng Zhang

Thesis submitted in fulfilment of the requirements for the degree of

Doctor of Philosophy

under the supervision of Dr Harry Far
A/Prof Shami Nejadi

University of Technology Sydney
Faculty of Engineering and Information Technology

January 2024

Certificate of Original Authorship

I, *Xiaofeng Zhang*, declare that this thesis is submitted in fulfilment of the requirements for the award of *Doctor of Philosophy*, in the *School of Civil and Environmental Engineering (Faculty of Engineering and Information Technology)* at the University of Technology Sydney.

This thesis is wholly my own work unless otherwise referenced or acknowledged. In addition, I certify that all information sources and literature used are indicated in the thesis.

This document has not been submitted for qualifications at any other academic institution.

This research is supported by the Australian Government Research Training Program.

Signature:

Production Note:
Signature removed prior to publication.

Date:
29/01/2024

ACKNOWLEDGEMENT

I would like to take this opportunity to express my heartfelt gratitude to the people who have contributed to the successful completion of my PhD thesis. First of all, I would like to thank my supervisor, Dr. Harry Far, for his guidance, support, and patience throughout the research process. His insightful comments and suggestions have helped me to refine my ideas and arguments, and his unwavering encouragement has kept me motivated and focused.

I would also like to extend my sincere thanks to my co-supervisor, A/Professor Shami Nejadi, for his invaluable assistance and expertise. His constructive feedback has been instrumental in shaping the scope of my research, and his dedication to my project is truly inspiring.

In addition, I would like to express my gratitude to the assessors of my thesis, Dr. Mina Mortazavi and A/Professor Sanjay Nimbalkar. Their thoughtful and thorough reviews have helped me to identify and address the weaknesses and limitations of my work, and their constructive criticism has challenged me to think more deeply and critically about my research.

Last but not least, I would like to thank my family, especially my parents, for their unwavering love, support, and encouragement. Without their constant support and encouragement, I would not have been able to pursue my academic dreams and achieve my goals. Their sacrifices and dedication have been the cornerstone of my success, and I am forever grateful for their love and support.

Thank you all for your contributions and support.

LIST OF PUBLICATIONS RELATED TO THIS RESEARCH

PEER-REVIEWED JOURNAL PAPERS

1. Zhang, X. F. and Far, H. 2022. Effects of dynamic soil-structure interaction on seismic behaviour of high-rise buildings. Bulletin of Earthquake Engineering, 20, 3443-3467. DOI: 10.1007/s10518-021-01176-z

2. Zhang, X. F. and Far, H. 2022. Seismic behaviour of high-rise frame-core tube structures considering dynamic soil-structure interaction. Bulletin of Earthquake Engineering, 20, 5073-5105. DOI: 10.1007/s10518-022-01398-9

3. Zhang, X. F. and Far, H. 2023. Seismic response of high-rise frame-shear wall buildings under the influence of dynamic soil-structure interaction. International Journal of Geotechnical Engineering, 23(9), 04023141. DOI: 10.1061/IJGNAI.GMENG-8451

TABLE OF CONTENTS

LIST OF FIGURES

LIST OF TABLES

LIST OF ABBREVIATIONS

ABC	Artificial boundary condition
AS	Australian standards
ASCE	American society of civil engineers design code
ATC	Applied technology council
BD	Bedrock depth
BSSC	Building seismic safety council
FEM	Finite element method
FIM	Foundation input motion
FEMA	Federal emergency management agency
HWR	Height width ratio
IBC	International building code
JSCE	Japan society of civil engineers
NBCC	National building code of Canada
NEHRP	National earthquake hazards reduction program
NZS	New Zealand standards
PBEE	Performance-based earthquake engineering
PSA	Pseudo spectral acceleration
RC	Reinforced concrete
SDOF	Single degree of freedom
SSI	Soil-structure interaction
SSPSI	Seismic soil-pile-structure interaction

SSSI	Structure-soil-structure interaction
TMD	Tuned mass damper
USCS	Unified soil classification system

LIST OF NOTATIONS

$2a$	width of the foundation
A_b	influencing area of the boundary node
c	damping coefficient
c'	effective cohesion
$\boldsymbol{C_b}$	damping coefficient of viscous-spring boundary.
C_{BT}	damping coefficients of dampers in tangential direction
C_{BN}	damping coefficients of dampers in normal direction
c_h	damping in the horizontal direction
c_p	P wave velocity of the soil deposit
c_s	shear wave velocity of the soil deposit
c_θ	damping in the rotational direction
E_c	modulus of elasticity
$\boldsymbol{F_b}$	equivalent node force
f_m	natural frequency of the shaking table test model
f_{max}	the highest wave frequency
f_p	natural frequency of the prototype
f'_c	characteristic compressive strength of concrete
G	shear modulus
G_{max}	maximum shear modulus
h	height of the superstructure
k	stiffness

$\boldsymbol{K_b}$	spring stiffness of viscous-spring boundary
K_{BT}	stiffness coefficients of springs in tangential direction
K_{BN}	stiffness coefficients of springs in normal direction
k_h	stiffness in the horizontal direction
k_θ	stiffness in the rotational direction
m	mass
M_w	moment magnitude of earthquake in Richter scale
$\boldsymbol{n}$	cosine vector of the normal direction
R	distance from the wave source to boundary nodes
T_{fix}	fundamental period of fixed base structure
T_{fle}	fundamental period of flexible base structure
$\boldsymbol{u_b^{ff}}$	free field displacement vector at artificial boundary nodes
u_g	free field motion
$\tilde{u}_g$	equivalent input motion
$\boldsymbol{v_b^{ff}}$	free field velocity vector at artificial boundary nodes
V_{fix}	base shear of fixed base structure
V_{fle}	base shear of flexible base structure
V_s	shear wave velocity
α, β	mass and stiffness damping coefficient
α_T, α_N	modified coefficients
γ_c	cyclic shear strain
δ	maximum inter-storey drift
δ_{fix}	maximum inter-storey drift of fixed base structure

δ_{fle}	maximum inter-storey drift of flexible base structure
Δ	maximum lateral deflection
Δ_0	base displacement relative to the free field motion
Δ_d	distortion component of the lateral deflection
Δ_t	maximum lateral deflection at the top of the system
Δ_θ	rocking component of the lateral deflection
λ	geometric scaling factor
ξ	damping ratio
ξ_0	hysteretic damping of the fixed base SDOF system
$\tilde{\xi}$	equivalent damping ratio
ρ	density of the soil deposit
$\boldsymbol{\sigma_b^{ff}}$	free field stress tensor
σ_y	yield stress of the concrete material
ω_0	natural frequency of the fixed base SDOF system
$\tilde{\omega}$	equivalent natural frequency
φ'	effective friction angle

ABSTRACT

It is widely believed that soil-structure interaction (SSI) can improve a building's ability to withstand earthquakes. However, recent earthquakes and studies have highlighted the disastrous consequences of ignoring SSI effects, causing conflicting opinions on its impact on the seismic behaviour. As a result, some contemporary design codes choose to ignore SSI or only consider its beneficial effects. Moreover, previous research has mainly focused on low or mid-rise moment frames, and impacts of SSI on commonly used structural systems of high-rise buildings have received little attention.

In this study, a soil-foundation-structure model based on finite element software was employed to examine SSI effects on high-rise buildings. The validity of the model was confirmed through shaking table tests. The study explores a range of superstructure and substructure parameters to compare the seismic response of rigidly and flexibly supported structures. Moreover, beneficial and detrimental scenarios concerning SSI were identified, and code-based procedures that offer a secure and cost-effective structural design approach were developed.

The study demonstrates that compared to structures modeled with a rigid base, those modeled with a flexible base that incorporates SSI effects exhibit amplified lateral deflections and inter-storey drifts to varying degrees. While piled foundations can mitigate the foundation rocking, the displacement response of piled foundation models may not necessarily be smaller than that of compensated foundation models. Blindly increasing the rigidity of the foundation and subsoil without considering SSI effects may not improve structural safety or economic efficiency.

Furthermore, the study found that SSI can significantly increase the base shear for both piled foundation structures and classical compensated foundation structures supported by C_e soil. In contrast, SSI has a beneficial effect on classical compensated

foundation structures supported by D_e and E_e soil types, as it reduces the base shear. In terms of the displacement response, SSI generally increases the inter-storey drifts for almost all cases examined, which has a negative impact on the high-rise buildings. When the subsoil exhibits sufficient stiffness, the amplification coefficient for base shear is nearly equivalent to the amplification coefficient for inter-storey drifts after considering SSI. In contrast, as the soil stiffness decays, inter-storey drifts are amplified, and the base shear is reduced.

Finally, based on these findings, code-based procedures were developed to provide a safe and economical structural design method. Designers can easily determine the base shear of high-rise flexible base structures without conducting laborious numerical computations during the design process.

Chapter 1 INTRODUCTION

1.1 Background

In the last decade, with the reduction of available urban construction land and the consequent rise in land prices, there has been an increasing trend towards the construction of high-rise buildings with multiple underground storeys. As highlighted by Al Agha et al. (2021) and Segaline et al. (2022), frame-core tube structures and frame-shear wall structures have emerged as particularly popular choices among the various structural forms of tall buildings. This is because these types of structures combine the flexible layout and high ductility of frame structures with the large stiffness and high bearing capacity of shear wall structures, as highlighted by Gao et al. (2005).

One of the primary benefits of frame-core tube buildings and frame-shear wall buildings is their ability to serve as a dual lateral force resistance system, providing excellent abilities to resist wind loads and earthquake effects. When subjected to earthquake action, the shear wall (or core tube) serves as the first line of defense, while the frame acts as the second line of defense (Lu 2005; Son et al. 2017). As such, frame-core tube structures and frame-shear wall structures with multiple basement storeys have become the most common structural forms of tall buildings in earthquake-prone areas, as noted by Ayala et al. (2022). Overall, these structures represent a highly effective means of mitigating the risks associated with earthquakes, while also providing a flexible layout for modern urban architecture.

In the structural design, it has been tried to make high-rise buildings safe and stable under different loads, especially when buildings are built on a site with poor geotechnical conditions in an earthquake-prone area. This is because the effects of horizontal loads on high-rise buildings are not linear but increase rapidly with the increase of the building height. For instance, in the presence of horizontal forces,

structures experience an overturning moment that is proportional to the square of their height, and the top of the structure deflects laterally in a manner that is proportional to the fourth power of its height (Gao et al. 2005). As a result, with the increment of building height, lateral displacement will undoubtedly become the main controlling factor in the structural design. Additionally, the structure can deform in any direction under strong earthquakes, and sometimes the displacement can be large, so the key design problem is to avoid excessive deformation that will lead to building collapse.

In the conventional design methodology, there is a clear distinction between the design of the superstructure and the substructure. The underlying assumption is that the superstructure is rigidly fixed to the substructure and impacts of soil-structure interaction (SSI) is considered negligible. As a result, the substructure is primarily designed to bear the vertical load, horizontal load, and moment induced by the superstructure (El Ganainy and El Naggar 2009). This traditional design approach, however, has been challenged by various factors, such as the dynamic nature of the soil-structure system, the emergence of new construction materials, and the need for more economical and sustainable design solutions.

While the traditional method has served its purpose for many years, it has its limitations in accurately predicting the structural behaviour of a building. The assumption of rigid base conditions leads to an oversimplified representation of the complex SSI mechanisms that can affect the building's performance during seismic events or other dynamic loads. Moreover, designing the substructure solely based on the loads induced by the superstructure may not be optimal, resulting in an over-designed or under-designed foundation.

In fact, when the building's foundation is constructed on solid rock, the motion induced by an earthquake is similar to the free field motion, and the rigid base assumption is reasonable. However, in the case of a soft soil medium, the seismic response can be different. The foundation of such structures can resist large

deformations due to its rigidity, leading to inconsistent input motion compared to free field motion. Additionally, according to Wolf and Deeks (2004), the seismic response of the superstructure has the potential to cause deformation of the underlying ground soil, which in turn can modify the input motion. This highlights the significant role that the interaction between the superstructure and the underlying soil plays in the seismic behaviour of the structure, resulting in a feedback loop (Tabatabaiefar et al. 2013; Tabatabaiefar 2016; Tabatabaiefar et al. 2017; Far 2019; Al Agha et al. 2021). This feedback loop is known as SSI, as noted by Saleh et al. (2018) and Anand and Satish Kumar (2018), where the behaviour of the soil influences the structural response and vice versa.

SSI is a highly interdisciplinary field that lies at the intersection of several technical disciplines (Kausel 2010). Engineers have recognised the significance of the interaction between soil and foundation since the early 20th century, which marked the beginning of the development of SSI as a field of study. It has since progressed rapidly, especially in recent decades due to the advancements in technology and numerical simulation tools (Roesset 2013).

The focus of SSI research has shifted from employing purely analytical methods to solve highly simplified mathematical calculations to addressing real and complex structure-foundation-soil models. These models may include irregularly shaped foundations constructed in the inhomogeneous or layered subsoil and take into account complicated factors such as material nonlinearity of the superstructure and substructure elements, and geometric nonlinearity. With the emergence of high-performance computers and advanced numerical simulation tools, researchers are now able to perform more accurate and complex simulations that consider the realistic characteristics of the structures and the soil, leading to better predictions of seismic performance and enhanced earthquake-resistant design (Kausel 2010; Roesset 2013).

1.2 Significance of SSI

It is widely believed in previous studies that considering SSI can improve the seismic performance of structures (Veletsos and Meek 1974), and there are the following reasons to support this view. Firstly, because of the flexibility of the ground, the foundation of buildings incorporating the dynamic SSI has two more degrees of freedom: horizontal movement and rotation. The increase of degrees of freedom can lower the stiffness of the overall system, and thus elongating its natural period. Moreover, because of both kinematic interaction and inertial interaction effects, the motion input on the structure base deviates from the free field motion (Anand and Satish Kumar 2018), and this is the second point to consider. According to the response spectrum theory, the seismic base shear force, in force-based methods of calculating seismic demand, is determined by multiplying the building weight with the pseudo spectral acceleration (PSA) at the first-mode period (normalised by g). Therefore, the elongation of the fundamental natural period and the modification of the input motion can alter the seismic demand of structures (Seed et al. 1976). In addition, when the flexible-base structure (considering the SSI) is in vibration, a significant amount of energy is dissipated into the soil through radiation damping caused by wave propagation and hysteresis damping of soil material, which makes the effective damping ratio of the structures founded on soft soils is generally greater than that of the rigidly supported structure (Wolf 1985). This effect tends to reduce the seismic demand of structures.

As a result, it is widely believed in previous studies that SSI is beneficial to the seismic behaviour of buildings and many current structural design codes recommend reducing the overall seismic coefficient when considering SSI or completely ignoring SSI (NZS1170.5 2007; NBCC 2010; GB 50011 2010; IBC 2012). Despite the commonly accepted design consideration, observations from several earthquake-damaged sites have shown that it can be harmful. For instance, during the 1985 Mexican earthquake,

a completely different outcome was observed, with the soft ground soil leading to a significant amplification of the seismic forces. (Sharma et al. 2018). In addition, as shown in Figure 1.1 and Figure 1.2, Yashinsky (1998) and Mylonakis and Gazetas (2000) provide remarkable examples, such as damage in piled foundation bridge and the failure of expressways, that demonstrate the incorrect and misleading nature of the rigid base assumption. Furthermore, lessons learned from recent earthquakes, such as the 2011 Christchurch earthquake of New Zealand and the 2011 Tohoku-Oki earthquake of Japan have also shown the importance of considering SSI effects for accurate prediction of the seismic response and ensuring building safety during an earthquake (Bagheri et al. 2018).

Recent studies have also provided evidence that supports the possibility of SSI impacting the lateral deformations of superstructures through horizontal movement and rotation of the foundation (Guin and Banerjee 1998; Tabatabaiefar and Clifton 2016; Far 2019). In performance-based design, deformation-related parameters are frequently employed as indicators of damage, which makes considering SSI particularly important. Additionally, the stability of the overall structure can be impacted by the amplification of structural lateral deformation and the secondary P-Delta effect. Thus, it is especially crucial to account for SSI in the design of high-rise and slender buildings. Several studies have emphasised the importance of this consideration, including Fatahi et al. (2011), Samali et al. (2011), and Tabatabaiefar et al. (2012).

As a result, there are conflicting opinions regarding the effect of SSI on the seismic behaviour of the building, as noted by Mylonakis and Gazetas (2000) and Far and Flint (2017). Due to the complexity of SSI and the lack of consensus among researchers, there are very few structure design codes that provide guidelines related to SSI. Consequently, considering SSI in the design practice of common and prevalent building typologies worldwide has been a rarity (Anand and Satish Kumar 2018).

These reasons highlight the need to critically investigate the impacts of SSI, and the development of a simple but accurate design program to analyse SSI problems is necessary (Sharma et al. 2018).

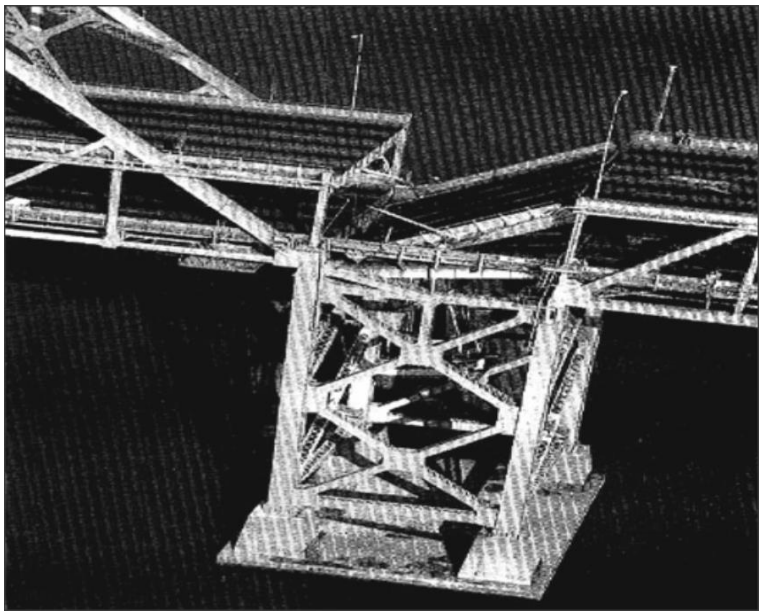

Figure 1.1 Fallen deck at Pier E9 of the East Bay crossing during Loma Prieta Earthquake, 1989 (after Yashinsky 1998)

Figure 1.2 Hanshin Expressway collapse during Kobe Earthquake, 1995 (after Mylonakis and Gazetas 2000)

In the present investigation, a numerical soil-foundation-structure model established

in finite element software Abaqus and verified by shaking table tests is used to critically explore the effects of SSI on high-rise frame-core tube and frame-shear wall structures. The seismic behaviour of high-rise buildings with different structural heights, height-width ratios (HWR), foundation types, soil types and bedrock depths (BD) are studied. The results including maximum lateral deflections (Δ), foundation rocking, inter-storey drifts and storey shear forces for the rigidly supported and flexibly supported structures are discussed and compared. The newly developed 3D numerical soil-structure model can be employed to explore similar SSI problems. By analysing the seismic response of a great number of high-rise buildings cases, the beneficial and detrimental scenarios for high-rise buildings considering SSI are identified and code-based procedures are developed to provide a safe and economical structural design method.

1.3 Aims and Objectives

The main aim of this study is to investigate seismic behaviour of high-rise buildings with different structural systems, structural heights, HWRs as well as foundation types, BDs and soil types. The primary objectives of this study can be summarised as follows:

- To develop a novel numerical soil-structure model to study seismic behaviour of high-rise buildings considering SSI.
- To verify the newly developed numerical model as a valid and reliable tool for conducting SSI analyses.
- To study the effects of variation in structure heights, HWRs as well as foundation types, BDs and soil types on seismic behaviour of high-rise frame-core tube structures.
- To study the effects of variation in structure heights, HWRs as well as foundation types, BDs and soil types on seismic behaviour of high-rise frame-shear wall structures.

- To compare the seismic performance of fixed base structures with flexible base structures to identify the beneficial and detrimental scenarios for high-rise buildings considering SSI.
- To develop standard-based procedures to provide a safer structural design method.

1.4 Organisation of the Thesis

This thesis is organised into six chapters. The current chapter presents the background, significance of SSI, and objectives of this study, while the remaining five chapters are outlined below.

Chapter 2 first illustrates the influence of SSI with a classic single degree of freedom (SDOF) system, and then discusses the mechanism and principle of SSI in detail. Afterwards, various parametric studies on seismic response of different structures with different foundation characteristics incorporating SSI as available in existing literature are introduced. In addition, a broad review of contemporary seismic codes that account for the impact of SSI on structural response is provided.

Chapter 3 describes how the 3D numerical soil-structure numerical model is established in finite element software Abaqus 6.14. In this process, a 15-storey reinforced concrete (RC) moment frames model with fixed and flexible base conditions is established in Abaqus. After that, the seismic performance of the numerical model under four different earthquake records are studied and compared with experimental shaking table tests to verify the accuracy of the numerical model. The validated 3D numerical model is utilised in the next phase of the research to investigate the seismic response of high-rise frame-core tube structures and frame-shear wall structures, taking into account SSI and varying parameters.

Chapter 4 and Chapter 5 conduct extensive parametric studies on frame-core tube structures and frame-shear wall structures, respectively. The parameters include structural heights, HWR, foundation types, soil types and BD. For each case, four

different seismic records are applied to investigate the seismic response (Δ, foundation rocking, inter-storey drifts and storey shear forces) of the superstructure. As a result, this study has calculated 72 rigid base cases and 720 flexible base cases. Afterwards, seismic responses of rigid base and flexible base structures are compared to identify the beneficial and detrimental scenarios considering SSI. Finally, code-based procedures are formulated to establish a structural design method that is both secure and cost-effective.

Chapter 6 summarises the current investigation with conclusions, as well as recommendations for further research. Additionally, a list of references is included.

Chapter 2 LITERATURE REVIEW

2.1 General

Seismic design codes and standards have traditionally focused on protecting human life by ensuring buildings do not collapse during earthquakes of a specific intensity. However, this approach has shifted in recent decades towards performance-based earthquake engineering (PBEE), which aims to ensure the structural integrity of a building by prioritising its ability to meet its intended function during and after an earthquake (Fardis 2010). Unlike previous strength-based design principles, PBEE uses performance levels to indicate the condition of a structure after being exposed to a specific hazard level. Performance levels are classified as fully operational, operational, life safe, near collapse, or collapse, according to the Vision 2000 Committee (1995) and FEMA (1997). For engineers, the most common performance indicators are ductility demand, and inter-storey drifts (Kramer 2008). The five qualitative performance levels mentioned earlier correspond to quantitative maximum inter-storey drifts (δ) of <0.2%, <0.5%, <1.5%, <2.5%, and >2.5%, respectively.

However, recent studies have shown that the inclusion of SSI can impact a structure's performance level. Low and mid-rise frame buildings have been found to experience increased inter-storey drifts when SSI is considered, potentially causing the structure to shift from a life safe zone to near collapse or even collapse levels (Tabatabaiefar 2012; Far 2019). Therefore, it is crucial to examine the impact of SSI on various types of structural systems, taking into account commonly used superstructure and foundation types in real-life scenarios, to gain a comprehensive understanding of their seismic response. Several parameters, including seismic record characteristics, foundation type and depth, soil modulus, shear wave velocity (V_s), and superstructure geometry and natural period, can influence the behaviour of any structure-soil system during seismic loading (Anand and Satish Kumar 2018).

To ensure the success of PBEE in practice, it is important to have reliable and accurate seismic hazard assessments, as well as properly calibrated analytical models that accurately predict the performance of structures under seismic loading. One of the challenges in PBEE is the lack of consensus among experts on the appropriate performance levels for different building types and occupancy categories, which can lead to inconsistencies in design and retrofit decisions. Nevertheless, the PBEE approach has gained widespread acceptance and is now adopted in many seismic design codes and standards worldwide.

The incorporation of SSI effects in PBEE has also gained significant attention in recent years, as it can have a significant impact on the seismic response of structures. The SSI effect can influence the structural response through changes in stiffness, damping, and natural period. Therefore, accurate modeling of SSI is crucial in PBEE to ensure the desired performance levels are achieved. Recent studies have shown that SSI can lead to increased inter-story drifts and shifts in performance levels, highlighting the need for a comprehensive understanding of SSI effects on various structural systems and foundation types.

This chapter offers an in-depth discussion on the impact of SSI on the seismic performance of structures. The discussion begins with a simple SDOF system to demonstrate the effects of SSI on the structural response during earthquake events. Through this, readers can gain a fundamental understanding of the mechanisms behind SSI and its potential impact on the seismic behaviour of a structure. The chapter then proceeds to explore the mechanics and principles of SSI, analysing the complex interactions between the soil and the foundation of the structure in detail. Additionally, a great number of parametric studies on the seismic response of various structures with different foundation characteristics and incorporating SSI are presented, drawing on existing literature. These studies provide valuable insights into the influence of SSI on the response of different types of structures. The chapter also

provides a comprehensive summary of contemporary seismic codes that consider the effects of SSI on structural behaviour. These codes outline the procedures and methodologies used to incorporate SSI effects in seismic design, offering valuable guidance to engineers and designers.

2.2 Mechanisms and Principles of SSI

The SDOF model is a widely used representation of a building structure, especially for low-rise or single-storey buildings. It is characterised by a dominant mode of vibration and is employed to illustrate the influence of SSI on the seismic response of the superstructure, as described by Wolf (1985). By using this simplified model, the underlying mechanisms and principles of SSI can be understood more easily. The SDOF system consists of the mass (m), stiffness (k), and damping coefficient (c) of the structure, and its natural frequency (ω_0) is determined by the m and k values as per Equation (2.1), while the hysteretic damping (ξ_0) can be computed using Equation (2.2) when the structure is fixed on the base.

$$\omega_0 = \sqrt{\frac{k}{m}} \tag{2.1}$$

$$\xi_0 = \frac{c\omega_0}{2k} \tag{2.2}$$

In contrast, when the subsoil is compliant and the superstructure is flexibly supported, the foundation possesses the capacity to undergo translation and rotation. The dynamic characteristics of this system are commonly illustrated in Figure 2.1, which employs translational and rotational springs and dashpots to represent the system. In this model, the horizontal stiffness and damping are represented by k_h and c_h, respectively, while k_θ and c_θ denote the stiffness and damping in the rotational direction. Additionally, the model comprises other variables such as h (height of the superstructure), $2a$ (foundation width), Δ_0 (base displacement relative to the free field motion, u_g), Δ_θ (lateral displacement induced by foundation rocking), Δ_d (structural distortion), and Δ_t (total lateral displacement).

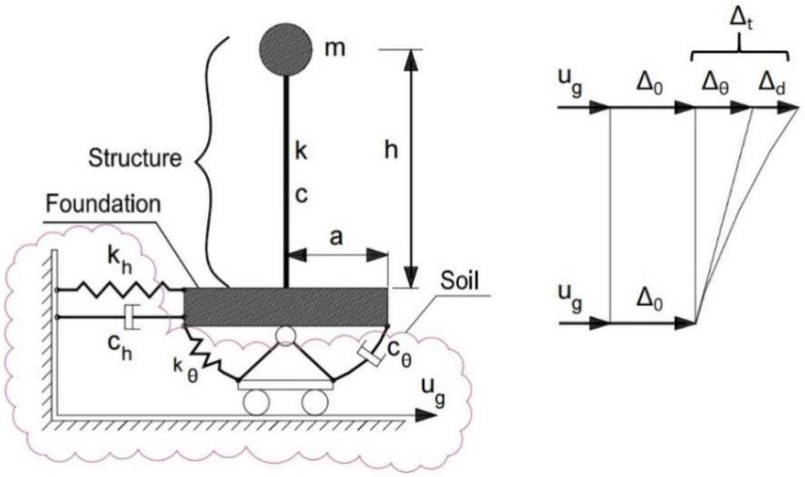

Figure 2.1 The SDOF and idealised discrete system to represent the soil-structure system (after Wolf 1985)

The system described above is then substituted with an equivalent model, which is depicted in Figure 2.2.

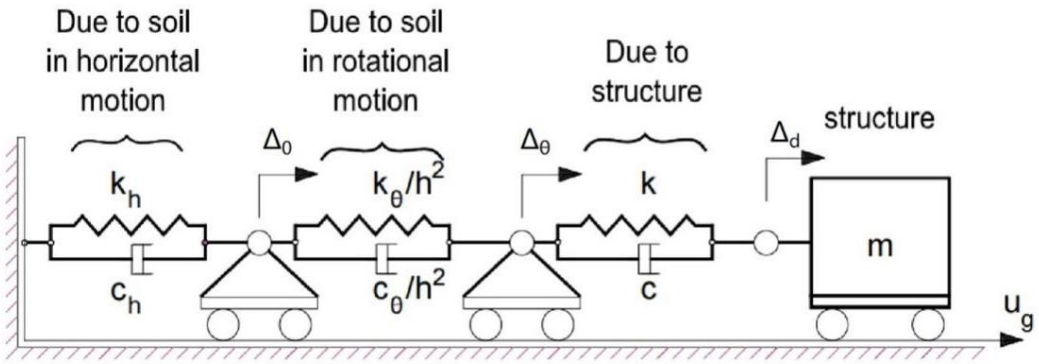

Figure 2.2 Equivalent system (after Wolf 1985)

The equation in matrix form for the motion of the system shown in Figure 2.2 is expressed as Equation (2.3), as presented by Wolf (1985). This equation provides a mathematical representation of the complex interactions between the superstructure and the subsoil. It incorporates the translational and rotational stiffness and damping coefficients of the foundation, as well as the structural parameters such as the mass, stiffness, and damping coefficient of the superstructure.

$$\begin{bmatrix} k_h + k_\theta / h^2 & -k_\theta / h^2 & 0 \\ -k_\theta / h^2 & k_\theta / h^2 + k & -k \\ 0 & -k & k \end{bmatrix} \begin{Bmatrix} \Delta_0 \\ \Delta_0 + \Delta_\theta \\ \Delta_0 + \Delta_\theta + \Delta_d \end{Bmatrix}$$
$$+ \begin{bmatrix} c_h + c_\theta / h^2 & -c_\theta / h^2 & 0 \\ -c_\theta / h^2 & c_\theta / h^2 + c & -c \\ 0 & -c & c \end{bmatrix} \begin{Bmatrix} \dot{\Delta}_0 \\ \dot{\Delta}_0 + \dot{\Delta}_\theta \\ \dot{\Delta}_0 + \dot{\Delta}_\theta + \dot{\Delta}_d \end{Bmatrix} \tag{2.3}$$
$$+ \begin{bmatrix} 0 & 0 & 0 \\ 0 & 0 & 0 \\ 0 & 0 & m \end{bmatrix} \begin{Bmatrix} \ddot{\Delta}_0 \\ \ddot{\Delta}_0 + \ddot{\Delta}_\theta \\ \ddot{\Delta}_0 + \ddot{\Delta}_\theta + \ddot{\Delta}_d \end{Bmatrix} = \begin{Bmatrix} 0 \\ 0 \\ -m \end{Bmatrix} \ddot{u}_g$$

Where:

$$\xi = \frac{c}{2k\omega}; \xi_h = \frac{c_h}{2k_h\omega_h}; \xi_\theta = \frac{c_\theta}{2k_\theta\omega_\theta}; \omega_s = \sqrt{\frac{k}{m}}; \omega_h = \sqrt{\frac{k_h}{m}}; \omega_\theta = \sqrt{\frac{k_\theta}{mh^2}} \tag{2.4}$$

After solving these equations:

$$\Delta_0 = \frac{\omega_s^2}{\omega_h^2} \frac{1+2i\xi}{1+2i\xi_h} \Delta_d; h_\theta = \frac{\omega_s^2}{\omega_\theta^2} \frac{1+2i\xi}{1+2i\xi_\theta} \Delta_d \tag{2.5}$$

Structural distortion, Δ_d, is expressed as Equation (2.6):

$$\left(1 + 2\xi - \frac{\omega^2}{\omega_s^2} - \frac{\omega_s^2}{\omega_h^2} \frac{1+2i\xi}{1+2i\xi_h} \frac{\omega_s^2}{\omega_\theta^2} \frac{1+2i\xi}{1+2i\xi_\theta}\right) \Delta_d = \frac{\omega^2}{\omega_s^2} u_g \tag{2.6}$$

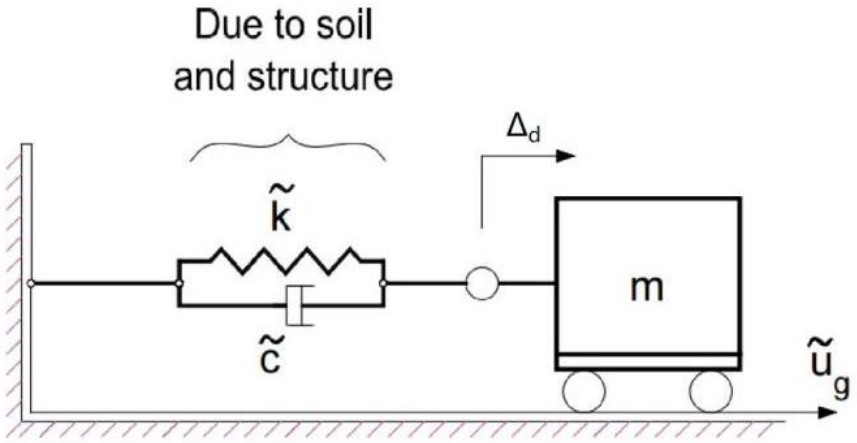

Figure 2.3 Equivalent SDOF system (after Wolf 1985)

Figure 2.3 illustrates the scenario in which the system in Figure 2.2 is substituted with an equivalent SDOF system that enforces the same Δ_d and has the same m. The equivalent natural frequency ($\widetilde{\omega}$), equivalent damping ratio ($\widetilde{\xi}$), and equivalent input motion ($\widetilde{u}_g$) are expressed as Equations (2.7), (2.8) and (2.9), respectively:

$$\frac{1}{\widetilde{\omega}^2} = \frac{1}{\omega_s^2} + \frac{1}{\omega_h^2} + \frac{1}{\omega_\theta^2} \tag{2.7}$$

$$\widetilde{\xi} = \frac{\widetilde{\omega}^2}{\omega_s^2}\xi_s + \frac{\widetilde{\omega}^2}{\omega_h^2}\xi_h + \frac{\widetilde{\omega}^2}{\omega_\theta^2}\xi_\theta \tag{2.8}$$

$$\widetilde{u}_g = \frac{\widetilde{\omega}^2}{\omega_s^2}u_g \tag{2.9}$$

In Wolf's (1985) study, it was revealed that incorporating SSI into the equivalent SDOF model, as presented in Equation (2.7), results in a lower natural frequency ($\widetilde{\omega}$) compared to the fixed base system's natural frequency (ω_0). Essentially, SSI can cause a significant reduction in the natural frequency of the structure, highlighting its crucial role in seismic performance. On the other hand, Equation (2.8) shows that the damping ratio of the equivalent SDOF model with SSI ($\widetilde{\xi}$) is generally higher than the fixed base counterpart's damping ratio (ξ_0). This suggests that SSI can contribute to enhancing the damping capacity of the structure, which is a desirable property in mitigating seismic response. It is worth noting that these findings hold for typical soils and foundations and may vary for different soil conditions and structural configurations.

In reality, the effects of SSI on the complex soil-foundation-structure systems are much more intricate and multifaceted than those captured by the simplified SDOF model. This is because SSI involves a variety of factors such as soil amplification, kinematic interaction, and inertial interaction, as explained by several researchers in the field. These three mechanisms are integral to the theory of SSI and have been

extensively studied in the literature.

Firstly, during an earthquake, seismic waves propagate through the ground and can be amplified by certain types of soils. Therefore, even before the structures are constructed, the motion of the free field is distinct from that of the bedrock, and this modification is called the soil amplification effect. This can result in greater damage to buildings, infrastructure, and other structures located on or in the vicinity of the soil. The severity of the soil amplification effect depends on a number of factors, including the frequency content of the seismic waves, the thickness and type of soil layers, and the distance from the earthquake source (Anand and Satish Kumar 2018). It can be significant in regions with soft soil layers, where the seismic waves can be amplified several times, resulting in much stronger shaking of the superstructure. However, technically the amplification effect is not a part of actual SSI.

Secondly, as shown in Figure 2.4, excavating and inserting the ideally massless and relatively rigid foundation into the soil further modify the foundation input motion (FIM). This is because the relatively rigid foundation filters out waves with a wavelength shorter than the size of the foundation (Hradilek and Luco 1970), thereby decreasing the energy of the input motion. Consequently, the FIM considering kinematic interaction is a more suitable motion for analysing structural response than the free field motion.

Finally, inertial interaction (Figure 2.5) occurs when the superstructure of a building generates inertial forces during an earthquake event. These forces can induce additional deformations in the soil and internal forces at the top of the foundation, which in turn, modifies the FIM (Mittal and Samanta 2021). Inertial interaction can be significant when the superstructure is heavy, resulting in a large inertia force, which can cause significant deformation to the foundation.

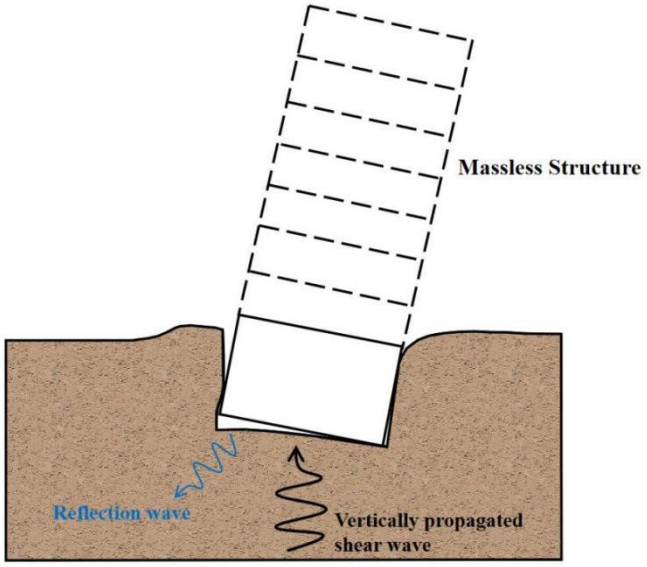

Figure 2.4 Visualisation of kinematic interaction

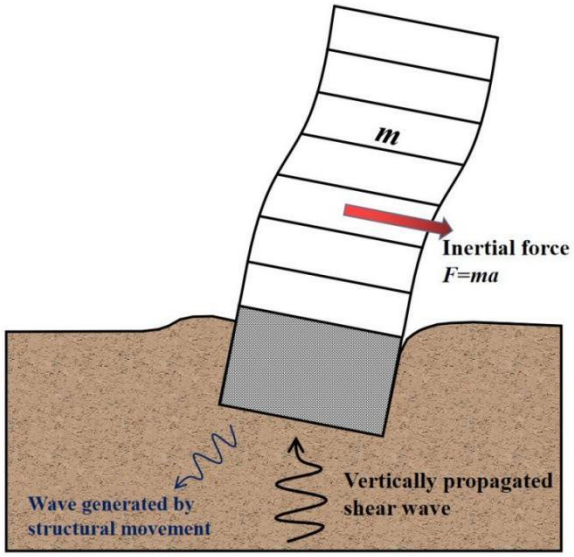

Figure 2.5 Visualisation of inertial interaction

Drawing on the three aforementioned principles of SSI, a solution that encompasses three steps has been developed to quantify the effects of SSI. Known as the substructure method, this approach considers the principles of SSI individually, as proposed by Kausel (2010). The substructure method is a three-step solution that aims to quantify the SSI effects by systematically breaking down the problem into smaller

components:

- Step 1: Evaluation of the FIM. This refers to the motion that would be present at the foundation base, assuming that both the structure and foundation have zero mass. In this stage, the impact of kinematic interaction is taken into account.
- Step 2: Calculation of the impedance function. In substructure analysis, the impedance function serves as a representation of the stiffness and damping properties of the substructure model. This step is crucial, as it accounts for inertial interaction effects. Gazetas (1991) devised a complete system of algebraic equations and dimensionless charts to calculate the various components of impedance functions, which are widely employed today.
- Step 3: The seismic analysis of the structure founded on a flexible base characterized by the impedance function and under the action of the FIM motion is performed. This step takes into account the effects of both kinematic and inertial interactions and is essential in accurately predicting the response of the structure to seismic loads.

The substructure method offers a more timesaving and computationally efficient solution for conducting parametric research (Anand and Satish Kumar 2018). However, the inclusion of soil nonlinearity presents a challenge for this approach (Scarfone et al. 2020), which relies on the superposition principle (Wolf 1998). As a matter of fact, SSI nonlinearity encompasses various aspects, such as geometric and material nonlinearity in different parts of the model, which may result in material yielding, soil liquefaction, as well as separation and slippage between foundation elements and subsoil elements. Additionally, it is important to note that soil stiffness may degrade under cyclic loading. Researchers like Kramer (1996) and Darendeli (2001) typically provide cyclic strain-dependent shear modulus curves, which are often utilised to account for soil stiffness degradation under cyclic loading.

In contrast to the substructure method, the direct method enables the analysis of both the soil and superstructure in a single step. It has been regarded as the most precise approach for SSI simulations, as it does not require the assumption of superposition and is better equipped to replicate the intricate nature of dynamic SSI (Borja et al. 1994; Far 2019). Nevertheless, the direct approach will probably require a lot of computational effort, including not only a suitable soil constitutive description, but also an appropriate simulation of the foundation elements, and the contact behaviour between the foundation and subsoil. Fortunately, with the advent of powerful computers, it became possible to analyse large soil-structure models with complex natures, such as irregularly shaped superstructures, embedded or pile foundations, and inhomogeneous and inelasticity of the subsoil.

2.3 Seismic Behaviour of Structures Considering SSI: Superstructure Parameters

The study of the influence of SSI on the seismic behaviour of structure-soil models with different superstructure systems and substructure types has been a topic of great interest (Anand and Satish Kumar 2018). In the last two decades, there has been significant progress in SSI research due to advancements in computational power and modeling techniques. The investigations in this field can broadly be categorised into two groups. The first category comprises researchers who have studied the positive and negative effects of SSI, while the second category comprises researchers who have aimed to identify the parameters and factors that affect the SSI effects. In this section, we will focus on the influence of various superstructure parameters on the seismic behaviour of buildings that incorporate SSI. These parameters include superstructure types, structure heights, and HWRs, as reported in the existing literature.

Carbonari et al. (2011) carried out a study on the seismic performance of a 6-storey frame-shear wall structure with pile foundations under the action of moderate

earthquakes using linear SSI analysis. The findings of the study revealed seismic shear forces in the columns were amplified, while these forces decreased in the shear wall when compared to the rigid base model. Furthermore, the study observed that there was a substantial increase in the transfer of shear forces from shear walls to frames with an decrease in the stiffness of ground soil.

Subsequently, Carbonari et al. (2012) employed the substructure method to examine the seismic response of the structure accounting for nonlinearity of the subsoil, and the nonlinearity were incorporated by equivalent linear method. The research demonstrated that SSI amplified the lateral deflection of the structure, and the response of the coupled shear wall framed structures was notably affected by foundation rocking. Similar to the previous study, SSI reduced the shear force at the shear wall base and increased it at the frame base.

Ganjavi and Hao (2012) conducted detailed parameter study on nonlinear multi-degree freedom systems under the impact of 30 earthquake records. The study's aim was to explore how SSI influences the distribution of ductility demands of the structure. This study systematically investigated the impacts of various factors, including the natural period, inelastic behaviour level, storey number, and damping factors. The results revealed that, irrespective of whether the structure was fixed based or rested on soft soils with longer natural periods, the earthquake reaction of the structure was primarily influenced by the target ductility demand value rather than the natural period. This was despite the fact that almost all seismic codes do not consider ductility demands.

Li et al. (2014) performed a numerical simulation on the seismic behaviour of the 632m Shanghai Tower using the substructure method. They developed a numerical model for the tower, which consisted of a detailed finite element simulation for the upper structure and a simplified analytical model for the foundation and the surrounding soil. The study involved simulating the collapse process of the tower

while considering SSI and exploring impacts of SSI on failure sequences and collapse resistance. The study results revealed that when SSI was taken into account, the natural period of the Shanghai Tower was elongated and the collapse margin ratio increased, leading to a reduction in seismic demand. Furthermore, SSI had a moderate influence on the failure sequences of the building during strong earthquakes, but only a minor influence on final failure modes.

Ghandil and Behnamfar (2017) employed the direct method to investigate the nonlinear behaviour of moment frames that were founded on a soft soil medium. This study analysed the inter-storey drifts, shear forces, and ductility demands of structures using both a fixed base model and a model that incorporated SSI through nonlinear time-history analysis. This study revealed that effects of SSI increased inter-storey drifts and ductility demands, particularly in the lower storeys of the structure.

Shirzadi et al. (2020) performed a study to explore effects of torsion on seismic responses of structures while considering SSI. The study focused on numerical models of four, eight, and twelve-storey steel structures that consisted of special frames founded on the soft subsoil. The study results showed that SSI caused an increase of up to 30% in the inter-storey drift of the first storey. Additionally, SSI amplified the plastic hinge rotation of the upper storeys, and this phenomenon was more significant in taller buildings.

Yang et al. (2020) carried out a set of shaking table tests on 12-storey RC building frames resting on pile foundations that incorporated nonlinear viscous dampers to investigate the impacts of SSI. They also developed and validated a numerical model to better understand the seismic behaviour of soil-foundation-structure systems with viscous dampers. This study found that SSI decreased the inter-storey drifts but increased the overall deformation. Therefore, the authors concluded that not considering SSI may result in a unsafe assessment of the dynamic properties of the RC buildings.

In the study of Arboleda-Monsalve et al. (2020), the authors investigated the earthquake reaction of 40-storey buildings while incorporating SSI. The study examined four different configurations: rigid base frame structure, frame structure considering SSI, rigid base frame-shear walls structure, and frame-shear walls structure considering SSI. The findings revealed that incorporating SSI in the model altered the seismic demands of the high-rise buildings, particularly with respect to inter-storey drifts, storey accelerations, and earthquake caused settlements. Furthermore, the study revealed that under the action of strong earthquakes, direct financial losses increased by 33% due to SSI.

Fathi et al. (2020) employed finite element method (FEM) to evaluate effects of SSI on the out-of-plane behaviour of an ancient Iranian building. The findings revealed that SSI had a noteworthy mitigating influence on the acceleration response, as it eliminated the effective mode vectors from the resonance region of the acceleration response spectra. Conversely, the displacement response spectra indicated a dramatic amplification in the deformation of the building due to SSI.

Radkia et al. (2020) performed a study on the seismic behaviour of asymmetric sliding structures with steel frame systems under horizontal and vertical earthquake effects, incorporating the impact of SSI. The research involved dynamic analysis of one, five, and ten-story buildings with 20%, 40%, and 60% irregularity using nonlinear FEM. The results indicated that seismic isolation had a considerable impact on the dynamic behaviour of structures with regard to inter-story drift and storey accelerations, particularly in one-story structures. Structural irregularities, however, did not considerably affect the seismic behaviour of the building. The study also revealed changing the soil type from II to III could be beneficial for tall buildings, as it led to a reduction in displacement and acceleration.

Mercado et al. (2021) explored influences of structural modelling on the nonlinear seismic behaviour of subsoil using a nonlinear inelastic-degrading model. The study

found that seismic responses in linear-elastic models were unrealistic and inaccurate in comparison to nonlinear high-rise building models. As a result, the authors concluded that incorporating nonlinear behaviour in the models is crucial for accurately predicting the seismic behaviour of structures founded on subsoil.

Kamal and Inel (2021) conducted an investigation on the seismic performance of RC frame building models with five, eight, ten, thirteen, and fifteen storeys and no structural irregularity. The demand measure utilised was the roof drift ratio. Twenty seismic record parameters were chosen as intensity measures. The study findings indicated that velocity-related parameters could serve as a reliable damage indicator for mid-rise buildings on soft subsoil, as they effectively reflected inelastic displacement demands. Among the parameters, Housner Intensity exhibited the strongest correlation.

Zhang et al. (2022) conducted earthquake vulnerability assessments of a 20-storey steel moment-resisting frame building with the tuned mass damper (TMD), while also considering the effects of SSI. The results showed the TMD could significantly mitigate the structural demands. However, SSI effects had an adverse impact on the fragility of the building, particularly during strong earthquakes.

Kamal et al. (2022) assessed the impact of structure-soil-structure interaction (SSSI) and SSI on the seismic response of mid-rise high ductility RC buildings situated on loose subsoil. The results suggested that incorporating SSI amplified the lateral deformation of the buildings by up to 15% compared to rigid base models.

According to the findings and conclusions drawn from the literature, it can be inferred that incorporating SSI effects in dynamic analysis generally results in an increase in the fundamental natural period of the model, inter-story drift, lateral displacement, and plastic hinge rotation, as well as a decrease in seismic demand and acceleration response. However, the majority of previous studies have focused on mid-rise

buildings, highlighting the need for further analysis of SSI effects on high-rise buildings with different structural systems. Therefore, additional investigations are necessary to analyse the impacts of SSI on high-rise buildings with distinct structural systems. Understanding the effects of SSI on these types of structures is crucial for accurately predicting their response to earthquakes and designing effective seismic retrofitting strategies. By conducting further research in this area, engineers and architects can ensure that their designs are better equipped to withstand seismic events and protect the lives and property of building occupants.

2.4 Seismic Behaviour of Structures Considering SSI: Substructure Parameters

The foundation system plays a crucial role in the complex problem of SSI, serving as the interface between the superstructure and the ground soil. Therefore, it is widely acknowledged as the most critical element of the SSI system. Over the years, several researchers have conducted studies to investigate the impact of various foundation system and subsoil characteristics on SSI analysis. This section summarises the findings from existing literature on the effects of different substructure parameters, including foundation types, foundation sizes, and subsoil characteristics, on the seismic performance of structures when considering SSI effects. By examining these parameters, we can gain a better understanding of the critical factors that influence the seismic response of structures under SSI conditions.

Han (2002) carried out an investigation on a 20-storey structure founded on a pile foundation, considering fixed base, linear soil-structure model, and nonlinear soil-structure model. This study examined the impact of the pile foundation deformation on the response of high-rise buildings and compared the findings with buildings constructed on shallow foundations. The findings indicated that considering the nonlinearity of piles resulted in shorter natural periods of the structures and improved displacements compared to the linear system. Additionally, buildings with raft or mat

foundations typically have longer natural periods compared to piled-supported buildings, resulting in more significant displacement amplitudes in both superstructures and foundations. The study also showed that the system's damping is underestimated, and stiffness is overestimated, highlighting the limitations of traditional design codes that do not consider effects of SSI in representing the real performance of tall buildings.

Galal and Naimi (2008) studied impacts of SSI on the nonlinear responses of 20-storey RC frames under different near-fault earthquake records. It is found that the inclusion of SSI resulted in a decrease in base shear and an increase in inter-storey drifts. The influence of SSI was more significant in soft and medium ground soil but had less and negligible influence in stiff and sound ground soil. The study suggests that structural designers should carefully consider whether SSI effects is positive or negative to seismic responses of structures.

Similar conclusions can be found in Tabatabaiefar and Massumi (2010). In this study, SSI effects on RC moment frames was investigated using the direct method. The findings showed it is imperative to take account of the influence of SSI for moment frames higher than 7-storey constructed on a soft soil medium.

El Ganainy and El Naggar (2009) conducted a study on the earthquake reaction of 5, 10, and 15-storey frame steel buildings with shallow foundations and one, three, and five basement storeys. The findings indicated effects of SSI varied depending on the soil type. For structures on stiff soil, SSI decreased the storey shear forces and moment demands, while for those on soft soil, it increased the base storey shear and moment demands. These results challenge the commonly held belief that SSI is always beneficial for reducing seismic demand. The study also demonstrated that the impact of SSI on structures with basement stories was similar to that of the rigid base model, and as basement storeys increased, the SSI effects became less apparent. Furthermore, the study found that SSI caused significant deformations of structural components,

with dynamic SSI resulting in an increase in deformations of 50% to 300% for buildings founded on soil class E. Such deformations can increase the lateral deflection of the entire building, leading the authors to conclude SSI have a detrimental effect on the behaviour of buildings.

Maheshwari and Sarkar (2011) examined the impact of higher loading amplitude on different dynamic property factors of a soil-pile group model. Additionally, they analysed the inertial interaction resulting from a four-storey portal frame built on the pile group-soil subsystem. The authors discovered that the interaction effect of the group was more noticeable, and the nonlinearity effect was more significant when the soil was softer. The fundamental period of the structure was lengthened because of SSI and the peak response tended to decrease, which was attributed to the influence of the superstructure's inertial interaction.

To explore SSI impacts on a 10-storey RC frame structure resting on a shallow foundation, Tabatabaiefar et al. (2013) employed the direct method. They analysed three types of soil with V_s of less than 600 m/s and both elastic and inelastic models to explore the impact of SSI on the structure's performance level. Results showed that structures founded on D_e and E_e soil type significantly increased their deformation and thus altered their performance level, suggesting the traditional design method excluding SSI is unsafe. Furthermore, the study revealed that compared to rigidly supported models, SSI causes a decrease in base shear, while the deformation-related indicators increase relatively. The influence of SSI become more pronounced with decreasing stiffness of ground soils.

Next, Tabatabaiefar and Fatahi (2014) delved further into the subject by investigating the impact of structural height on the soil-structure model. Their research findings demonstrated SSI exerts a dramatic influence on the performance level of mid-rise (5~15 storey) RC frame structures resting on D_e and E_e class soils. Building upon the data and outcomes of the aforementioned studies, Tabatabaiefar et al. (2014a)

developed a comprehensive empirical formula to estimate the seismic lateral deflections of the frame structure, which considers SSI effects.

To investigate the influence of seismic soil-pile-structure interaction (SSPSI) on RC frame structures, Hokmabadi et al. (2014; 2015) conducted a set of shaking table tests and used a fully nonlinear 3-dimensional numerical model with FLAC 3D. The study focused on three different scenarios: fixed base models, structures resting on raft foundations, and structures resting on floating (frictional) pile foundations. The results indicated that SSPSI increased the lateral displacement and inter-storey drifts in the soil-foundation-structure model. Additionally, the study found that the lateral deflections in piled foundation structures were reduced compared to shallow foundation models, as floating pile foundations could decrease the rocking components.

Similarly, a set of shaking table tests were carried out by Fatahi et al. (2014) to assess the influence of various types of foundations on the soil-structure system. The study evaluated a rigid base structure without SSI, a shallow foundation-supported structure, a floating pile-supported structure, and an end-bearing-supported structure. The findings revealed that the inclusion of SSPSI led to increased lateral displacements and inter-storey drifts in the experimental model, ultimately altering the structure's performance level.

Yeganeh et al. (2015) examined the impact of SSI on excavations adjacent to buildings using FEM. In this research, the structures considering the subsoil and the excavation-structure interaction model as well as the rigid base model were investigated. The study found the type of building model adjacent to the excavation had a significant effect on various factors.

Luo et al. (2016) performed 3D dynamic analyses of the structure-pile-soil system using both equivalent linear and nonlinear soil models. The study compared the

outcomes obtained from the two models and found the acceleration was underestimated when using the equivalent linear soil model. The authors suggested that the fully nonlinear constitutive model should be used to accurately account for soil behaviour in the SSPSI system. Additionally, the study introduced impacts of pile foundations on the dynamic behaviour of the system. The pile foundations were found to restrain foundation rocking, resulting in a reduced displacement response of the soil and structure during the soil and pile interaction.

Van Nguyen et al. (2016; 2017) conducted numerical simulations on a 15-storey frame structure to examine the impact of foundation size, such as shallow foundation width and pile length, on seismic response with consideration of SSI. The findings indicated that foundation size exerts a significant influence on building performance and should be considered in structural design. The study also found that increasing the length of floating piles resulted in larger maximum lateral displacements due to the piles' ability to absorb additional energy. Furthermore, the seismic response of end-bearing piles cannot be easily compared with floating piles as a result of the different load-bearing mechanisms. The end-bearing piles significantly affects the attracted kinematic forces during earthquakes.

Khazaei et al. (2017) conducted a research study aimed at assessing influences of SSI on the seismic behaviour of various buildings through 3D FEM using Abaqus software. The study employed two commonly used methods: the direct method and the cone model method, which is one of the substructure methods. The comparison of the maximum lateral displacement and storey shear forces calculated from the two methods revealed the cone model method demonstrated good agreement with the direct method. The findings of the study revealed the lateral displacement of the building increased with an increase in the number of storeys. This implies the upper storeys were more affected by SSI than the lower storeys. Additionally, the responses of storey shear were found to be greatly influenced by the rigidity of the foundation

and soil. The outcome of the study indicated the inclusion of SSI resulted in a decrease in the base shear for both 5- and 20-storey buildings in comparison to the rigid base model.

Bagheri et al. (2018) utilised numerical simulations to investigate SSPSI effects on 15-storey and 30-storey frame structures that were founded on six different piled foundation types. The target of this study is to investigate the optimal numbers, locations, and configurations of piles. The numerical findings indicated the performance levels of the flexibly supported structures were influenced by several factors, including the lengths, diameters, area replacement ratios, and distances between piles. This study also revealed SSPSI had a dramatic impact on the distribution of shear forces on the structures, resulting in a reduction of the shear forces.

To explore the effect of the V_s on the seismic behaviour of 20-storey high-rise buildings and end bearing piled foundations, Xu and Fatahi (2019) utilised FLAC 3D software to conduct a numerical simulation. The study focused on two distinct soil profiles, namely the in-situ soil profile and equivalent average soil profile. The study analysed and discussed the internal forces and the displacement of the superstructure and the pile. The findings revealed that when compared with the equivalent average profile, the utilisation of an in-situ V_s profile resulted in a decreased seismic demand of the structure.

Choinière et al. (2019) illustrated a simple linear method to evaluate seismic demands of shear wall buildings considering SSI. In this paper two methods (a rotational spring under the core and a more complex springs and dashpots system) to consider the effects of SSI were compared. Besides, a rigidly based model with code foundation factors was also established. Then, these approaches were used to evaluate a 12-storey RC shear wall building. The simulation results indicated that the aforementioned approaches were accurate in computing seismic demands. Due to the extremely soft

soil type E, linear analysis methods proved inadequate in accurately simulating the seismic performance of structures, necessitating the use of nonlinear analysis.

The influence of SSI on a 20-storey frame-shear wall building was examined by Scarfone et al. (2020) through 3D nonlinear dynamic time history analyses. This study investigated three different categories of foundations, namely shallow foundation, classic compensated foundation, and piled foundation. The findings indicated that the increase in foundation flexibility resulted in the reduction of seismic demand and an increase in foundation rotation.

Qaftan et al. (2020) carried out a study on the seismic performance of a scaled 15-storey RC frame-shear wall structure. The study found that the structure constructed on the pile raft foundation exhibited approximately 30% lower rotation compared with the raft foundation supported structures.

In their research on the seismic demands of piled structures while considering SSI effects, Akbari et al. (2021) analysed the behaviour of a ten-storey building with frames, braces, and rigid floors, using soft, medium, and dense sand as the three soil types. Results of this research indicated that increasing soil stiffness can lead to an amplification of the shear force at the structure's base. Additionally, the internal forces such as bending moment and shear force in the pile decreased smoothly with an increase in soil depth.

Al Agha et al. (2021) utilised the direct method to explore how soil type affects the seismic response of 16-storey wall-framed dual structures. By comparing soft and stiff soil, the authors found that the base shear of structures resting on soft soil decreased, while the values in the stiff soil model remained relatively unchanged in comparison with the rigid base model. In terms of the arrangement of RC shear walls, the structure with peripheral RC shear walls located at the corners exhibited the smallest deformation and base shear compared to the other models with stiff soil. Nevertheless,

the best arrangement was found to be the structure with the core RC shear wall constructed on soft soil, which displayed the smallest displacement and shear force.

In the investigation carried out by Ansari et al. (2021), the seismic vulnerability of buildings ranging from 12 to 24 storeys was examined based on their foundation type and layout. The study revealed that utilising flexible pile caps, as opposed to rigid pile caps, resulted in a decrease in seismic fragility and base shear induced by earthquakes. Additionally, the use of flexible pile caps also led to a reduction in pile head forces and deflection, ultimately improving the seismic performance of the structure-pile model during ground excitation. These findings suggest that incorporating flexible pile caps can mitigate damage caused by earthquakes and enhance overall structural resilience. Furthermore, the results indicate that the seismic vulnerability of buildings founded on soft subsoil can be underestimated if SSI is not considered, particularly under the impact of a strong earthquake.

Shabani et al. (2021) assessed seismic responses of mid-rise buildings situated near the crest and toe of a slope using three-dimensional numerical simulation. The study found that incorporating the topography soil-structure system increased the storey displacement and base shear in the structure. For instance, in topography SSI analyses, the 10 and 15-storey buildings experienced a 71% and 29% increase in maximum lateral displacement, respectively. Furthermore, the base shear in these buildings increased by 109% and 78% relative to their SSI counterparts. The study also found that the rocking angle of the foundation increased by 97% and 83% in the topography SSI system as compared to the SSI. These findings suggest that accounting for topography SSI effects can enhance the accuracy of building design near the crest of a slope.

Zomorodian et al. (2021) conducted research to assess the dynamic response of a 20-storey steel structure resting on a mat foundation founded on layered soil under the action of a series of strong seismic excitations. The study concluded that the most

reliable type of soil for this soil-structure model under both far-field and near-field earthquakes is dense sandy soil, while the most crucial case is the soft clay soil. The results also showed that the maximum average drift ratio under earthquakes far from faults was 1.24%, while the highest drift ratio was about 1.31% in near-fault earthquakes. Furthermore, this study found that the drift ratio was higher on the first and last floors of the structure. Overall, these findings suggest that understanding the type of soil and its effect on the seismic response of a structure is crucial in determining the most reliable and suitable design for the building's foundation.

Nasab et al. (2021) analysed the impact of SSI on the seismic retrofit of soft first-storey buildings. The findings illustrated the inclusion of SSI increased the seismic response and seismic demand for retrofit devices, particularly in structures founded on soft soils.

Adhikary and Deoda (2022) investigated the seismic behaviour of a 100-meter-tall tower constructed on a deep ground soil, considering various loading and boundary conditions. Using the finite element program SAP 2000, authors assessed the impact of soil depth on the seismic performance of the tower. The study found SSI can either amplify or reduce the shear force and the lateral deflection of the structure. The authors' final determination was that the earthquake reaction of the structure is non-monotonic with regards to the soil depth, and the significance of the ductility demand on the model under the action of SSI effects cannot be overlooked.

Bariker and Kolathayar (2022) utilised Abaqus software to conduct a set of SSI analyses on a 25-story building with a shear wall supported by a finned-pile mat subjected to far-field seismic records. The seismic performance was investigated through a time-history analysis of the finned-pile mat, which had varying fin-lengths, and compared with the findings of the conventional piled-mat. The results illustrated the use of finned-pile mats considerably decreased the building's vibrations and seismic effects, with increasing fin-length leading to a further reduction in these

effects. Additionally, increasing the fin-length also resulted in a reduction of the drifting bound.

An effective numerical model was created by Wang and Yang (2022), which takes into account the nonlinearities of both a RC frame and subsoil. The model was verified by a shaking table test before detailed parameter study were performed to examine the dynamic SSI effect. The results showed the shear force of the pile-supported frame increased with a larger pile dimension. Additionally, the consideration of SSI could dramatically increase the structural base shear under some conditions, with growth rates exceeding 30%.

Liang et al. (2023) proposed a refined finite element model that utilises a user-defined element to analyse the seismic behaviour of tall buildings founded on fluid-saturated soil, accounting for the dynamic characteristics of two-phase media and SSI. The model was then used to analyse a 51-story building with a frame-core tube system under the action of six earthquake records. Additionally, a rigid base model was incorporated to explore the SSI effect under the same circumstances. The findings of this study indicate that the SSI reduces acceleration and story shear force, but increases the deformation, inter-story drifts, and storey shear force. Its effects may not always result in conservative seismic performance evaluations for high-rise buildings. Therefore, it is crucial to incorporate SSI in the performance-based seismic design of high-rise buildings to obtain a comprehensive understanding of their seismic performance.

As a result of previous research, it has become apparent that there are contradictory opinions regarding the effects of SSI, which can be attributed to variations in methods, models, and parameters used in studies. Many studies have demonstrated the negative impacts of SSI on structures, such as increased inter-storey drifts, lateral displacements, plastic hinge rotation, and base shear. Examples of such studies include Tabatabaiefar and Fatahi (2014), Ghandil and Behnamfar (2017), El Ganainy

and El Naggar (2009), Radkia et al. (2020), and Van Nguyen et al. (2017). Conversely, some researchers have reached opposite conclusions, indicating a decrease in deformation and shear forces. Examples of such studies include Yang et al. (2020), Galal and Naimi (2008), Bagheri et al. (2018), and Ansari et al. (2021).

To summarise, structures with different foundation types and layouts show varying seismic responses in dynamic SSI analysis. In general, the use of piled foundations can reduce foundation rocking and minimise the lateral displacement of superstructures. However, the seismic demand may increase since piled foundations tend to absorb more earthquake energy. With decreasing stiffness of ground soils, SSI effects become more apparent and critical. The seismic behaviour of structures resting on stiff soil will likely be similar to fixed base cases. Nevertheless, the current research primarily focuses on low or mid-rise moment frames and fails to consider the differences in seismic performance between low and high-rise structures. Additionally, the seismic behaviour of frame-shear wall structures differs from frame structures due to the significant influence of foundation rotation on the former (Sharma et al. 2018).

Therefore, it is essential to investigate the seismic behaviour of high-rise buildings with varying structural systems, superstructure geometries, foundation and soil types, and bedrock depths, while taking into account SSI. Moreover, despite the numerous studies highlighting the adverse effects of SSI, the issue of distinguishing between beneficial and detrimental scenarios in SSI analysis remains unresolved. As a result, further research is necessary to determine the optimal conditions for SSI in various scenarios.

Additionally, it should be noted that the complexity of SSI and the lack of consensus in research findings make it challenging to establish reliable design guidelines for structures subjected to seismic loads. Although numerous methods for analysing SSI have been proposed, there is still a need for further research to develop accurate and efficient modeling techniques that can account for the dynamic behaviour of soil and

structures.

In summary, despite the progress made in understanding the effects of SSI on the seismic performance of structures, there are still many challenges that need to be addressed to ensure safe and reliable designs. Further research is needed to develop more accurate and efficient modeling techniques and establish reliable design guidelines. With the increasing frequency of earthquakes and the growing demand for high-rise buildings, addressing these challenges has become more critical than ever.

2.5 Review of Building Code Provisions Related to SSI

Considering the significance of factoring in SSI during dynamic structural analyses, as highlighted in Sections 2.3 and 2.4, it is crucial to integrate SSI considerations into seismic codes and standards worldwide. Nevertheless, only a small number of international codes include provisions for incorporating SSI. The reason for this could be the absence of a consensus among researchers regarding how SSI affects the seismic performance of structures, as noted by Anand and Satish Kumar (2018). In the upcoming sections, a critical review and discussion of existing international seismic codes that relate to SSI will be conducted.

2.5.1 United States

ASCE 7-10 (2010) provides the option to decrease the base shear force by considering SSI. This is accomplished by amending the natural period and damping of the rigid base structure. To avoid excessive reduction in base shear, a limit is imposed to ensure that the revised design base shear does not fall below 70% of the original value. The National Earthquake Hazard Reduction Program (NEHRP) created guidelines for this limit in FEMA (2015), prescribing the maximum reduction in base shear as a function of the response modification factor. These recommendations propose smaller design base shear reduction factors for structure-soil systems with larger response modification. Following this, ASCE 7-16 (2016) incorporated these instructions.

Chapter 19 of ASCE 7-16 (2016) suggests two approaches for conducting a linear seismic evaluation: the SSI modified general design response spectrum (specified in the code) and an SSI modified site-specific response spectrum (to be established by the design engineer). To account for non-linear soil effects, the design process recommends utilising the equivalent linear method, which involves calculating the reduced V_s and shear modulus based on the soil category and the design seismic records. To incorporate kinematic interaction in the design process, ASCE 7-16 (2016) enables the use of a non-linear response history procedure, which involves utilising acceleration histories scaled to a site-specific response spectrum. This necessitates modeling both the superstructure and substructure in a non-linear fashion.

2.5.2 Europe

According to EN 1998-5 (2004), in the design process of slender structures or structures with significant second-order effects (P-Delta effects), it is necessary to take into account the dynamic SSI. Moreover, structures that rely on piles or have substantial and deeply embedded foundations are also mandated to consider SSI. While EN 1998-5 (2004) determines the structures that necessitate the incorporation of SSI in the design process, there are no particular instructions given for computing the crucial components of SSI from a technical standpoint.

2.5.3 Japan

Similarly, JSCE 15 (2007) also recommends that the design of certain structures, including bridge abutments, retaining walls, underground structures, as well as piled and caissons foundation structures, should consider the SSI effects. However, the structural designer has the freedom to decide whether to model the structure and substructure as a whole or separately, and choose between the direct or substructure method.

2.5.4 China

GB 50011 (2010) provides a general recommendation that the influence of SSI does

not require consideration. However, for high-rise buildings constructed in areas with high seismic intensity on soil category III and IV with box foundations or piled raft foundations, it is permissible to consider the influence of SSI. Additionally, for buildings with an HWR of less than 3, the code offers a calculation formula for determining the horizontal seismic shear reduction coefficient of each storey.

2.5.5 India

IS 1893-3 (2014) and IS 1893-4 (2015) state that SSI should be incorporated into the design of bridges and industrial structures when the structure is resting on deep foundations in soft subsoil. Although it has been noted SSI may decrease seismic shear and increase lateral displacements in some cases, neither code provides provisions for analysing the effects of SSI, nor does the specialist literature address this issue.

2.5.6 New Zealand

Similar to the majority of the codes referenced earlier, NZS 1170.5 (2007) does not provide any explicit directives for integrating SSI into the design procedure. However, it does refer to the use of a structural performance factor, which is dependent on the seismic resisting system's material, type, and period, as well as the structure's damping and interaction with the ground soil.

2.5.7 Australia

AS1170.4 (2007) does not explicitly incorporate SSI effects in the seismic design of buildings. Therefore, structural designers using this standard are unable to consider these important effects in their analysis and design methodologies.

2.6 Summary

This chapter presents a comprehensive overview of mechanisms and principles of SSI, as well as various parametric studies on the structure-soil model that are available in the literature. Additionally, international codes and standards related to SSI are examined, including their guidelines and provisions. To begin with, a simplified

SDOF system has demonstrated that SSI effects can cause a natural period elongation and an increase in the damping ratio of structures. Nonetheless, in practical settings, this procedure can be quite intricate, as it encompasses numerous variables, including the amplification effect of the soil, the kinematic interaction between the foundation and the soil, as well as the inertial interaction between the structure and the foundation. Furthermore, the advantages and disadvantages of the direct method and substructure method are discussed, and it is concluded that the direct method is the most appropriate method for conducting dynamic SSI analyses.

Additionally, this review introduced effects of SSI and various parameters on various categories of structural and foundation systems. It is apparent that previous studies have primarily focused on low or mid-rise moment frames, while the commonly used structural systems in the design of tall buildings are rarely explored.

Moreover, the review of various codes and standards reveals that many of the renowned international seismic codes do incorporate conditions for considering SSI, but they still lack guidelines on the evaluation and integration of SSI in design practice. Some of these codes only take into account the beneficial effects of SSI by reducing base shear force, while underestimating the detrimental effect such as the increase of displacements and its influence on the performance levels of buildings. Out of codes that are covered in this section, the American standard places greater emphasis on design methodologies and other linear models related to SSI, with ASCE 7-16 (2016) being the most advanced standard in structural design practice that considers SSI. The development of well-drafted SSI protocols will undoubtedly receive appreciation from structural design practitioners. Therefore, it is essential to establish code procedures that address and mitigate the adverse impacts of SSI on the design of structures subjected to seismic activity.

Chapter 3 DEVELOPMENT AND VALIDATION OF 3D NUMERICAL MODEL

3.1 Introduction

Numerical simulations have become increasingly popular in recent years as a powerful tool for studying SSI. This is because of their ability to accurately replicate the complex properties of both the superstructure and substructure and capture the realistic interactions between the soil and structure. Accurately modeling SSI is crucial to guarantee that any parameter studies carried out are precise and dependable. Therefore, the main objective of this chapter is to validate the accuracy of a novel 3D numerical model that is developed based on the finite element software Abaqus 6.14. This model will be used to study SSI.

The chapter begins by offering a comprehensive description of the numerical model developed in Abaqus 6.14. This model is a 3D finite element model that includes a detailed representation of both the structure and soil element, as well as their interaction. Additionally, the boundary conditions and seismic motion input method are also described to offer a complete understanding of the model development process.

Following this, the experimental shaking table tests are presented in detail. Properties of the prototype structure, the scaling process, as well as the design and assembly of the scaled model are introduced. At the same time, the direct method is employed to numerically simulate the identical soil-structure model in the shaking table tests.

Finally, the accuracy of the novel 3D numerical model is evaluated by comparing the results derived from both the numerical simulations and experimental shaking table tests. The next phase of this research involves utilising this validated model to investigate the seismic response of high-rise buildings through numerical simulations

while considering various parameters related to SSI.

3.2 Numerical Model of the Superstructure

Abaqus 6.14 software (Dassault Systèmes SIMULIA 2012) is adopted to simulate the soil-structure system. The objective of this modeling approach is to maintain precision while achieving a high level of computational efficiency, and this is achieved through the selection of 4-node general-purpose shell elements with reduced integration and hourglass control (S4R) to simulate slabs and shear walls, and three-dimensional 2-node linear beam elements (B31) to simulate beams and columns. In addition, the elastic-perfectly plastic behaviour is implemented in the superstructure elements. Notably, the superstructures in parameter study are all RC structures; thus, the damping ratio is set at 5%, and the concrete's yield stress (σ_y) is assumed to be equivalent to the compressive strength (f'_c).

3.3 Numerical Model of the Subsoil

According to Rayhani and Naggar (2008), the soil domain's length should be no less than five times the width of the superstructure. Given the variable nature of the superstructure height and HWR employed in this study, the width of the superstructure ranges from 10 m to 30 m, resulting in horizontal dimensions of the soil domain that range between 50 m and 150 m. Moreover, the depth of the bedrock is assumed to be no more than 30 m, as the most significant amplification effects occur within the top 30 m of subsoil.

To model the soil domain, 8-node solid elements with reduced integration and hourglass control (C3D8R) are utilised. The adoption of reduced integration helps prevent locking phenomena. When meshing the ground soil, the guideline proposed by Gazetas (1983) is employed. According to this guideline, the height of the soil element should range from 1/5 to 1/8 of V_s/f_{max}, where f_{max} represents the highest wave frequency of the seismic records considered. To guarantee the accuracy while limiting the dimension of soil elements, seismic records used in this study are filtered to

prevent frequencies above 25 Hz, and the process of filtering is achieved by using Fast Fourier Transform technique.

To consider the nonlinear characteristics of soil elements, Mohr-Coulomb failure criterion is adopted. Specifically, the cohesion and internal friction angle are specified, along with the tension cut-off option. To address the nonlinearity of the ground soil, the cyclic shear strain (γ_c) depended shear modulus ratio (G/G_{max}) reduction curves (see Figure 3.1) and damping ratio (ξ) curves (see Figure 3.2) developed by Sun et al. (1998) and Seed et al. (1986) are utilised. The strain-compatible values of soil damping and shear modulus are determined iteratively under the influence of various earthquakes. The detailed steps of this process have been described in previous works such as Fatahi and Tabatabaiefar (2014) and Van Nguyen et al. (2017). To account for the energy loss in the subsoil during an earthquake event, Rayleigh damping is employed. The damping coefficients are calculated based on two soil frequencies that adequately capture the range of selected seismic records, as described by Park and Hashash (2004).

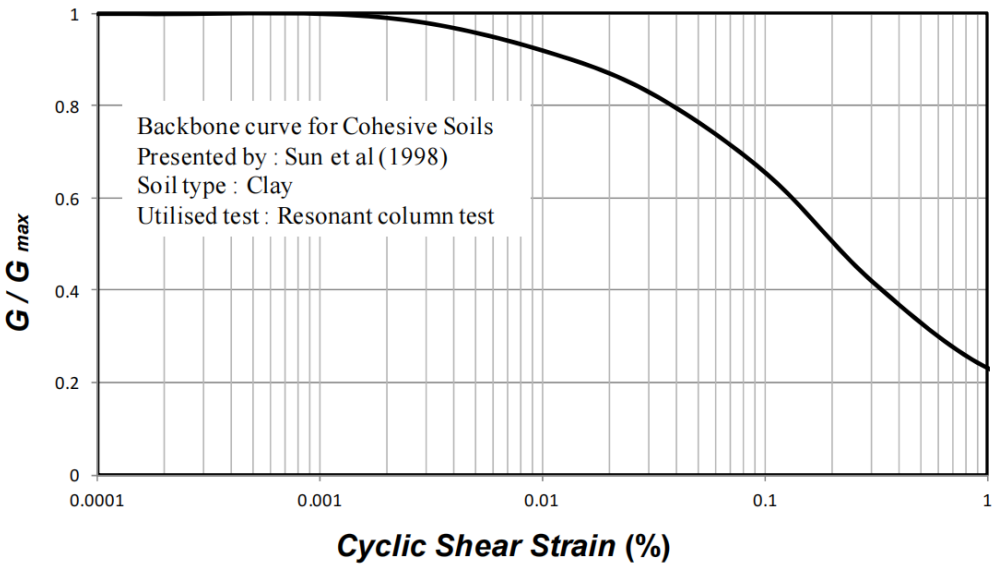

(a)

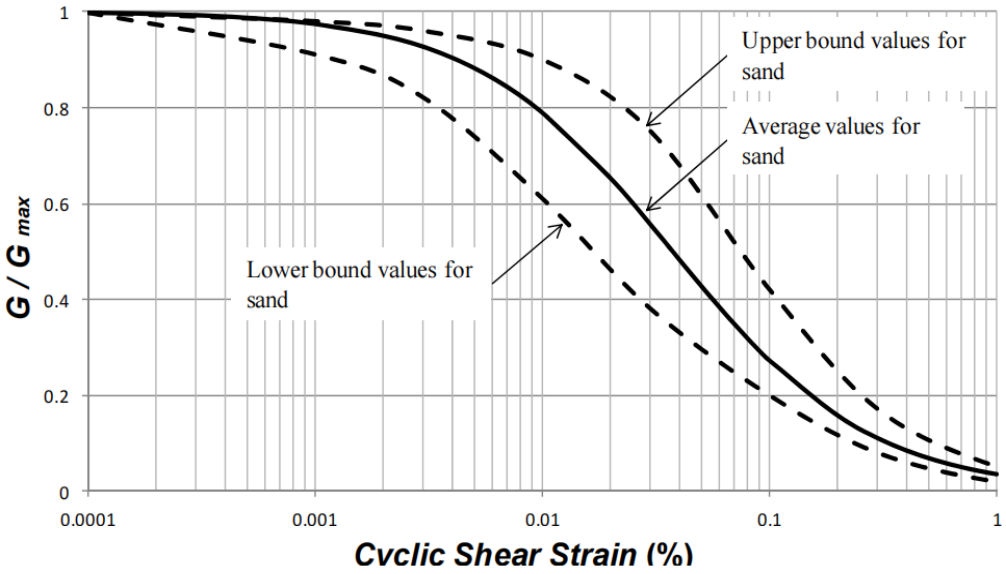

(b)

Figure 3.1 Relations between G/G_{max} versus γ_c for (a) cohesive soil (Sun et al. 1998)

(b) cohesionless soil (Seed et al. 1986)

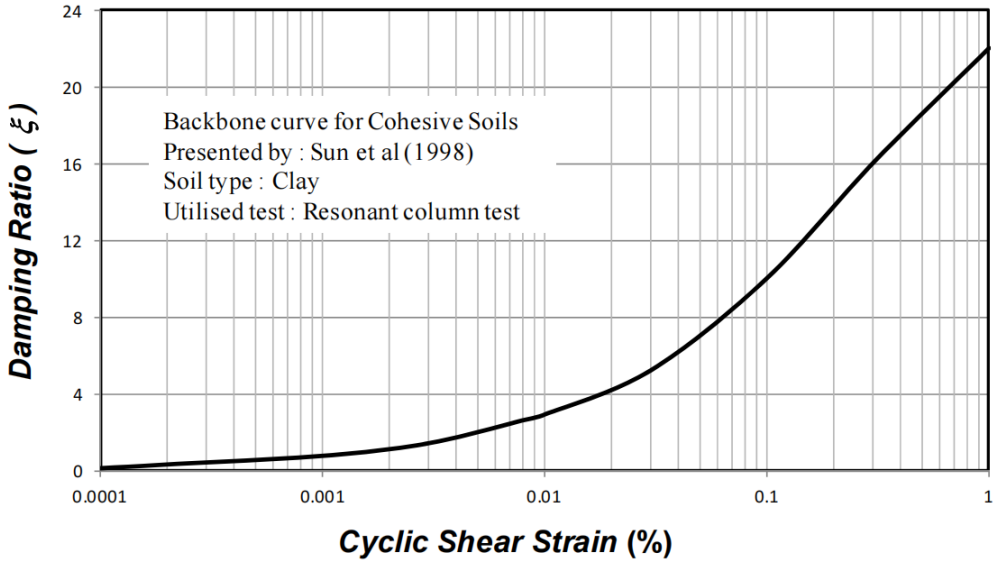

(a)

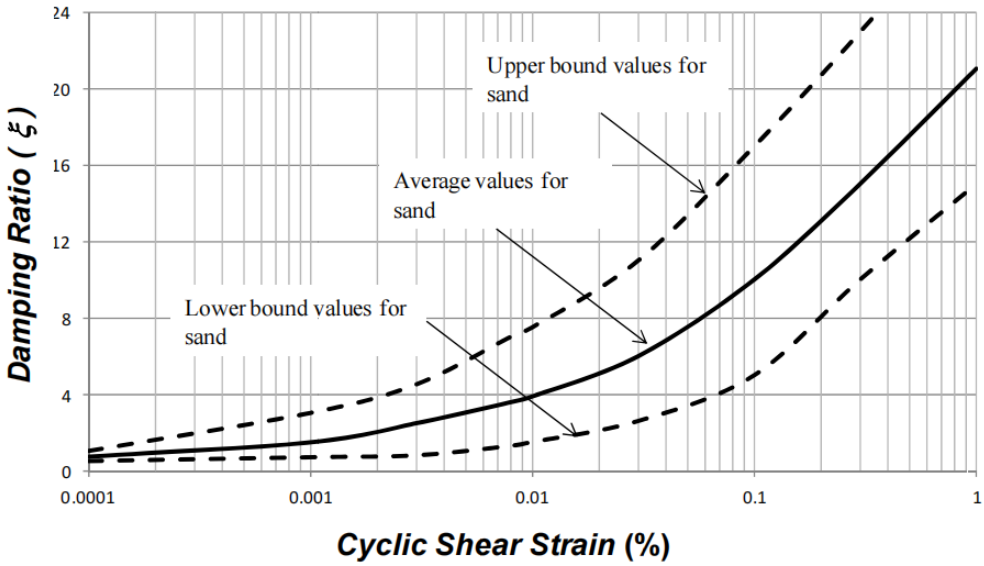

(b)

Figure 3.2 Relations between ξ versus γ_c for (a) cohesive soil (Sun et al. 1998) (b) cohesionless soil (Seed et al. 1986)

3.4 Contact Surface

To replicate the interaction between the foundation's bottom surface (referred to as the master surface) and the soil medium's top surface (known as the slave surface) under seismic loading conditions, Abaqus employs a surface-to-surface contact method. This technique involves using a finite sliding formulation and a surface-to-surface discretisation approach to achieve the desired objective.

The mechanical behaviour of the contact surfaces in the numerical simulation is separated into two categories: normal behaviour and tangential behaviour. The former uses a hard contact method, which utilises Lagrange Multipliers to enforce contact constraints, as explained by Van Nguyen et al. (2017). On the other hand, the latter employs a penalty friction formulation and utilises contact-pressure-dependent data to replicate the Mohr-Coulomb failure criterion between the contact surfaces of the foundation and soil. This allows the simulation to accurately replicate the frictional forces that arise between the foundation and soil during seismic loading.

3.5 Boundary Conditions

When utilising numerical methods to solve the dynamic SSI problem, it is often necessary to extract a finite calculation area from an infinitely vast soil medium. To prevent the impact of reflected waves, we apply an artificial boundary condition (ABC), specifically a viscous-spring boundary, on the lateral and bottom surfaces of the subsoil domain. Compared to a viscous boundary, the viscous-spring boundary can effectively absorb the energy of scattering waves on the boundary while simultaneously capturing the recovery ability of semi-infinite ground, without any issues of high-frequency instability or low-frequency drift, as explained by Gu et al. (2007).

To implement the viscous-spring boundary, a common technique is to apply parallel springs and dampers in one normal and two tangential directions at the boundary nodes, as depicted in Figure 3.3 and previously described by Gu et al. (2007). The mechanical coefficients of these springs and dampers are determined based on the characteristics of the surrounding soil medium, and their calculation formula is presented as Equation 3.1 and 3.2:

$$K_{BT}=\alpha_T\, G/R,\ C_{BT}=\rho\, c_s \tag{3.1}$$

$$K_{BN}=\alpha_N\, G/R,\ C_{BN}=\rho\, c_p \tag{3.2}$$

Where K_{BT}, K_{BN} are the stiffness coefficients of springs in tangential and normal directions, respectively; C_{BT}, C_{BN} are the damping coefficients of dampers in tangential and normal directions, respectively; α_T, α_N are modified coefficients and their value referred to the study of Liu et al. (2006), $\alpha_T=0.67$, $\alpha_N=1.33$; R is the distance from the wave source to boundary nodes; ρ and G are the density and shear modulus of the soil deposit, respectively; c_s and c_p are shear and P wave velocity of subsoil, respectively.

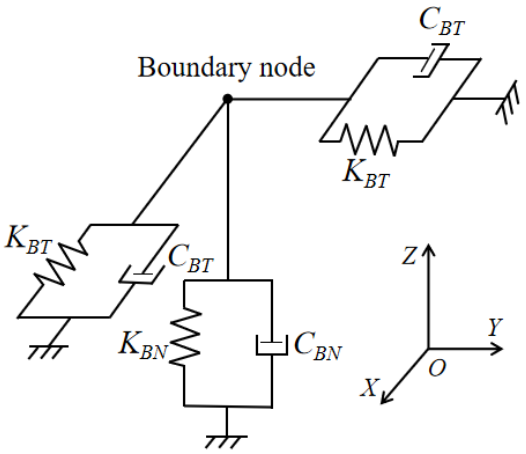

Figure 3.3 Viscous-spring boundary

3.6 Input of Earthquake Motions

After the implementation of the viscous-spring boundary, it is essential for the artificial boundary node to conform to the free field motion in order to supply conditions identical to those of the infinite subsoil. Typically, a one-dimensional free field grid is positioned along the periphery of the model, running parallel to the main grid, and connected to the main grid nodes by means of springs and dampers. However, this approach often results in an increased number of elements, and it can be difficult to implement in Abaqus because of the great number of required boundary nodes. In this study, the free field motion is transformed into an equivalent node force, denoted as $\boldsymbol{F_b}$, and applied to the boundary nodes (Ma et al. 2020).

The proposed approach involves several steps. Firstly, the free-field strain of the boundary is determined by applying the geometric equation, and subsequently, the stress on the boundary is obtained by applying the stress-strain relationship. Using the boundary node balance relationship, the equivalent earthquake load on the boundary node is then calculated, yielding the $\boldsymbol{F_b}$. Finally, $\boldsymbol{F_b}$ is applied in the form of concentrated forces on the boundary nodes of the soil domain, allowing for the implementation of seismic wave input.

The $\boldsymbol{F_b}$ comprises three parts: the first two parts are used to compensate for the influence of springs and dashpots, and the third part is the free field stress on the boundary:

$$\boldsymbol{F_b} = (\boldsymbol{K_b u_b^{ff}} + \boldsymbol{C_b v_b^{ff}} + \boldsymbol{\sigma_b^{ff}}\, \boldsymbol{n})\, A_b \tag{3.3}$$

Where $\boldsymbol{u_b^{ff}} = [u_x\ v_y\ w_z]^{\mathrm{T}}$ is free field displacement vector at artificial boundary nodes, $\boldsymbol{v_b^{ff}} = [v_x\ v_y\ v_z]^{\mathrm{T}}$ is free field velocity vector at artificial boundary nodes, $\boldsymbol{\sigma_b^{ff}}$ is the free-field stress tensor which can be derived from the geometric equation and linear elastic material stress-strain relationship, $\boldsymbol{K_b}$ is spring stiffness of viscous-spring boundary, $\boldsymbol{C_b}$ is damping coefficient of viscous-spring boundary; A_b is the influencing area of the boundary node; $\boldsymbol{n}$ is the cosine vector of the normal direction outside the boundaries.

By following the approach outlined by Ma et al. (2020) and implementing a simple MATLAB program, it is possible to calculate the amplitudes of $\boldsymbol{F_b}$ in all three directions for each node. These amplitudes can then be recorded in an amplitude file which can subsequently be read into the inp file of Abaqus, enabling the application of $\boldsymbol{F_b}$ on the viscous-spring boundary. After the completion of this task, it will be possible to analyse the seismic response of soil-structure models when subjected to earthquake acceleration records.

3.7 The Setup of Shaking Table Tests

To validate the accuracy of the numerical modelling technique, shaking table tests were conducted on a 15-storey frame structure. The outcomes of the numerical simulation were subsequently compared with the results obtained through the experimentation. This comparative analysis aims to assess the reliability and veracity of the numerical model in accurately evaluating the dynamic behaviour of the building under seismic loads.

The prototype subjected to shaking table tests is a 15-storey frame structure constructed on a shallow foundation. With a natural frequency of 0.384 Hz and a total

mass of 953 tonnes, the structure is situated on clayey soil characterised by a V_s of 200 m/s and a mass density of 1470 kg/m^3. In the scaling process, the objective is to achieve "dynamic similarity" between the model and the prototype, wherein both experience equivalent forces. Therefore, the approach formulated by Meymand (1998) is employed. The first prerequisite is that the shaking table experiment is performed under the condition of gravitational acceleration of Earth surface, which is approximately 9.81 m/s^2, ensuring that the model and prototype accelerations are identical. Next, it is necessary to develop a model with a comparable density to the prototype. Upon establishing the scaling condition of acceleration and density, the scaling relationships for other variables, such as mass, time, length, etc., is possible to formulate and present in relation to a geometric scaling factor (λ). Through a comparison of shaking table parameters (including the dimensions, payload capacity, and overturning moment) and model characteristics at different λ values, λ of 1:30 is determined to be the optimal scaling factor for shaking table tests while complying with shaking table constraints. As such, λ=1:30 is adopted in this research.

Thus, to achieve geometric similarity, the height, length, and width of the scaled model in shaking table tests can be conveniently computed to be 1.5 meters, 0.4 meters, and 0.4 meters, respectively. In addition to the geometric dimensions, it is necessary to scale the natural frequency of the prototype by $\lambda^{-1/2}$ (5.480) to attain dynamic similarity. Consequently, the natural frequency and mass of the scaled model are determined to be 2.11 Hz and 106 kg, respectively.

Subsequently, the scaled model was designed and constructed using steel plates for columns (500×40×2 mm), slabs (400×400×5 mm), and the foundation (500×500×10 mm), as illustrated in Figure 3.4. The assembled structure has a mass of 104 kg and a natural frequency of 2.19 Hz, which closely aligns with the computed values mentioned above. Similarly, the V_s and mass density of soil in shaking table tests are determined to be 36 m/s and 1470 kg/m^3. The completed soil-structure model utilised

in shaking table tests is depicted in Figure 3.5. Further information regarding shaking table tests can be obtained from Fatahi et al. (2015), Tabatabaiefar and Mansoury (2016), and Tabatabaiefar (2016).

Figure 3.4 Completed fixed base model of shaking table tests

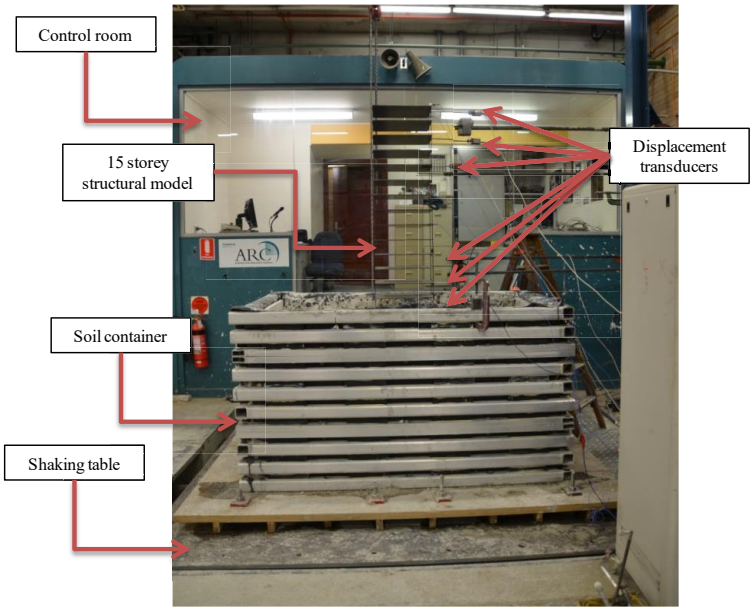

Figure 3.5 Completed soil-structure model of shaking table tests

3.8 Validation of 3D Numerical Model

The identical rigid base numerical model (Figure 3.6) and flexible base numerical model (Figure 3.7) were also established in Abaqus software. The same modeling

techniques introduced earlier were used to establish these models. Shell elements were selected in Abaqus to model steel columns and slabs of frame structures, while solid elements were used to simulate the subsoil. Based on the frequency extraction results from Abaqus, the natural frequency of the numerical model is 2.21 Hz, which indicated a close agreement with the experimental results.

The damping ratio of the scaled frame structure was also determined. It was found to be approximately 1.1%. According to the 1st and 2nd vibration frequencies of the frame, two damping coefficients (α and β) were obtained. The damping coefficient α was found to be 2.297, while the damping coefficient β was found to be 0.0004. These values are crucial for accurately simulating the damping behaviour of the numerical model.

Based on the previously introduced backbone curve, the soil strain-compatible parameters under various earthquake records were determined and are presented in Table 3.1. As the shear strain amplitude induced by each seismic record differs, the resulting values of G/G_{max} and ξ vary accordingly. Additionally, Table 3.1 provides the computed Rayleigh damping parameters for the different earthquake records.

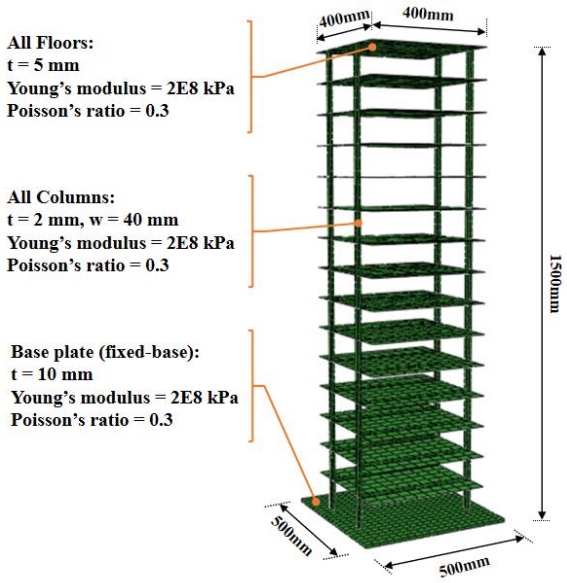

Figure 3.6 Numerical model of this scaled fixed base frame structure in Abaqus

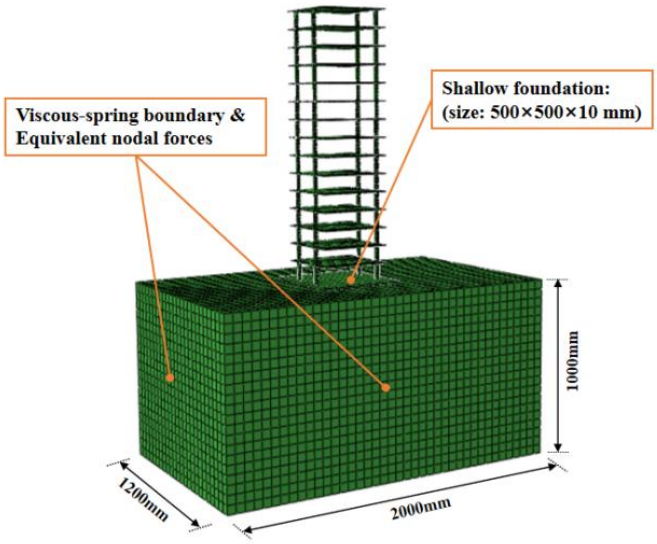

Figure 3.7 Numerical grid of soil-structure model in Abaqus

Table 3.1 Adopted strain-compatible parameters and damping parameters

Scaled earthquake records	G/G_{max}	ξ	Damping coefficients
El-Centro	0.48	14.0%	α=5.245 β=0.0028
Hachinohe	0.36	17.1%	α=2.540 β=0.0071
Kobe	0.33	17.5%	α=5.885 β=0.0039
Northridge	0.25	19.8%	α=6.534 β=0.0044

To validate the efficacy of the numerical simulation method discussed in the previous section, time-history analyses were carried out on both the numerical models and shaking table experiments using four different seismic records. The specifics of the chosen seismic records are outlined thoroughly in Chapter 4.

In accordance with Tabatabaiefar et al. (2014b), a scaling relationship of $\lambda^{-1/2}$=5.480 was utilised to calculate the natural frequency of the model (f_m) according to the natural frequency of the prototype (f_p), while the scaling relationship between the model and prototype accelerations was set at 1.0. This implies that the earthquake magnitude remains consistent with that of the prototype. To implement this scaling

relationship, the original earthquake records had to be scaled by a factor of 5.480 by reducing the time steps. The acceleration records for the four chosen earthquakes were then plotted in Figure 3.8 to showcase the resulting scaled data.

In order to compare the results attained from the numerical models with those from the shaking table tests, the Δ of the frame structure obtained from these two approaches was calculated. The outcomes of the time-history analyses using the numerical models and the shaking table tests are compared in Figures 3.9 and 3.10, respectively.

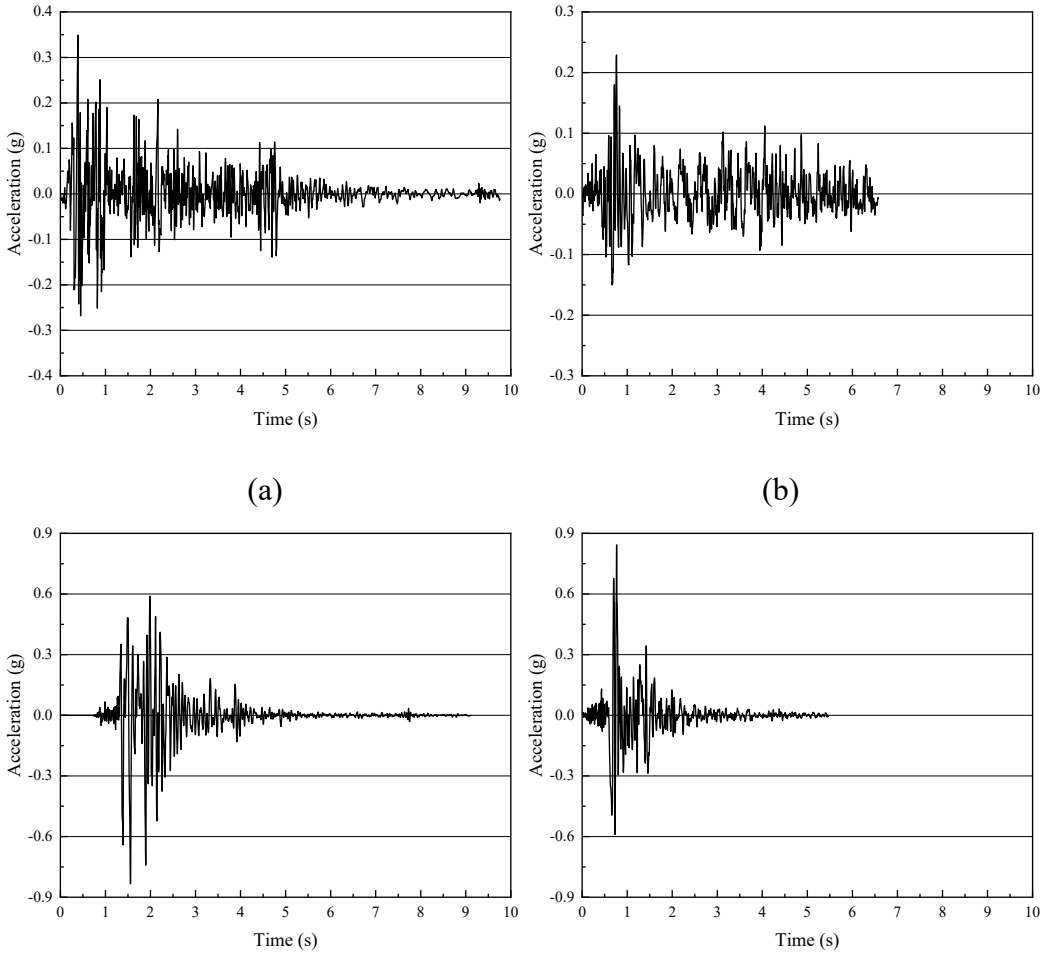

Figure 3.8 Scaled seismic records: (a) El Centro (b) Hachinohe (c) Kobe (d) Northridge earthquake

Figure 3.9 reveals that the rigid base and flexible base numerical models both

demonstrate a remarkable level of precision in simulating the seismic performance of structures when exposed to different earthquake records. The trends and values of the seismic response in the numerical simulations are consistent with the findings of shaking table tests, indicating a high level of agreement. Figure 3.10 illustrates the error of the average Δ, which were found to be 8.8% and 5.6% in fixed base and flexible base cases, respectively. The results imply that the numerical soil-structure model can effectively simulate the behaviour of the actual soil-structure system with a satisfactory level of accuracy. As such, this model presents a suitable and reliable tool for conducting additional SSI analysis.

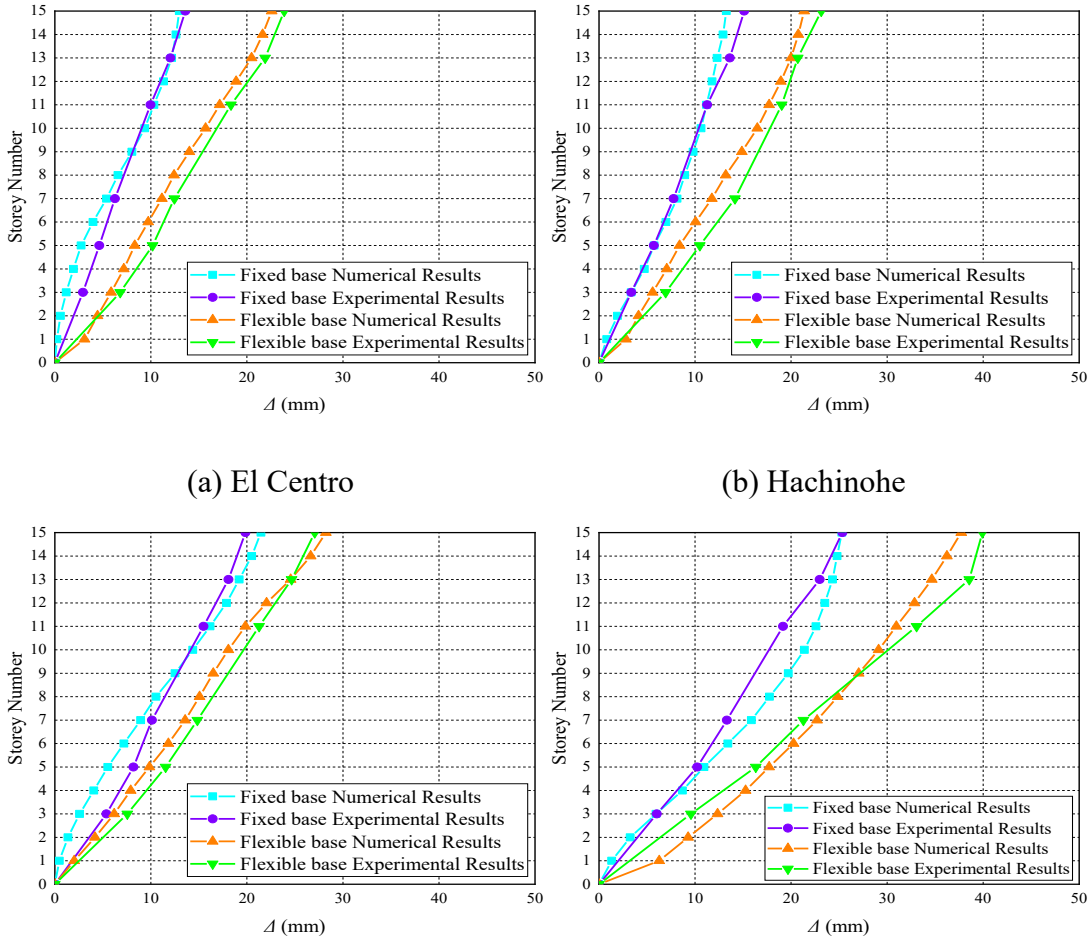

(a) El Centro (b) Hachinohe

(c) Kobe (d) Northridge

Figure 3.9 Numerical and experimental Δ of fixed base and flexible base models under the four scaled earthquakes

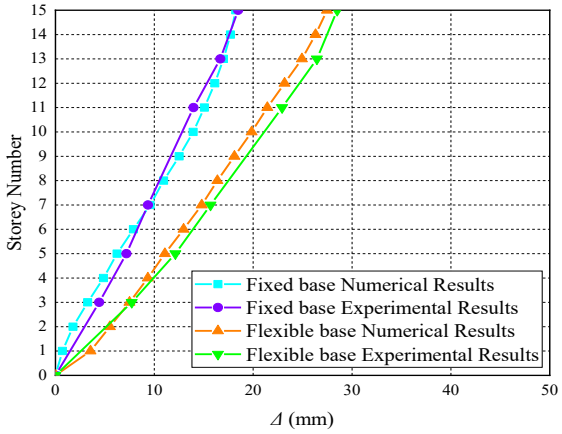

Figure 3.10 Average values of Δ of numerical model and experimental model

3.9 Summary

This chapter presents a novel and enhanced numerical simulation technique for analysing SSI based on the finite element software Abaqus 6.14. The simulation method accounts for the superstructure, subsoil, and contact surface, and the setup of boundary conditions and the input method for seismic record are also illustrated.

Following this, shaking table tests were carried out on a scaled 15-story frame structure model subjected to four scaled earthquake motion records. In parallel, identical numerical simulations were performed using the technique introduced in this chapter.

In the final step, a comparative analysis was conducted to evaluate the precision of the proposed 3D numerical model, utilising the results obtained from numerical simulations and shaking table tests. The Δ value of the rigid base model and the soil-structure model was utilised to demonstrate the accuracy and reliability of the proposed numerical model. Based on these results, the validated 3D numerical model will be employed in the subsequent phase of the study to examine the earthquake response of high-rise frame-core tube structures and frame-shear wall structures, considering various parameters related to SSI. The primary objective of this research is to provide significant insights and practical recommendations for the design and analysis of such structures in seismic zones.

Chapter 4 PARAMETRIC STUDIES ON FRAME-CORE TUBE STRUCTURES

4.1 Introduction

The analysis of SSI can be sorted into two primary groups. The first group includes studies that examine the positive and negative SSI impacts on earthquake behaviour of structures. The second group involves investigations that endeavors to identify the parameters and various factors that impact the criticality of SSI effects. This chapter employs the soil-foundation-structure model that was developed and validated in Chapter 3 to comprehensively explore the effects of SSI on high-rise frame-core tube structures. To achieve this objective, a range of superstructure and substructure parameters are considered. This analysis provides an improved comprehension of the seismic behaviour of tall buildings that considers SSI. Furthermore, by analysing the seismic response of a great number of cases, the beneficial and detrimental scenarios for high-rise frame-core tube structures considering SSI can be identified. Code-based procedures are then developed based on these scenarios to provide a safe and economical structural design method.

4.2 Overview of the Frame-core Tube Structure-Soil Numerical Model

In 1972, the International Conference on Tall Buildings classified tall buildings into four groups based on their height, as documented by Mukand et al. (1973). These categories included buildings with (1) 9~16 storeys (up to 50 meters); (2) 17~25 storeys (up to 75 meters); (3) 26~40 storeys (up to 100 meters); (4) over 40 storeys (super tall buildings). Consequently, the present study considers three typical high-rise building heights: 20 storeys (60 meters), 30 storeys (90 meters), and 40 storeys (120 meters). Furthermore, the high-rise buildings' HWRs examined in this study are four, five, and six, and each building has three spans in each direction. Two common

foundation types are employed in this study: end-bearing piled foundation and classical compensated foundation. The foundation embedment depth is assumed to be nine meters, with three basement storeys. Since the majority of soil amplification effects occur within the initial 30 meters of the soil profile, the BDs are assumed to be 10 m, 20 m, and 30 m, which is consistent with the majority of contemporary seismic codes (ATC 1996; Building Seismic Safety Council 2003). Only the top 30 meters from the ground surface are taken into account by these seismic codes when evaluating local site effects.

4.2.1 Characteristics of the Adopted Frame-core Tube Structure

Figure 4.1 (a) depicts the standard floor plan view of RC frame-core tube structures. AS3600 (2018) and AS1170.4 (2007) were referred to in designing the structural sections for buildings of various heights and widths using SAP2000 software. Nonlinear time history analyses were then performed on fixed base structures with various parameters under four seismic records (Figure 4.2) to ensure that all the δ remained below 1.5%, which is considered a life-safe level. The four seismic records consist of two near and two far earthquake accelerations to conduct a comprehensive investigation on earthquake responses of frame-core tube structures.

The structures employed grade 40 concrete with a characteristic compressive strength (f'_c) of 40 MPa, modulus of elasticity (E_c) of 32.8 GPa, and unit weight of 24.5 kN/m^3 (AS3600 2018). To simplify the modelling procedure in subsequent finite element analyses, structures of the same height were assigned the same dimensions for their structural sections, regardless of their HWRs. Table 4.1 summarises the dimensions of structural elements.

The superstructures in this study are anchored to soil deposits that possess varying geotechnical properties, which are detailed in Table 4.2 as described by Tabatabaiefar et al. (2014b). To evaluate the seismic response of the buildings, the maximum V_s of the ground soil was selected to be 600 m/s, as indicated by Tabatabaiefar et al. (2013).

This selection was made because, in general, the impact of SSI is deemed to be negligible when V_s exceeds 600 m/s.

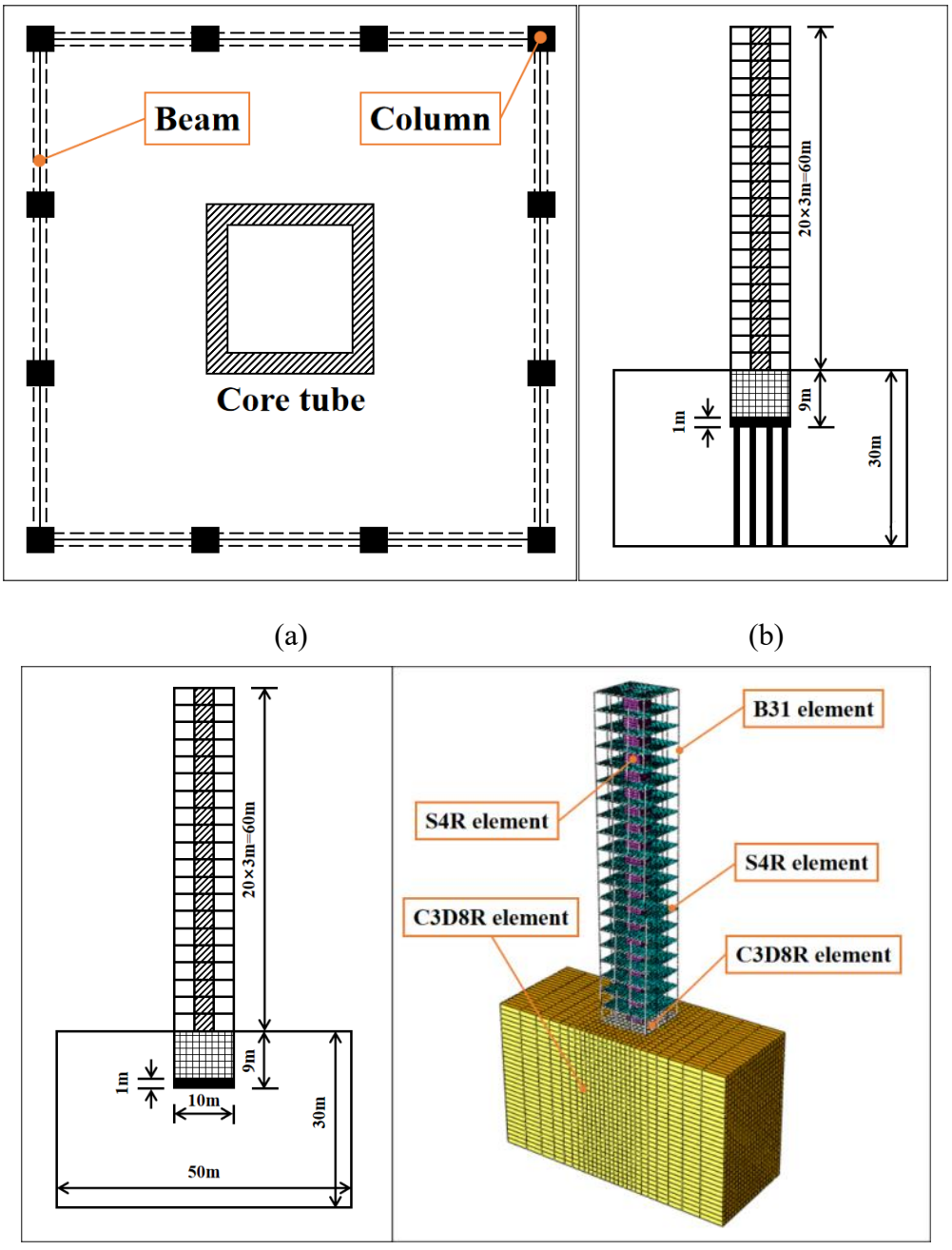

Figure 4.1 Characteristics of the adopted frame-core tube structure (a) plan view of standard floor (b) 20-storey frame-core tube structure with end bearing piled foundation (c) 20-storey frame-core tube structure with classical compensated foundation (d) the finite-element model

Table 4.1 Summary of dimensions of structural beams, columns and thickness of slabs and shear walls (m)

Structures	Levels	Columns	Beams	Core tube	Slabs
20-storey	1~5	0.55×0.55	0.40×0.40	0.55	0.25
	6~10	0.50×0.50	0.40×0.40	0.50	0.25
	11~15	0.45×0.45	0.40×0.40	0.45	0.25
	16~20	0.40×0.40	0.40×0.40	0.40	0.25
30-storey	1~10	0.70×0.70	0.50×0.50	0.70	0.25
	11~20	0.60×0.60	0.50×0.50	0.60	0.25
	21~30	0.50×0.50	0.50×0.50	0.50	0.25
40-storey	1~10	1.00×1.00	0.50×0.80	0.80	0.25
	11~20	0.90×0.90	0.50×0.80	0.70	0.25
	21~30	0.80×0.80	0.50×0.80	0.60	0.25
	31~40	0.70×0.70	0.50×0.80	0.50	0.25

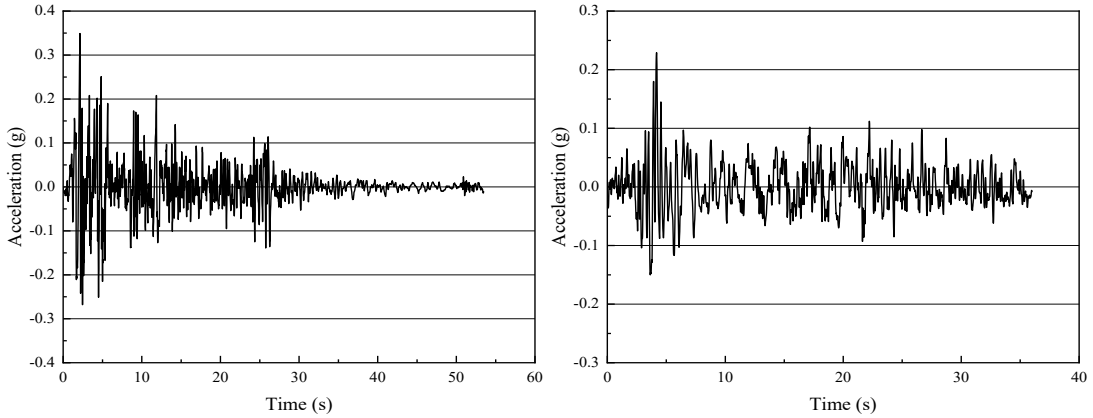

(a) (b)

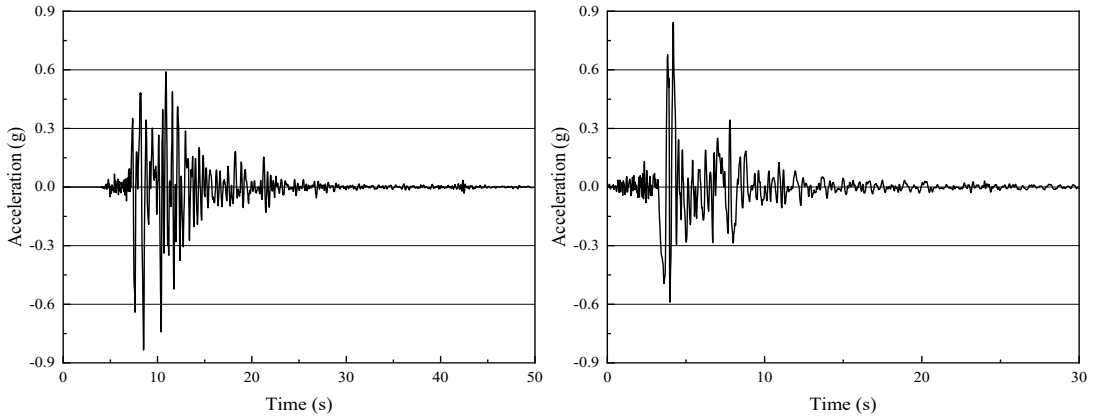

(c) (d)

Figure 4.2 Earthquake records: (a) El Centro (b) Hachinohe (c) Kobe (d) Northridge

earthquake

In recent times, there has been a growing trend towards using piled foundations for buildings. Piled foundations are a type of foundation system that transfers the upper loads through soft soil to deeper, stiffer soil or rock. For this study, an end-bearing piled foundation was selected, as demonstrated in Figure 4.1 (b). In this type of foundation system, all piles are rigidly connected to the bottom slab of the basement, and the pile toes are fixed firmly in every direction.

The arrangement and properties of piled foundation are illustrated in Figure 4.3 and Table 4.3, respectively. The pile foundation was designed to ensure that the applied loads were safely transferred to the underlying soil or rock. The arrangement and characteristics of the pile foundation were carefully selected to ensure the stability and safety of the structure.

What is more, the classical compensated foundation was chosen for comparison with the piled foundation model. The compensated foundation in building design is generally defined as a foundation that is deep enough so that the weight of the building is roughly equal to the total soil weight removed from the building position, allowing the soil weight to compensate for the building weight. When the foundation bottom pressure is exactly equal to the soil gravity stress, the additional stress at the foundation bottom is zero. This means that in theory, the foundation will not experience any settlement or shear failure. One of the advantages of the compensated foundation is that it is relatively simple and cost-effective to construct compared to other types of foundations. It is also suitable for use in areas where the soil is relatively uniform and stable.

The compensated foundation tends to induce larger foundation rotation, resulting in more significant lateral deflection of the superstructure. Thus, this study employs the classical compensated foundation and piled foundation, both of which have three basement floors overlying a 1m-thick RC base slab (Figure 4.1 b and c). The bearing

capacity and maximum settlement requirements for both types of foundation are met (Bowles 2001).

Table 4.2 Parameters of the subsoil

Soil type (AS1170)	V_s (m/s)	Unified classification (USCS)	G_{max} (kPa)	Poisson's ratio	Soil density (kg/m^3)	c' (kPa)	φ' (degree)	Plasticity Index
C_e	600	GM	623,400	0.28	1730	5	40	-
D_e	320	CL	177,300	0.39	1730	20	19	20
E_e	150	CL	33,100	0.40	1470	20	12	15

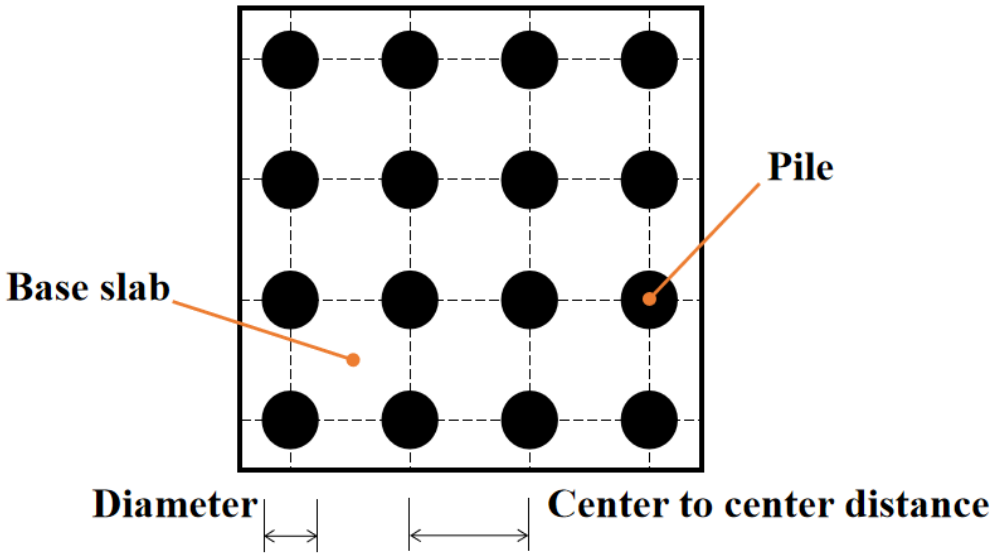

Figure 4.3 The pile arrangement used in this study

Table 4.3 Pile diameters and centre to centre distances

Storey number	HWR	Diameter (m)	Centre to centre distance (m)
20	4	1.2	4
	5	1.2	3
	6	1.2	2.6
30	4	1.5	6
	5	1.5	5
	6	1.5	4
40	4	2	8
	5	2	6
	6	2	5

4.2.2 Numerical Analysis

The numerical simulation method introduced in Chapter 3 is employed for the soil-structure model, including the modelling techniques for the superstructure and subsoil, contact surface properties as well as boundary conditions and loading methods. To consider the nonlinearity of the subsoil, the cyclic shear strain (γ_c)-dependent shear modulus (G/G_{max}) curves and damping ratio (ξ) curves presented in Figures 3.1 and 3.2 are utilised for cohesive soils (D_e and E_e soil) and cohesionless soils (C_e soil).

After setting up the numerical model for the soil-structure models with distinct parameters, the next step involves subjecting the rigid base and flexible base models to four bedrock earthquake ground motions, as depicted in Figure 4.2. It is worth noting that each of these ground motions has different seismic characteristics, which are summarised in Table 4.4. To accurately model the nonlinear behaviour of soil in the ground, the strain-compatible parameters and Rayleigh damping parameters are obtained for the four earthquake acceleration records. These parameters are presented in Table 4.5.

Table 4.4 Earthquake ground motions adopted in this study

Earthquake	Country	Year	PGA (g)	M_w (R)	T (s) Duration	Type	Hypocentral distance (km)	Record type
El Centro	USA	1940	0.349	6.9	56.5	Far field	15.69	Bedrock record
Hachinohe	Japan	1968	0.229	7.5	36.0	Far field	14.1	Bedrock record
Kobe	Japan	1995	0.833	6.8	50.0	Near field	7.4	Bedrock record
Northridge	USA	1994	0.843	6.7	30.0	Near field	9.2	Bedrock record

Table 4.5 Adopted strain-compatible parameters and damping parameters

Soil types	Earthquake records	G/G_{max}	ξ	Damping coefficients
E_e	El-Centro	0.57	11.1%	α=0.769 β=0.012
	Hachinohe	0.60	10.4%	α=0.284 β=0.024
	Kobe	0.35	17.0%	α=1.043 β=0.021
	Northridge	0.21	23.5%	α=1.415 β=0.029
D_e	El-Centro	0.71	7.8%	α=0.5337 β=0.0084
	Hachinohe	0.72	7.1%	α=0.1936 β=0.0162
	Kobe	0.55	11.7%	α=0.7179 β=0.0141
	Northridge	0.46	13.7%	α=0.825 β=0.0169
C_e	El-Centro	0.53	6.2%	α=0.4242 β=0.0067
	Hachinohe	0.53	6.2%	α=0.1691 β=0.0142
	Kobe	0.22	11.1%	α=0.6811 β=0.0134
	Northridge	0.215	11.2%	α=0.6744 β=0.0138

4.3 Results and Discussions

4.3.1 Lateral Deflection

The results are presented in Figures 4.4 to 4.18, which show the Δ of frame-core tube structures with 20, 30, and 40 storeys, varying in HWRs, foundation types, soil types, and BDs under fixed base and flexible base situations. The flexible base structures show higher Δ for almost all the cases, regardless of the structural height, HWRs, BDs, foundation and soil types. This is because after considering SSI, the degree of freedom of the soil-structure system increases and the natural period of the system is prolonged, resulting in an increase value of displacement according to the displacement response

spectrum curve. Consequently, the displacement response of high-rise frame-core tube structures is amplified.

Upon analysing the findings, it was also found that the Δ of piled foundation structures displays negligible variation with respect to the type of soil, provided that the superstructure parameters remain constant. In contrast, the displacement response of the classical compensated foundation structures shows a significant degree of variation, particularly in the presence of far-field earthquakes. These observations lead to the conclusion that end bearing pile foundation-supported structures are less susceptible to the effects of soil type when compared to classical compensated foundation-supported structures.

Furthermore, it should be noted that the Δ of piled foundation structures are not necessarily smaller than those of classical compensated foundation structures. For instance, when subjected to far-field earthquakes, the deformation of piled foundation structures (which have little difference between each other) is generally smaller than that of classical compensated foundation structures resting on the E_e soil type. However, when subjected to near-field earthquakes, the deformation of piled foundation structures does not decrease significantly compared to that of classical compensated foundation structures. It is worth mentioning that under far-field earthquake excitations, as the soil type changes from C_e to E_e, the Δ of structures gradually increases, particularly for classical compensated foundation structures. On the other hand, under near-field earthquakes, the deformation of structures typically decreases as the subsoil modulus decreases.

It is worth noting that the effects of the HWR on the Δ are multifaceted. While the increase in the building width can enhance the stability of structures and reduce foundation rotation, it also implies an increase in the mass of the building, leading to a rise in inertial force and structural distortion during seismic activity. Therefore, the Δ exhibits distinct patterns as the HWR varies. Additionally, compared with other

parameters related to the superstructure and substructure, the effects of BD do not seem significant. In order to provide a more comprehensive comprehension of the impact of the main elements in this investigation, such as soil type, HWR, and BD, the earthquake reactions of structures under the action of four seismic records will be averaged and analysed in detail in subsequent sections of this chapter.

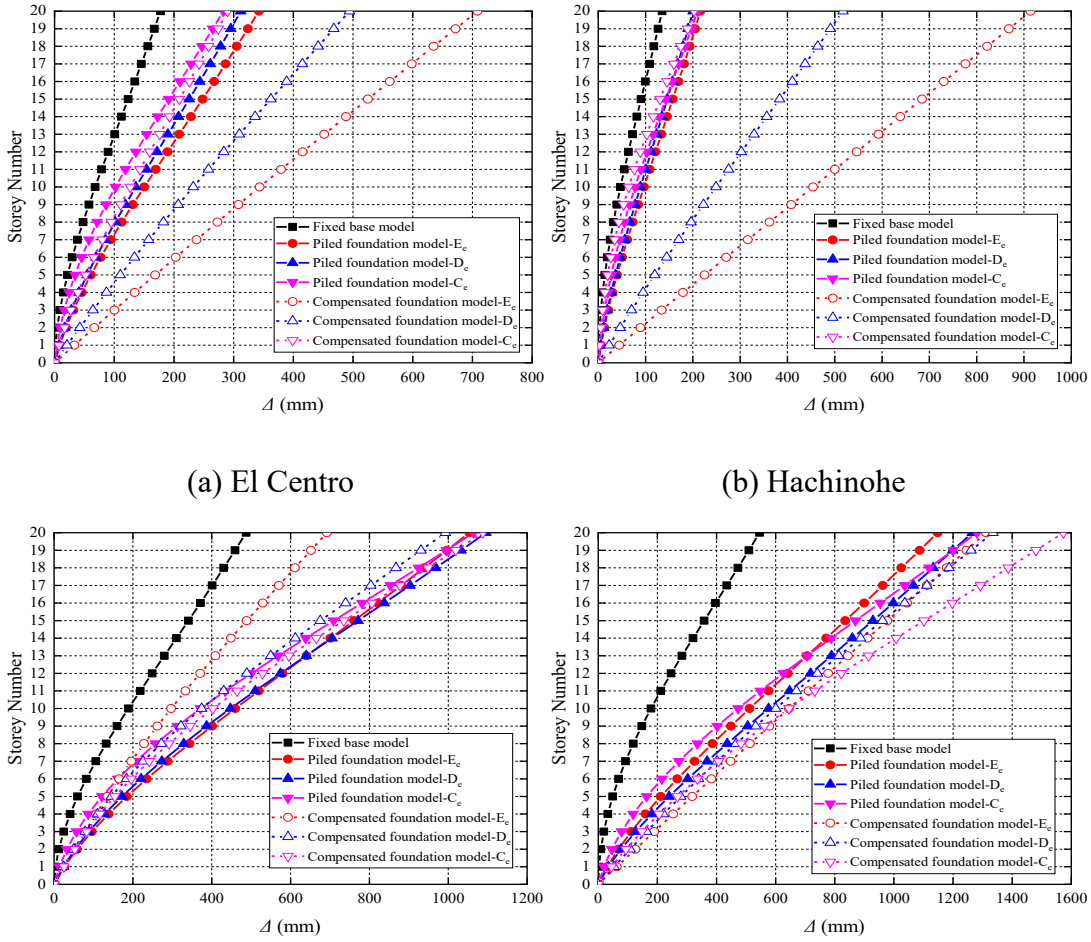

(a) El Centro (b) Hachinohe

(c) Kobe (d) Northridge

Figure 4.4 Lateral deflections of 20-storey structure (HWR=6, BD=30) under the four seismic records

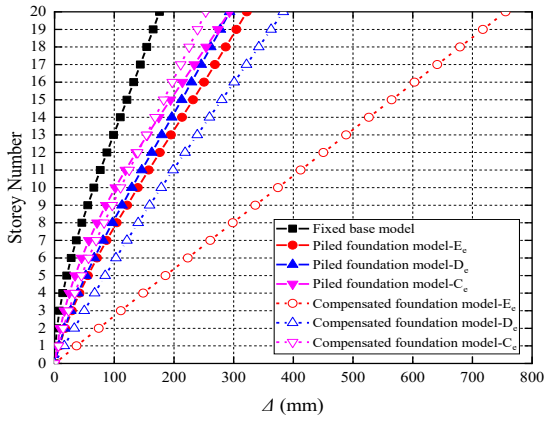

(a) El Centro

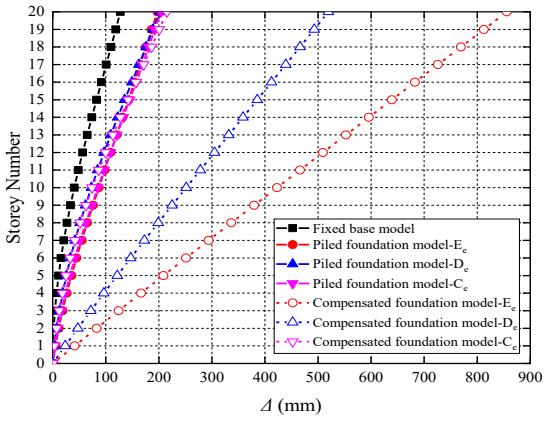

(b) Hachinohe

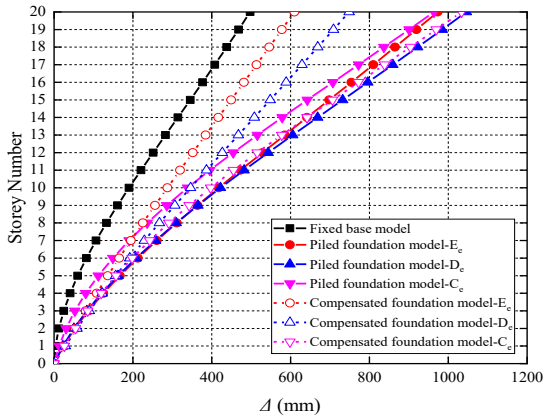

(c) Kobe

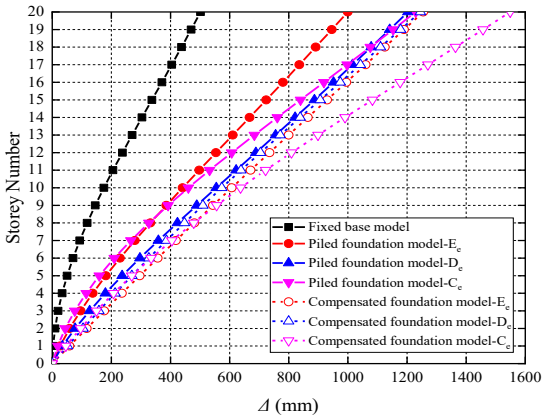

(d) Northridge

Figure 4.5 Lateral deflections of 20-storey structure (HWR=5, BD=30) under the four seismic records

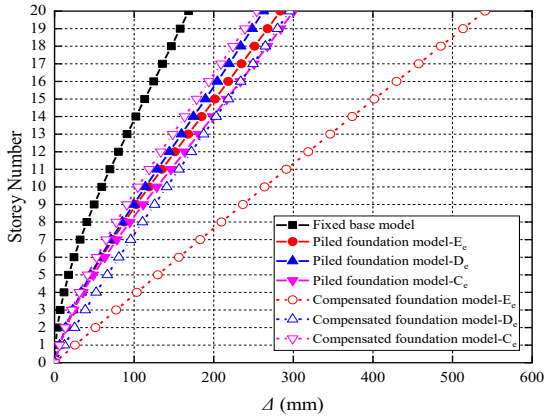

(a) El Centro

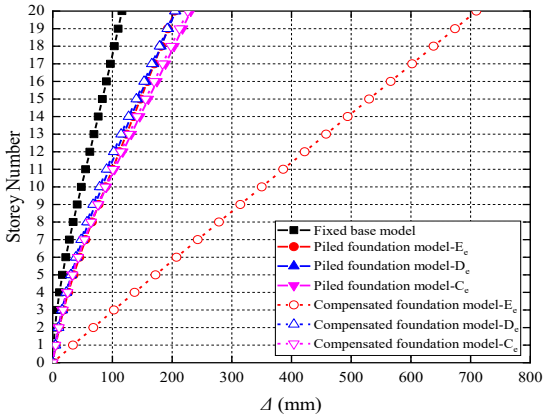

(b) Hachinohe

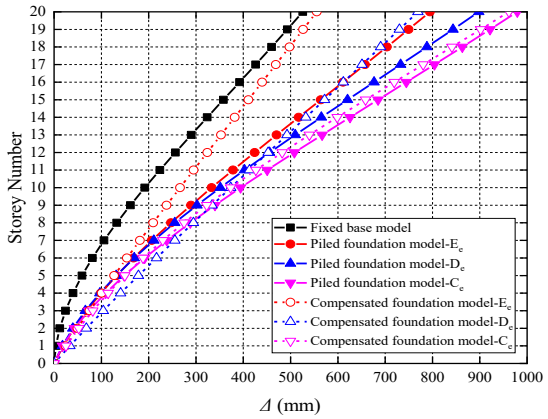

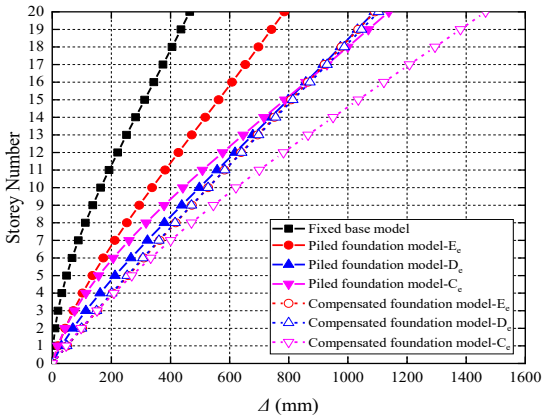

(c) Kobe (d) Northridge

Figure 4.6 Lateral deflections of 20-storey structure (HWR=4, BD=30) under the four seismic records

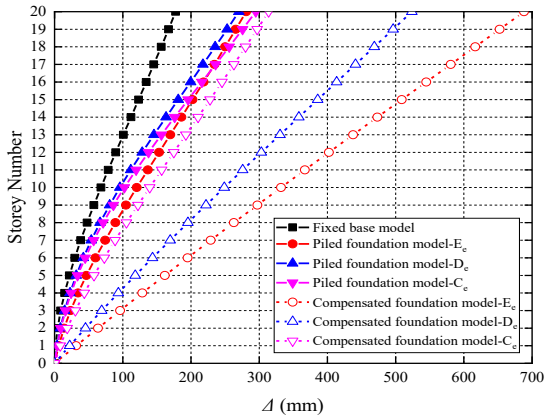

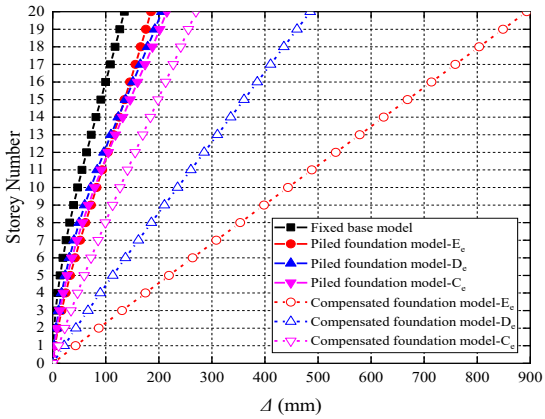

(a) El Centro (b) Hachinohe

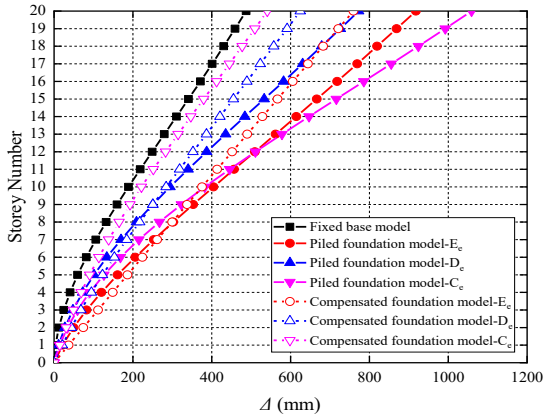

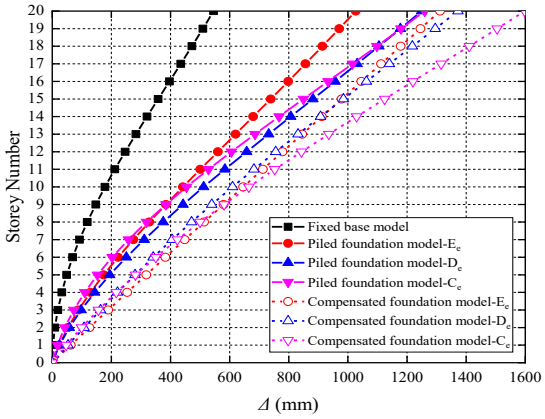

(c) Kobe (d) Northridge

Figure 4.7 Lateral deflections of 20-storey structure (HWR=6, BD=20) under the four seismic records

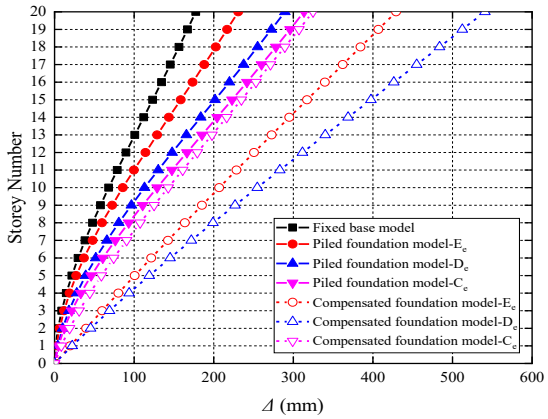

(a) El Centro

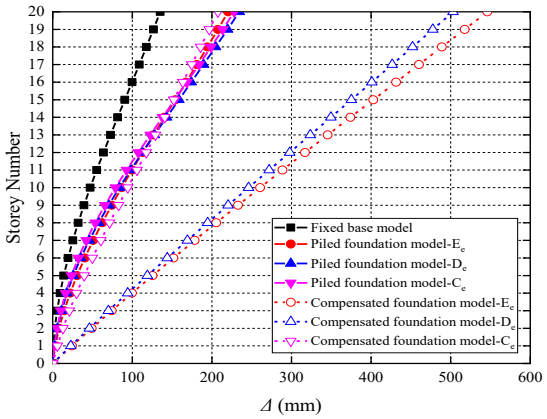

(b) Hachinohe

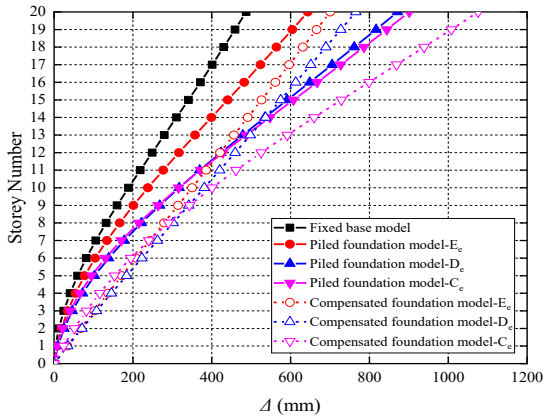

(c) Kobe

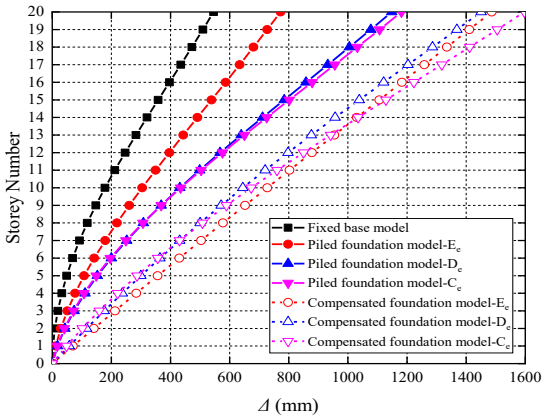

(d) Northridge

Figure 4.8 Lateral deflections of 20-storey structure (HWR=6, BD=10) under the four seismic records

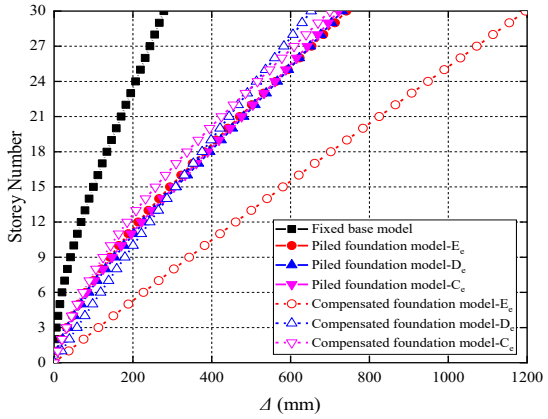

(a) El Centro

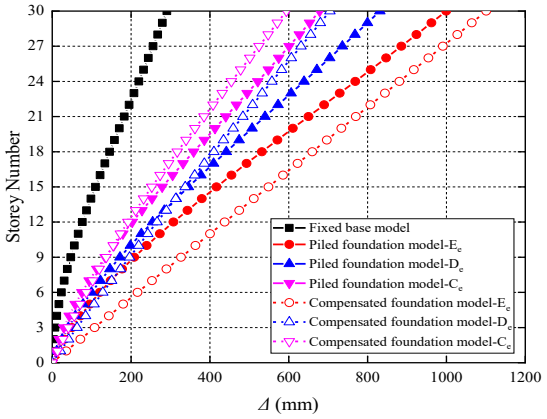

(b) Hachinohe

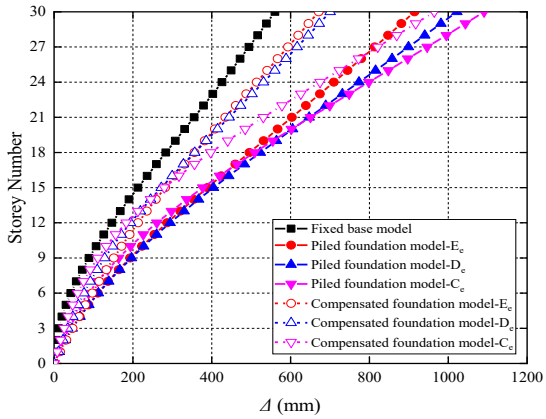

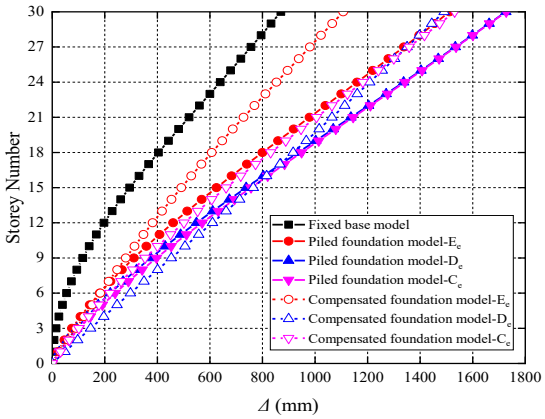

(c) Kobe (d) Northridge

Figure 4.9 Lateral deflections of 30-storey structure (HWR=6, BD=30) under the four seismic records

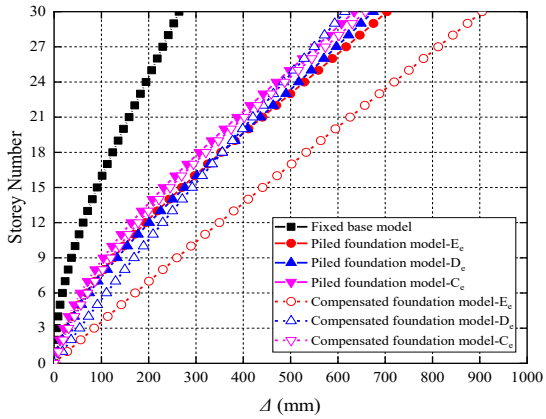

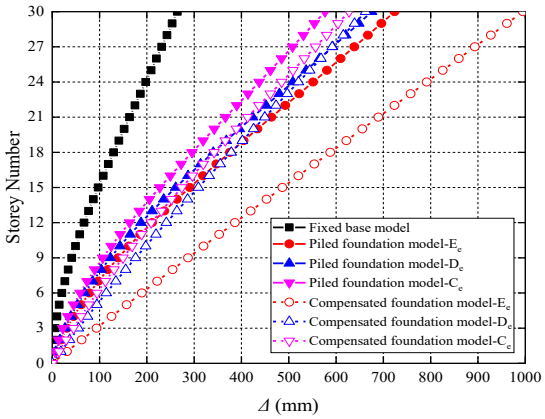

(a) El Centro (b) Hachinohe

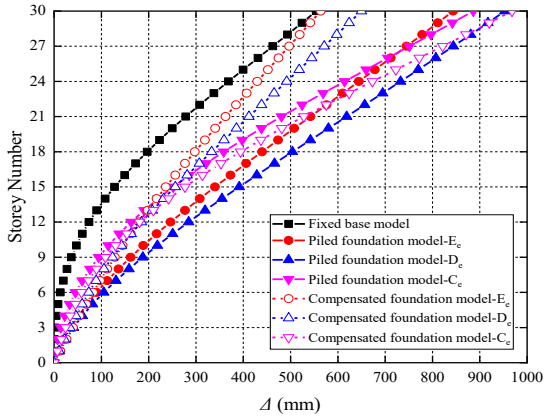

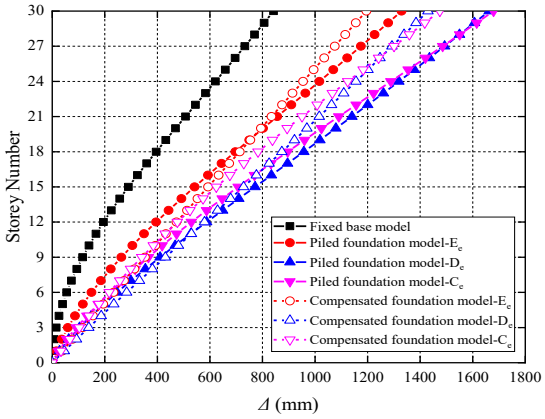

(c) Kobe (d) Northridge

Figure 4.10 Lateral deflections of 30-storey structure (HWR=5, BD=30) under the four seismic records

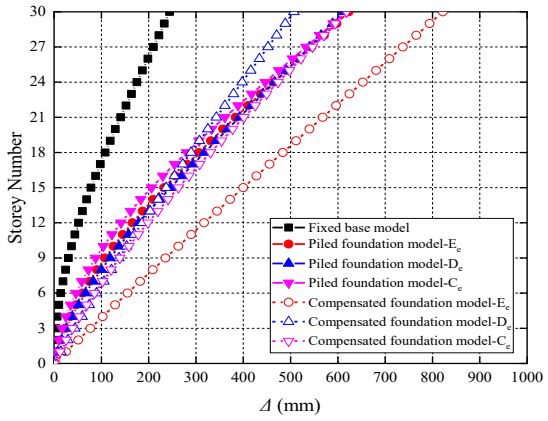

(a) El Centro

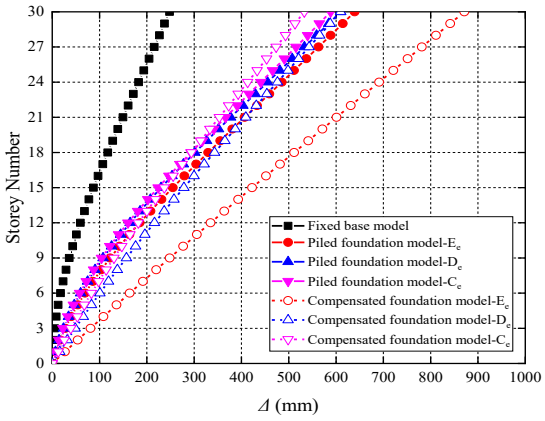

(b) Hachinohe

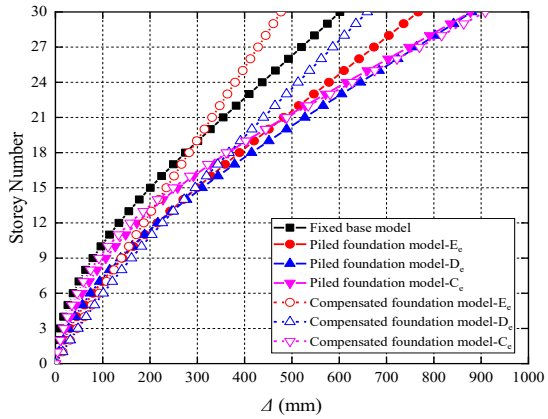

(c) Kobe

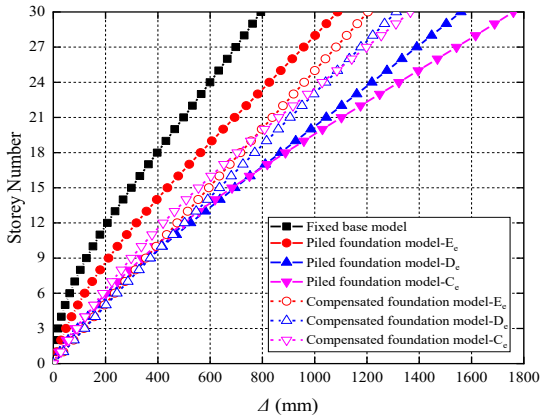

(d) Northridge

Figure 4.11 Lateral deflections of 30-storey structure (HWR=4, BD=30) under the four seismic records

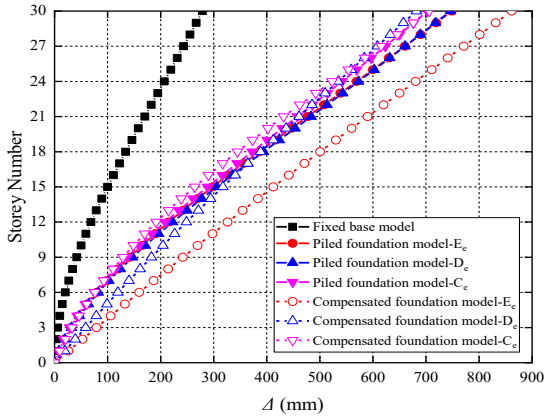

(a) El Centro

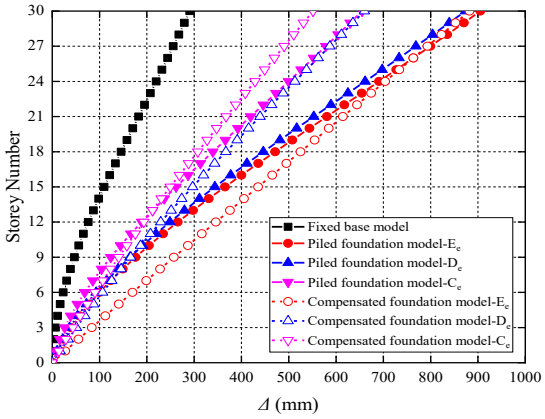

(b) Hachinohe

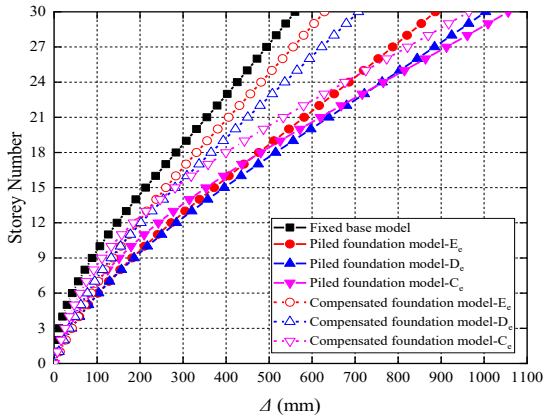

(c) Kobe

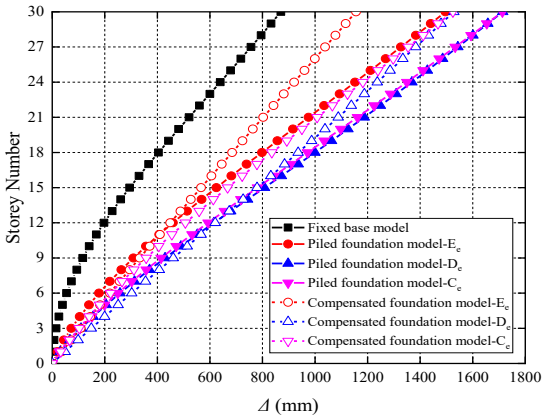

(d) Northridge

Figure 4.12 Lateral deflections of 30-storey structure (HWR=6, BD=20) under the four seismic records

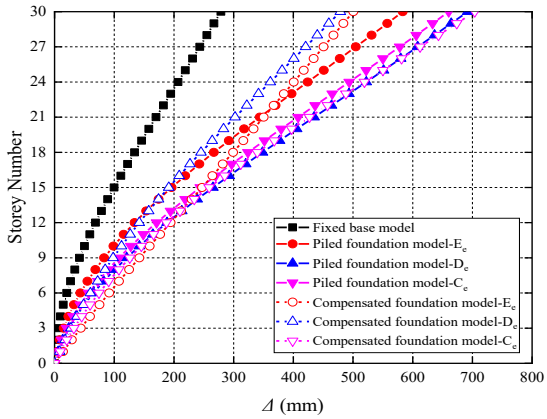

(a) El Centro

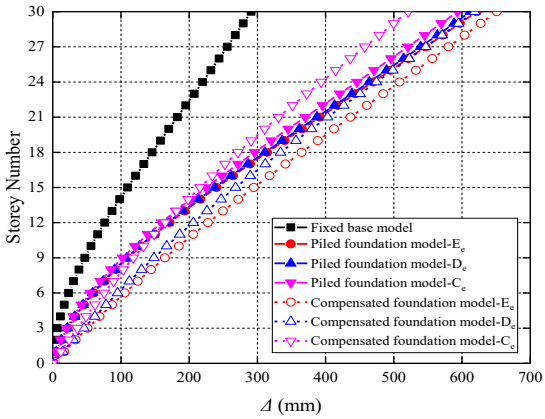

(b) Hachinohe

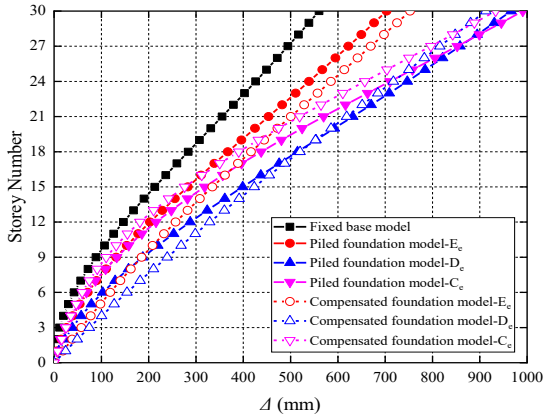

(c) Kobe

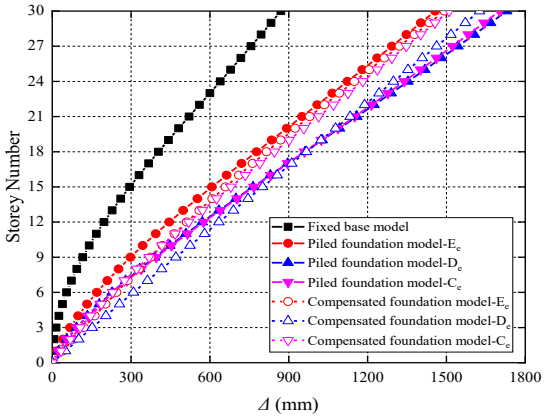

(d) Northridge

Figure 4.13 Lateral deflections of 30-storey structure (HWR=6, BD=10) under the four seismic records

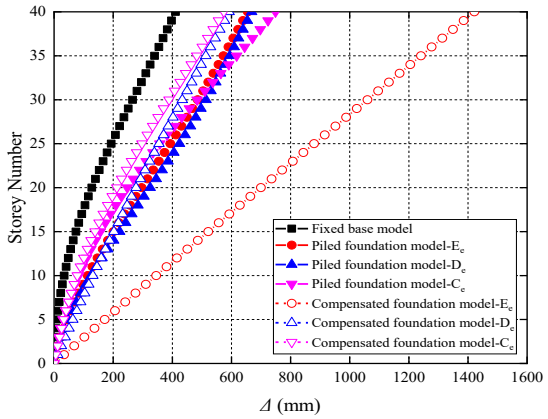

(a) El Centro

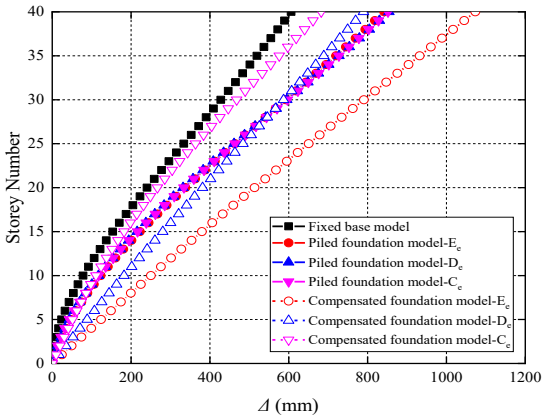

(b) Hachinohe

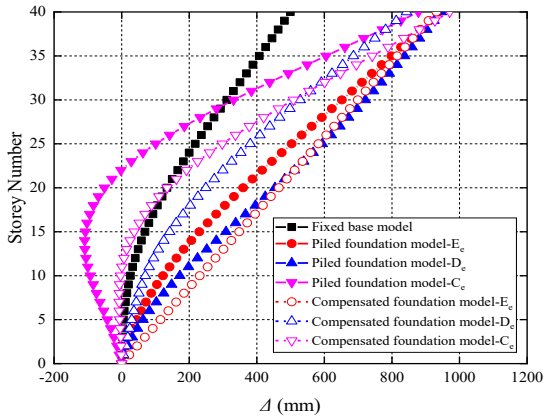

(c) Kobe

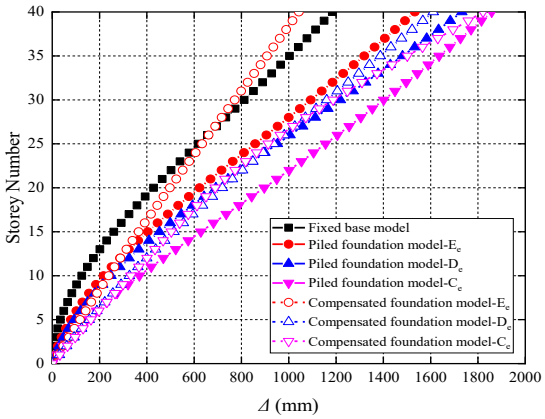

(d) Northridge

Figure 4.14 Lateral deflections of 40-storey structure (HWR=6, BD=30) under the four seismic records

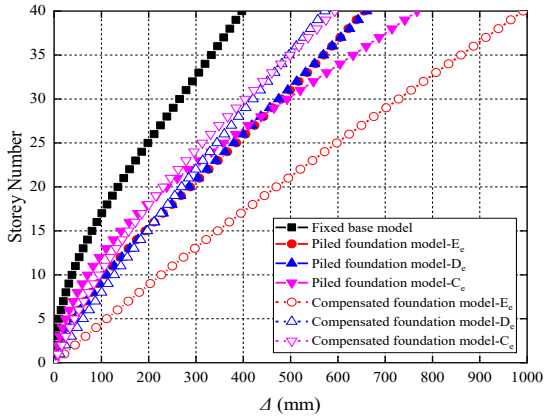

(a) El Centro

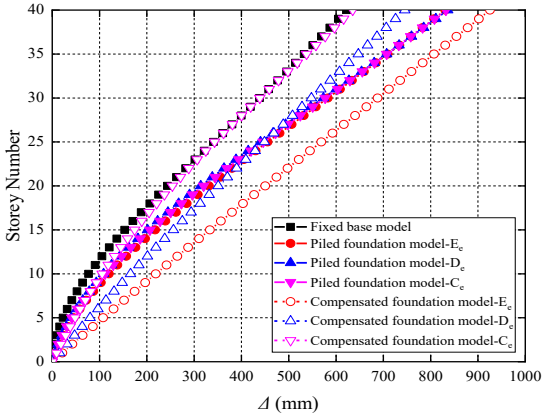

(b) Hachinohe

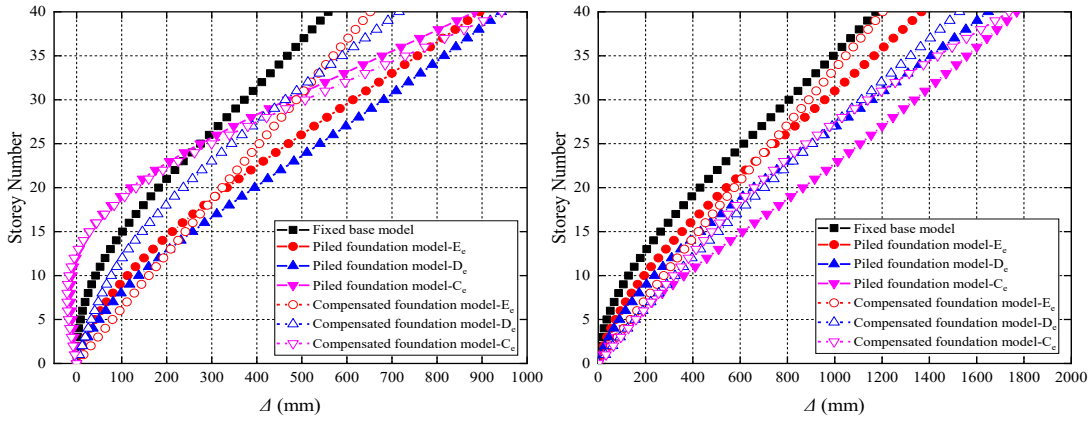

(c) Kobe (d) Northridge

Figure 4.15 Lateral deflections of 40-storey structure (HWR=5, BD=30) under the four seismic records

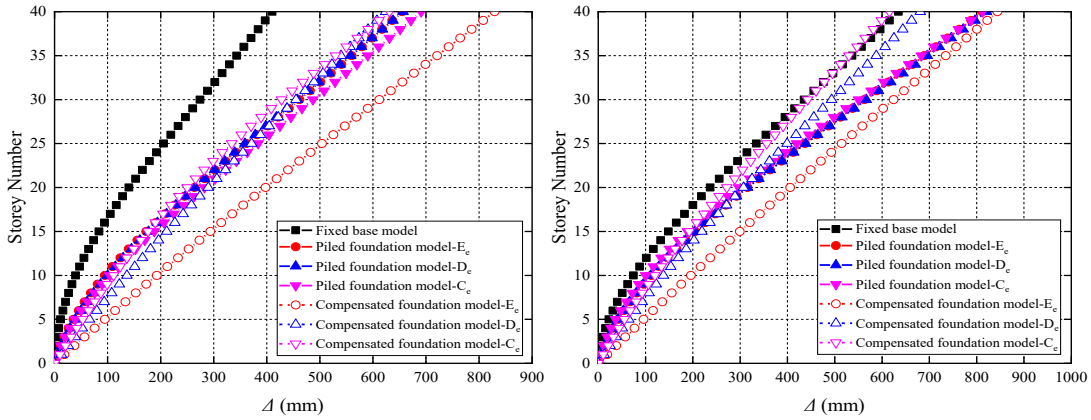

(a) El Centro (b) Hachinohe

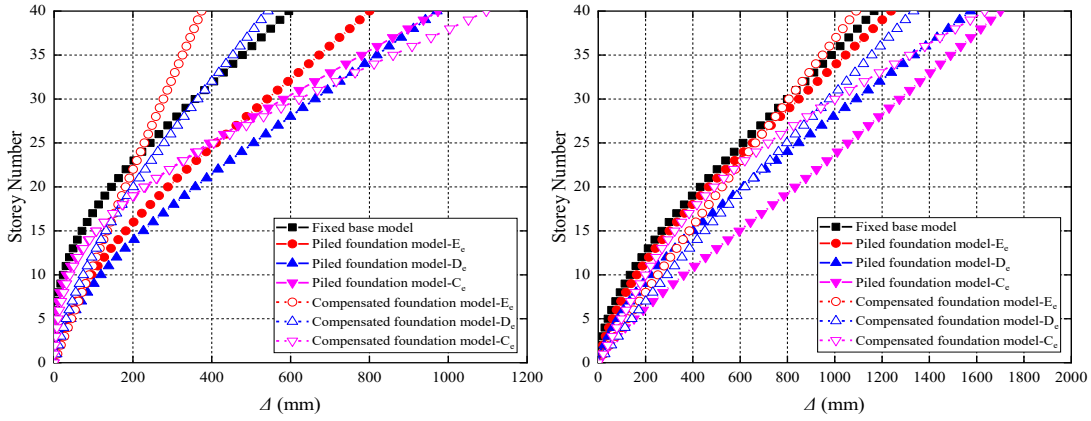

(c) Kobe (d) Northridge

Figure 4.16 Lateral deflections of 40-storey structure (HWR=4, BD=30) under the four seismic records

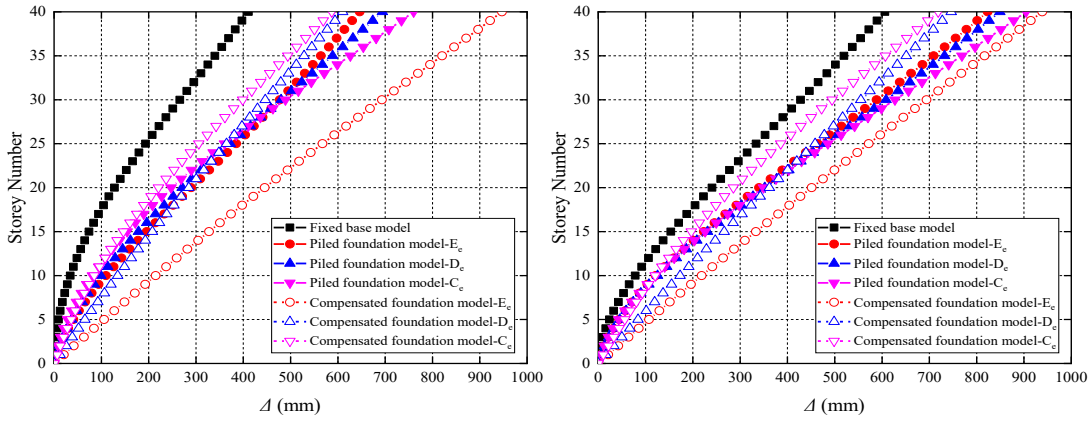

(a) El Centro (b) Hachinohe

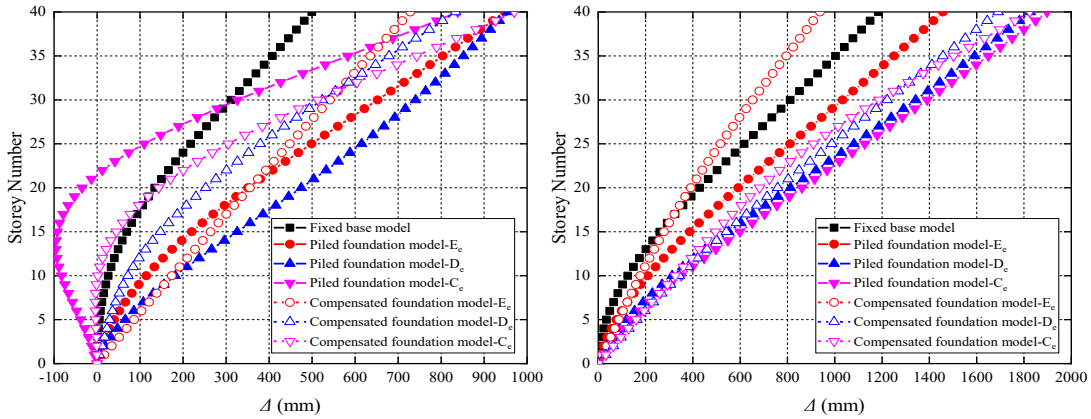

(c) Kobe (d) Northridge

Figure 4.17 Lateral deflections of 40-storey structure (HWR=6, BD=20) under the four seismic records

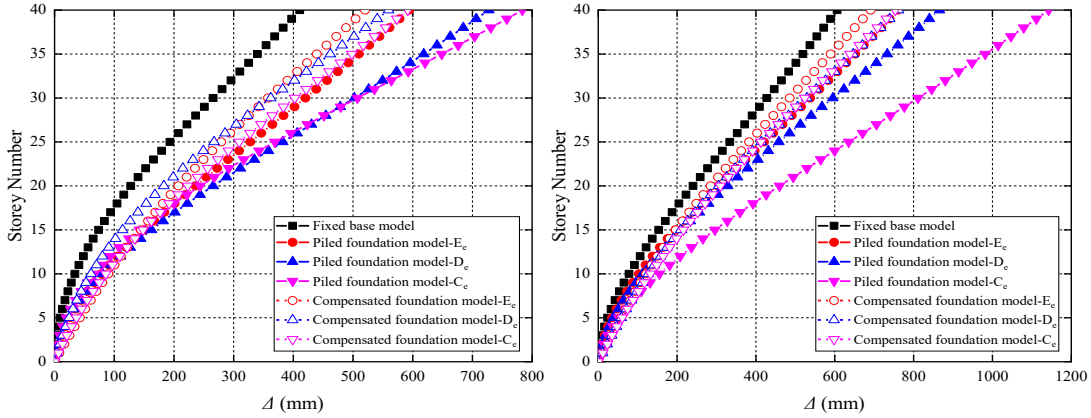

(a) El Centro (b) Hachinohe

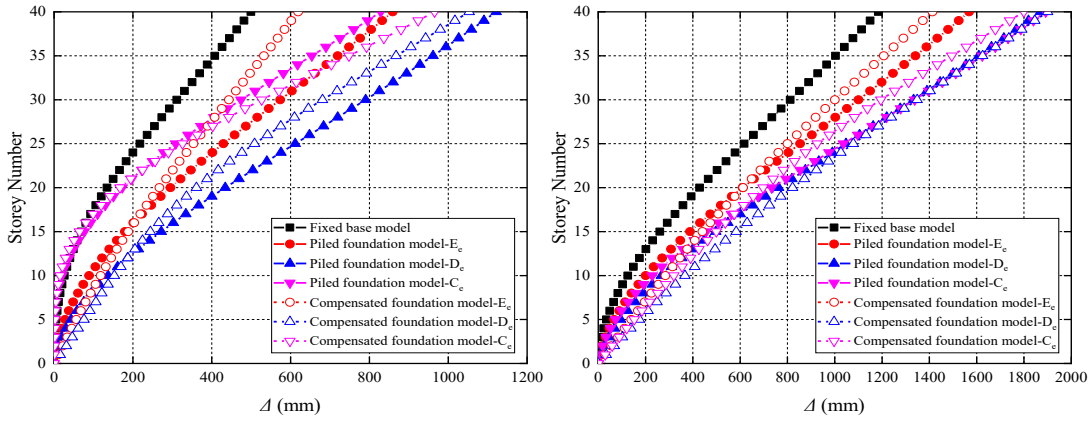

(c) Kobe (d) Northridge

Figure 4.18 Lateral deflections of 40-storey structure (HWR=6, BD=10) under the four seismic records

4.3.2 Foundation Rocking

In contrast to fixed base structures, those modelled with soil include both rocking and distortion components in their lateral deflections (Kramer 1996). Tables 4.6 to 4.11 present the proportion of foundation rocking-induced lateral deflection (Δ_θ) in the total deflection of the top floor (Δ_t) for structures with different parameters. The influence of structure width on the rotation of the structure is insignificant, whereas the soil type significantly affects the foundation rocking, especially in classical compensated foundation-supported models. Similarly, pile foundations can effectively restrain the rotation of the foundation. For classical compensated foundation structures founded on E_e soils, the Δ_θ accounts for more than 90% of the total displacement on average, indicating a greater likelihood of overall building rotation. In contrast, this proportion in piled foundation models is typically less than 30%. Moreover, the effects of BD are negligible for classical compensated foundation-supported models; however, for piled foundation models, this proportion decreases considerably with decreasing BD. This reduction in pile length leads to a dramatic increase in the stiffness of the piles.

However, according to the findings presented in section 4.2.1, while end-bearing piled foundations may effectively mitigate foundation rocking, it is not necessarily the case

that the Δ exhibited by piled foundation structures will be smaller than those observed in classical compensated foundation structures.

Table 4.6 The proportion of lateral deflection caused by foundation rocking (Δ_θ/Δ_t) of 20-storey structures with different HWRs (%)

HWR	Earthquake record	Piled foundation model			Compensated foundation model		
		E_e soil	D_e soil	C_e soil	E_e soil	D_e soil	C_e soil
6	El Centro	29.29	26.73	13.16	94.85	82.18	31.50
	Hachinohe	30.97	27.62	15.77	96.06	85.98	14.74
	Kobe	28.04	24.59	12.19	81.30	45.90	42.63
	Northridge	28.90	24.42	10.60	95.83	81.16	47.21
5	El Centro	28.43	26.83	10.17	97.62	83.44	33.13
	Hachinohe	29.65	21.35	13.94	94.67	86.87	18.33
	Kobe	28.29	24.49	11.53	87.74	76.21	46.59
	Northridge	30.79	24.35	10.27	92.52	83.22	52.63
4	El Centro	24.78	23.79	13.51	94.57	77.76	29.00
	Hachinohe	25.47	23.37	10.51	92.99	34.69	28.96
	Kobe	26.95	22.19	12.25	89.52	85.45	49.06
	Northridge	28.41	21.78	10.58	92.30	88.93	59.07

Table 4.7 The proportion of lateral deflection caused by foundation rocking (Δ_θ/Δ_t) of 20-storey structures with different BDs (%)

BD	Earthquake record	Piled foundation model			Compensated foundation model		
		E_e soil	D_e soil	C_e soil	E_e soil	D_e soil	C_e soil
30	El Centro	29.29	26.73	13.16	94.85	82.18	31.50
	Hachinohe	30.97	27.62	15.77	96.06	85.98	14.74
	Kobe	28.04	24.59	12.19	81.30	45.90	42.63
	Northridge	28.90	24.42	10.60	95.83	81.16	47.21
20	El Centro	15.72	11.81	7.45	92.12	82.53	30.97
	Hachinohe	16.11	13.73	9.61	95.23	84.49	60.62
	Kobe	16.45	13.32	9.25	97.68	69.01	42.71
	Northridge	14.66	14.18	7.47	95.21	79.00	47.89
10	El Centro	5.97	3.92	3.37	90.55	79.91	31.11
	Hachinohe	6.35	3.33	3.10	87.07	85.40	32.11
	Kobe	6.60	3.28	2.98	94.74	87.09	41.02
	Northridge	5.68	2.89	2.33	93.76	80.68	48.63

Table 4.8 The proportion of lateral deflection caused by foundation rocking (Δ_θ/Δ_t) of 30-storey structures with different HWRs (%)

HWR	Earthquake record	Piled foundation model			Compensated foundation model		
		E_e soil	D_e soil	C_e soil	E_e soil	D_e soil	C_e soil
6	El Centro	22.18	23.05	12.68	93.66	87.91	32.03
	Hachinohe	24.60	23.23	12.51	96.36	85.64	64.57
	Kobe	24.08	22.65	12.08	74.36	57.21	32.25
	Northridge	26.08	24.71	12.65	84.72	94.51	57.75
5	El Centro	17.09	17.63	9.35	92.01	85.52	34.03
	Hachinohe	18.46	17.03	10.84	92.07	78.83	64.75
	Kobe	17.42	18.26	9.40	73.31	58.93	30.58
	Northridge	17.73	15.95	7.47	97.14	93.88	63.68
4	El Centro	16.77	18.03	7.92	91.49	83.94	47.07
	Hachinohe	18.84	16.83	15.98	90.29	73.60	64.77
	Kobe	17.65	14.54	4.50	96.84	72.44	20.77
	Northridge	18.29	15.69	5.92	96.67	89.11	63.27

Table 4.9 The proportion of lateral deflection caused by foundation rocking (Δ_θ/Δ_t) of 30-storey structures with different BDs (%)

BD	Earthquake record	Piled foundation model			Compensated foundation model		
		E_e soil	D_e soil	C_e soil	E_e soil	D_e soil	C_e soil
30	El Centro	22.18	23.05	12.68	93.66	87.91	32.03
	Hachinohe	24.60	23.23	12.51	96.36	85.64	64.57
	Kobe	24.08	22.65	12.08	74.36	57.21	32.25
	Northridge	26.08	24.71	12.65	84.72	94.51	57.75
20	El Centro	26.65	22.55	10.23	90.48	75.93	32.71
	Hachinohe	27.60	22.46	10.07	92.22	66.99	73.46
	Kobe	27.69	20.97	9.74	70.41	52.06	31.87
	Northridge	23.66	22.42	10.92	93.93	89.16	58.60
10	El Centro	9.02	7.83	5.01	84.83	54.60	33.33
	Hachinohe	10.38	7.92	5.93	76.90	70.74	64.64
	Kobe	17.64	7.24	5.88	77.27	76.51	31.86
	Northridge	17.76	8.61	9.04	82.29	79.35	60.11

Table 4.10 The proportion of lateral deflection caused by foundation rocking (Δ_θ/Δ_t) of 40-storey structures with different HWRs (%)

HWR	Earthquake record	Piled foundation model			Compensated foundation model		
		E_e soil	D_e soil	C_e soil	E_e soil	D_e soil	C_e soil
6	El Centro	18.94	19.60	9.09	95.27	81.73	37.20
	Hachinohe	16.80	15.88	15.63	92.36	85.32	61.86
	Kobe	14.14	16.45	4.23	98.08	49.88	15.18
	Northridge	14.65	15.33	13.39	91.59	77.78	64.56
5	El Centro	17.58	18.44	7.51	88.35	77.43	50.23
	Hachinohe	16.12	14.83	14.75	90.26	80.03	60.37
	Kobe	13.63	14.28	7.33	98.19	55.67	41.26
	Northridge	15.65	14.32	12.44	90.86	80.92	66.97
4	El Centro	13.57	14.64	9.02	89.03	79.13	63.17
	Hachinohe	13.26	12.85	11.87	87.74	67.26	61.39
	Kobe	11.31	11.19	3.38	94.30	58.43	15.65
	Northridge	12.47	10.67	10.41	91.00	84.90	43.69

Table 4.11 The proportion of lateral deflection caused by foundation rocking (Δ_θ/Δ_t) of 40-storey structures with different BDs (%)

BD	Earthquake record	Piled foundation model			Compensated foundation model		
		E_e soil	D_e soil	C_e soil	E_e soil	D_e soil	C_e soil
30	El Centro	18.94	19.60	9.09	95.27	81.73	37.20
	Hachinohe	16.80	15.88	15.63	92.36	85.32	61.86
	Kobe	14.14	16.45	4.23	98.08	49.88	15.18
	Northridge	14.65	15.33	13.39	91.59	77.78	64.56
20	El Centro	17.75	11.01	9.27	88.68	71.15	37.30
	Hachinohe	16.56	12.32	9.92	86.30	75.12	62.79
	Kobe	14.03	12.54	4.13	56.38	49.26	16.61
	Northridge	13.26	11.64	12.68	78.69	73.87	63.26
10	El Centro	5.76	3.88	2.78	67.39	39.97	38.14
	Hachinohe	5.56	4.46	2.85	66.77	62.34	61.67
	Kobe	6.08	4.27	2.62	78.08	66.95	20.11
	Northridge	3.80	3.39	2.55	81.52	72.90	59.07

4.3.3 Inter-storey Drifts

Figures 4.19 to 4.33 depict the inter-storey drifts of frame-core tube structures ranging from 20 to 40 storeys, with varying HWRs, foundation types, soil types, and BDs, for

both fixed base and flexible base conditions. The inter-storey drifts were determined by utilising the methodology prescribed in AS1170-4 (2007). The analysis revealed that the majority of flexible base cases exhibited an increase in the inter-storey drifts, with the maximum values exceeding 1.5% for several far-field and many near-field earthquake cases. This indicates that the performance levels shifted from life safe to near-collapse or collapse levels after considering SSI effects, as outlined in BSSC (1997).

In addition, for classical compensated foundation models, the inter-storey drifts generally exhibited an almost vertical line, signifying that the inter-storey drifts remain relatively constant with increasing structural height. This suggests that the lateral deflection induced by foundation rotation accounts for a significant portion of the total deflection observed in classical compensated foundation models. Furthermore, the inter-storey drifts of piled structures with identical height, HWR, and seismic record demonstrated no significant variance with respect to soil type, in contrast to classical compensated foundation cases. Notably, a substantial increase in inter-storey drift was observed for structures supported by C_e soil during near-field earthquakes and for structures with compensated foundations on E_e soil during far-field earthquakes. This is attributed to differences in the response spectra shapes between near and far earthquakes.

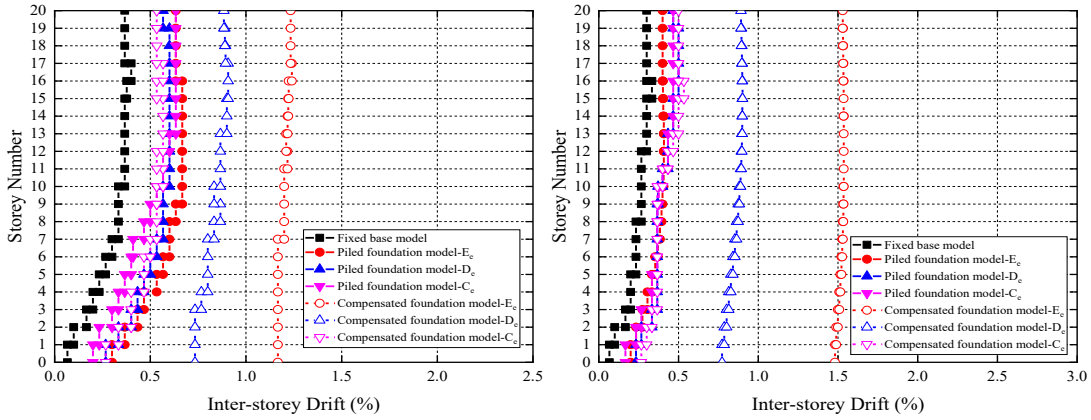

(a) El Centro (b) Hachinohe

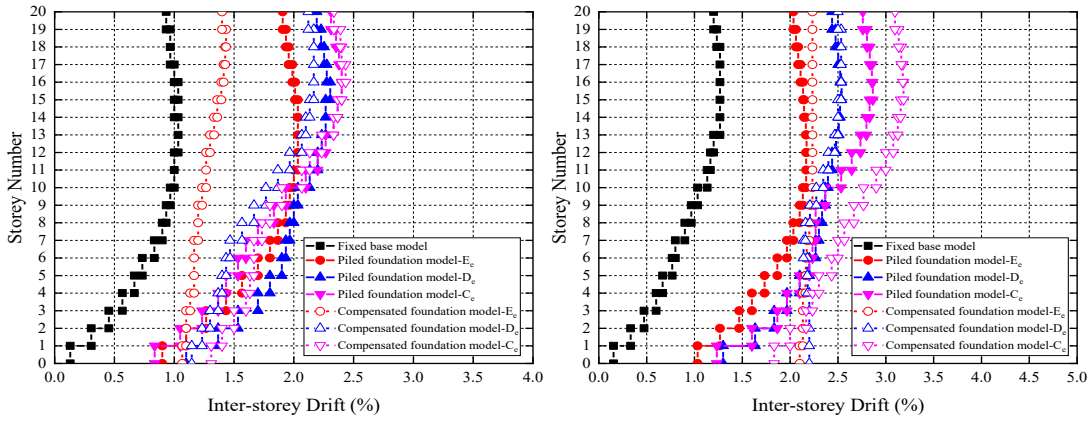

(c) Kobe (d) Northridge

Figure 4.19 Inter-storey drifts of 20-storey structure (HWR=6, BD=30) under the four seismic records

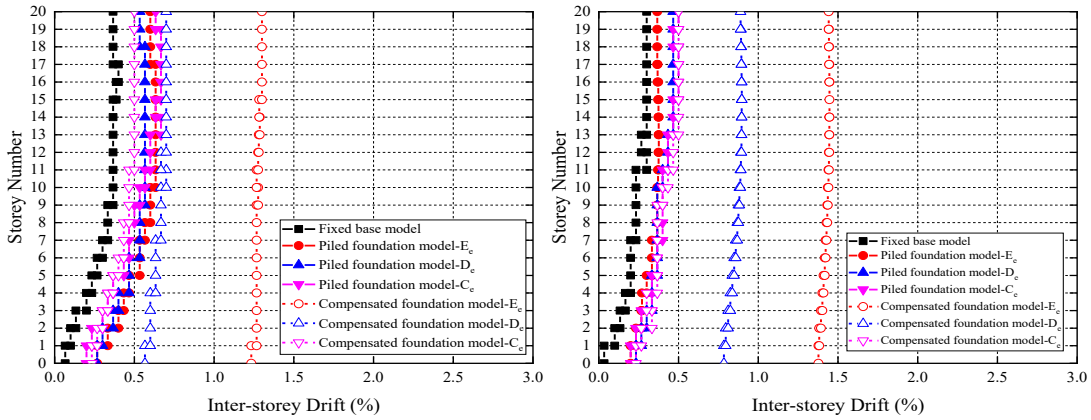

(a) El Centro (b) Hachinohe

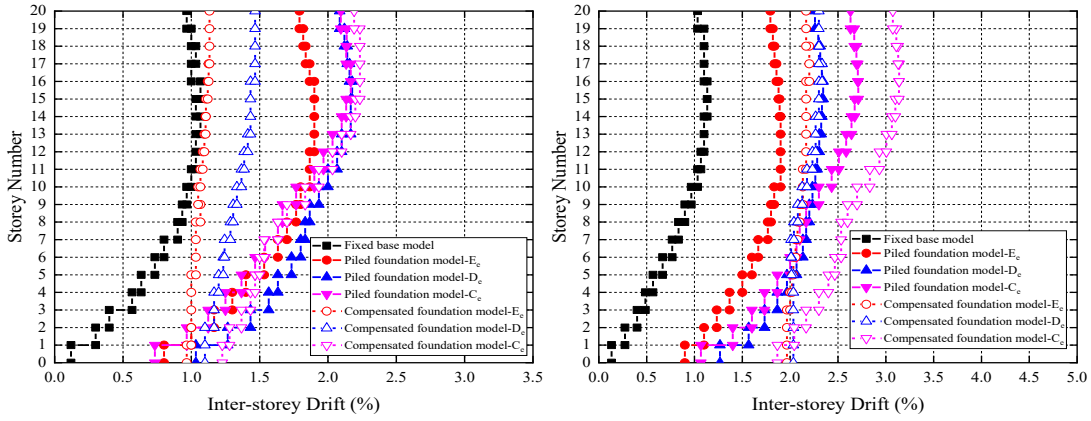

(c) Kobe (d) Northridge

Figure 4.20 Inter-storey drifts of 20-storey structure (HWR=5, BD=30) under the four seismic records

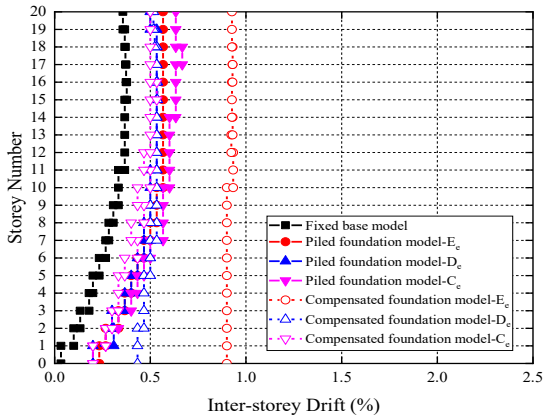

(a) El Centro

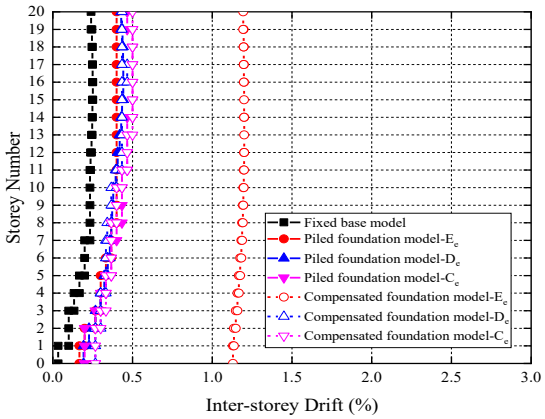

(b) Hachinohe

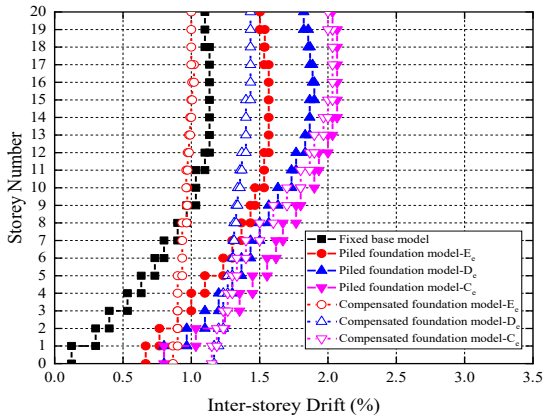

(c) Kobe

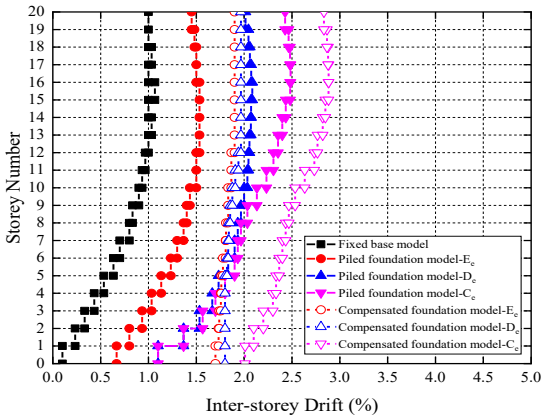

(d) Northridge

Figure 4.21 Inter-storey drifts of 20-storey structure (HWR=4, BD=30) under the four seismic records

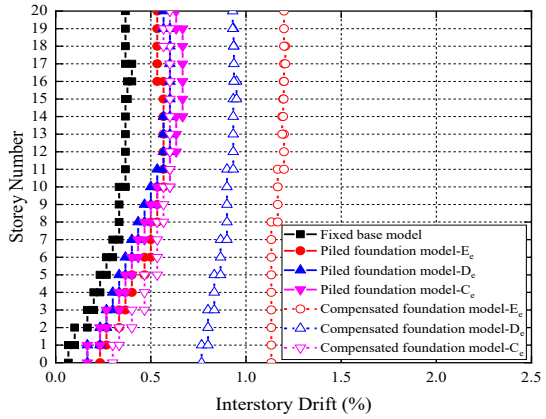

(a) El Centro

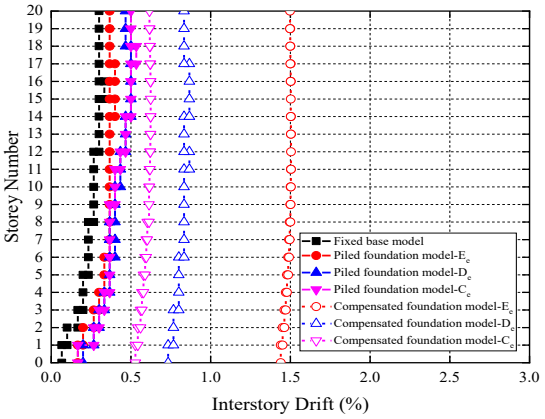

(b) Hachinohe

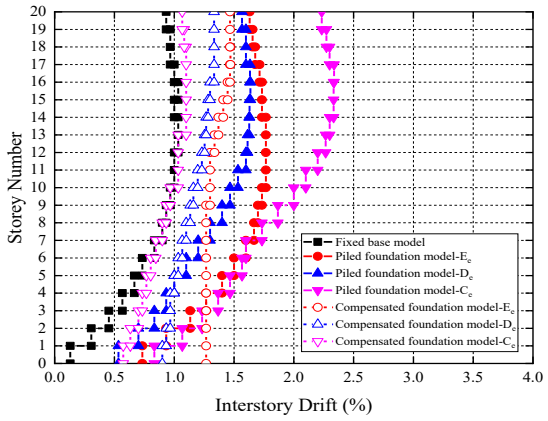

(c) Kobe

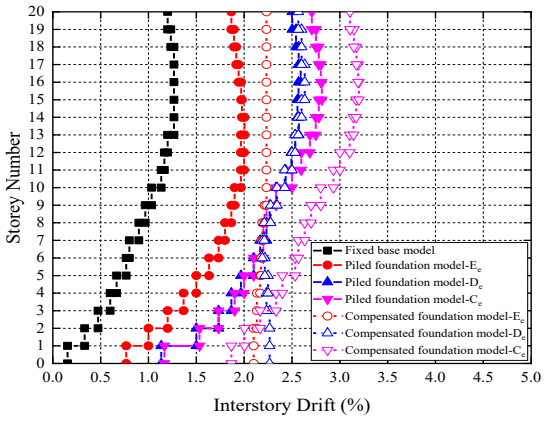

(d) Northridge

Figure 4.22 Inter-storey drifts of 20-storey structure (HWR=6, BD=20) under the four seismic records

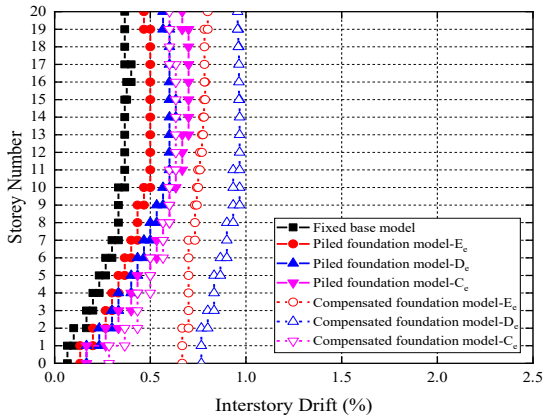

(a) El Centro

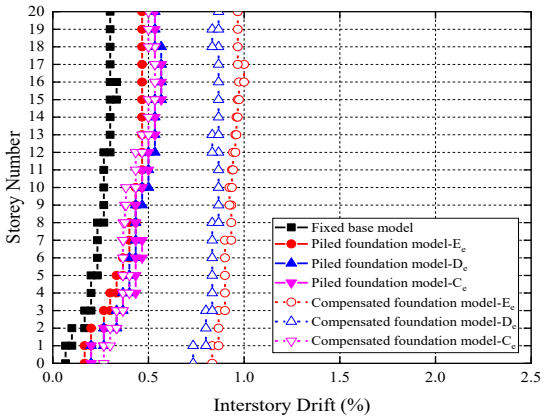

(b) Hachinohe

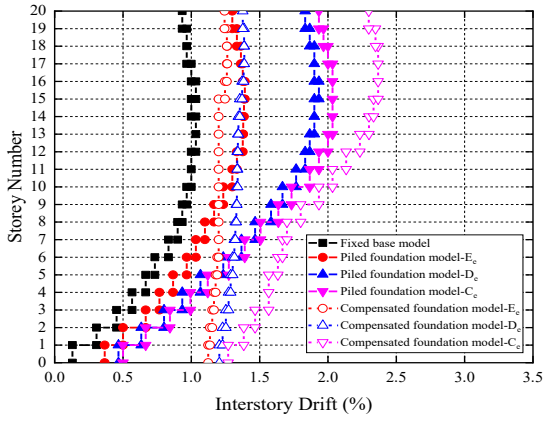

(c) Kobe

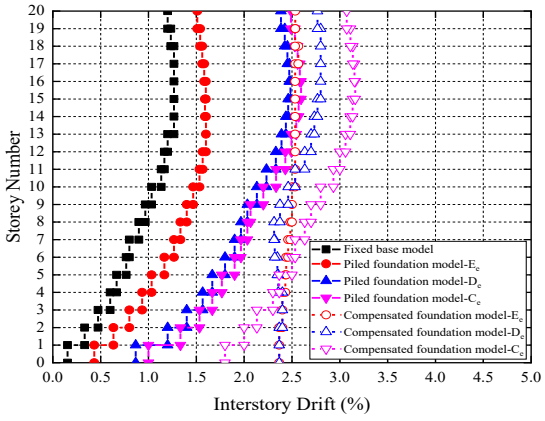

(d) Northridge

Figure 4.23 Inter-storey drifts of 20-storey structure (HWR=6, BD=10) under the four seismic records

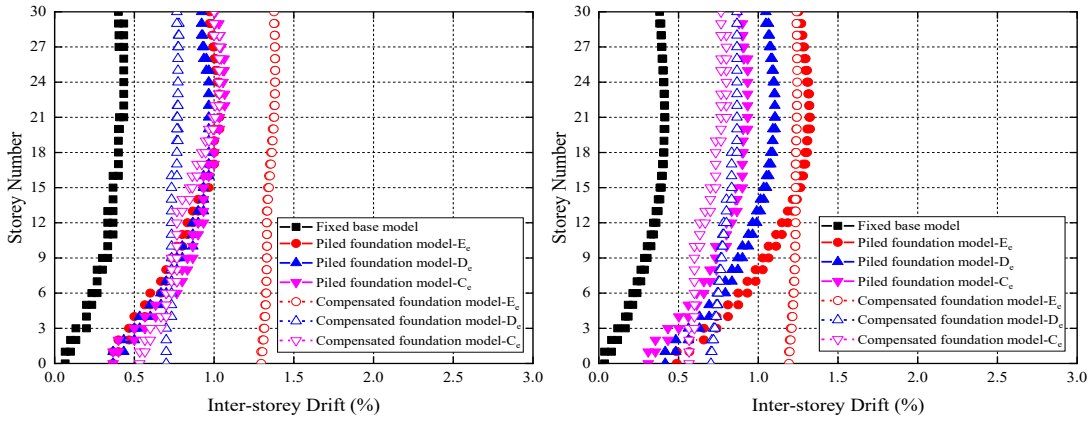

(a) El Centro (b) Hachinohe

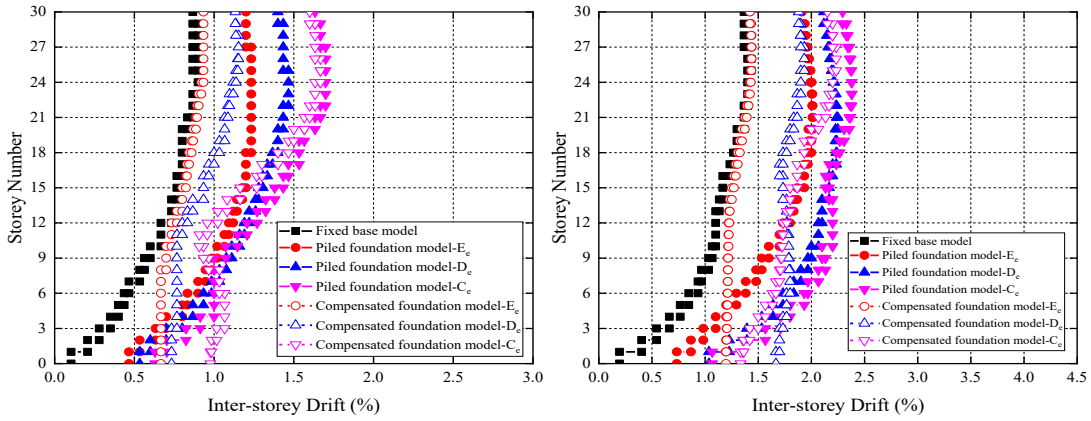

(c) Kobe (d) Northridge

Figure 4.24 Inter-storey drifts of 30-storey structure (HWR=6, BD=30) under the four seismic records

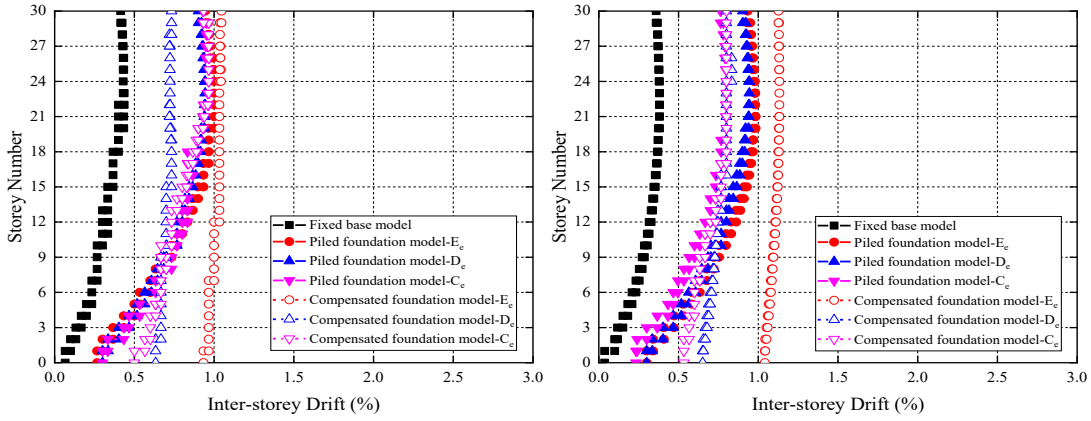

(a) El Centro (b) Hachinohe

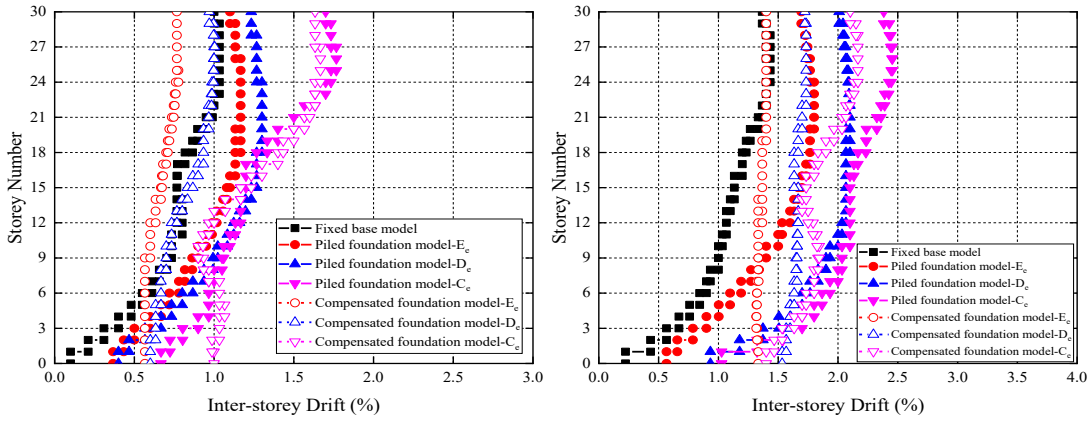

(c) Kobe (d) Northridge

Figure 4.25 Inter-storey drifts of 30-storey structure (HWR=5, BD=30) under the four seismic records

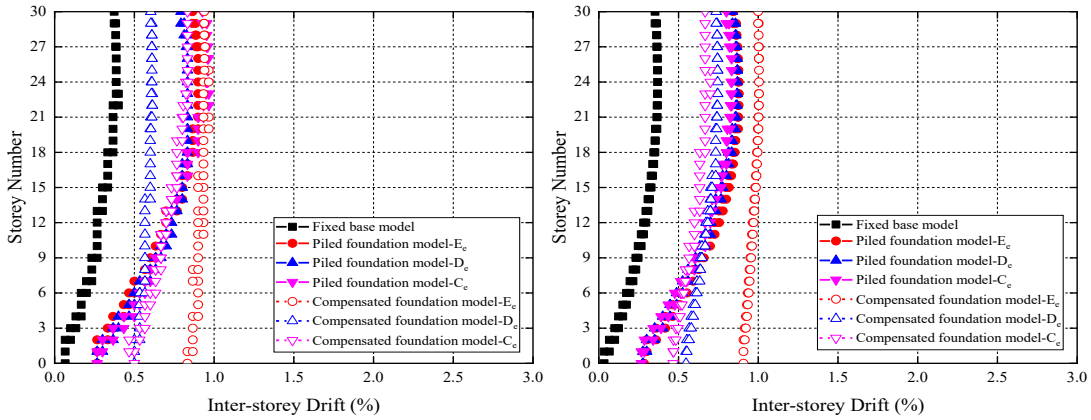

(a) El Centro (b) Hachinohe

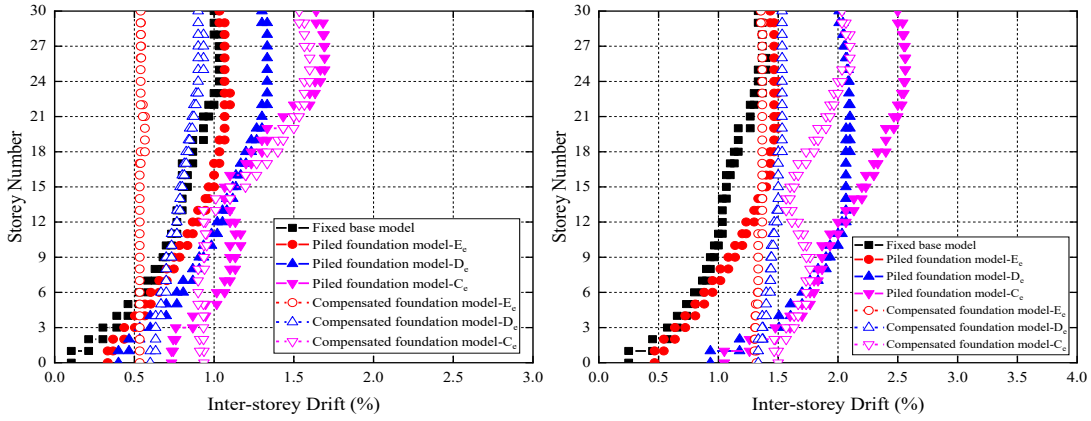

(c) Kobe (d) Northridge

Figure 4.26 Inter-storey drifts of 30-storey structure (HWR=4, BD=30) under the four seismic records

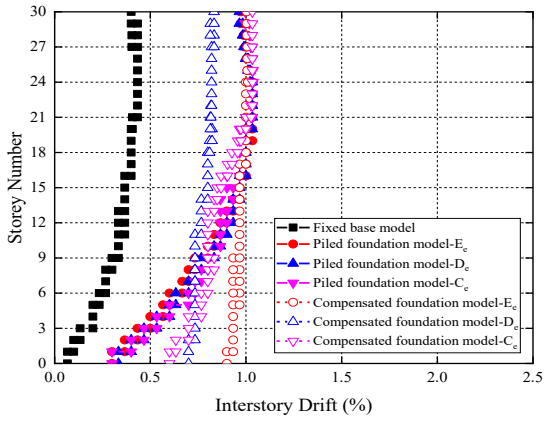

(a) El Centro

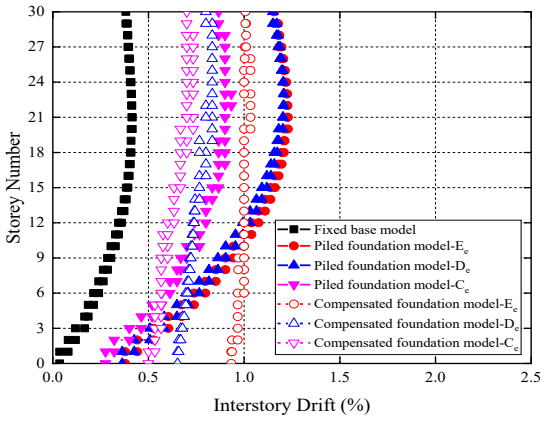

(b) Hachinohe

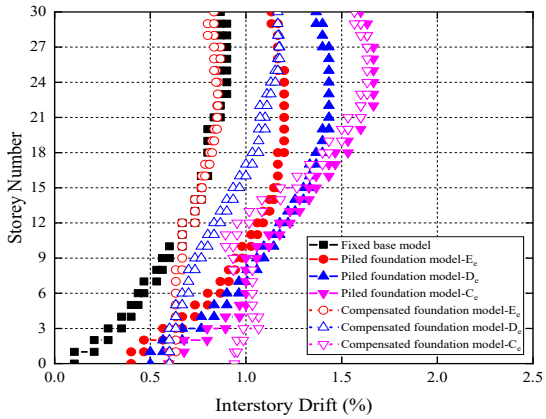

(c) Kobe

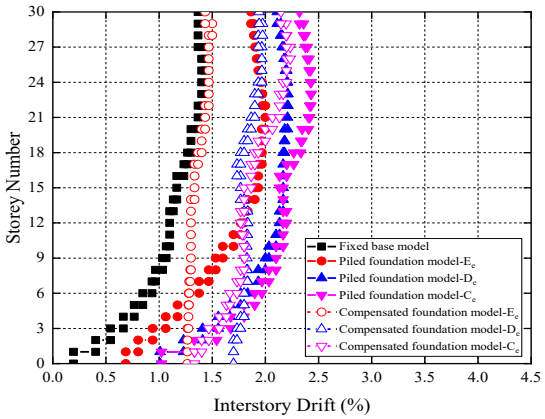

(d) Northridge

Figure 4.27 Inter-storey drifts of 30-storey structure (HWR=6, BD=20) under the four seismic records

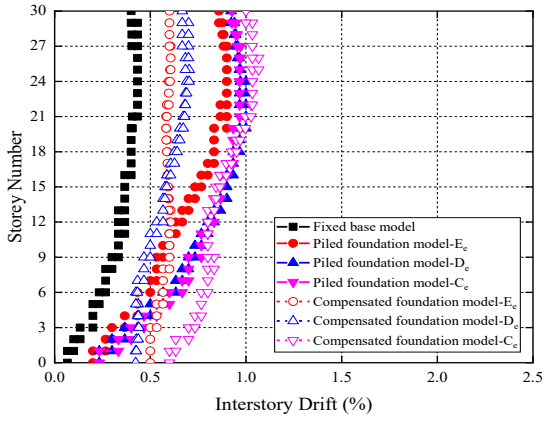

(a) El Centro

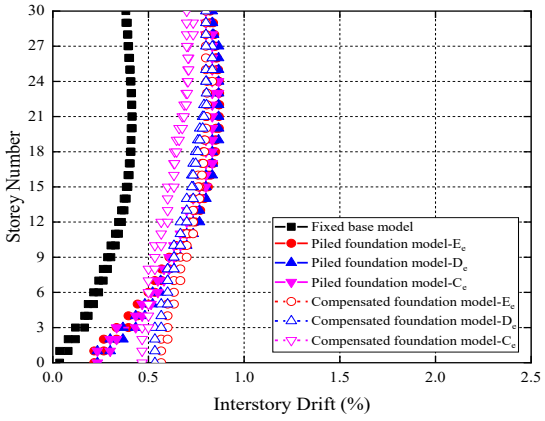

(b) Hachinohe

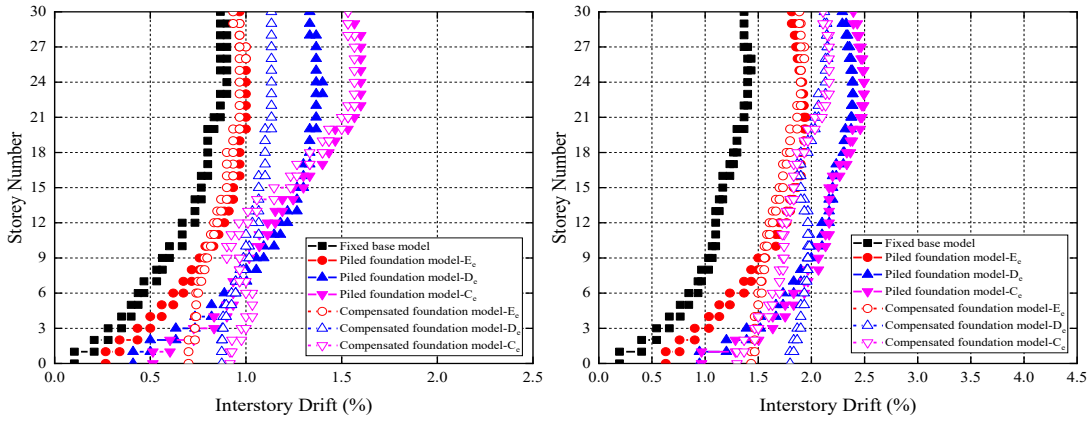

(c) Kobe (d) Northridge

Figure 4.28 Inter-storey drifts of 30-storey structure (HWR=6, BD=10) under the four seismic records

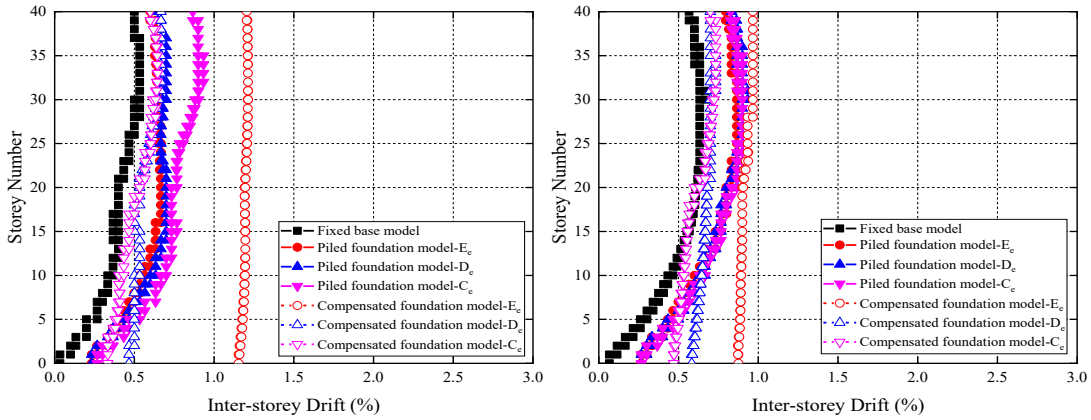

(a) El Centro (b) Hachinohe

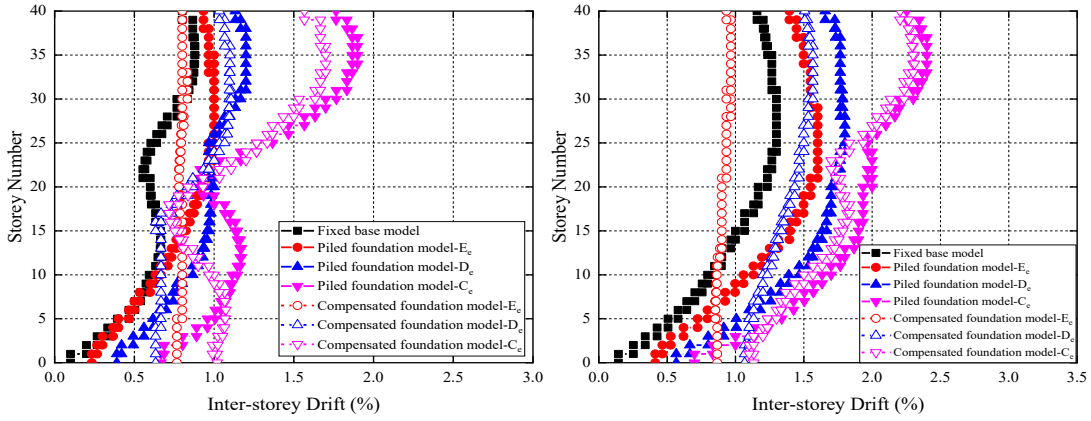

(c) Kobe (d) Northridge

Figure 4.29 Inter-storey drifts of 40-storey structure (HWR=6, BD=30) under the four seismic records

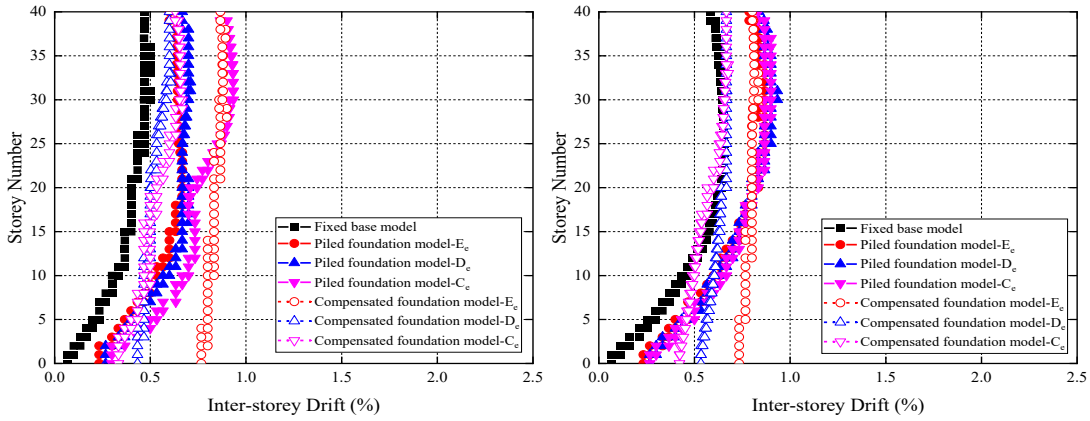

(a) El Centro (b) Hachinohe

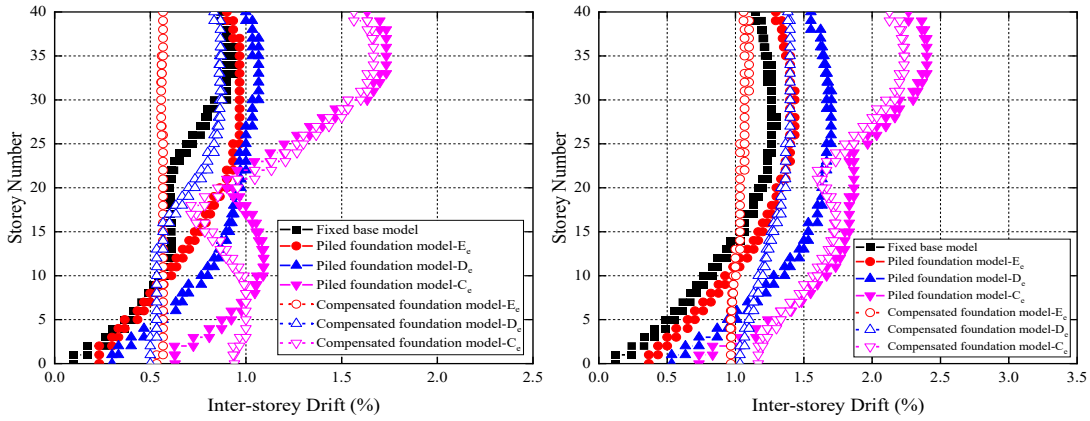

(c) Kobe (d) Northridge

Figure 4.30 Inter-storey drifts of 40-storey structure (HWR=5, BD=30) under the four seismic records

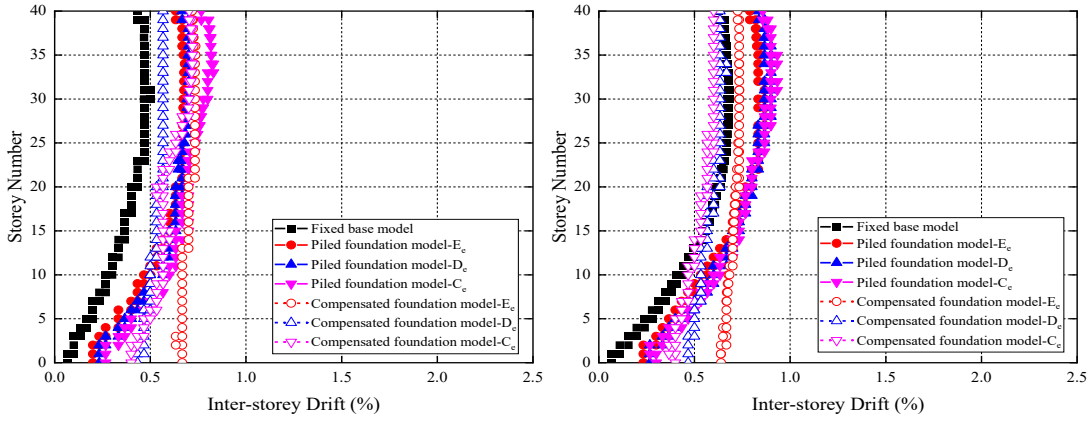

(a) El Centro (b) Hachinohe

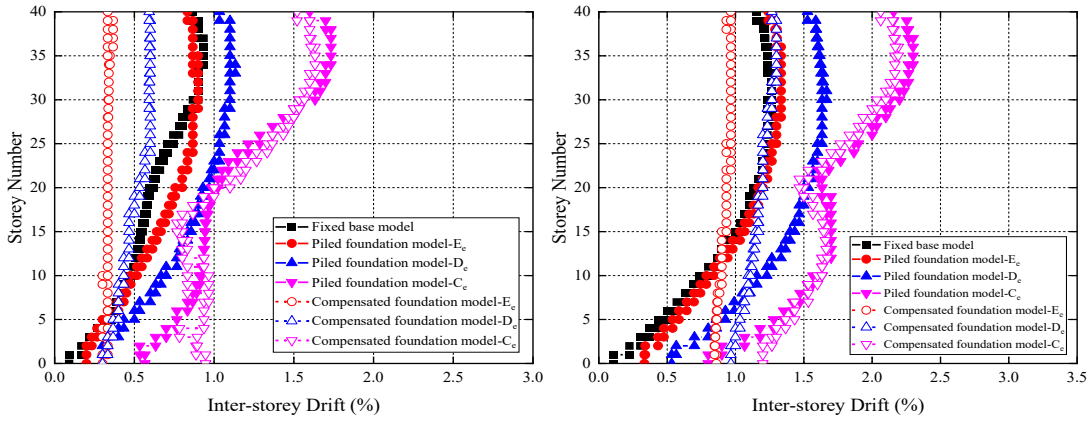

(c) Kobe (d) Northridge

Figure 4.31 Inter-storey drifts of 40-storey structure (HWR=4, BD=30) under the four seismic records

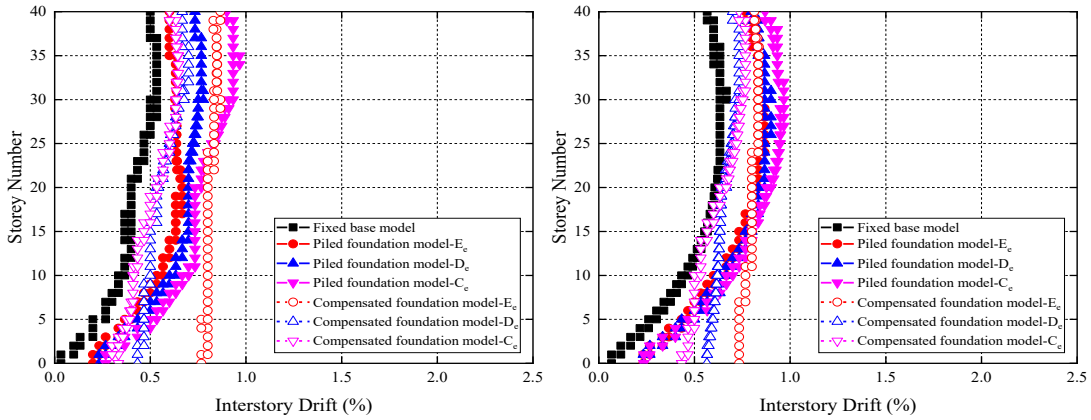

(a) El Centro (b) Hachinohe

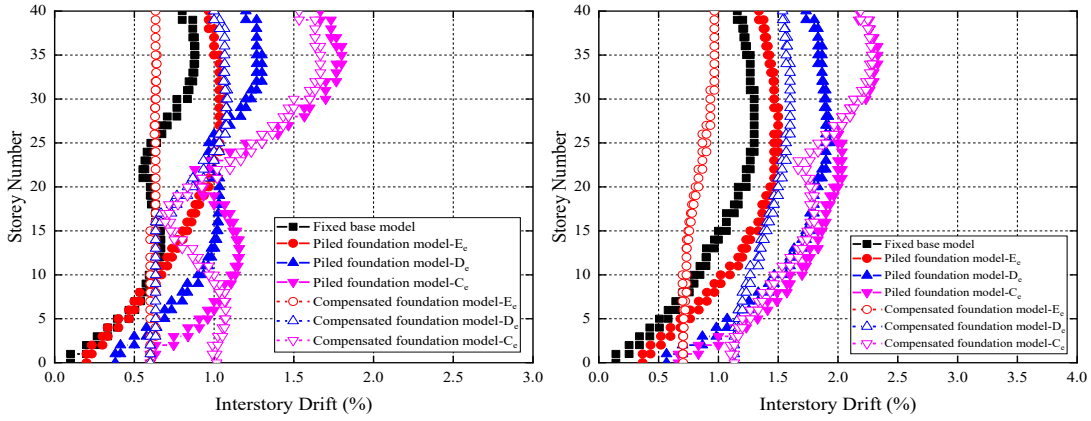

(c) Kobe (d) Northridge

Figure 4.32 Inter-storey drifts of 40-storey structure (HWR=6, BD=20) under the four seismic records

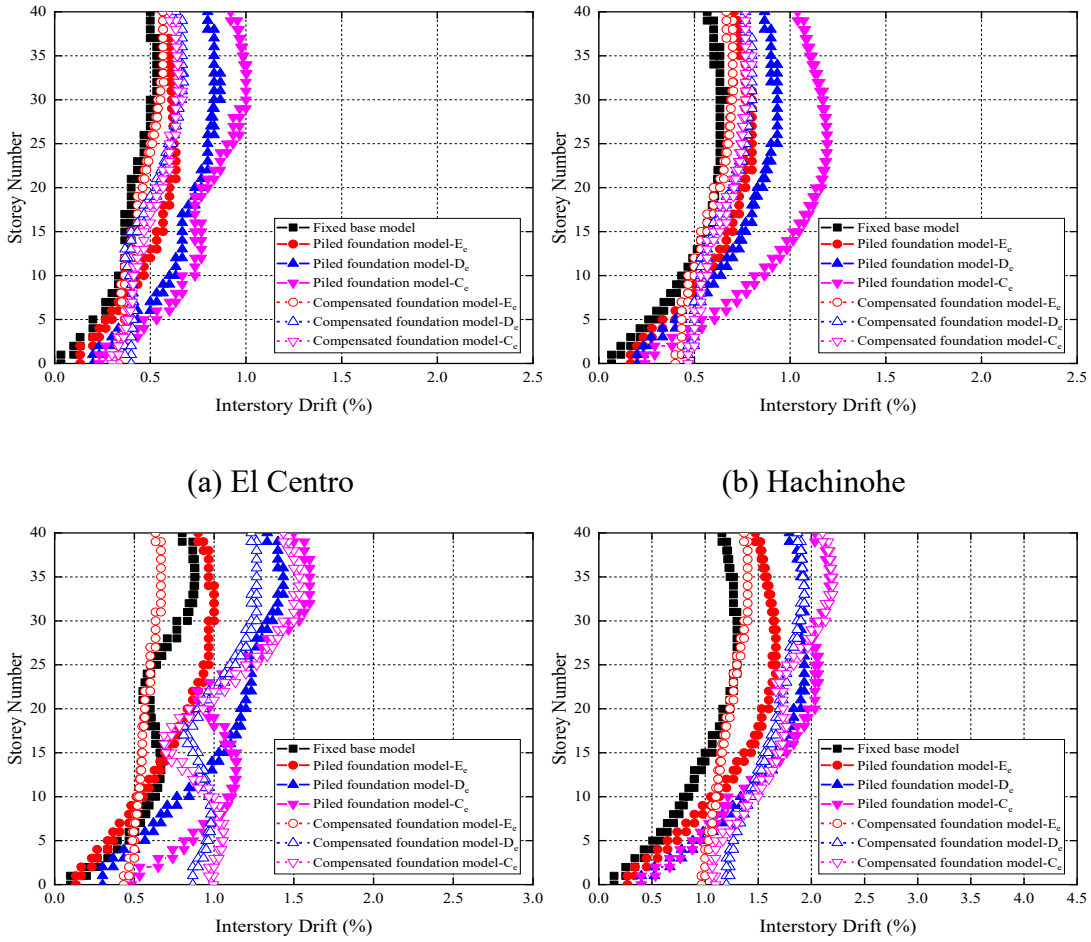

(a) El Centro (b) Hachinohe

(c) Kobe (d) Northridge

Figure 4.33 Inter-storey drifts of 40-storey structure (HWR=6, BD=10) under the four seismic records

4.3.4 Shear Force

Figures 4.34 to 4.48 present a comparison of the shear forces in structures subjected to various influencing factors. Incorporating SSI may cause an increase or decrease in the shear force of the structure, determined by the foundation type and soil type. For instance, the shear forces in classical compensated foundation structures constructed on soft soils, such as E_e and D_e, are typically lower than those observed in their fixed base counterparts, while the shear forces in classical compensated foundation and piled foundation structures resting on C_e soil are amplified. This implies that increasing the rigidity of the substructure can absorb more seismic energy, rendering

the traditional assumption that SSI always reduces the seismic demand of the structure invalid, as noted by Van Nguyen et al. (2017).

Consequently, while piled foundations may reduce foundation rocking, they may also increase the seismic shear force, leading to an increase in the lateral deformation of the superstructure. This finding provides an explanation for why the deformation of the piled foundation model may not necessarily be less than that of the classical compensated foundation model, as presented in sections 4.2.1 and 4.2.3.

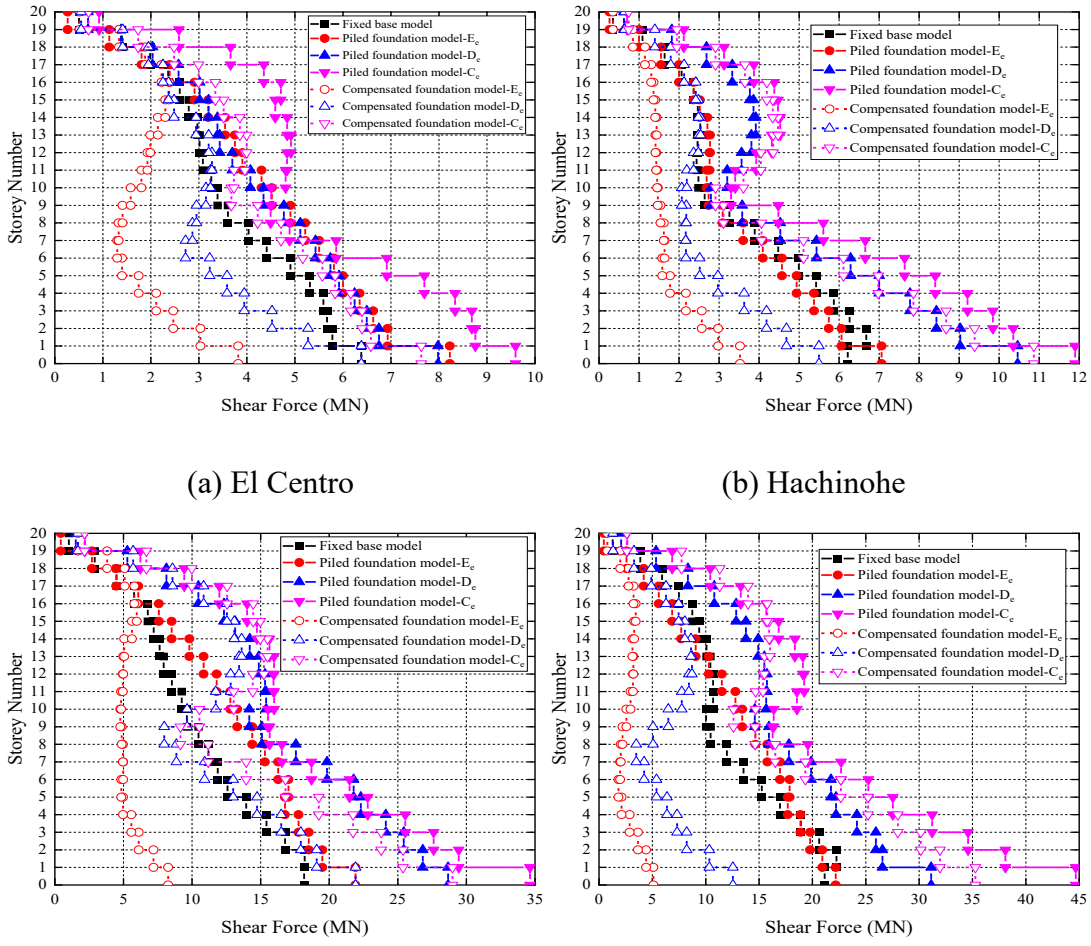

(a) El Centro (b) Hachinohe

(c) Kobe (d) Northridge

Figure 4.34 Storey shear forces of 20-storey structure (HWR=6, BD=30) under the four seismic records

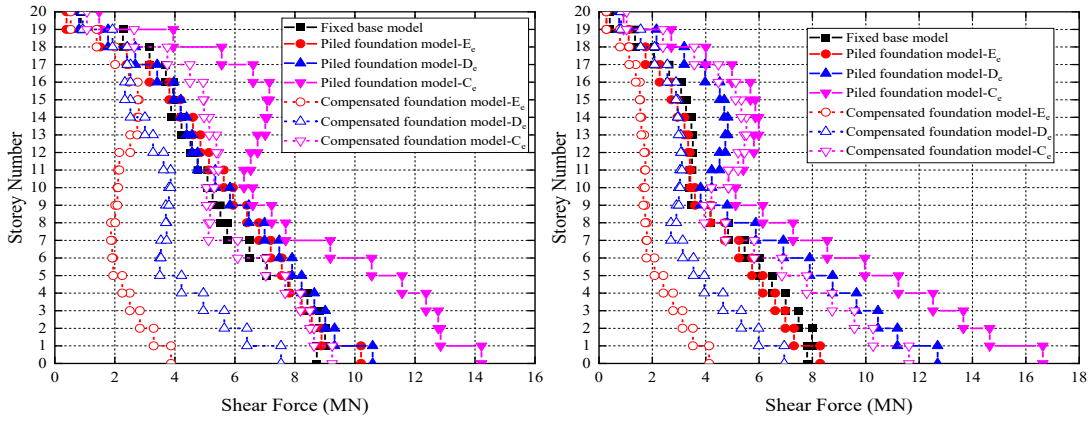

(a) El Centro (b) Hachinohe

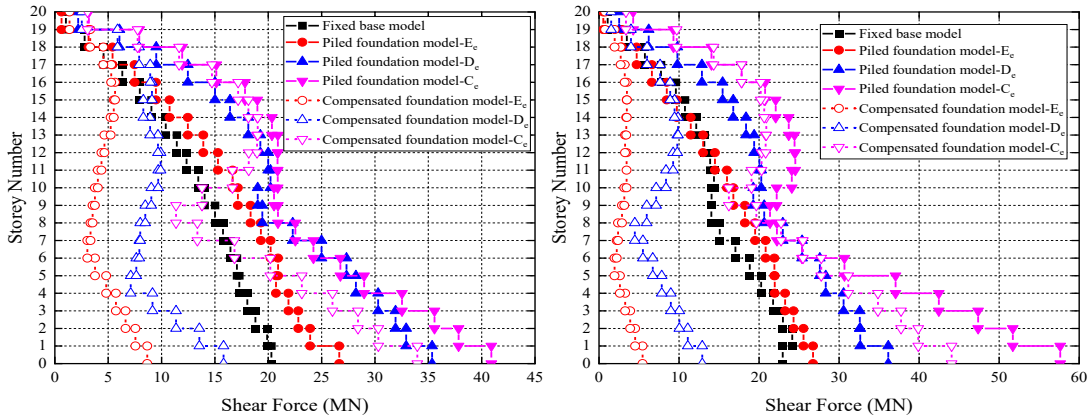

(c) Kobe (d) Northridge

Figure 4.35 Storey shear forces of 20-storey structure (HWR=5, BD=30) under the four seismic records

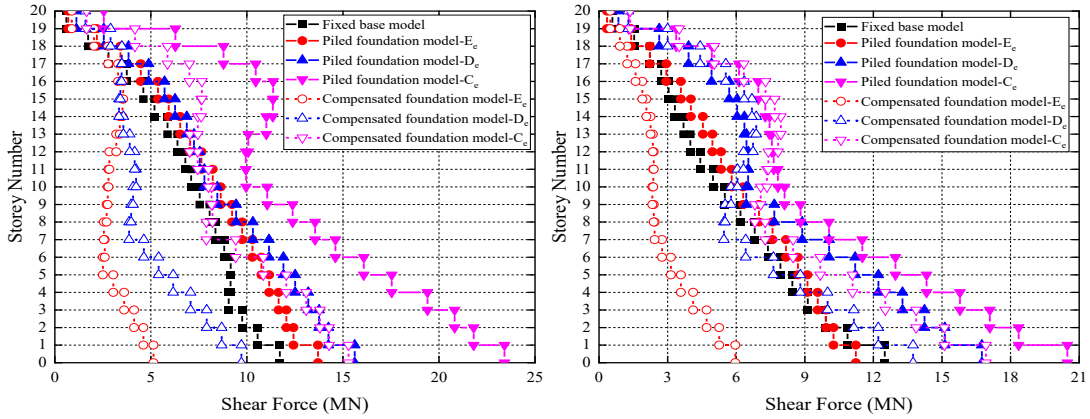

(a) El Centro (b) Hachinohe

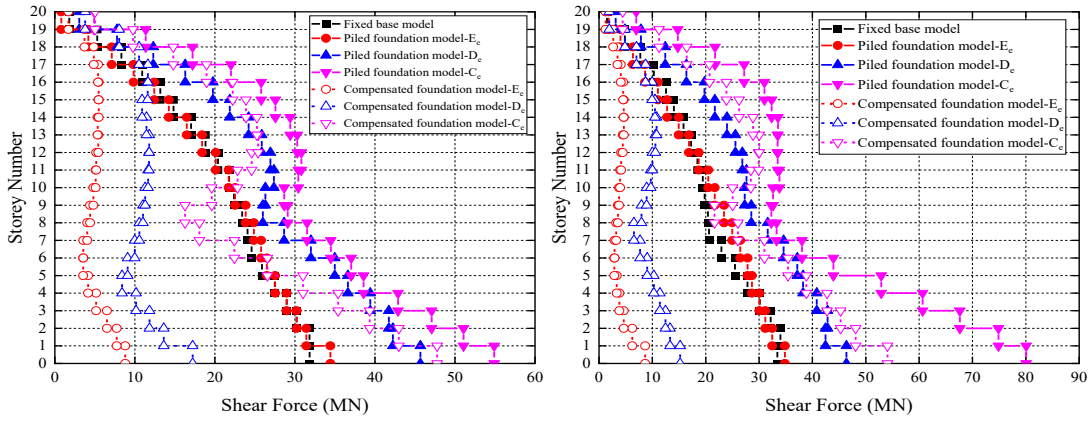

(c) Kobe (d) Northridge

Figure 4.36 Storey shear forces of 20-storey structure (HWR=4, BD=30) under the four seismic records

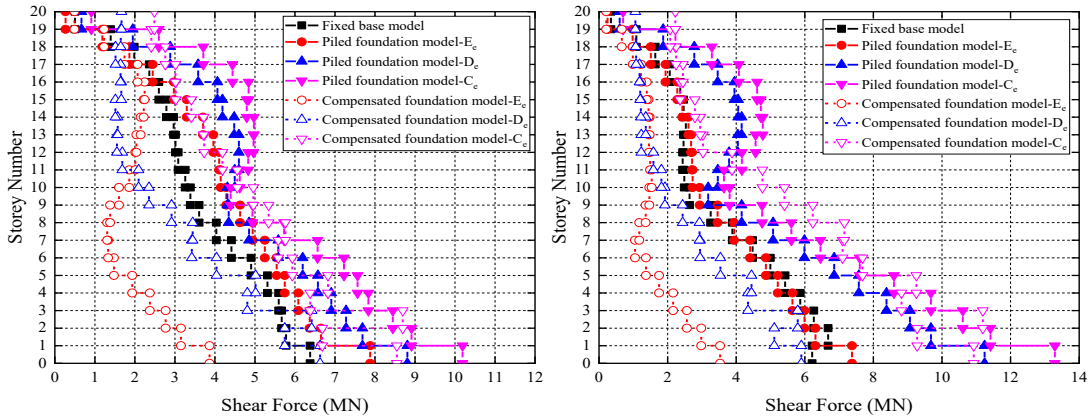

(a) El Centro (b) Hachinohe

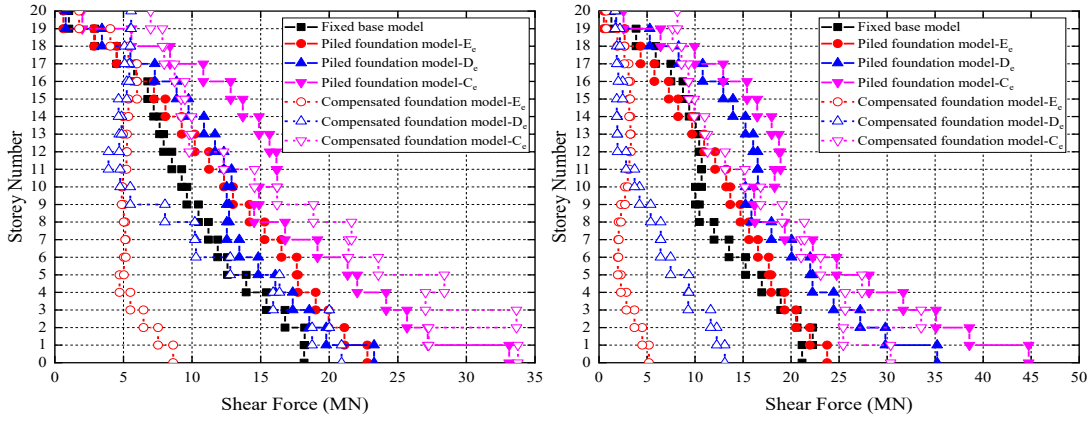

(c) Kobe (d) Northridge

Figure 4.37 Storey shear forces of 20-storey structure (HWR=6, BD=20) under the four seismic records

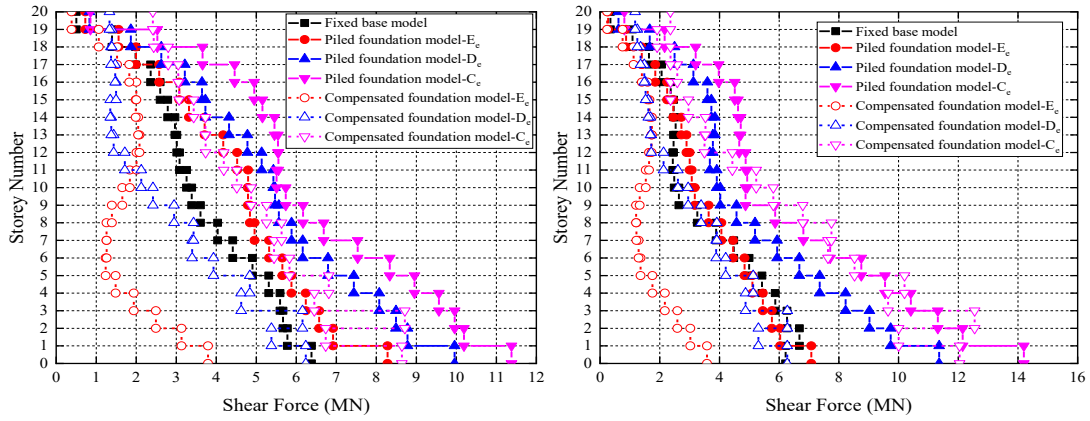

(a) El Centro (b) Hachinohe

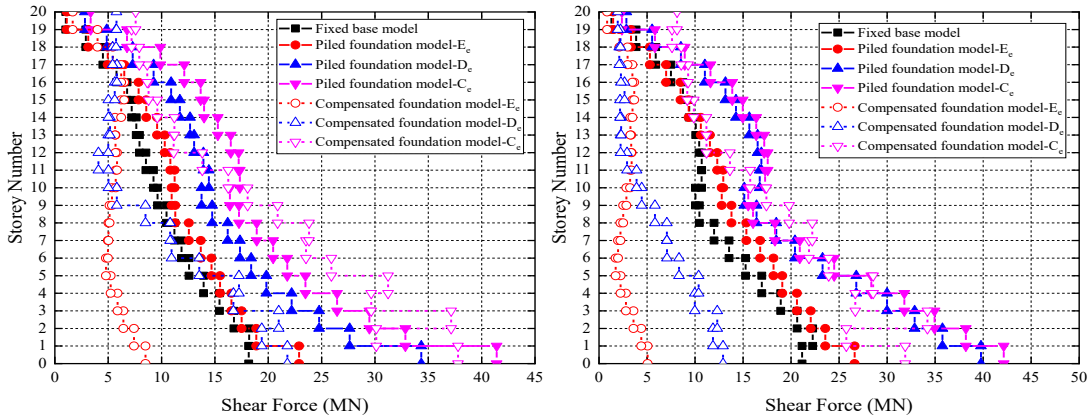

(c) Kobe (d) Northridge

Figure 4.38 Storey shear forces of 20-storey structure (HWR=6, BD=10) under the four seismic records

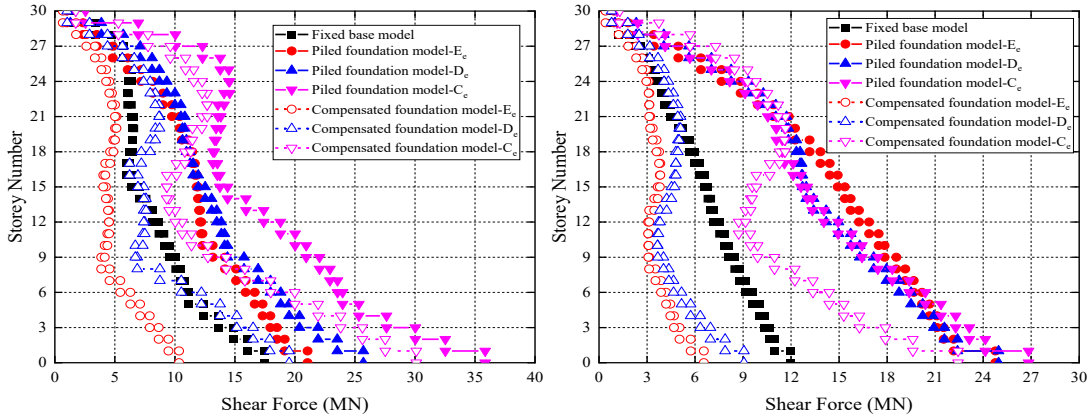

(a) El Centro (b) Hachinohe

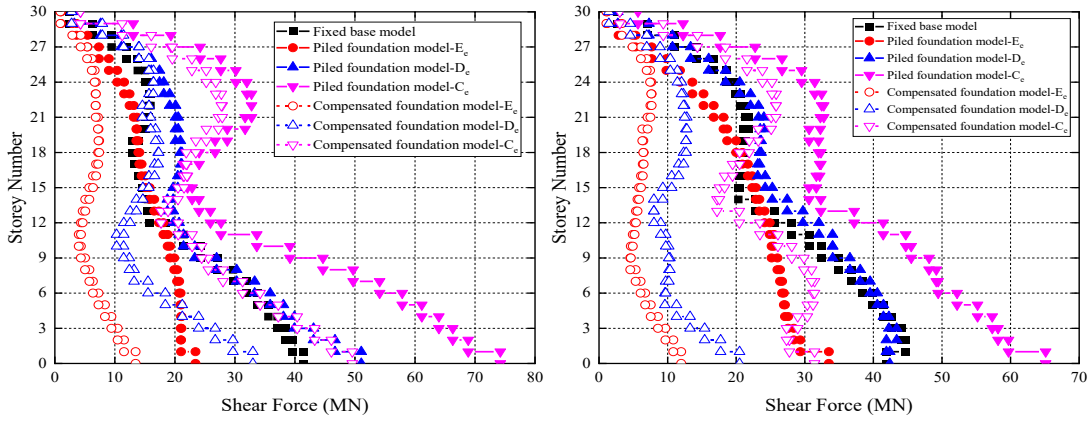

(c) Kobe (d) Northridge

Figure 4.39 Storey shear forces of 30-storey structure (HWR=6, BD=30) under the four seismic records

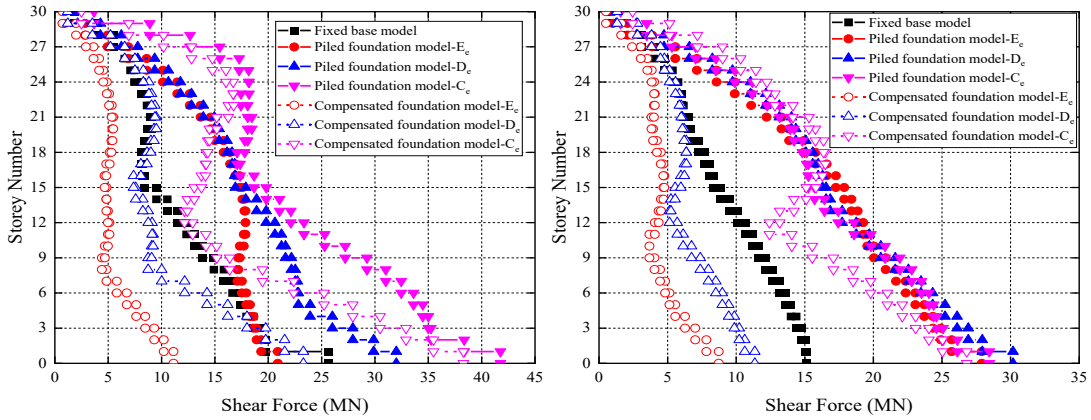

(a) El Centro (b) Hachinohe

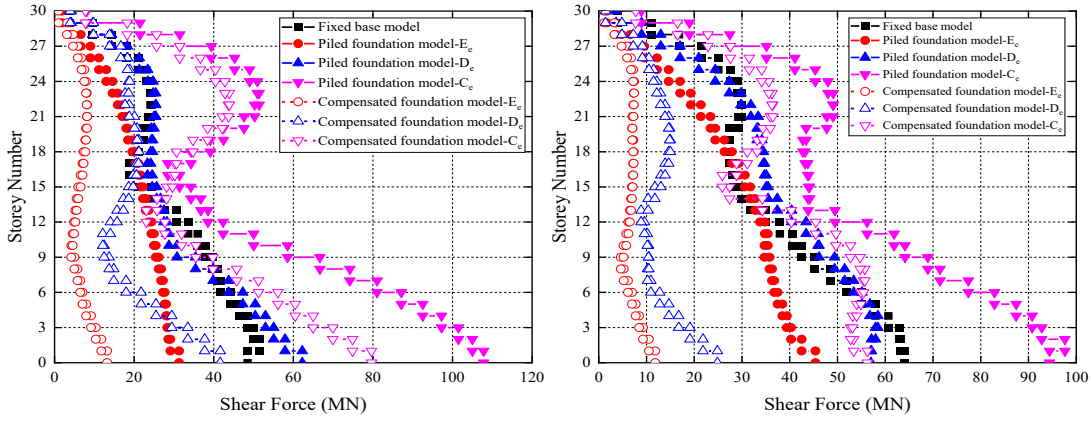

(c) Kobe (d) Northridge

Figure 4.40 Storey shear forces of 30-storey structure (HWR=5, BD=30) under the four seismic records

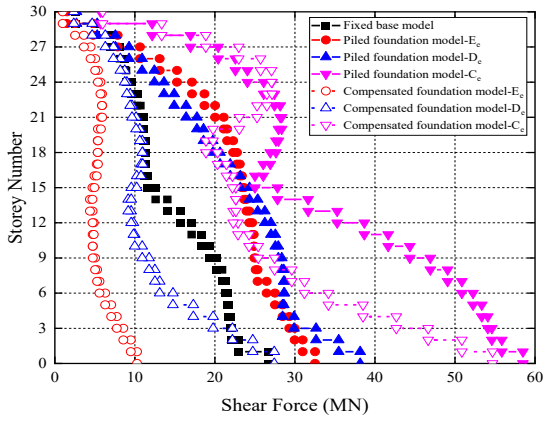

(a) El Centro

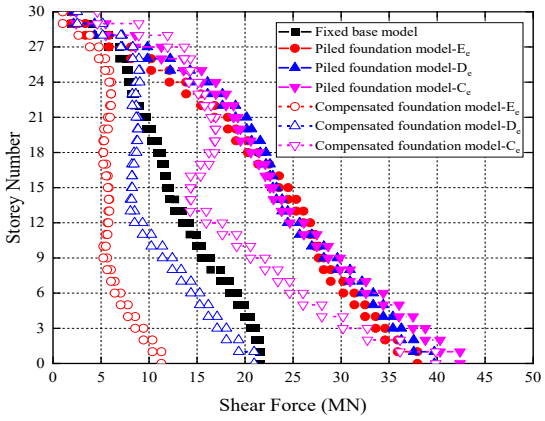

(b) Hachinohe

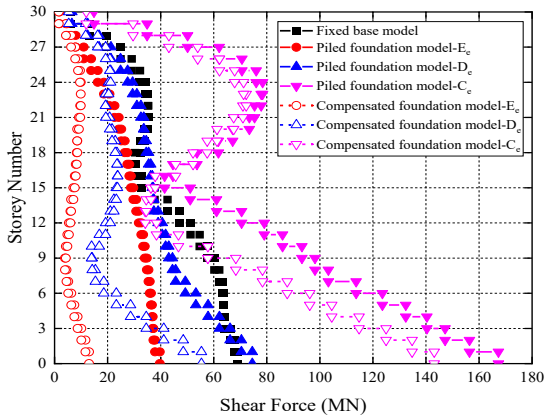

(c) Kobe

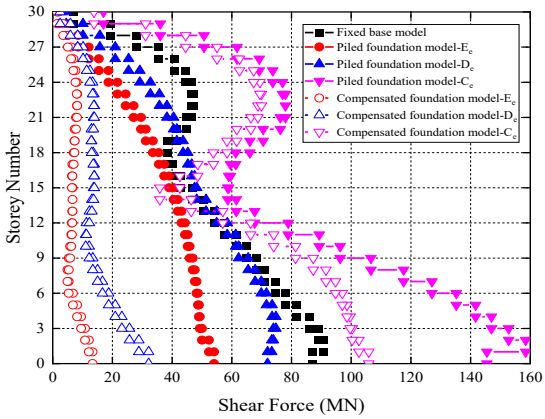

(d) Northridge

Figure 4.41 Storey shear forces of 30-storey structure (HWR=4, BD=30) under the four seismic records

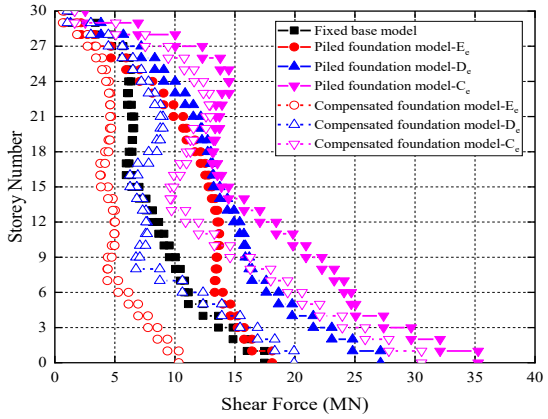

(a) El Centro

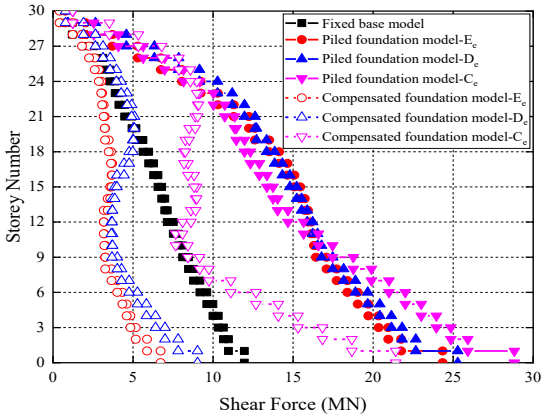

(b) Hachinohe

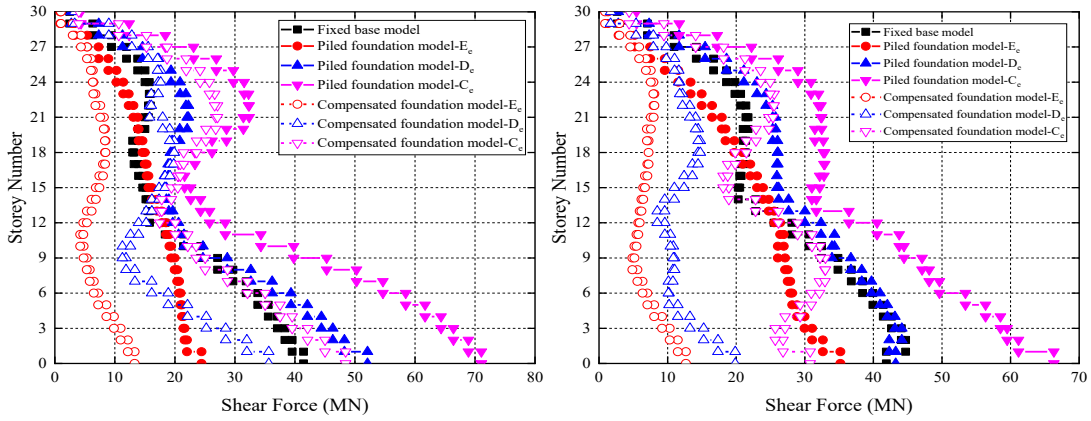

(c) Kobe (d) Northridge

Figure 4.42 Storey shear forces of 30-storey structure (HWR=6, BD=20) under the four seismic records

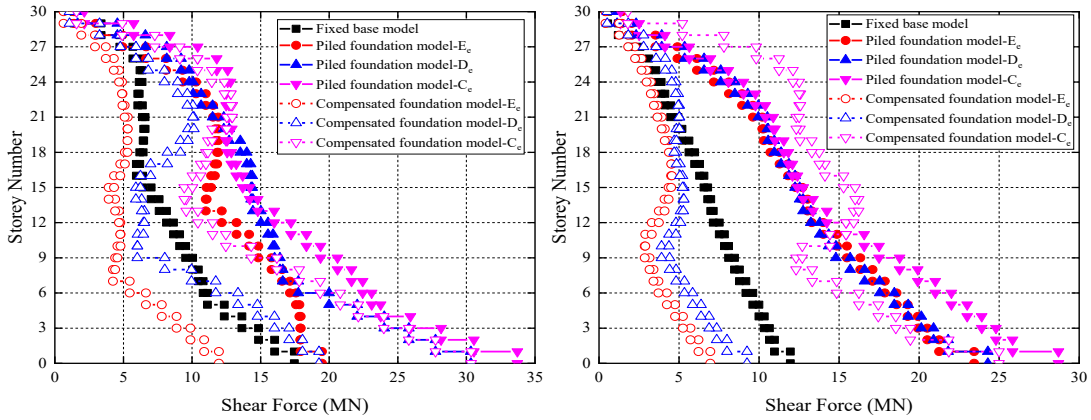

(a) El Centro (b) Hachinohe

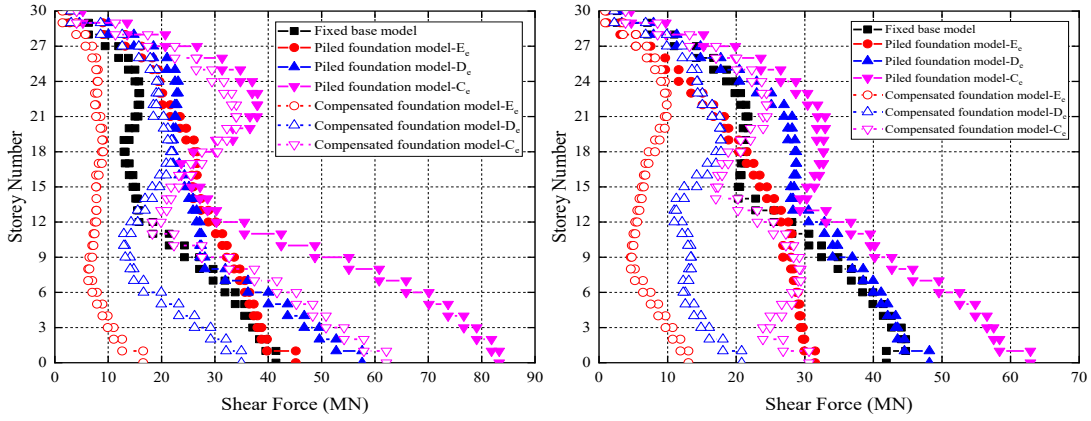

(c) Kobe (d) Northridge

Figure 4.43 Storey shear forces of 30-storey structure (HWR=6, BD=10) under the four seismic records

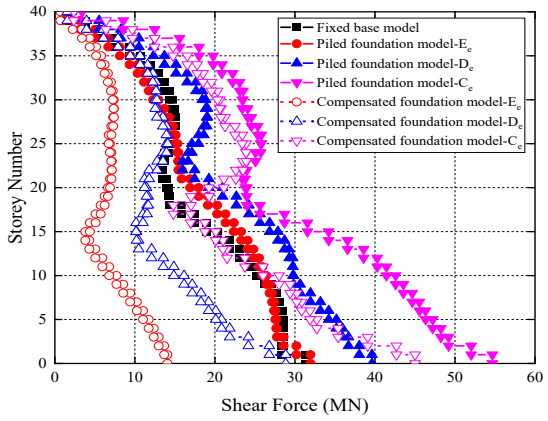

(a) El Centro

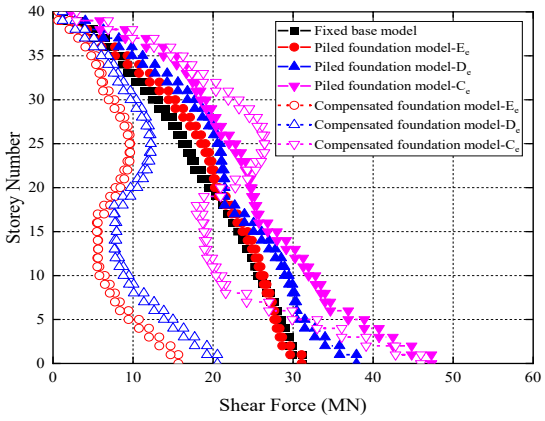

(b) Hachinohe

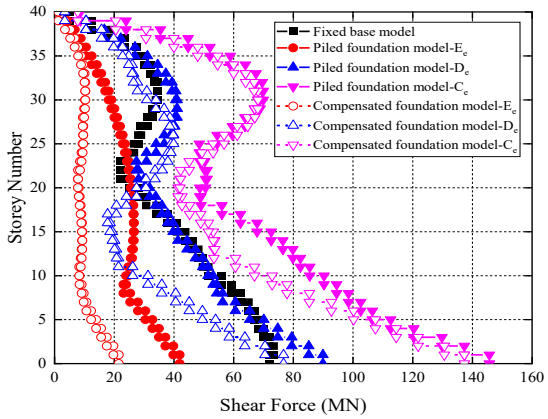

(c) Kobe

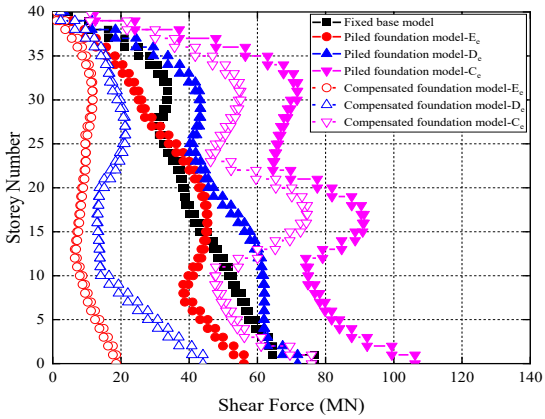

(d) Northridge

Figure 4.44 Storey shear forces of 40-storey structure (HWR=6, BD=30) under the four seismic records

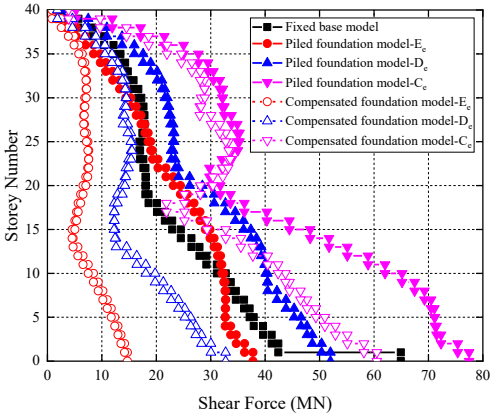

(a) El Centro

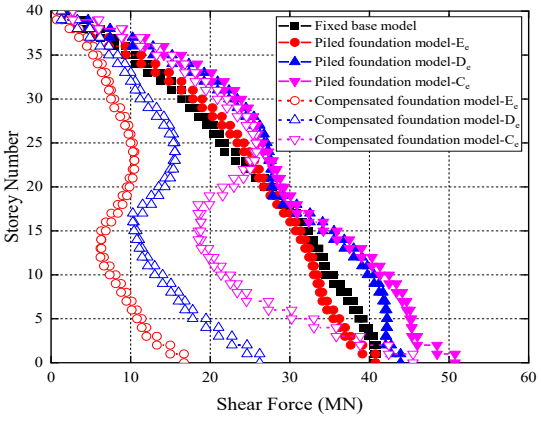

(b) Hachinohe

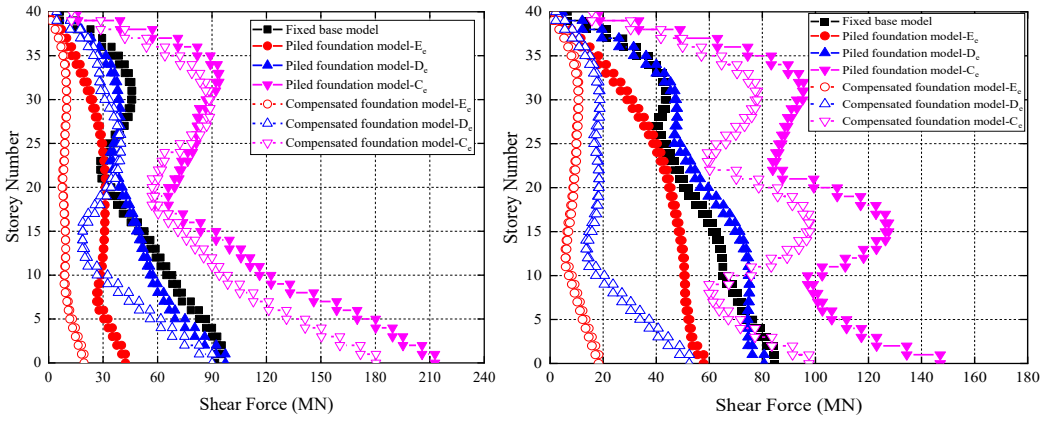

(c) Kobe (d) Northridge

Figure 4.45 Storey shear forces of 40-storey structure (HWR=5, BD=30) under the four seismic records

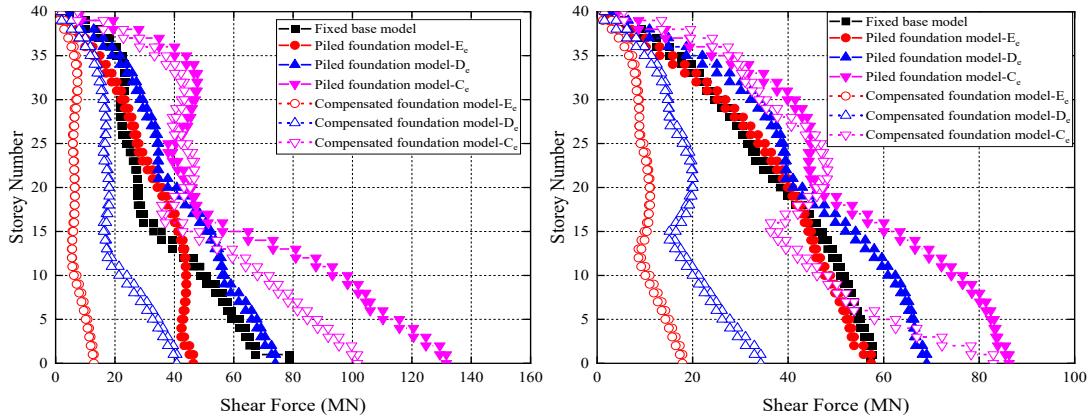

(a) El Centro (b) Hachinohe

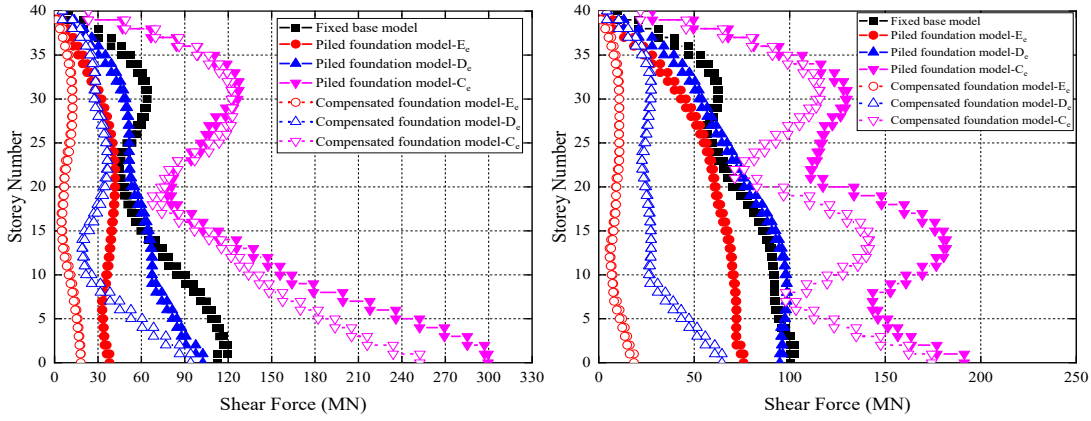

(c) Kobe (d) Northridge

Figure 4.46 Storey shear forces of 40-storey structure (HWR=4, BD=30) under the four seismic records

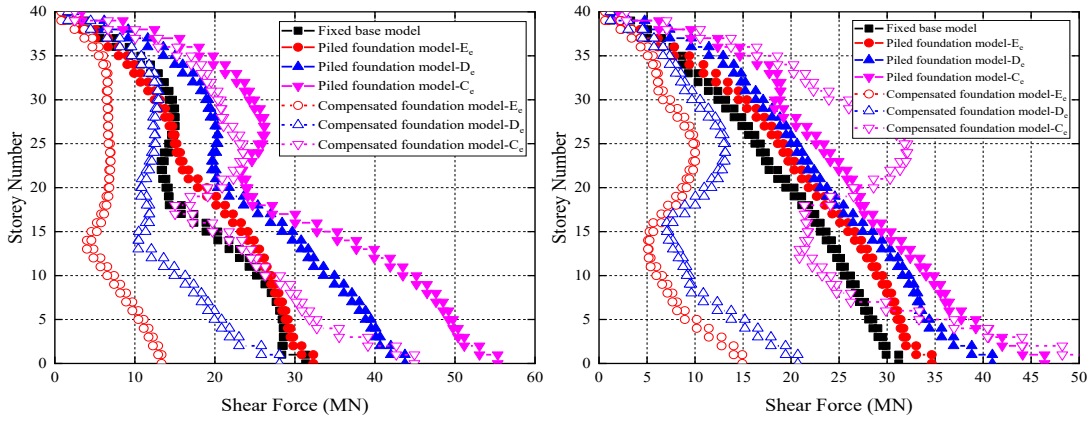

(a) El Centro (b) Hachinohe

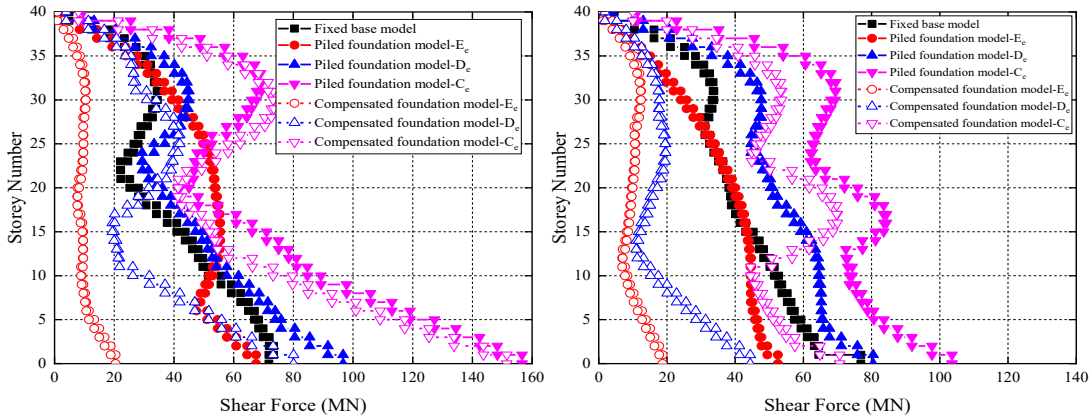

(c) Kobe (d) Northridge

Figure 4.47 Storey shear forces of 40-storey structure (HWR=6, BD=20) under the four seismic records

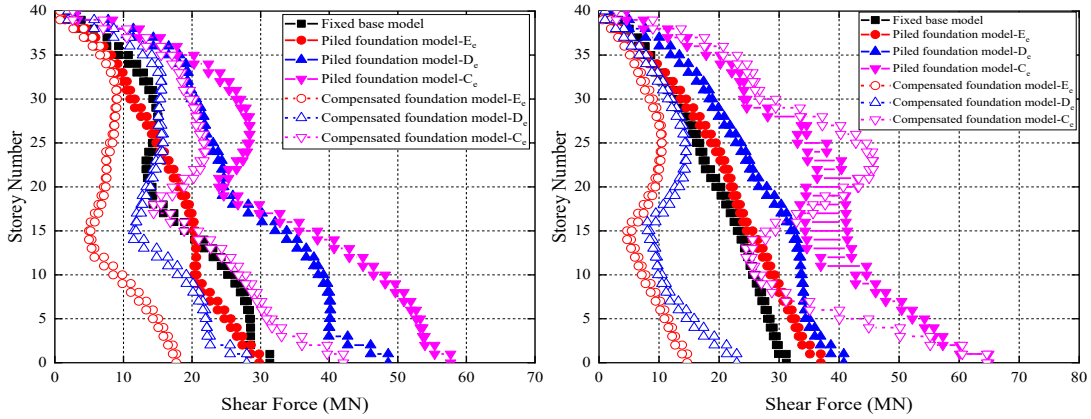

(a) El Centro (b) Hachinohe

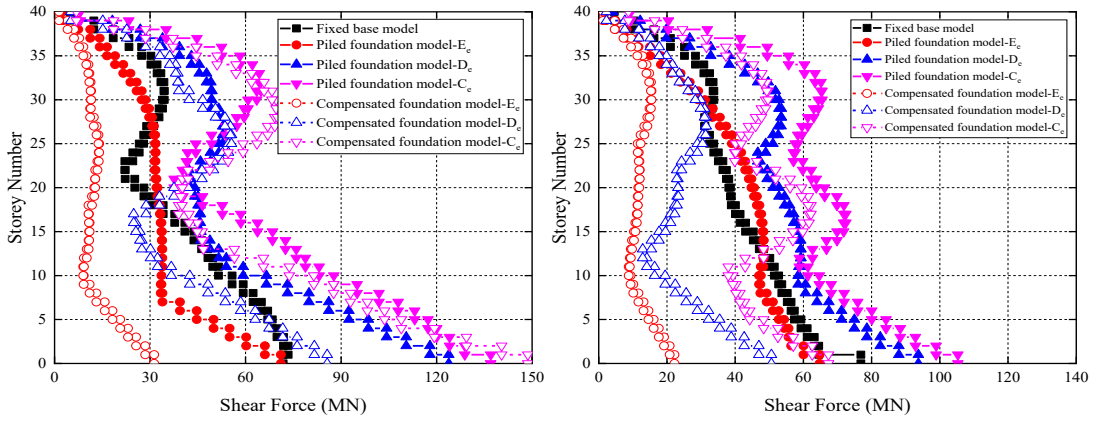

(c) Kobe (d) Northridge

Figure 4.48 Storey shear forces of 40-storey structure (HWR=6, BD=10) under the four seismic records

4.3.5 The Effects of Parameters on V_{fle}/V_{fix}

To facilitate a more intuitive comparison of the effects of various factors and to discuss the beneficial and detrimental influences of SSI on seismic performance, the present study utilises numerical soil-structure models to compute base shears (V_{fle}) and maximum inter-storey drifts (δ_{fle}) and normalises these results with those obtained from traditional rigid base models (V_{fix} and δ_{fix}). The resulting base shear ratio (V_{fle}/V_{fix}) or maximum inter-storey drifts ratio ($\delta_{fle}/\delta_{fix}$) values greater than 1 indicate that SSI amplifies base shear or maximum inter-storey drifts, thereby exerting a detrimental effect.

To provide a comprehensive analysis and clear demonstration of the impacts of superstructure and substructure parameters on high-rise frame-core tube structures, the values of V_{fle}/V_{fix} and $\delta_{fle}/\delta_{fix}$ are averaged under the action of four seismic records (Figure 4.2). Firstly, this study presents the values of V_{fle}/V_{fix} for classical compensated foundation structures and piled foundation structures with different superstructure and substructure parameters, as shown in Figures 4.49, 4.50, 4.51, 4.52, 4.53, and 4.54.

It is observed that, regardless of the foundation type, there is a significant increase in the values of V_{fle}/V_{fix} with an increase in the stiffness of the soil. Although the changes

in the HWR and BD can slightly affect this ratio, their influence is considerably less than that of the soil type.

For the classical compensated foundation structures, the values of V_{fle}/V_{fix} of structures constructed on C_e soil consistently exceed 1, indicating that stiff soil increases the base shear of frame-core tube structures when SSI is considered. In contrast, V_{fle}/V_{fix} of structures built on D_e and E_e soil types is less than 1, suggesting that base shear can be reduced when structures are built on medium or soft soils.

Piled foundation structures are observed to absorb more seismic energy during an earthquake event owing to the enhanced stiffness of the substructure system (Van Nguyen et al. 2017). Consequently, in almost all piled foundation cases, the values of V_{fle}/V_{fix} exceed 1, indicating that, under the parameters examined in this study, the seismic demand of frame-core tube structures established on a piled foundation is amplified after considering SSI. Therefore, for piled foundation structures, the effects of SSI on base shear are observed to be detrimental.

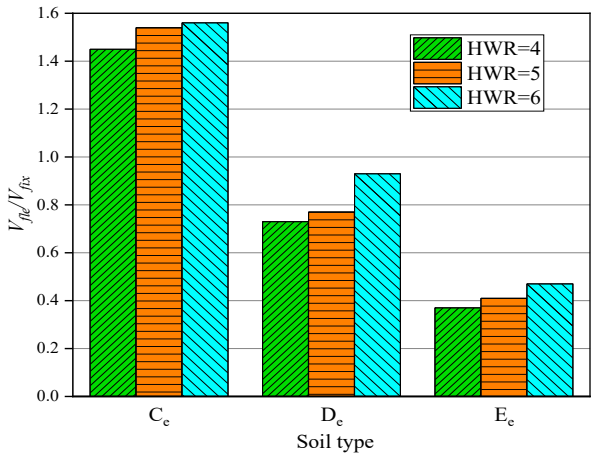

(a)

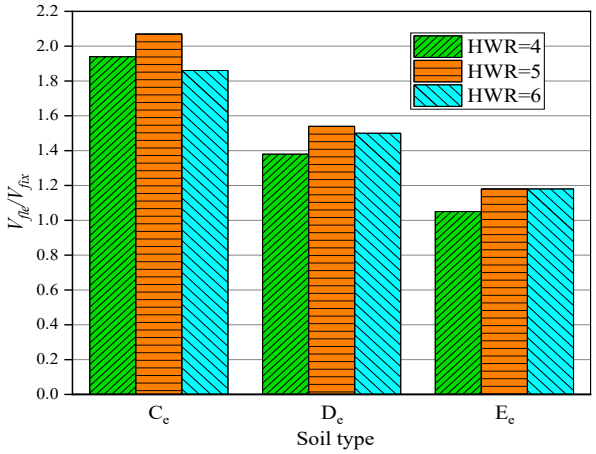

(b)

Figure 4.49 The value of V_{fle}/V_{fix} of 20-storey buildings with different HWRs (a) classical compensated foundation structure (b) piled foundation structure

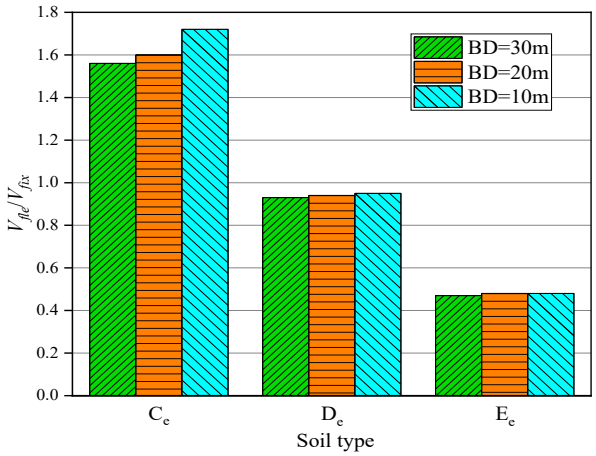

(a)

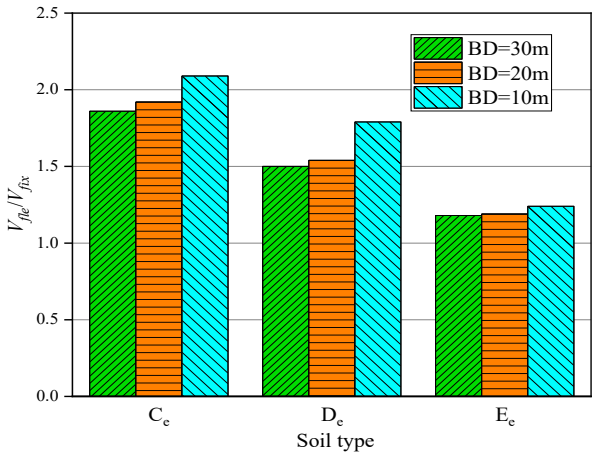

(b)

Figure 4.50 The value of V_{fle}/V_{fix} of 20-storey buildings with different BDs (a) classical compensated foundation structure (b) piled foundation structure

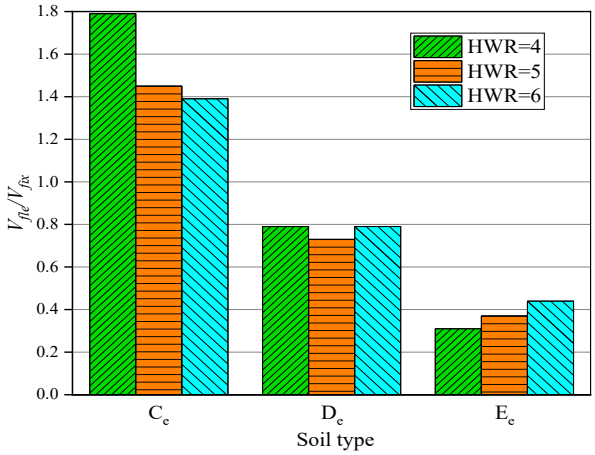

(a)

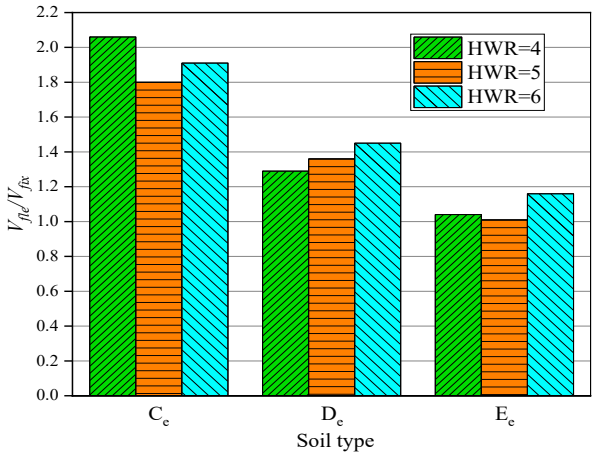

(b)

Figure 4.51 The value of V_{fle}/V_{fix} of 30-storey buildings with different HWRs (a) classical compensated foundation structure (b) piled foundation structure

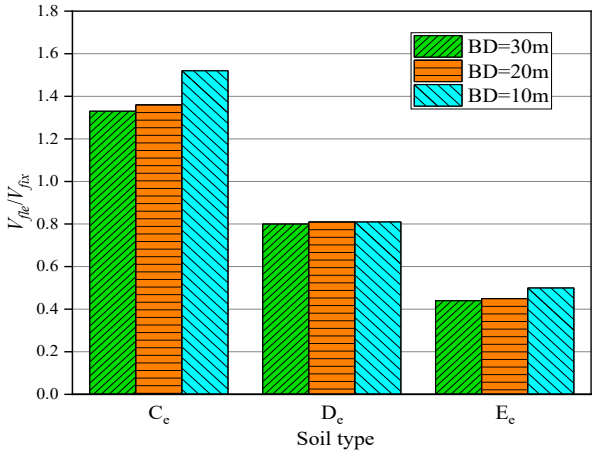

(a)

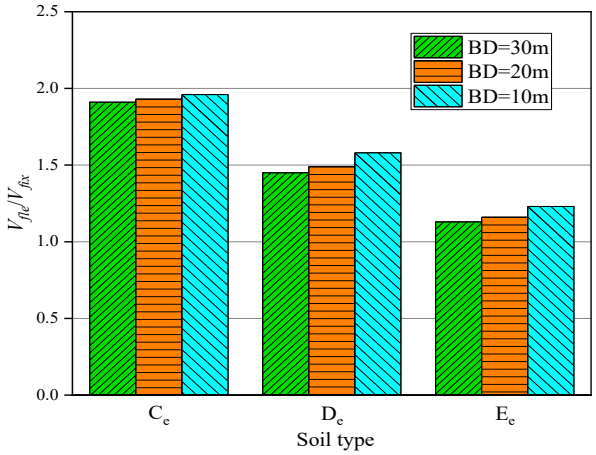

(b)

Figure 4.52 The value of V_{fle}/V_{fix} of 30-storey buildings with different BDs (a) classical compensated foundation structure (b) piled foundation structure

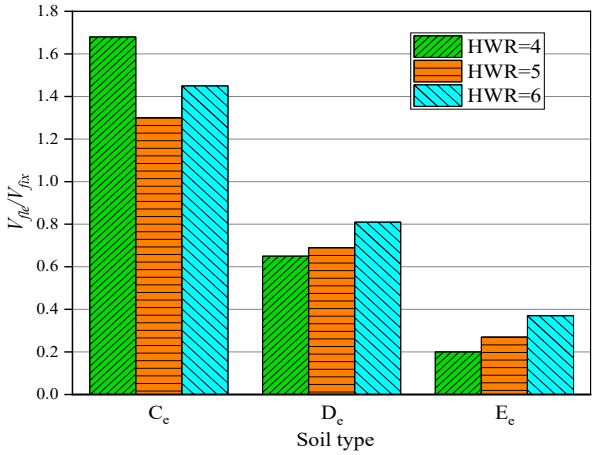

(a)

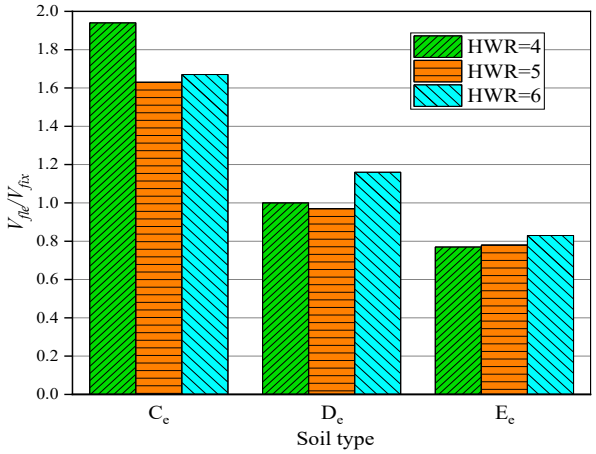

(b)

Figure 4.53 The value of V_{fle}/V_{fix} of 40-storey buildings with different HWRs (a) classical compensated foundation structure (b) piled foundation structure

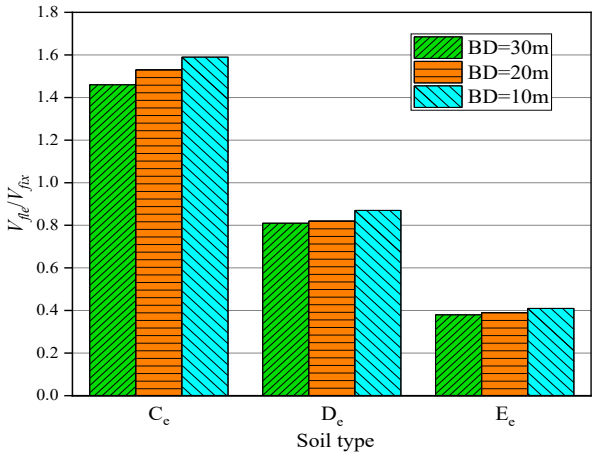

(a)

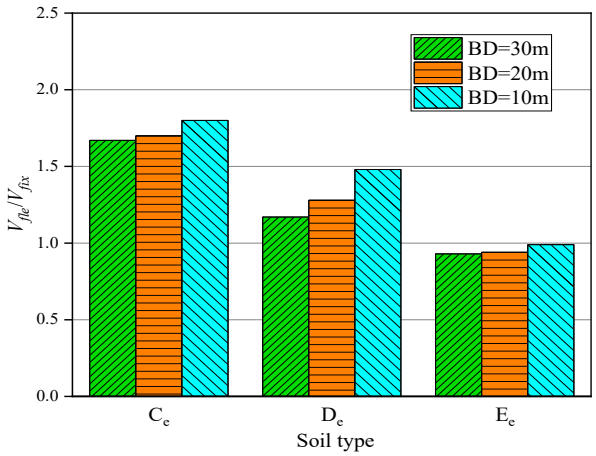

(b)

Figure 4.54 The value of V_{fle}/V_{fix} of 40-storey buildings with different BDs (a) classical compensated foundation structure (b) piled foundation structure

4.3.6 The Effects of Parameters on $\delta_{fle}/\delta_{fix}$

The values of $\delta_{fle}/\delta_{fix}$ are presented in Figures 4.55, 4.56, 4.57, 4.58, 4.59, and 4.60. It is obvious that SSI consistently increases the inter-storey drifts, as $\delta_{fle}/\delta_{fix}$ is observed to be greater than 1 in almost all cases examined in this study. This implies that SSI can modify the performance level of high-rise frame-core tube buildings. Moreover, varying the superstructure and substructure parameters produces different trends in the influence of SSI on the values of $\delta_{fle}/\delta_{fix}$. This is because the stiffness of the substructure has a complex influence on the deformation of the superstructure. On one hand, as stated earlier, the increased stiffness of the substructure system attracts more seismic energy to deform the superstructure. On the other hand, stiffer ground soil can limit the foundation rocking, thereby decreasing the deformation of the superstructure. Hence, when analysing SSI effects on the deformation of the superstructure, it is crucial to consider the base shear, inter-storey drift, and foundation rocking comprehensively.

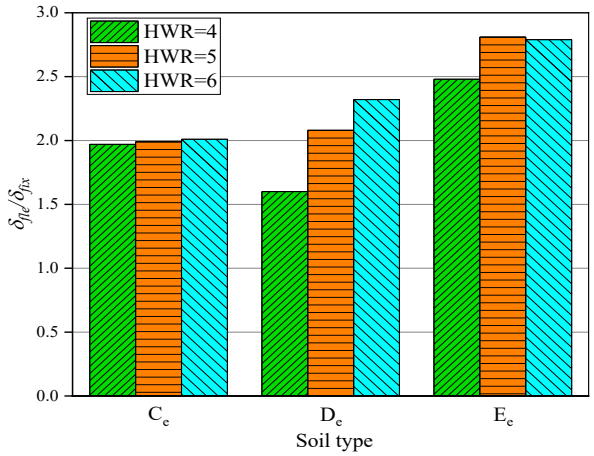

(a)

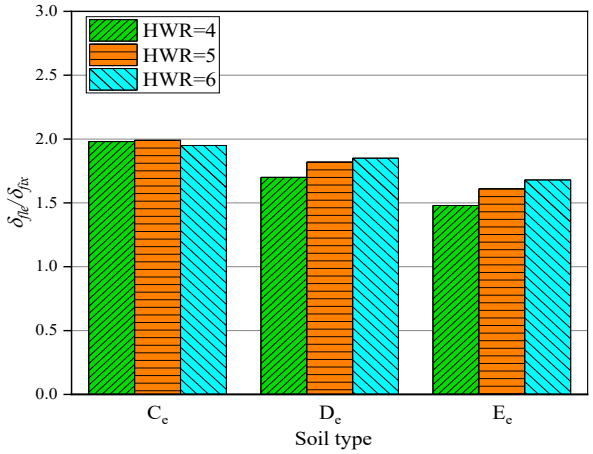

(b)

Figure 4.55 The value of $\delta_{fle}/\delta_{fix}$ of 20-storey buildings with different HWRs (a) classical compensated foundation structure (b) piled foundation structure

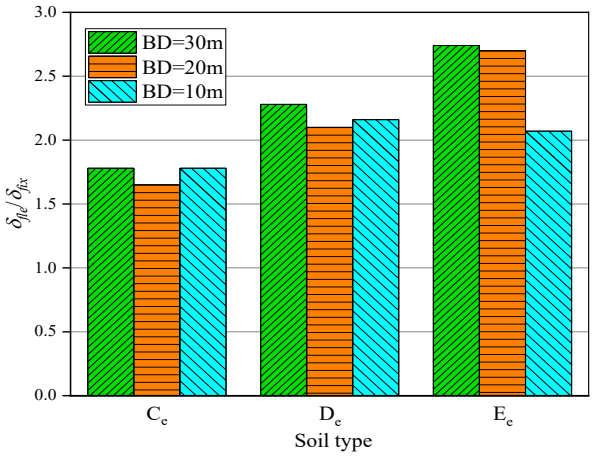

(a)

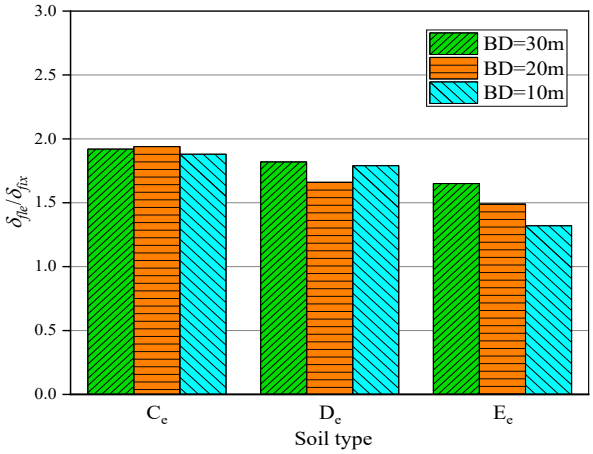

(b)

Figure 4.56 The value of $\delta_{fle}/\delta_{fix}$ of 20-storey buildings with different BDs (a) classical compensated foundation structure (b) piled foundation structure

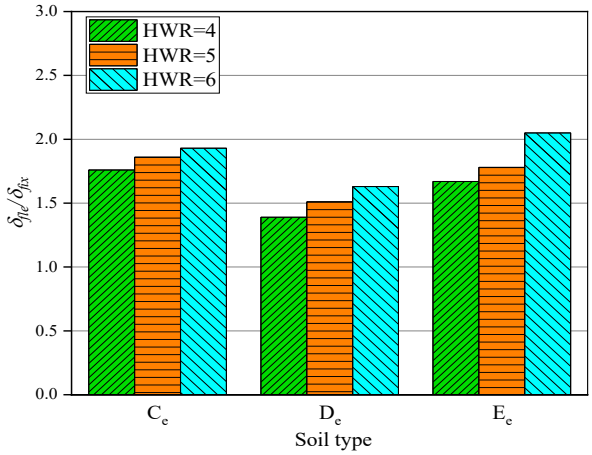

(a)

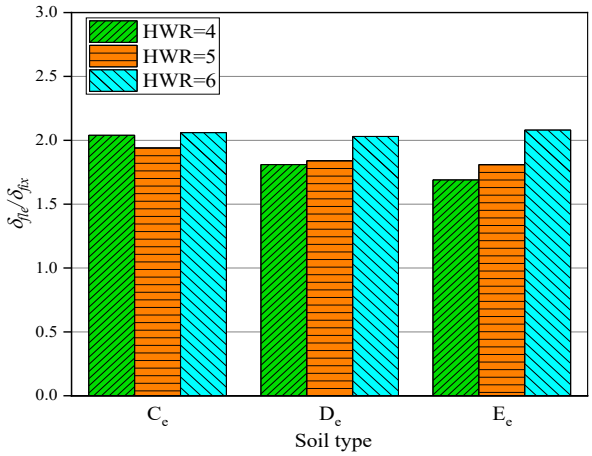

(b)

Figure 4.57 The value of $\delta_{fle}/\delta_{fix}$ of 30-storey buildings with different HWRs (a) classical compensated foundation structure (b) piled foundation structure

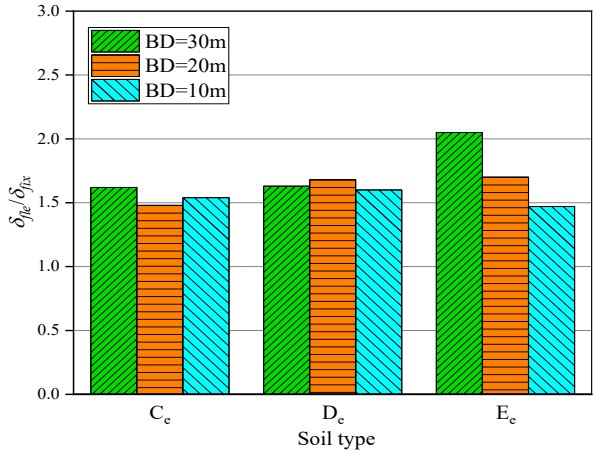

(a)

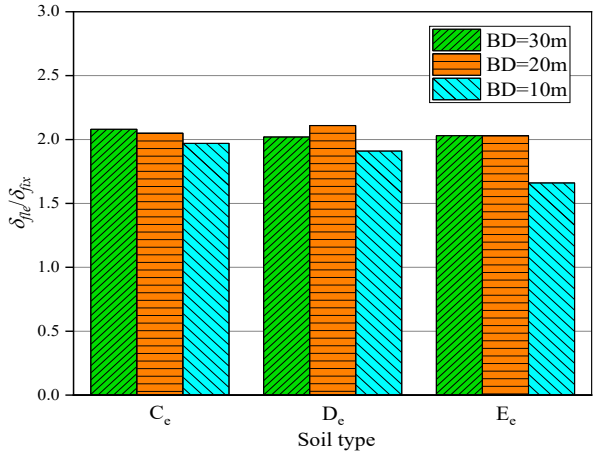

(b)

Figure 4.58 The value of $\delta_{fle}/\delta_{fix}$ of 30-storey buildings with different BDs (a) classical compensated foundation structure (b) piled foundation structure

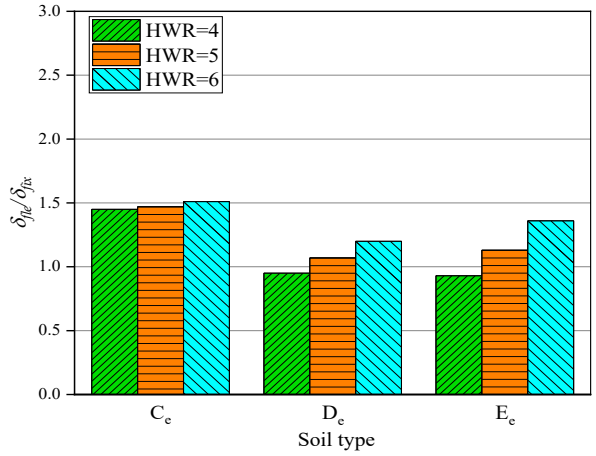

(a)

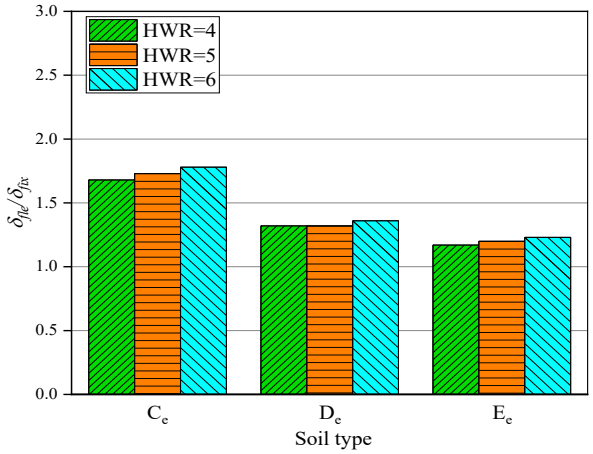

(b)

Figure 4.59 The value of $\delta_{fle}/\delta_{fix}$ of 40-storey buildings with different HWRs (a) classical compensated foundation structure (b) piled foundation structure

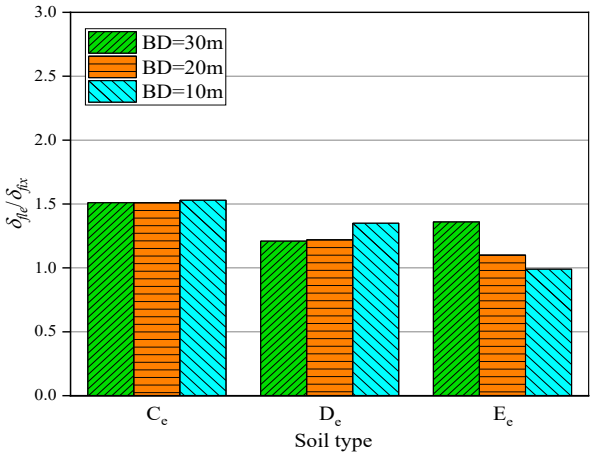

(a)

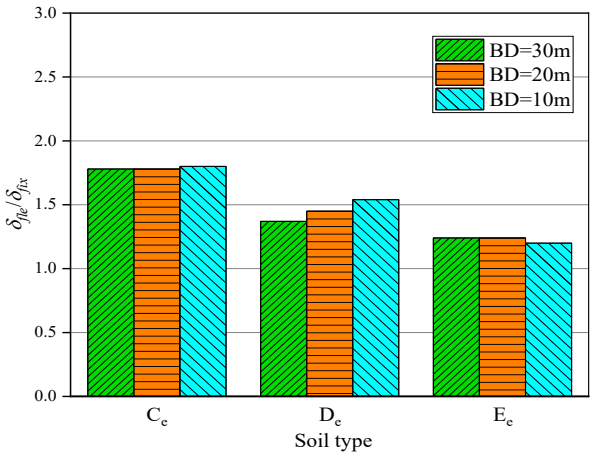

(b)

Figure 4.60 The value of $\delta_{fle}/\delta_{fix}$ of 40-storey buildings with different BDs (a) classical compensated foundation structure (b) piled foundation structure

According to Figure 2.1, it can be observed that the Δ_t of a structure is composed of two distinct components, Δ_θ and Δ_d (Kramer 1996). The Δ_d is closely associated with shear forces that are produced in the superstructure, while foundation rocking occurs due to the settlement on one side of the foundation and possible uplift on the other side, which is caused by inertial forces. To assess the significance of foundation rocking during seismic events, this study adopts the proportions of lateral deflection caused by foundation rocking (Δ_θ/Δ_t). To compute this value under different parameters, the moment when the Δ_t occurs in the time-history curve is recorded, as illustrated in Figure 4.61 (Hokmabadi et al. 2012). The foundation rocking angle at this moment is then multiplied by the height of the structure to determine the value of Δ_θ. Finally, the ratio Δ_θ/Δ_t can be calculated.

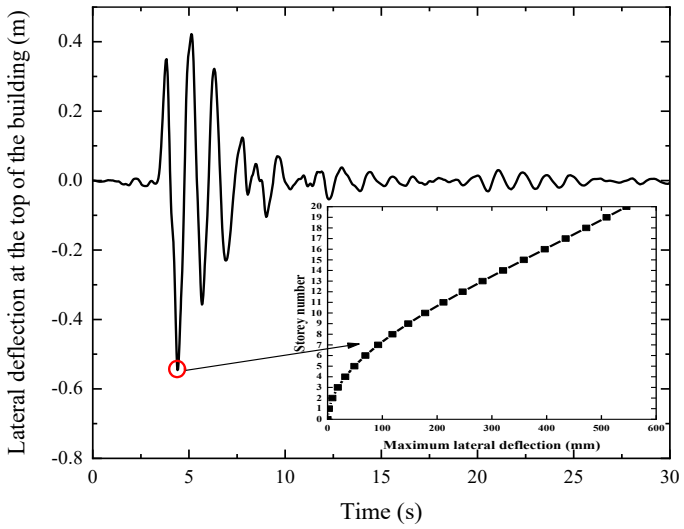

Figure 4.61 The determination of Δ_t (Take the 20-storey fixed base model subjected to Northridge earthquake as an illustration)

Figure 4.62 shows the relationship between $\delta_{fle}/\delta_{fix}$, V_{fle}/V_{fix}, and Δ_θ/Δ_t for various models with different superstructure and substructure parameters. When the subsoil exhibits sufficient stiffness, and the values of Δ_θ/Δ_t are small, specifically less than 0.5

for classical compensated foundation structures and less than 0.15 for piled foundation structures, the data points tend to be evenly distributed around the $y=x$ line. This distribution pattern indicates that the amplification coefficient for base shear is nearly equivalent to the amplification coefficient for inter-storey drifts after accounting for SSI. However, as the soil stiffness decreases and the values of Δ_θ/Δ_t increase, the data points start to shift downward and away from the $y=x$ line. This deviation implies that an increase in Δ_θ/Δ_t value amplifies the inter-storey drift and reduces the base shear of high-rise frame-core tube structures.

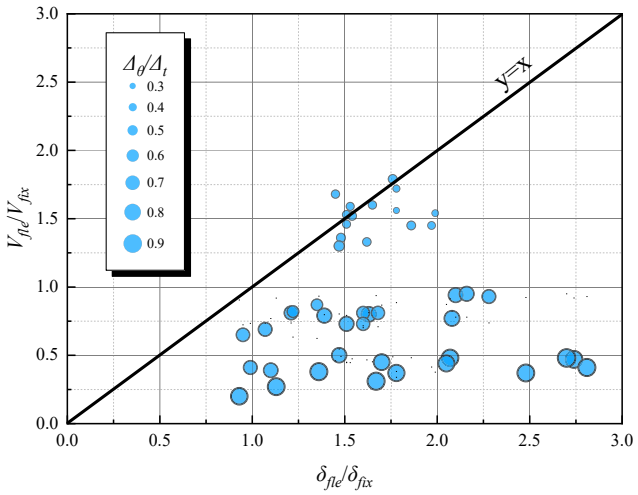

(a)

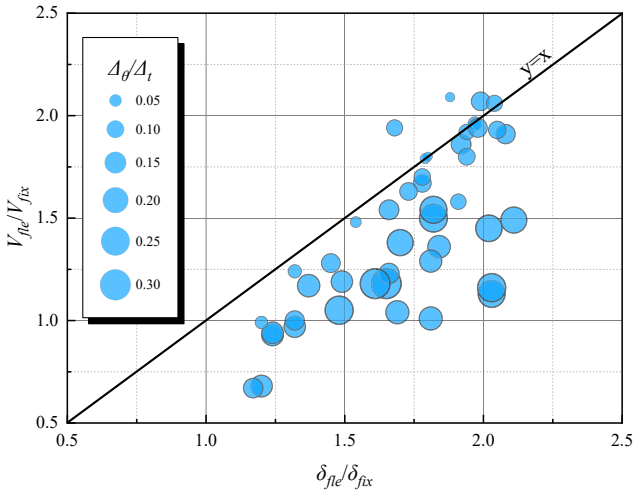

(b)

Figure 4.62 The relationship between $\delta_{fle}/\delta_{fix}$, V_{fle}/V_{fix} and Δ_θ/Δ (a) classical

compensated foundation structure (b) piled foundation structure

It is also noteworthy that the lateral displacement of the classical compensated foundation model is primarily dominated by Δ_θ, while the proportion of Δ_θ in the piled foundation model is relatively small, amounting to less than 30%. This observation is reasonable as end-bearing piles can efficiently constrain foundation rotation. Furthermore, the impact of SSI on seismic responses of buildings with different foundation types is evident from Figure 4.62. The majority of data points of the piled foundation model are located in the range of $\delta_{fle}/\delta_{fix}>1$, $V_{fle}/V_{fix}>1$, indicating that SSI has adverse effects irrespective of changes in model parameters. In contrast, for the classical compensated foundation model, structures with D_e and E_e soil types fall below the $V_{fle}/V_{fix}=1$ line, indicating that SSI has a favorable impact as it reduces the base shear of the superstructure, even if the inter-storey drifts remain amplified.

4.3.7 The Relationship between T_{fle}/T_{fix} and V_{fle}/V_{fix}

Based on the above analysis, it can be concluded that SSI has a detrimental effect on the inter-storey drifts of high-rise frame-core tube structures, while its impact on base shears is determined by the foundation type and subsoil stiffness. However, it is important to note that previous studies have mainly focused on the amplification of inter-storey drifts, neglecting the effect of SSI on the shear force. This is because most of the previous research has concluded that SSI can reduce the shear force of the superstructure. For instance, Tabatabaiefar et al. (2014a) developed an empirical formula to predict the value of $\delta_{fle}/\delta_{fix}$ and evaluate the performance level of buildings after considering SSI. Similarly, the present study aims to summarise the influence of SSI on the base shear of high-rise buildings and develop a straightforward and precise procedure to estimate the value of V_{fle}/V_{fix}.

Figure 4.63 displays the correlation between T_{fle}/T_{fix} and V_{fle}/V_{fix}, where T is the natural period of structures. As the substructure stiffness decreases and T_{fle}/T_{fix} increases, V_{fle}/V_{fix} linearly decreases. However, when it reaches a certain threshold, the value of

V_{fle}/V_{fix} stabilises and does not decrease further. Specifically, for classical compensated foundation structures, V_{fle}/V_{fix} reaches its minimum at 0.395 and remains stable thereafter, whereas for piled foundation structures, the minimum value is 1.046.

As a result, in structural design, practitioners can determine whether the base shear of the structure should be amplified or reduced after considering SSI, so as to make the structural design more economical and safer. The seismic codes can also refer to the above two values to specify different minimum values of reduced shear force based on the foundation type.

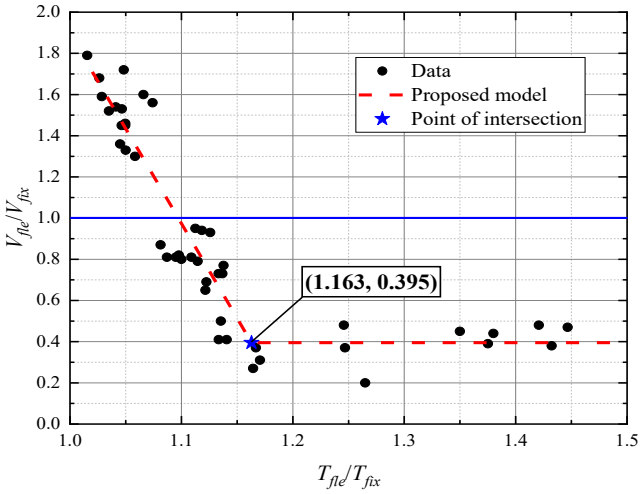

(a)

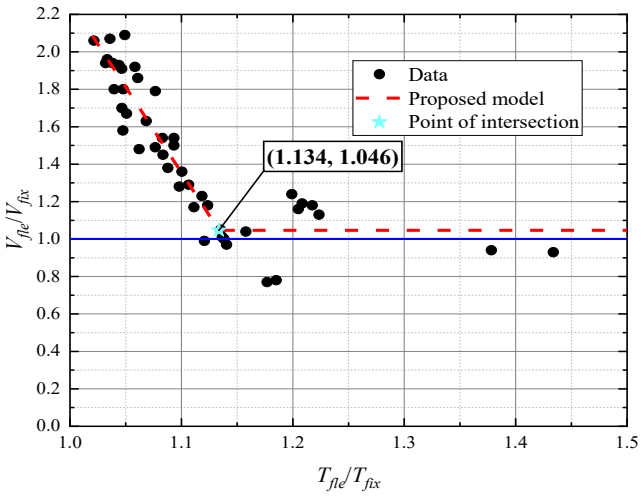

(b)

Figure 4.63 The relationship between T_{fle}/T_{fix} and V_{fle}/V_{fix} (a) classical compensated foundation structure (b) piled foundation structure

Moreover, straight line fittings were also performed on the descending sections in Figure 4.63. The fitting results of the classical compensated foundation structure (Equation 4.1) and piled foundation structure (Equation 4.2) are as follows, respectively:

$$V_{fle}/V_{fix}=11.0967-9.2024\ (T_{fle}/T_{fix}) \quad (4.1)$$

$$V_{fle}/V_{fix}=11.4066-9.1381\ (T_{fle}/T_{fix}) \quad (4.2)$$

The strong negative correlation between the variables is supported by the high linear correlation coefficients r=-0.9111 and -0.8811 for the classical compensated and piled foundation structures, respectively. Thus, designers can conveniently determine the V_{fle} value of high-rise frame-core tube structures by calculating V_{fix} and T_{fle}/T_{fix}, eliminating the need for laborious numerical computations during the design process. Furthermore, previous studies have proposed empirical formulas for the calculation of T_{fle}, which are available in Balkaya et al. (2012) and Renzi et al. (2013).

4.4 Summary

To comprehensively evaluate the effects of SSI on the seismic behaviour of high-rise frame-core tube structures, this chapter examines the impact of various superstructure and substructure parameters, such as HWR, foundation type, soil type, and BD, on 20-, 30-, and 40-storey buildings. The findings of numerical simulation including Δ, foundation rocking, inter-storey drifts and storey shear forces of fixed base cases and flexible base structures are obtained and compared to identify the positive and negative influence of SSI. The following conclusions can be drawn:

- In comparison to structures modeled with a rigid base, those modeled with a flexible base incorporating subsoil effects exhibit amplified Δ and inter-storey drifts to varying degrees, irrespective of factors such as HWR, foundation type, soil type, and BD. This highlights the significance of considering SSI in the

design process, as neglecting SSI effects may lead to underestimation of the structural response under seismic loading.

- The inter-storey drifts resulting from both near-field and far-field earthquakes have been found to exceed 1.5% in many cases, indicating that the seismic performance of structures may be altered by SSI. Thus, traditional design approaches that do not account for SSI may be inadequate in ensuring the safety of high-rise frame-core tube structures. This highlights the importance of incorporating SSI considerations in the design process to adequately assess and mitigate seismic risk.

- The use of piled foundations can effectively mitigate foundation rocking in comparison to classical compensated foundations. However, in many cases, the Δ of piled foundation models are the largest, particularly under the influence of near-field earthquakes. This can be explained by the fact that the shear forces in piled foundation structures are typically greater than those in both compensated foundation and fixed base structures. Therefore, while piled foundations may offer advantages over classical compensated foundations, their performance under seismic loading conditions should be carefully evaluated, and appropriate design measures should be implemented to ensure structural safety.

- When the superstructure parameters are held constant, the influence of soil type on the deformation of pile foundation structures is relatively minor, whereas it has a significant impact on classical compensated foundation structures, particularly in response to far-field earthquakes. Thus, the seismic performance of pile foundation structures is less vulnerable to variations in soil type when compared to classical compensated foundation structures. This suggests that incorporating piled foundations into the design of structures in seismically active regions may offer advantages in terms of reducing the impact of soil variability on structural response.

- The use of stiff soil can significantly limit foundation rocking, and this effect is particularly pronounced in classical compensated foundation-supported models. In cases where classical compensated foundations are built on soft soils, the lateral deflection resulting from foundation rocking constitutes a substantial portion of the total lateral deflection. Therefore, when designing structures with classical compensated foundations, attention should be given to soil properties to ensure that adequate stiffness is maintained to minimise the impact of foundation rocking on structural response.

- Incorporating SSI into structural analysis may result in either an increase or a decrease in the base shear of the structure, depending on the type of foundation and soil. As a consequence, increasing the stiffness of the foundation and subsoil without proper consideration of SSI effects may not necessarily enhance structural safety or economic efficiency, as it could lead to the excessive absorption of seismic energy. Therefore, SSI should be carefully evaluated in the design process to ensure that design measures are appropriately balanced to optimise both structural safety and economic efficiency.

- The displacement response of structures exhibits opposite trends under the action of different types of earthquakes. Therefore, the change in Δ and inter-storey drifts resulting from decreasing soil stiffness depends on the earthquake characteristics. Specifically, the impact of decreasing soil stiffness on structural response varies between near-field and far-field earthquakes and should be evaluated accordingly in the design process to ensure the appropriate selection of design measures for different earthquake scenarios.

- Irrespective of the foundation type, an increase in V_s of the subsoil can substantially increase the value of V_{fle}/V_{fix} for structures. Conversely, the HWR and BD have a relatively minor impact on this value. Therefore, in seismically active regions where the soil conditions vary, it is important to consider the V_s of

the subsoil in the design process to optimise the seismic performance of structures.

- The impact of substructure parameters on the value of $\delta_{fle}/\delta_{fix}$ is complex and multifaceted. In general, the increase of Δ_θ/Δ_t can amplify the inter-storey drifts and reduce the base shear of high-rise frame-core tube structures. Therefore, when designing structures with high-rise frame-core tube structures, it is essential to consider the effect of substructure parameters on $\delta_{fle}/\delta_{fix}$ to ensure that the design measures are appropriately balanced to optimise structural performance.

- The analysis conducted in this paper shows that SSI amplifies the value of $\delta_{fle}/\delta_{fix}$ for almost all cases studied. As a result, the effect of SSI is generally detrimental to the inter-storey drifts of high-rise buildings. Therefore, when designing high-rise buildings, it is crucial to take into account the potential impact of SSI.

- The findings of this study indicate that SSI amplifies the value of V_{fle}/V_{fix} for piled foundation structures and classical compensated foundation structures supported by C_e soil. However, for classical compensated foundation structures supported by D_e and E_e soil types, the effects of SSI are beneficial, as the value of V_{fle}/V_{fix} is reduced. These results highlight the need for a comprehensive evaluation of the potential impact of SSI on different types of foundation systems to ensure that the design measures adopted effectively address the specific requirements of each case.

- As the ratio of T_{fle}/T_{fix} increases, the value of V_{fle}/V_{fix} decreases linearly until it reaches a minimum value of 0.395 for classical compensated foundation structures or 1.046 for piled foundation structures. Beyond this point, the value of V_{fle}/V_{fix} remains constant. Based on these findings, current seismic codes may specify different minimum values of reduced shear force for different types of foundations to ensure adequate seismic performance of structures under different loading conditions.

Chapter 5 PARAMETRIC STUDIES ON FRAME-SHEAR WALL STRUCTURES

5.1 Introduction

In this chapter, a numerical simulation model previously developed and validated in Chapter 3 is utilised to comprehensively assess the effects of SSI on high-rise frame-shear wall structures, similar to the approach employed in Chapter 4. The study considers the same superstructure and substructure parameters to achieve the objective of improving understanding of the earthquake response of high-rise frame-shear wall structures. Through the analysis of numerous cases, both advantageous and disadvantageous scenarios for high-rise frame-shear wall structures subjected to SSI are identified. The findings of this study contribute to the development of code-based procedures that provide a safe and cost-effective structural design method.

5.2 Overview of the Frame-shear Wall Structure-Soil Numerical Model

This study considers frame-shear wall buildings with three different structural heights: 60m (20-storey), 90m (30-storey), and 120m (40-storey), each with three different HWRs of 4, 5, and 6 and three different BDs of 10m, 20m, and 30m. The arrangement of shear walls and columns is illustrated in Figure 5.1 (a). To comply with AS 1170.4 (2007), three soil types (C_e, D_e, and E_e) are adopted, and their geotechnical properties are presented in Table 4.2 (Tabatabaiefar and Fatahi 2014). Additionally, both end bearing piled foundation and classical compensated foundation (Figure 5.1 b and c) are taken into account. The arrangement and dimensions of piles for buildings of different heights, HWRs, and BDs are shown in Figure 4.3 and Table 4.3. For each model, two far-field and two near-field earthquake motions (Figure 4.2) are applied. Consequently, a total of 36 rigid base structures, excluding SSI effects, and 360 flexible base structures, including SSI effects, are evaluated in this chapter.

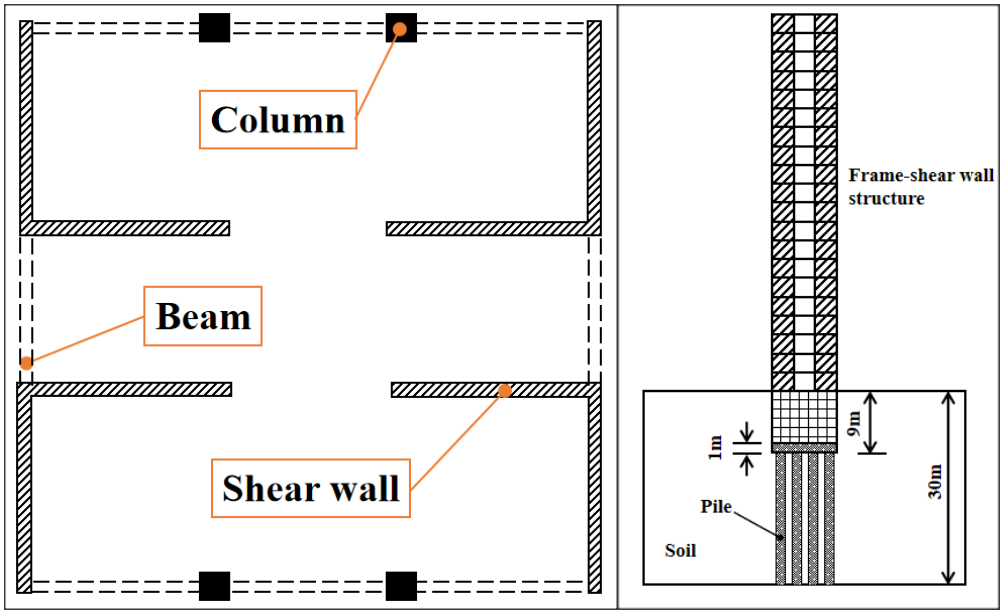

(a) (b)

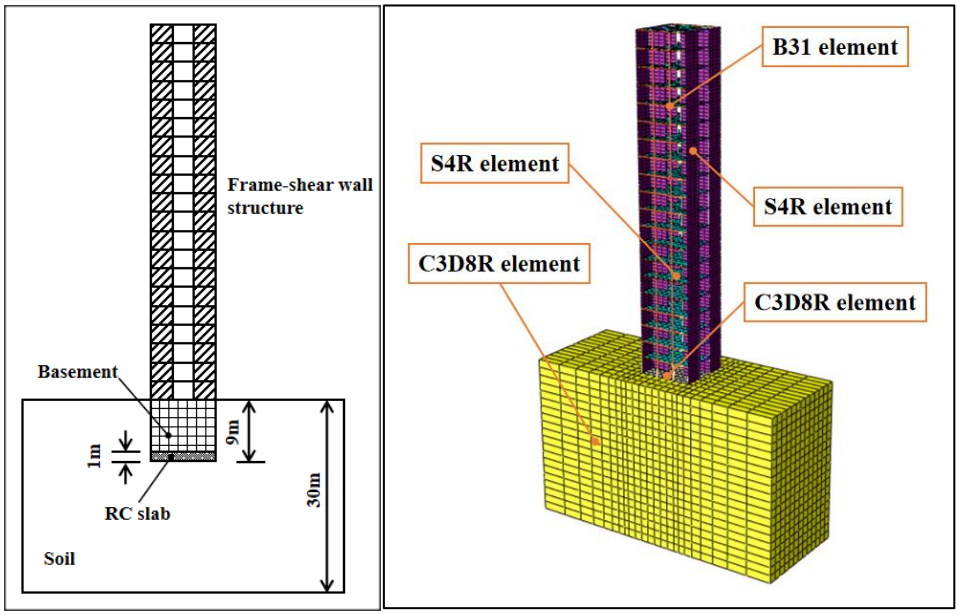

(c) (d)

Figure 5.1 Soil-structure model (a) plan view of the standard storey of the superstructure (b) end bearing piled foundation-supported structure (c) classical compensated foundation-supported structure (d) the finite-element model

The design of the structural sections was carried out utilising SAP2000 V 20 software in accordance with AS3600 (2018) and AS1170.4 (2007) standards. The f'_c, E_c, and unit weight of concrete were specified as 40 MPa, 32.8 GPa, and 24.5 kN/m^3,

respectively. To ensure the δ of all rigid base models were less than 1.5%, nonlinear time-history analyses were conducted using the earthquake records provided in Figure 4.2. Table 5.1 illustrates the dimensions of shear walls, columns, beams, and slabs for structures with varying heights. For the purpose of comparison, the frame-shear wall structures with different HWRs adopted the same component dimensions. After the determination of model parameters and the completion of fixed base structure design, the numerical simulation method introduced in Chapter 3 is employed for the parametric study of high-rise frame-shear wall structures.

Table 5.1 Summary of dimensions of structural beams, columns and thickness of slabs and shear walls (m)

Structures	Levels	Columns	Beams	Shear walls	Slabs
20-storey	1~5	0.55×0.55	0.40×0.40	0.55	0.25
	6~10	0.50×0.50	0.40×0.40	0.50	0.25
	11~15	0.45×0.45	0.40×0.40	0.45	0.25
	16~20	0.40×0.40	0.40×0.40	0.40	0.25
30-storey	1~10	0.70×0.70	0.50×0.50	0.70	0.25
	11~20	0.60×0.60	0.50×0.50	0.60	0.25
	21~30	0.50×0.50	0.50×0.50	0.50	0.25
40-storey	1~10	1.00×1.00	0.50×0.80	0.80	0.25
	11~20	0.90×0.90	0.50×0.80	0.70	0.25
	21~30	0.80×0.80	0.50×0.80	0.60	0.25
	31~40	0.70×0.70	0.50×0.80	0.50	0.25

5.3 Results and Discussions

5.3.1 Lateral Deflection

Figures 5.2 to 5.16 depict the Δ of 20-, 30-, and 40-storey frame-shear wall structures with varying structural heights, HWRs, foundation types, soil types, and BDs, under both rigid base and flexible base conditions. It is noteworthy that the lateral deflections of flexible base structures are significantly greater than those of rigid base structures. This is because the degree of freedom of the soil-structure system increases after considering SSI and the natural period is prolonged, and the displacement response

spectrum curve generally increases with the increase of the natural period of the system. Consequently, high-rise frame-shear wall buildings experience amplified displacement response.

Furthermore, similar to frame-core tube structures, the lateral deflection values of piled foundation models do not exhibit significant variations with changes in soil type. In contrast, classical compensated foundation models show remarkable variations in lateral deflection values, particularly during far-field earthquakes. Additionally, it can be observed that under near-field earthquakes, the lateral deflection values of piled foundation models are not substantially reduced compared to the classical compensation foundation model and may even increase in certain cases. Hence, the presence of a piled foundation does not necessarily guarantee a reduction in lateral deflections for structures, as it can absorb a greater amount of inertial energy while decreasing foundation rotation (Van Nguyen et al. 2017).

The impact of HWR on the Δ is complex. On the one hand, a wider building can enhance structural stability and decrease foundation rotation. However, a wider building also means greater mass, leading to increased inertial force and structural distortion during seismic excitations. Therefore, changes in HWR may result in varying patterns of Δ. Moreover, the effects of HWR and BD do not appear to be as significant as those of other superstructure and substructure parameters.

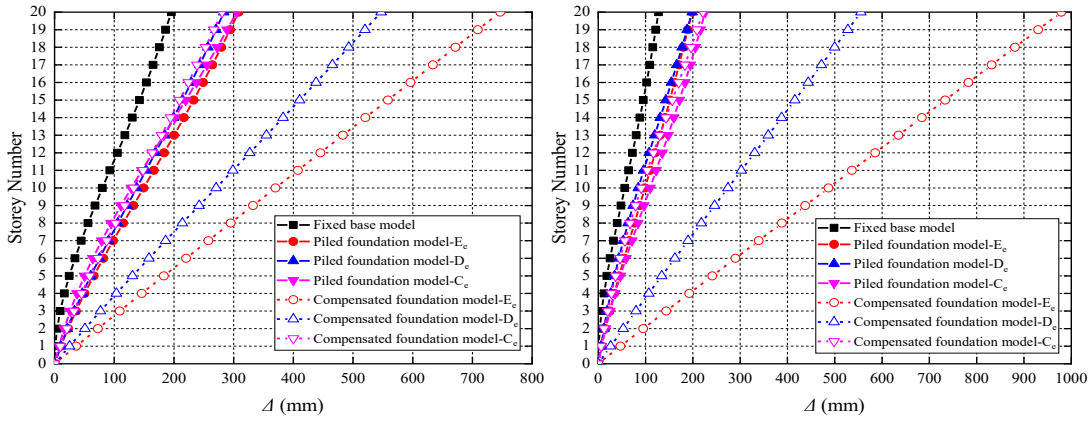

(a) El Centro (b) Hachinohe

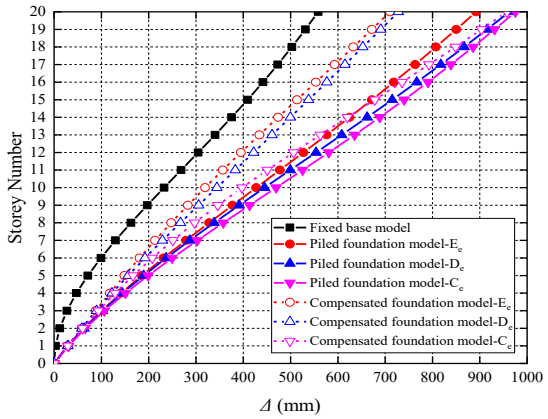

(c) Kobe

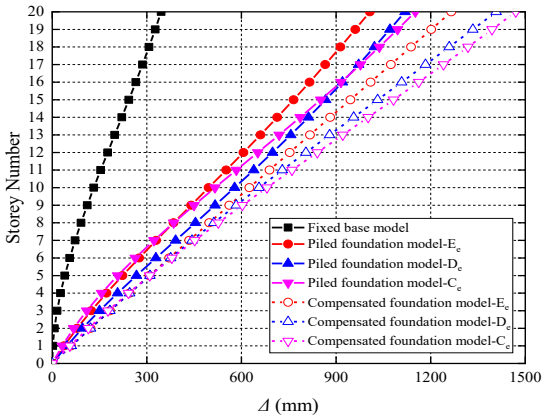

(d) Northridge

Figure 5.2 Lateral deflections of 20-storey structure (HWR=6, BD=30) under the four seismic records

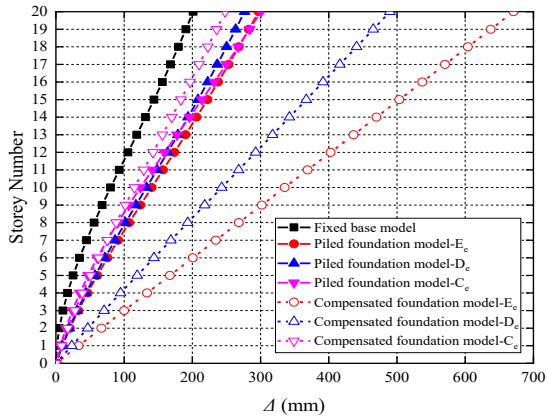

(a) El Centro

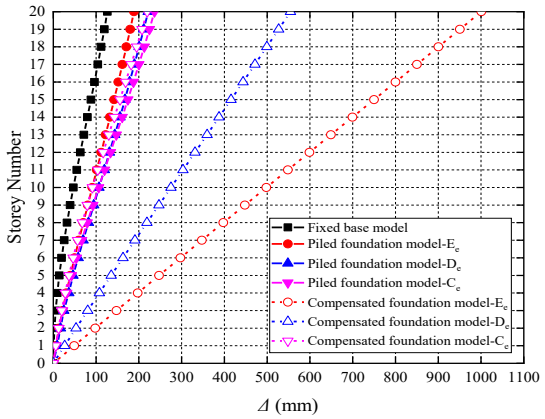

(b) Hachinohe

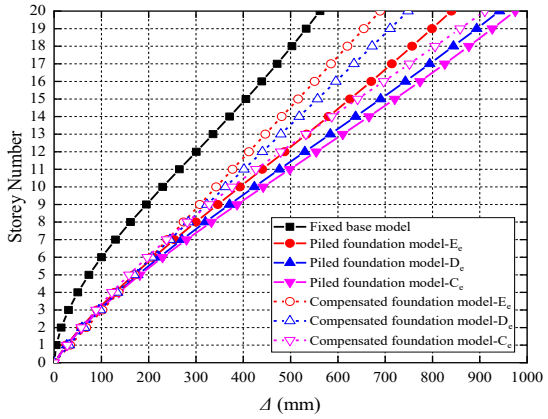

(c) Kobe

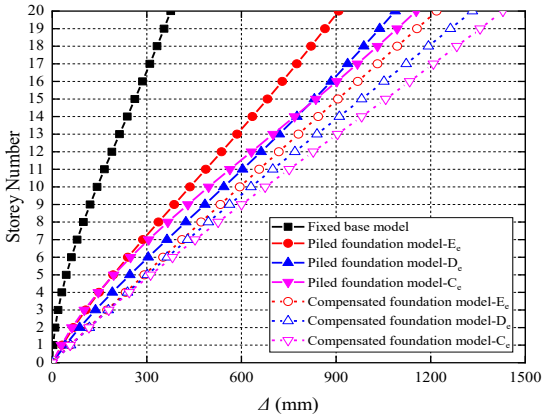

(d) Northridge

Figure 5.3 Lateral deflections of 20-storey structure (HWR=5, BD=30) under the four seismic records

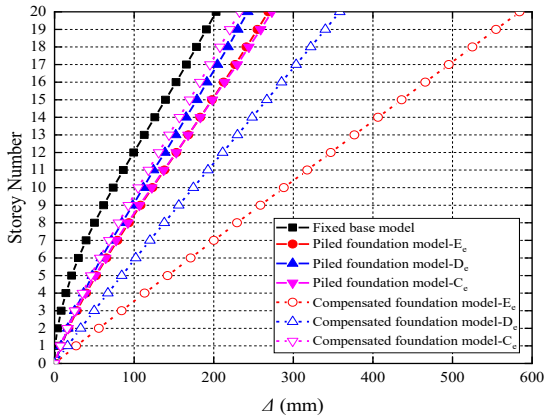

(a) El Centro

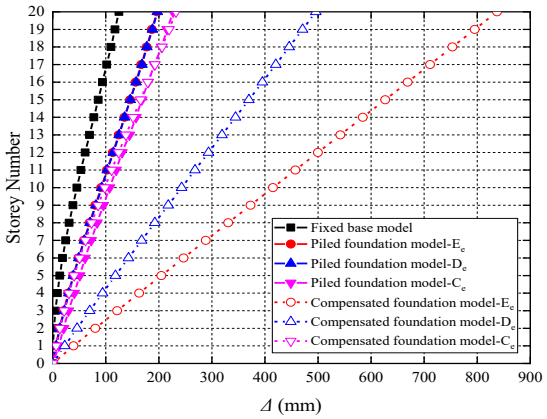

(b) Hachinohe

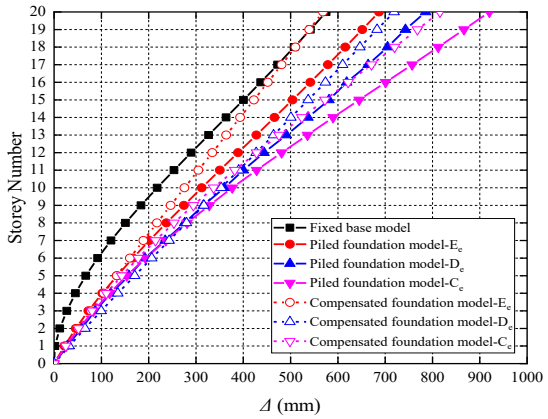

(c) Kobe

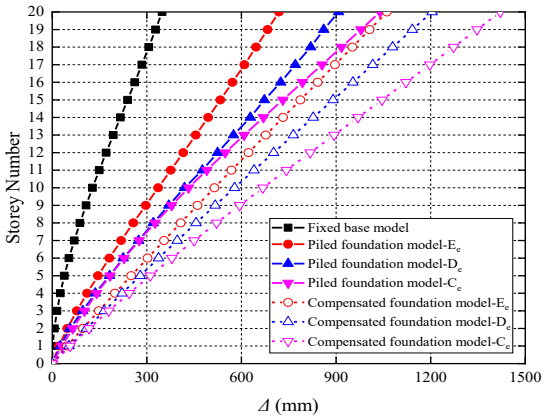

(d) Northridge

Figure 5.4 Lateral deflections of 20-storey structure (HWR=4, BD=30) under the four seismic records

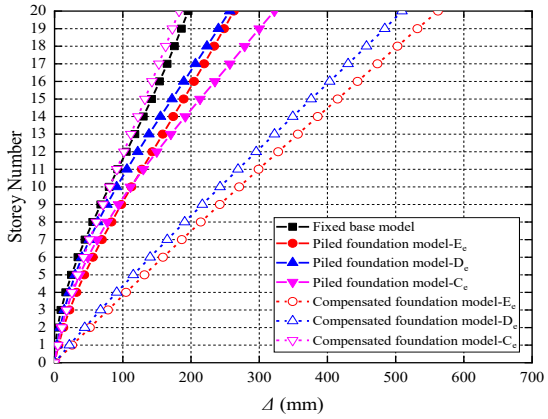

(a) El Centro

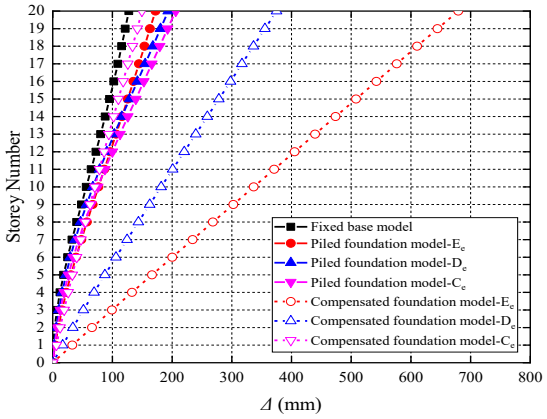

(b) Hachinohe

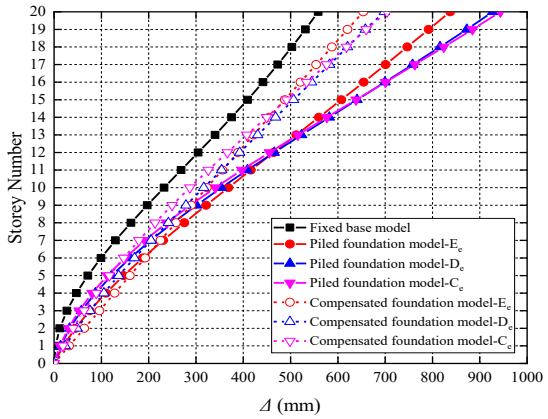

(c) Kobe

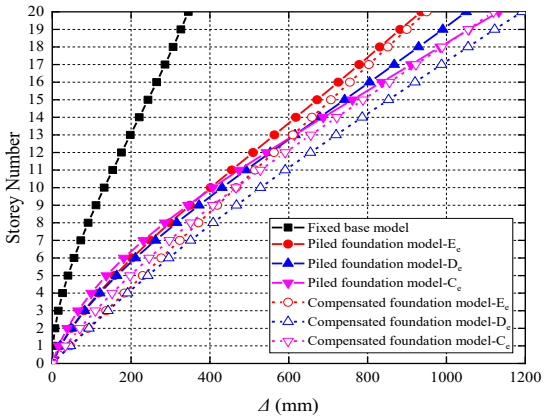

(d) Northridge

Figure 5.5 Lateral deflections of 20-storey structure (HWR=6, BD=20) under the four seismic records

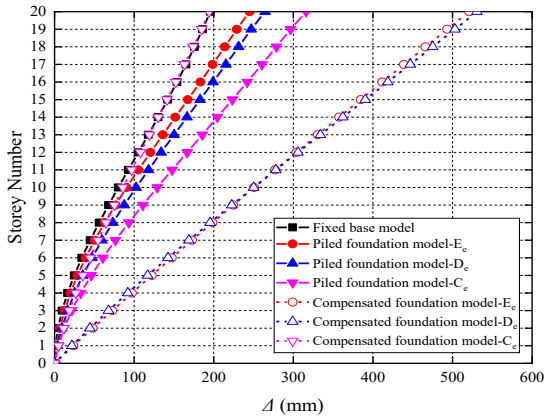

(a) El Centro

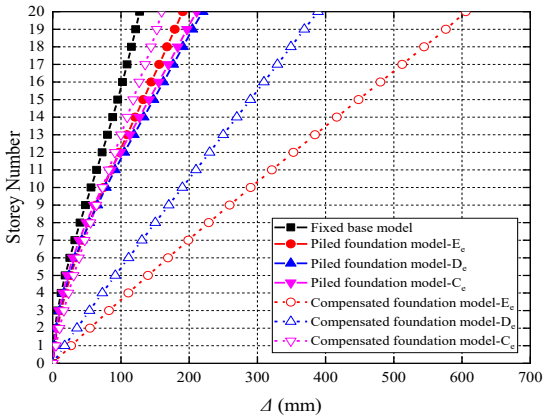

(b) Hachinohe

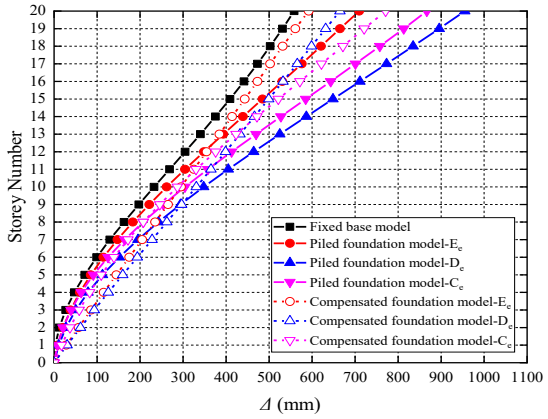

(c) Kobe

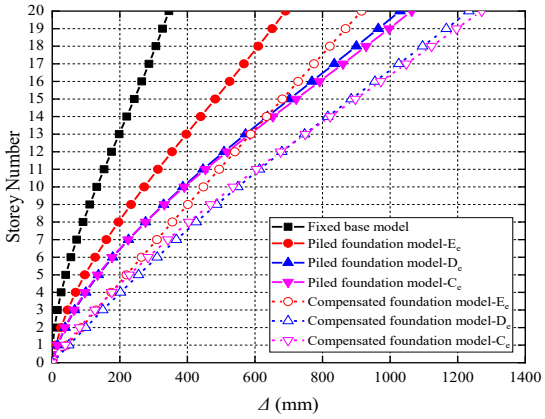

(d) Northridge

Figure 5.6 Lateral deflections of 20-storey structure (HWR=6, BD=10) under the four seismic records

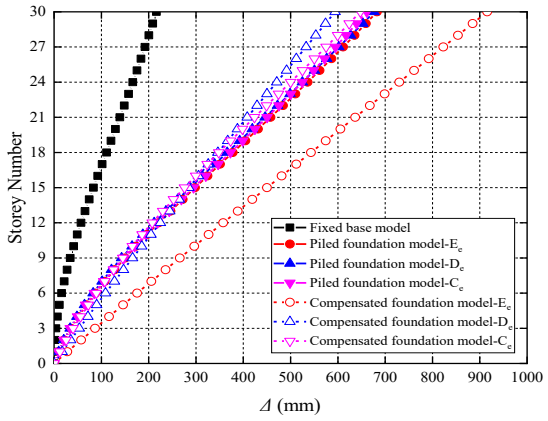

(a) El Centro

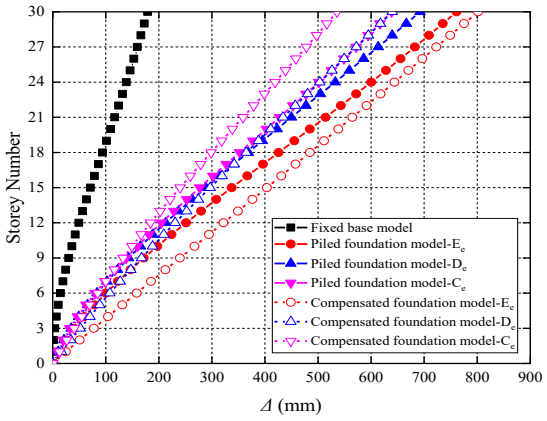

(b) Hachinohe

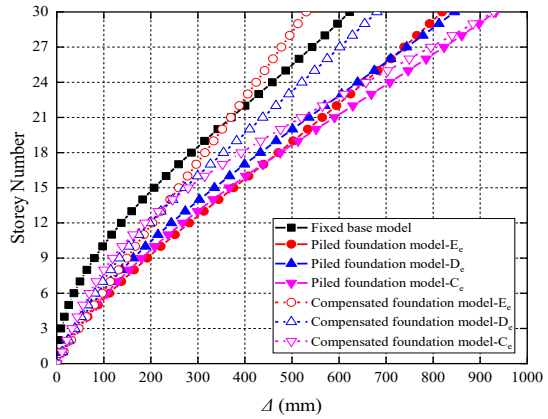

(c) Kobe

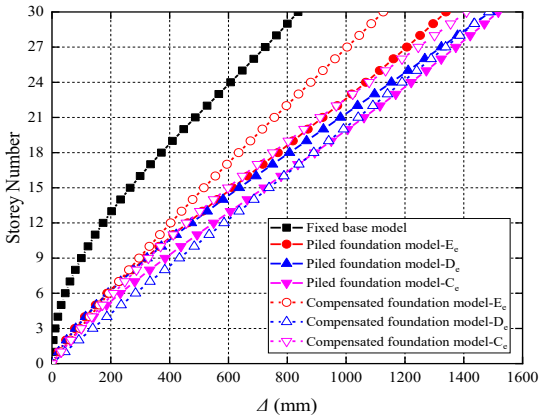

(d) Northridge

Figure 5.7 Lateral deflections of 30-storey structure (HWR=6, BD=30) under the four seismic records

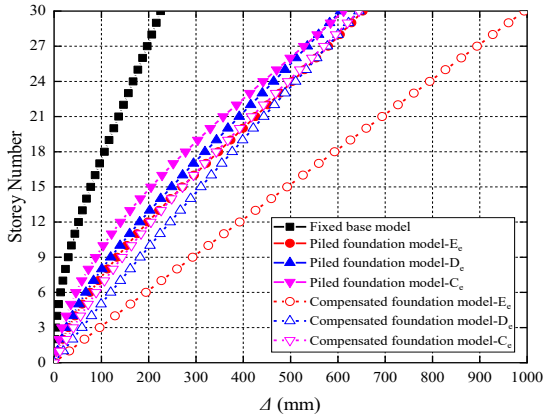

(a) El Centro

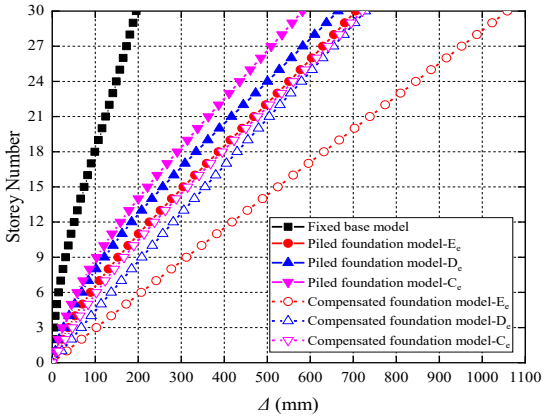

(b) Hachinohe

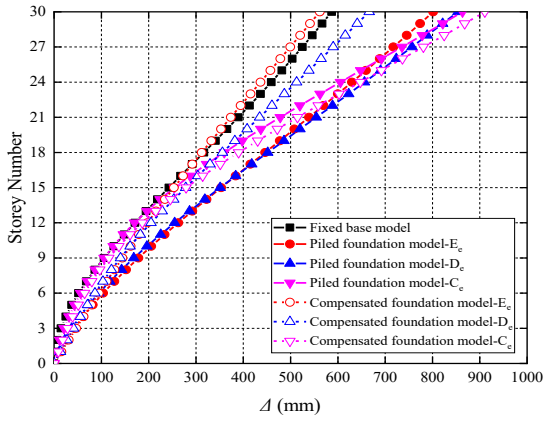

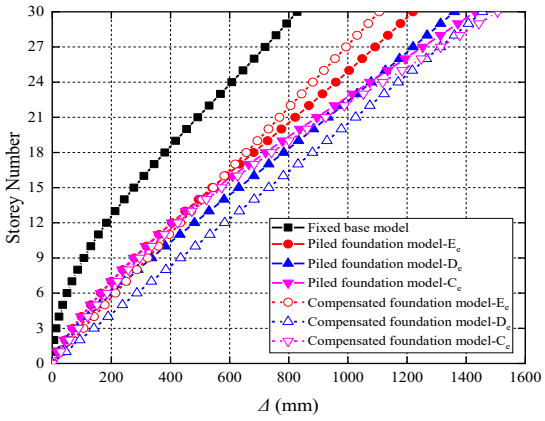

(c) Kobe (d) Northridge

Figure 5.8 Lateral deflections of 30-storey structure (HWR=5, BD=30) under the four seismic records

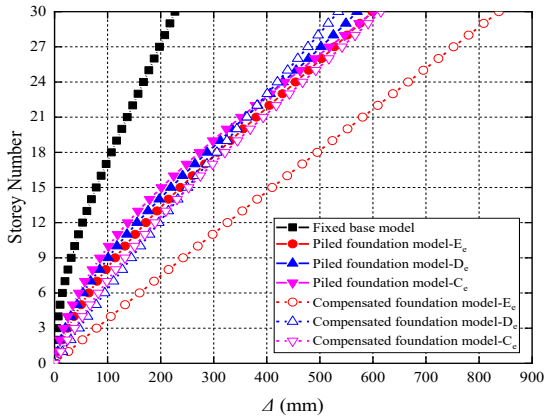

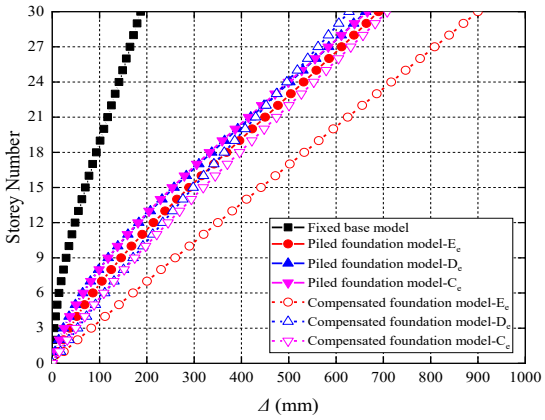

(a) El Centro (b) Hachinohe

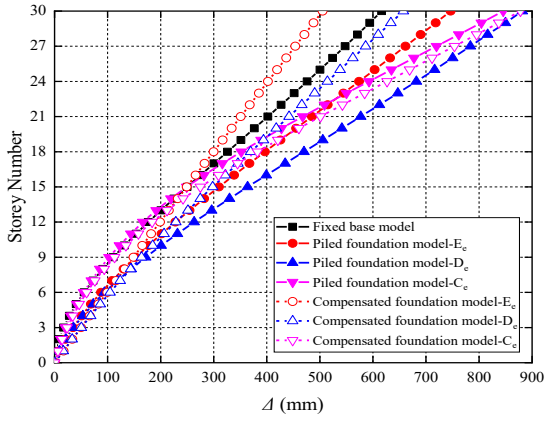

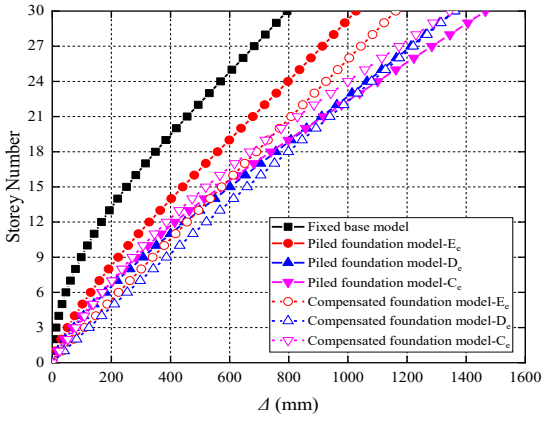

(c) Kobe (d) Northridge

Figure 5.9 Lateral deflections of 30-storey structure (HWR=4, BD=30) under the four seismic records

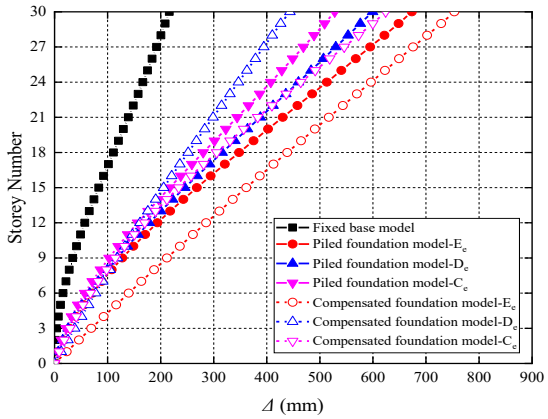

(a) El Centro

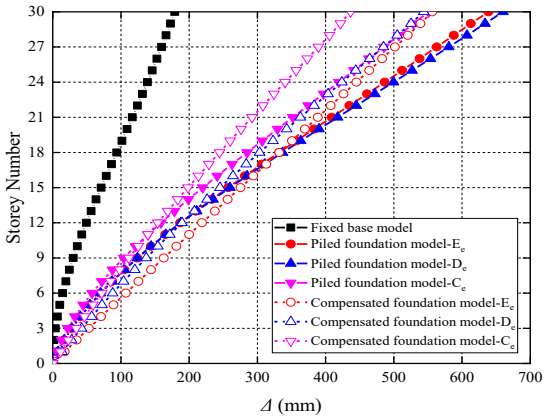

(b) Hachinohe

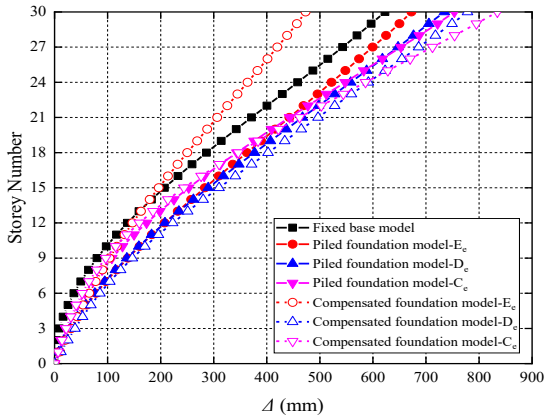

(c) Kobe

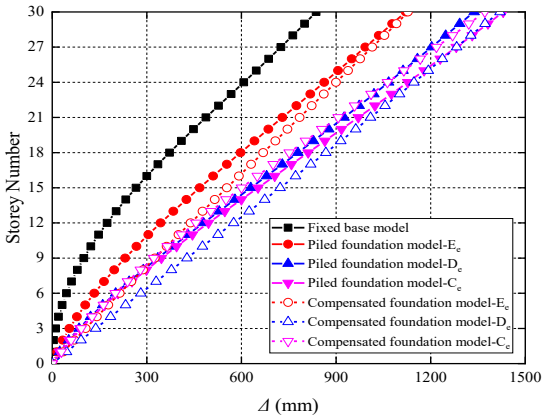

(d) Northridge

Figure 5.10 Lateral deflections of 30-storey structure (HWR=6, BD=20) under the four seismic records

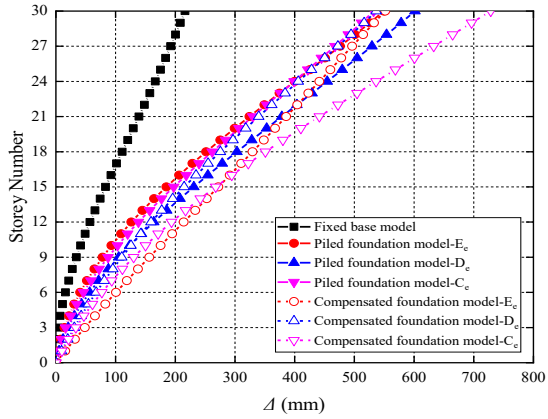

(a) El Centro

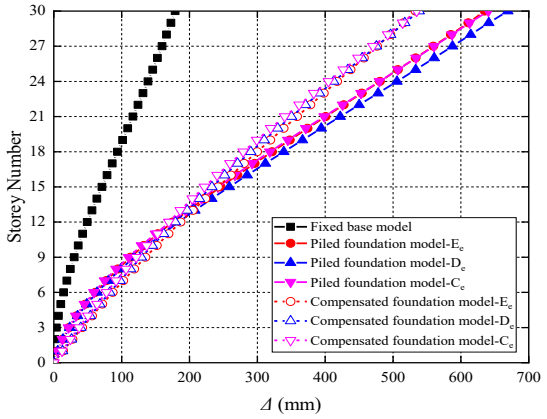

(b) Hachinohe

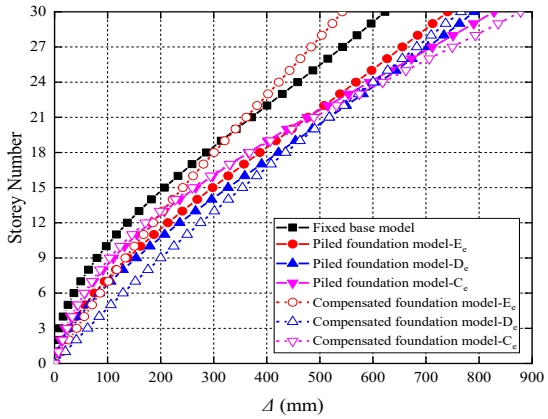

(c) Kobe

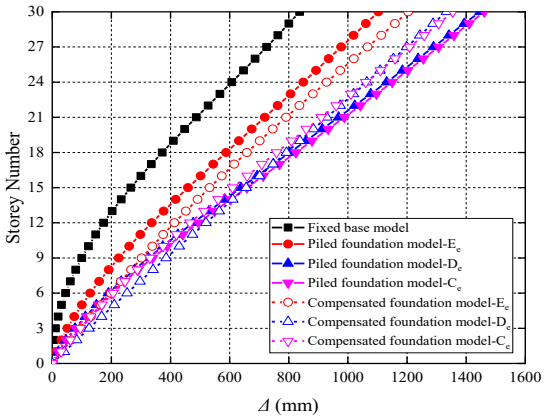

(d) Northridge

Figure 5.11 Lateral deflections of 30-storey structure (HWR=6, BD=10) under the four seismic records

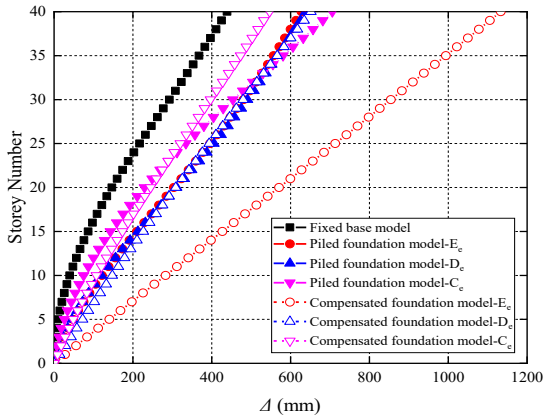

(a) El Centro

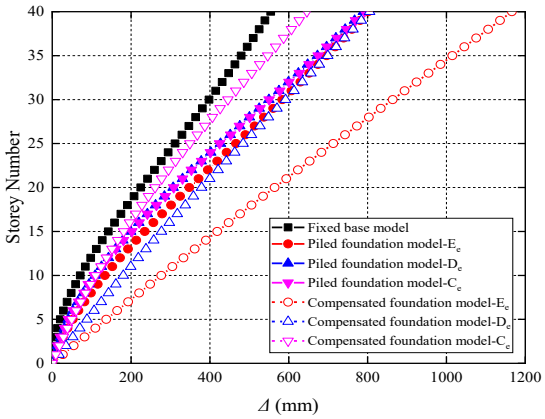

(b) Hachinohe

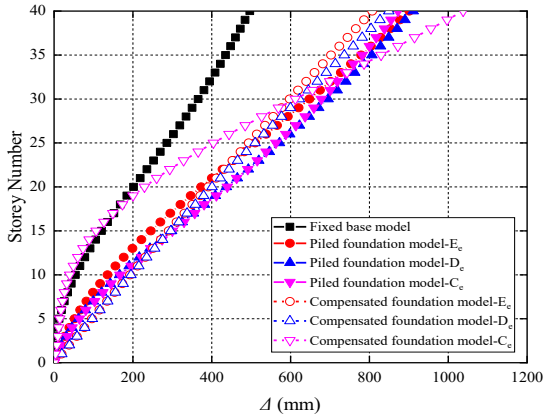

(c) Kobe

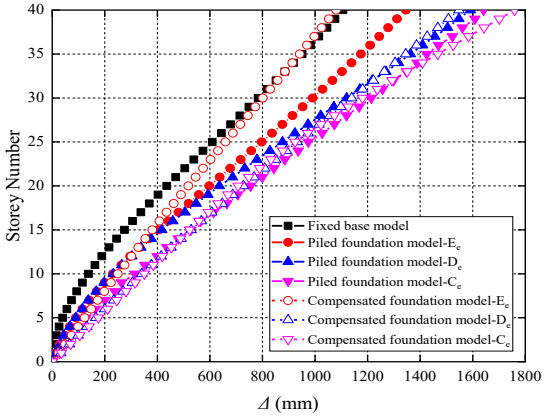

(d) Northridge

Figure 5.12 Lateral deflections of 40-storey structure (HWR=6, BD=30) under the four seismic records

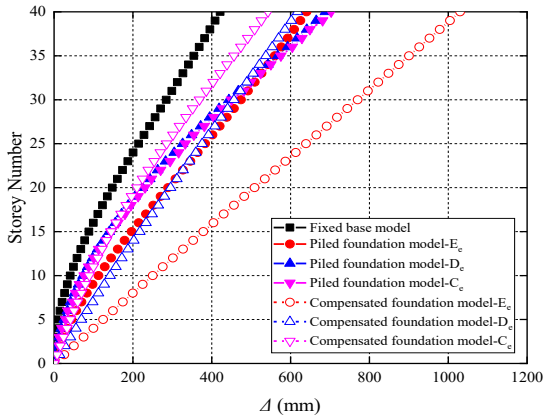

(a) El Centro

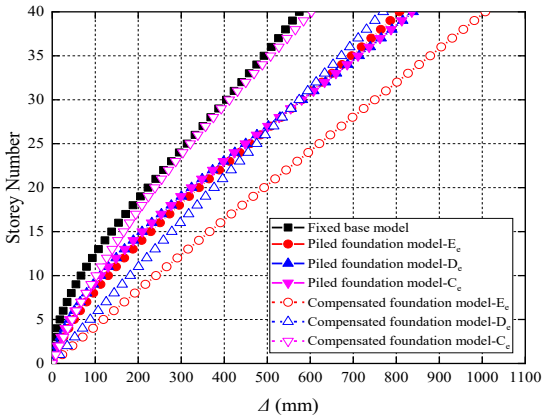

(b) Hachinohe

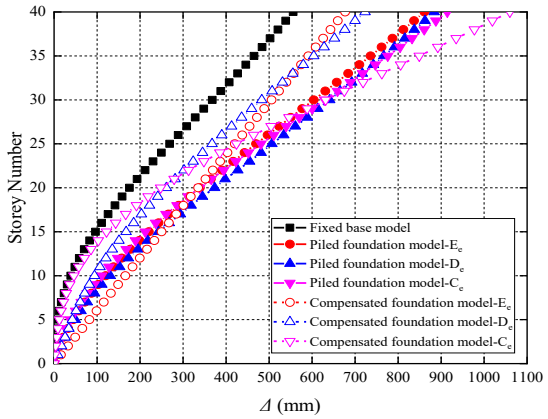

(c) Kobe

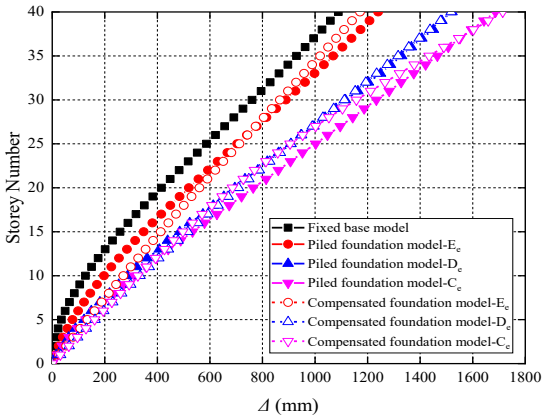

(d) Northridge

Figure 5.13 Lateral deflections of 40-storey structure (HWR=5, BD=30) under the four seismic records

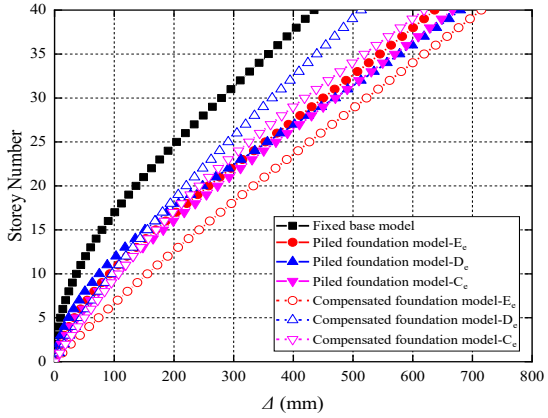

(a) El Centro

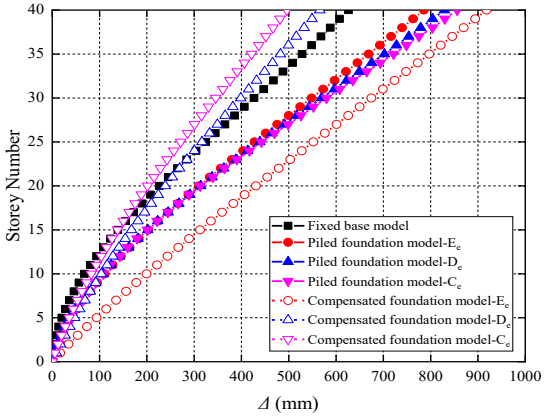

(b) Hachinohe

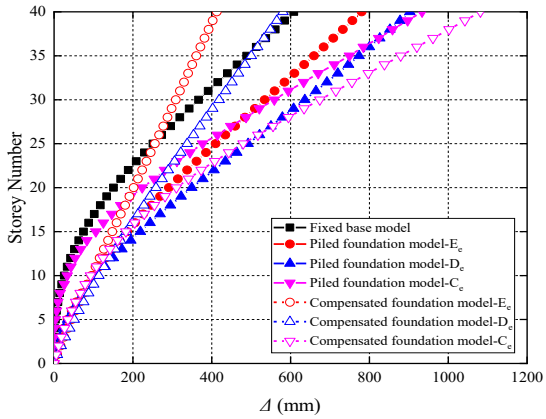

(c) Kobe

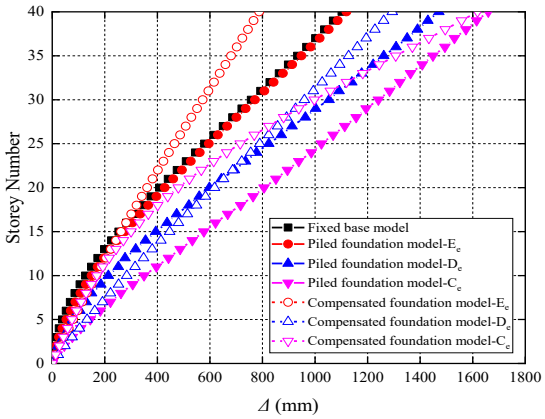

(d) Northridge

Figure 5.14 Lateral deflections of 40-storey structure (HWR=4, BD=30) under the four seismic records

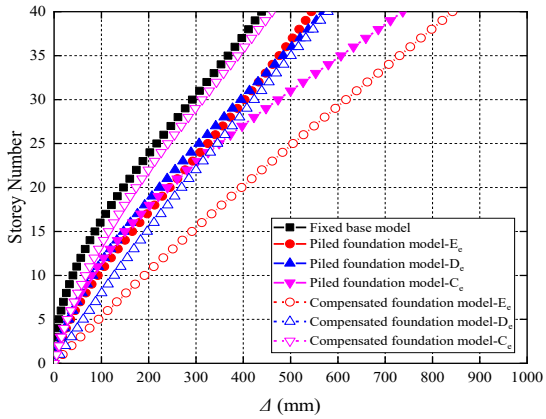

(a) El Centro

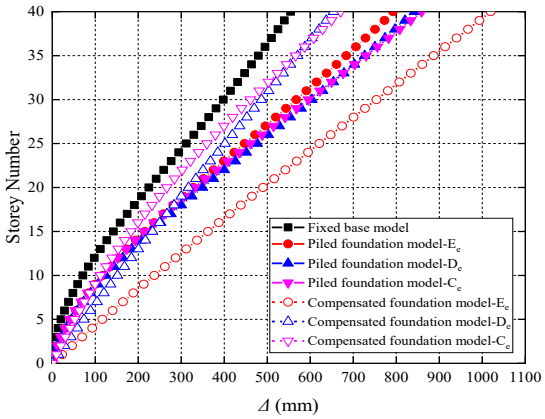

(b) Hachinohe

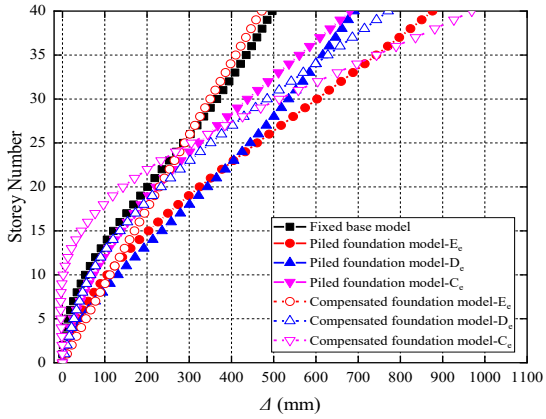

(c) Kobe

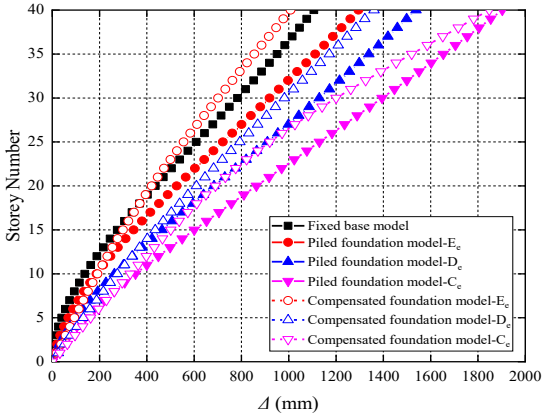

(d) Northridge

Figure 5.15 Lateral deflections of 40-storey structure (HWR=6, BD=20) under the four seismic records

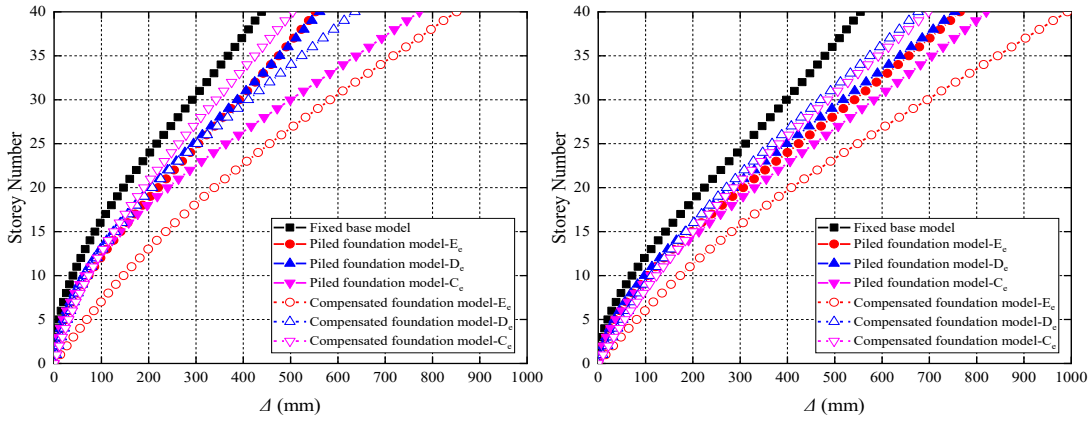

(a) El Centro (b) Hachinohe

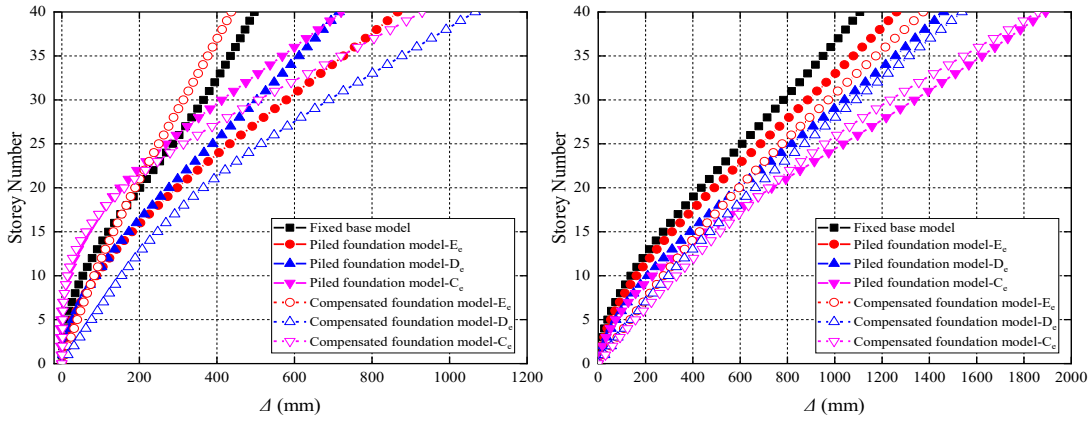

(c) Kobe (d) Northridge

Figure 5.16 Lateral deflections of 40-storey structure (HWR=6, BD=10) under the four seismic records

5.3.2 Foundation Rocking

Tables 5.2, 5.3, 5.4, 5.5, 5.6, and 5.7 present the proportion of foundation rocking-induced lateral deflection (Δ_θ) in the total deflection of the top floor (Δ_t) for 20-, 30-, and 40-story buildings with varying foundation types, soil types, HWRs, and BDs. The width of the structure appears to have minimal impact on the rotation of the building, while the soil type can significantly restrain foundation rocking. This effect is particularly evident in classical compensated foundation-supported structures. Similarly, pile foundations can effectively reduce foundation rotation. For classical compensated foundation structures on E_e soils, foundation rotation-induced

displacement accounts for over 90% of the total displacement, suggesting a greater likelihood of overall building rotation. In contrast, this proportion for piled foundation models is typically less than 40% and decreases notably with a decrease in BD due to the increased stiffness of the piles. However, as discussed in Section 5.2.1, although end-bearing piled foundations can effectively reduce foundation rocking, the Δ of piled foundation structures are not always smaller than those of classical compensated foundation structures. Furthermore, in comparison to frame-core tube structures, the value of Δ_θ/Δ_t for frame-shear wall structures increases slightly because these structures, with the same height and HWR, are heavier and induce more inertial force during earthquake events.

Table 5.2 The proportion of lateral deflection caused by foundation rocking (Δ_θ/Δ_t) of 20-storey structures with different HWRs (%)

HWR	Earthquake record	Piled foundation model			Compensated foundation model		
		E_e soil	D_e soil	C_e soil	E_e soil	D_e soil	C_e soil
6	El Centro	39.66	36.89	17.93	96.80	89.93	45.06
	Hachinohe	41.17	31.97	22.07	97.15	92.03	34.69
	Kobe	39.73	36.46	21.68	85.64	79.57	55.49
	Northridge	43.43	42.11	19.25	97.26	86.76	61.77
5	El Centro	38.38	36.11	15.39	98.26	91.56	44.98
	Hachinohe	40.00	39.17	16.95	97.15	92.89	35.69
	Kobe	39.55	34.38	20.73	98.65	84.46	56.99
	Northridge	44.11	42.16	18.29	95.19	88.59	68.86
4	El Centro	32.19	30.43	14.32	96.42	88.15	43.33
	Hachinohe	31.73	29.87	15.15	95.73	88.69	36.48
	Kobe	33.85	30.95	18.64	92.91	88.57	57.74
	Northridge	37.02	33.28	16.83	94.41	90.93	71.81

Table 5.3 The proportion of lateral deflection caused by foundation rocking (Δ_θ/Δ_t) of 20-storey structures with different BDs (%)

BD	Earthquake record	Piled foundation model			Compensated foundation model		
		E_e soil	D_e soil	C_e soil	E_e soil	D_e soil	C_e soil
30	El Centro	39.66	36.89	17.93	96.80	89.93	45.06
	Hachinohe	41.17	31.97	22.07	97.15	92.03	34.69
	Kobe	39.73	36.46	21.68	85.64	79.57	55.49
	Northridge	19.49	16.20	9.19	94.29	88.55	44.69
20	El Centro	25.91	15.31	14.55	95.39	92.79	48.93
	Hachinohe	21.15	18.41	16.91	96.63	86.50	54.91
	Kobe	22.39	20.65	9.01	96.87	87.26	62.52
	Northridge	10.25	9.63	4.25	92.73	86.37	42.39
10	El Centro	8.49	9.87	5.72	88.97	91.23	38.63
	Hachinohe	9.73	9.85	2.71	92.21	69.59	53.49
	Kobe	9.59	5.46	3.18	94.31	85.83	61.10
	Northridge	19.49	16.20	9.19	94.29	88.55	44.69

Table 5.4 The proportion of lateral deflection caused by foundation rocking (Δ_θ/Δ_t) of 30-storey structures with different HWRs (%)

HWR	Earthquake record	Piled foundation model			Compensated foundation model		
		E_e soil	D_e soil	C_e soil	E_e soil	D_e soil	C_e soil
6	El Centro	25.49	21.94	14.98	94.14	87.85	47.04
	Hachinohe	26.63	20.73	14.89	94.82	79.01	71.71
	Kobe	25.98	22.87	17.39	92.38	64.97	41.69
	Northridge	27.21	22.36	15.62	87.10	93.14	64.80
5	El Centro	23.21	22.2	12.04	95.22	89.06	47.89
	Hachinohe	24.59	23.58	11.66	95.56	89.15	51.33
	Kobe	24.53	23.56	15.97	84.05	70.26	35.75
	Northridge	24.65	24.43	15.44	96.53	96.67	58.57
4	El Centro	20.69	20.17	11.64	92.84	84.20	52.50
	Hachinohe	22.30	19.24	10.96	93.97	78.70	54.81
	Kobe	21.87	18.67	14.61	97.24	77.27	23.42
	Northridge	22.89	19.70	13.74	97.05	91.32	60.47

Table 5.5 The proportion of lateral deflection caused by foundation rocking (Δ_θ/Δ_t) of 30-storey structures with different BDs (%)

BD	Earthquake record	Piled foundation model			Compensated foundation model		
		E_e soil	D_e soil	C_e soil	E_e soil	D_e soil	C_e soil
30	El Centro	25.49	21.94	14.98	94.14	87.85	47.04
	Hachinohe	26.63	20.73	14.89	94.82	79.01	71.71
	Kobe	25.98	22.87	17.39	92.38	64.97	41.69
	Northridge	27.21	22.36	15.62	87.10	93.14	64.80
20	El Centro	23.78	20.03	12.11	91.83	77.67	46.52
	Hachinohe	28.89	22.51	11.21	91.30	61.91	66.63
	Kobe	22.99	21.61	15.45	94.10	67.11	40.73
	Northridge	26.23	22.08	11.92	89.51	89.01	66.97
10	El Centro	22.21	20.19	8.79	86.75	56.49	47.21
	Hachinohe	23.82	21.29	7.27	73.22	68.84	64.07
	Kobe	28.69	22.53	7.62	84.33	76.57	42.31
	Northridge	29.93	19.00	7.73	87.43	83.81	68.41

Table 5.6 The proportion of lateral deflection caused by foundation rocking (Δ_θ/Δ_t) of 40-storey structures with different HWRs (%)

HWR	Earthquake record	Piled foundation model			Compensated foundation model		
		E_e soil	D_e soil	C_e soil	E_e soil	D_e soil	C_e soil
6	El Centro	24.60	22.48	16.90	96.87	86.07	56.26
	Hachinohe	22.58	23.34	15.11	93.41	84.45	50.21
	Kobe	19.59	21.18	14.81	96.76	92.07	24.05
	Northridge	22.53	24.12	16.61	91.65	85.84	74.97
5	El Centro	21.25	21.98	13.56	92.83	83.77	56.63
	Hachinohe	20.09	21.67	12.82	92.30	86.12	49.37
	Kobe	16.87	14.81	10.96	98.65	63.00	12.43
	Northridge	19.28	16.8	13.16	91.46	85.42	70.72
4	El Centro	15.88	14.93	11.06	81.56	64.88	63.70
	Hachinohe	15.71	15.32	11.22	79.37	61.76	46.07
	Kobe	13.14	11.90	10.39	90.06	67.35	27.05
	Northridge	14.51	13.17	12.68	82.07	82.30	37.05

Table 5.7 The proportion of lateral deflection caused by foundation rocking (Δ_θ/Δ_t) of 40-storey structures with different BDs (%)

BD	Earthquake record	Piled foundation model			Compensated foundation model		
		E_e soil	D_e soil	C_e soil	E_e soil	D_e soil	C_e soil
30	El Centro	24.60	22.48	16.90	96.87	86.07	56.26
	Hachinohe	22.58	23.34	15.11	93.41	84.45	50.21
	Kobe	19.59	21.18	14.81	96.76	92.07	24.05
	Northridge	22.53	24.12	16.61	91.65	85.84	74.97
20	El Centro	22.33	12.09	15.49	91.63	74.01	55.99
	Hachinohe	21.57	21.19	11.15	87.87	74.25	51.85
	Kobe	16.81	14.66	8.25	58.11	88.72	26.09
	Northridge	17.79	13.53	14.49	81.97	84.83	71.33
10	El Centro	8.40	3.75	4.96	76.33	45.93	52.19
	Hachinohe	7.27	5.23	3.83	69.80	68.17	50.80
	Kobe	8.51	7.33	3.31	77.91	68.64	21.37
	Northridge	5.61	3.57	4.41	83.15	81.75	69.77

5.3.3 Inter-storey Drifts

The results presented in Figures 5.17 to 5.31 show the inter-storey drifts of frame-shear wall structures with different HWRs, foundation types, soil types, and BDs under fixed base and flexible base conditions. It is observed that the inter-storey drifts of flexible base cases have increased compared to fixed base cases. For many near-field earthquake cases and some far-field earthquake cases, the values of δ have exceeded 1.5%, indicating an alter in the performance level.

In classical compensated foundation models, the inter-storey drifts exhibit an almost vertical line, indicating that the inter-storey drifts change slightly with the structural height. This suggests the Δ_θ accounts for a significant part of the Δ_t in these models. However, in piled foundation models, inter-storey drifts do not change significantly with soil type when the structural height, HWR, BD, and seismic record are the same.

It is also worth noting that there is a considerable increase in inter-storey drifts for structures resting on C_e soil under near-field earthquakes and structures with compensated foundations resting on E_e soil under far-field earthquakes. This is related

to the difference between the shape of response spectra of near and far earthquakes.

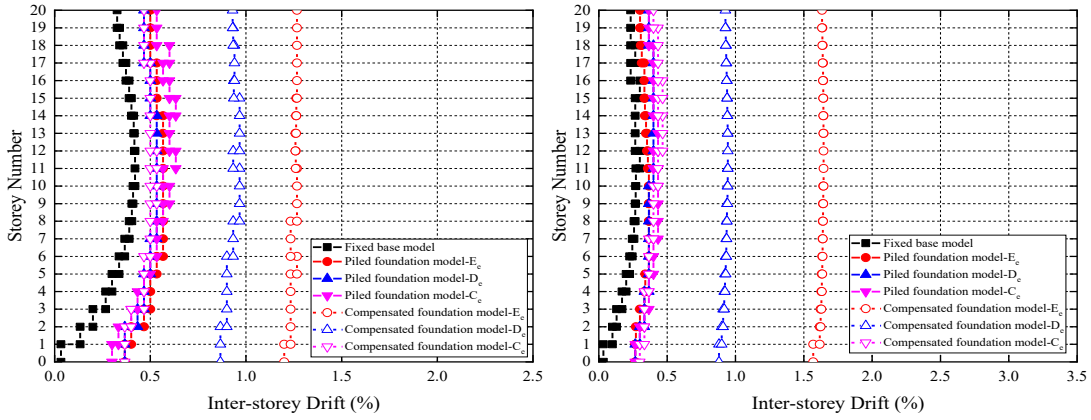

(a) El Centro (b) Hachinohe

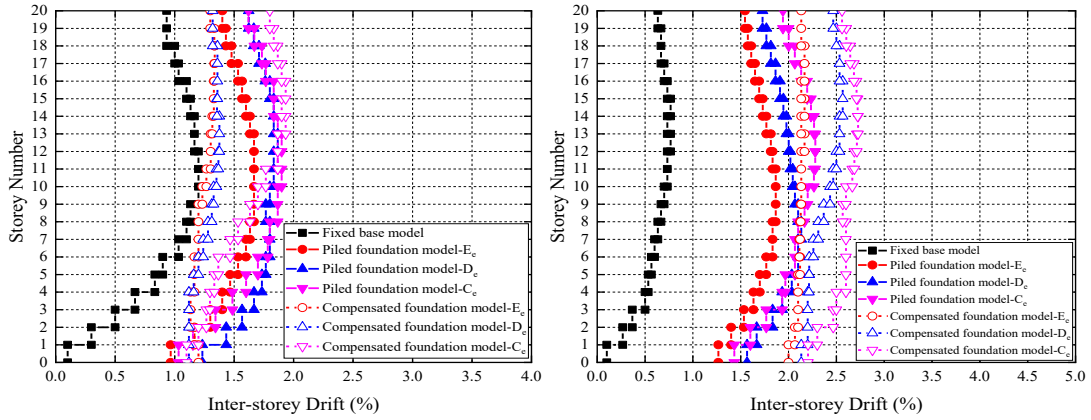

(c) Kobe (d) Northridge

Figure 5.17 Inter-storey drifts of 20-storey structure (HWR=6, BD=30) under the four seismic records

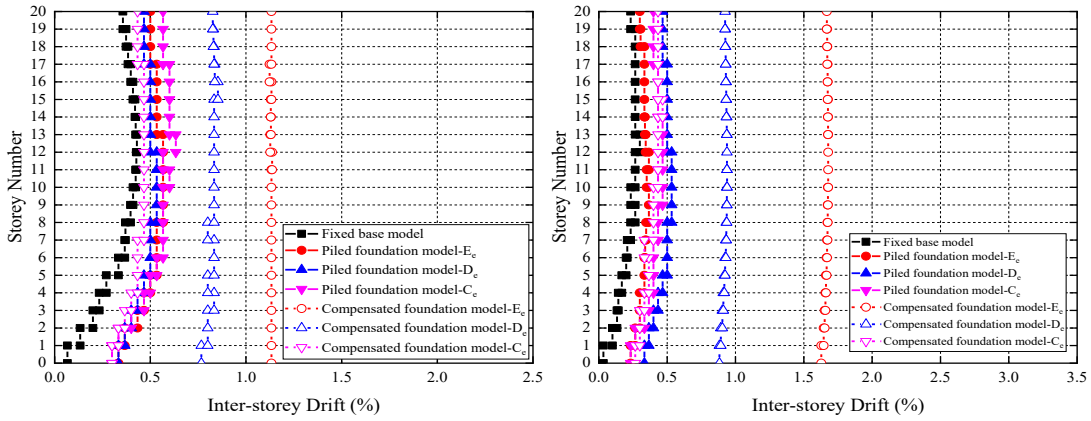

(a) El Centro (b) Hachinohe

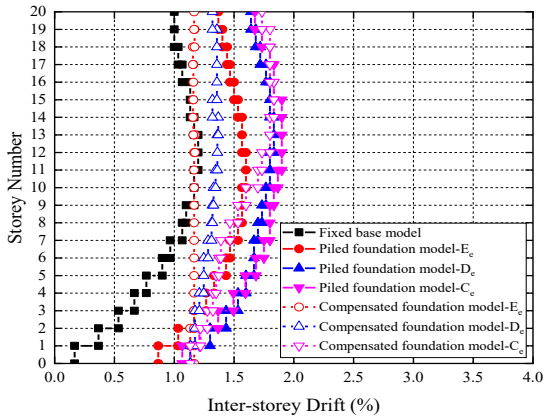

(c) Kobe

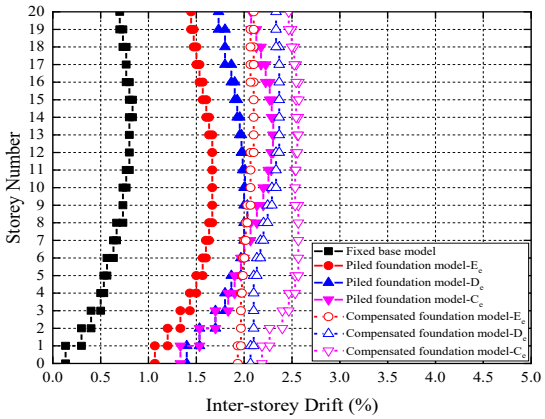

(d) Northridge

Figure 5.18 Inter-storey drifts of 20-storey structure (HWR=5, BD=30) under the four seismic records

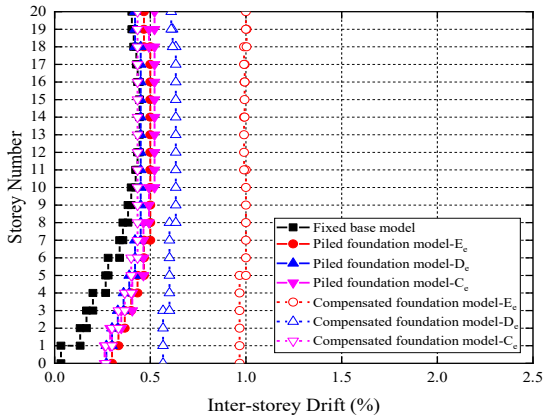

(a) El Centro

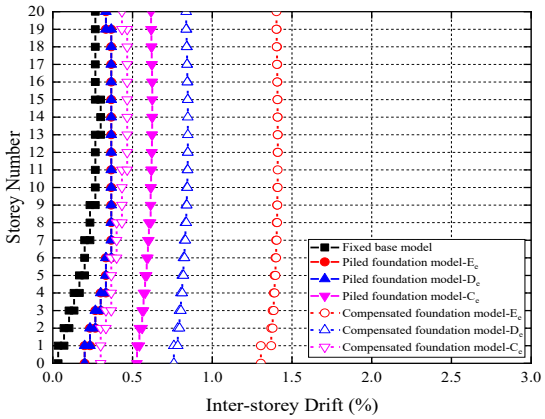

(b) Hachinohe

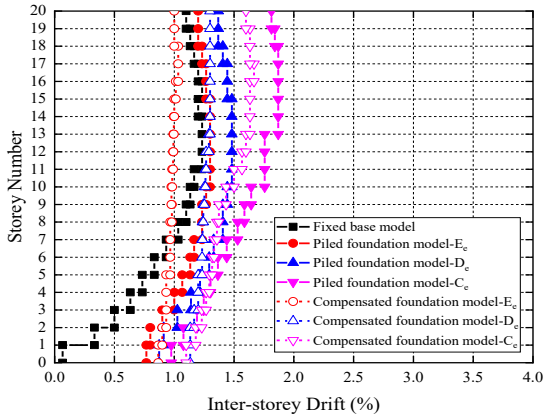

(c) Kobe

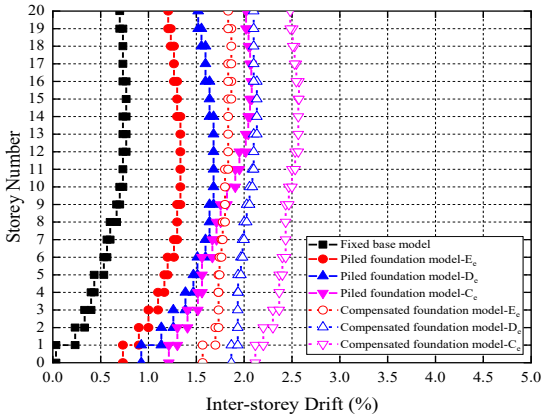

(d) Northridge

Figure 5.19 Inter-storey drifts of 20-storey structure (HWR=4, BD=30) under the four seismic records

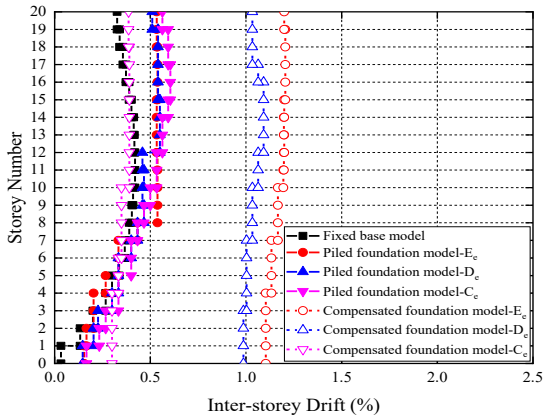

(a) El Centro

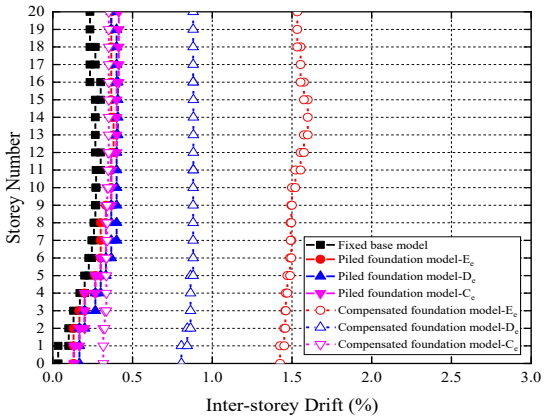

(b) Hachinohe

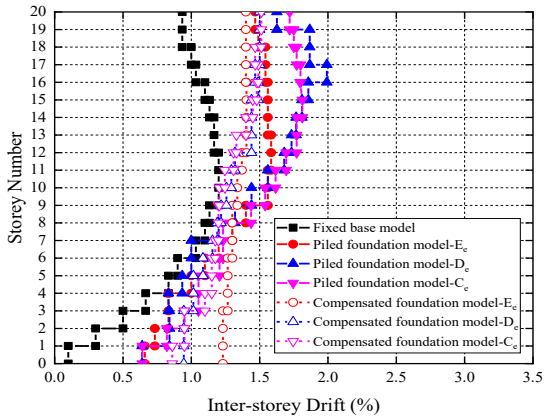

(c) Kobe

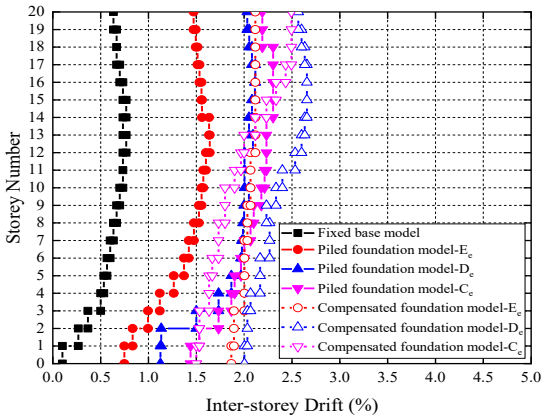

(d) Northridge

Figure 5.20 Inter-storey drifts of 20-storey structure (HWR=6, BD=20) under the four seismic records

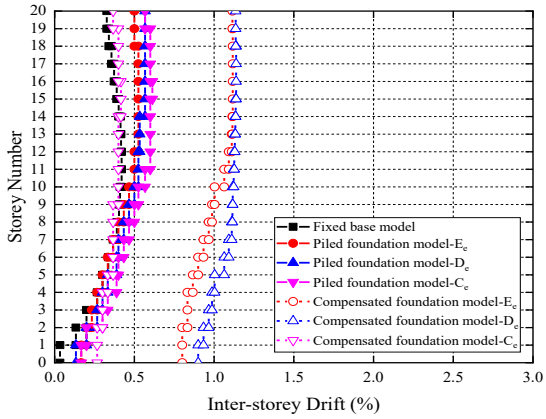

(a) El Centro

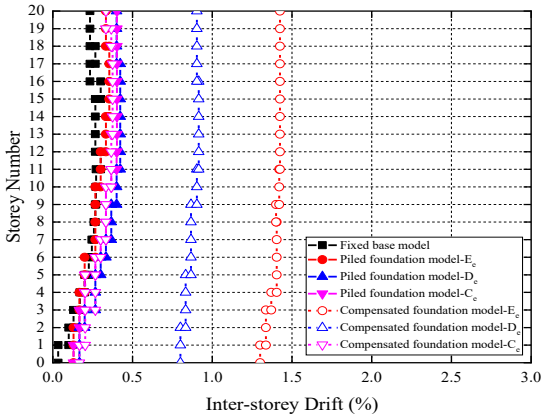

(b) Hachinohe

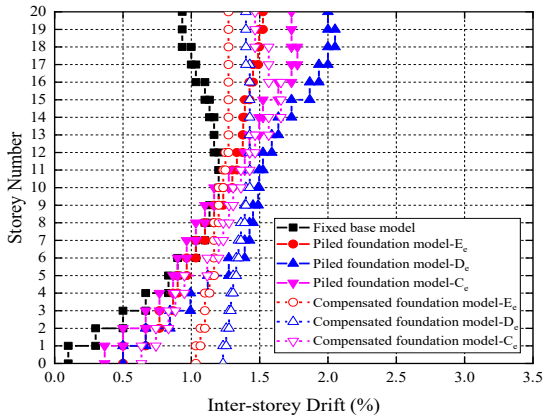

(c) Kobe

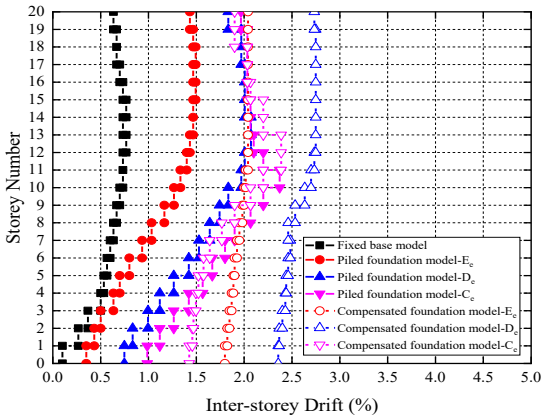

(d) Northridge

Figure 5.21 Inter-storey drifts of 20-storey structure (HWR=6, BD=10) under the four seismic records

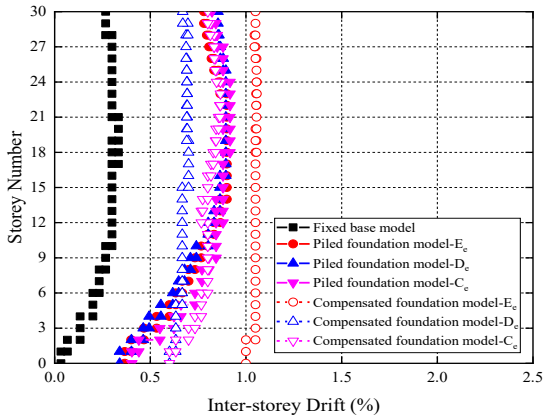

(a) El Centro

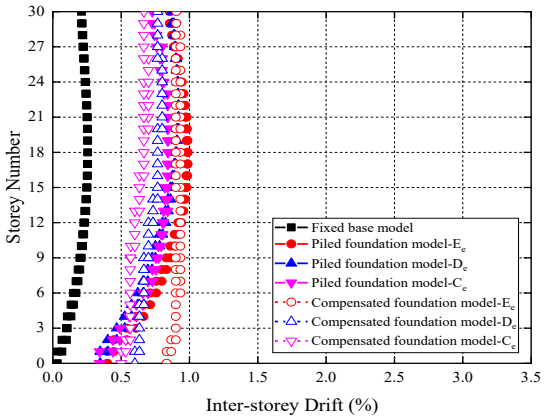

(b) Hachinohe

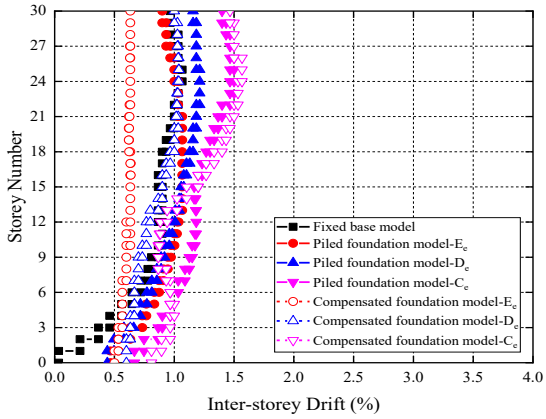

(c) Kobe

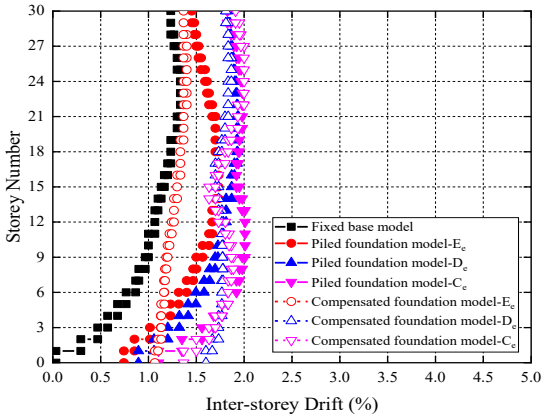

(d) Northridge

Figure 5.22 Inter-storey drifts of 30-storey structure (HWR=6, BD=30) under the four seismic records

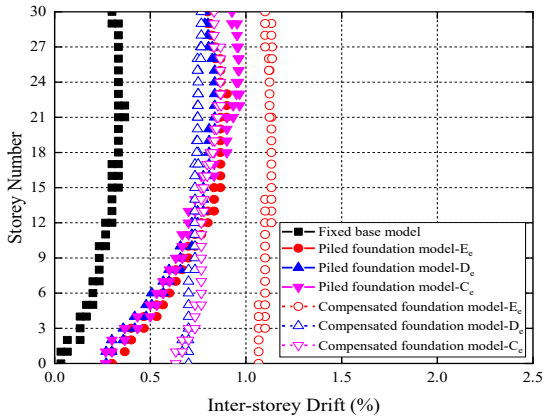

(a) El Centro

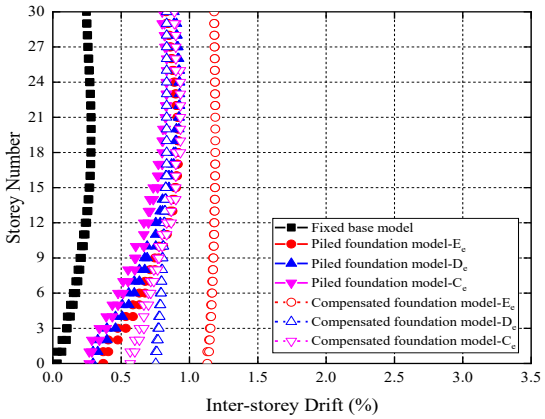

(b) Hachinohe

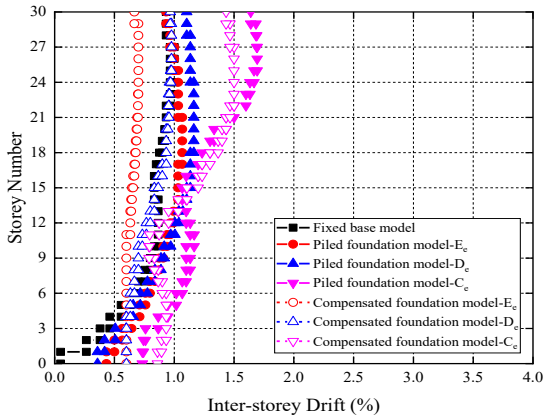

(c) Kobe

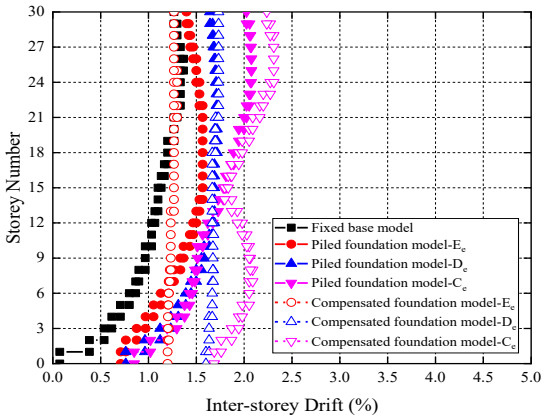

(d) Northridge

Figure 5.23 Inter-storey drifts of 30-storey structure (HWR=5, BD=30) under the four seismic records

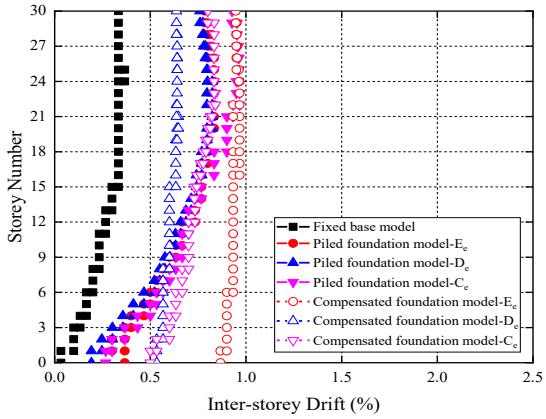

(a) El Centro

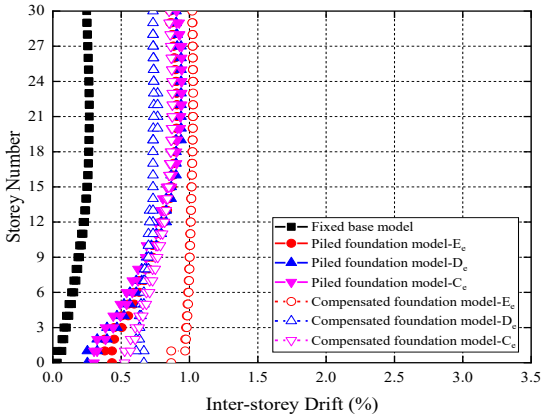

(b) Hachinohe

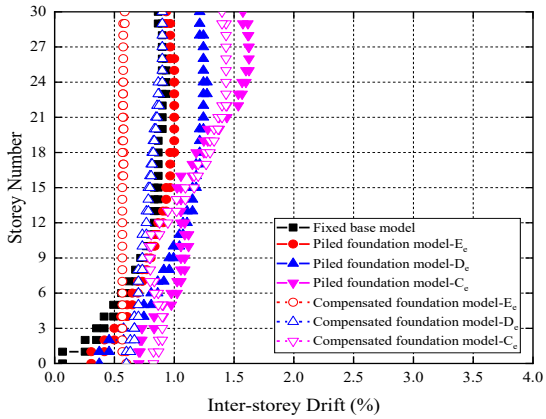

(c) Kobe

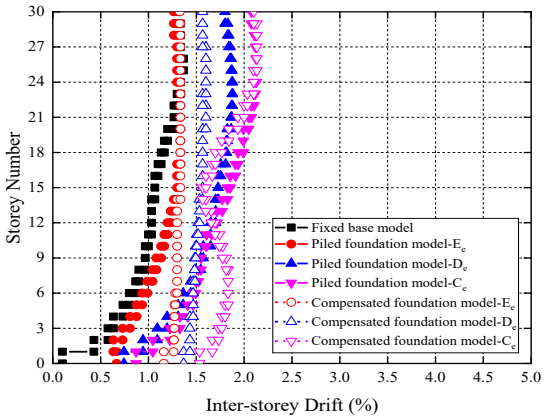

(d) Northridge

Figure 5.24 Inter-storey drifts of 30-storey structure (HWR=4, BD=30) under the four seismic records

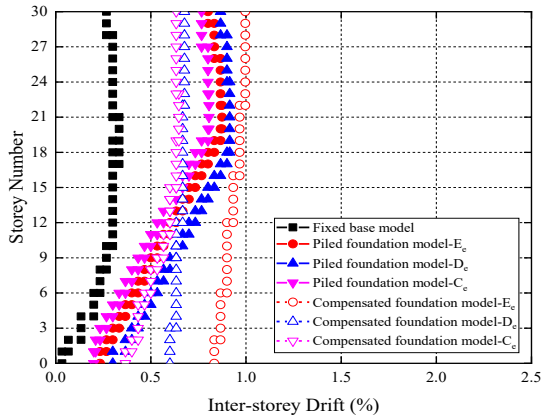

(a) El Centro

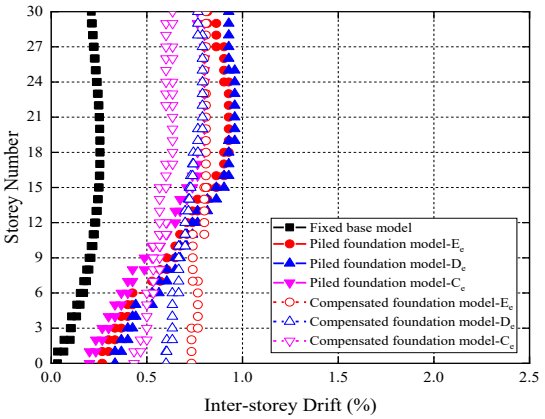

(b) Hachinohe

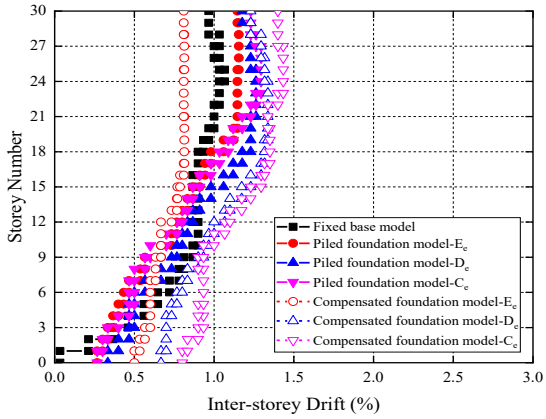

(c) Kobe

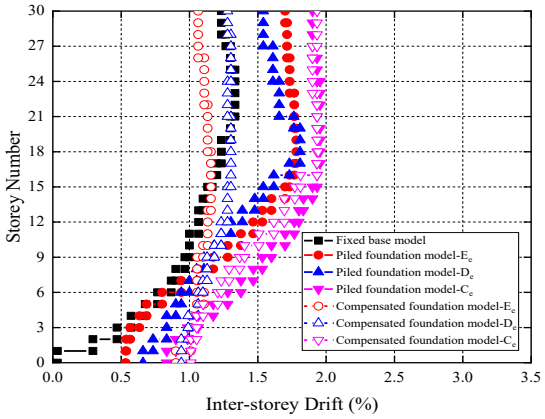

(d) Northridge

Figure 5.25 Inter-storey drifts of 30-storey structure (HWR=6, BD=20) under the four seismic records

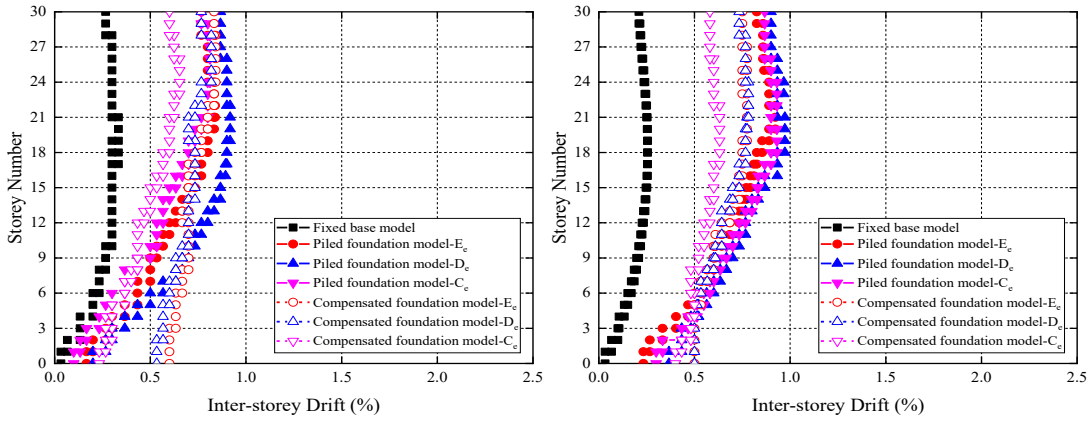

(a) El Centro (b) Hachinohe

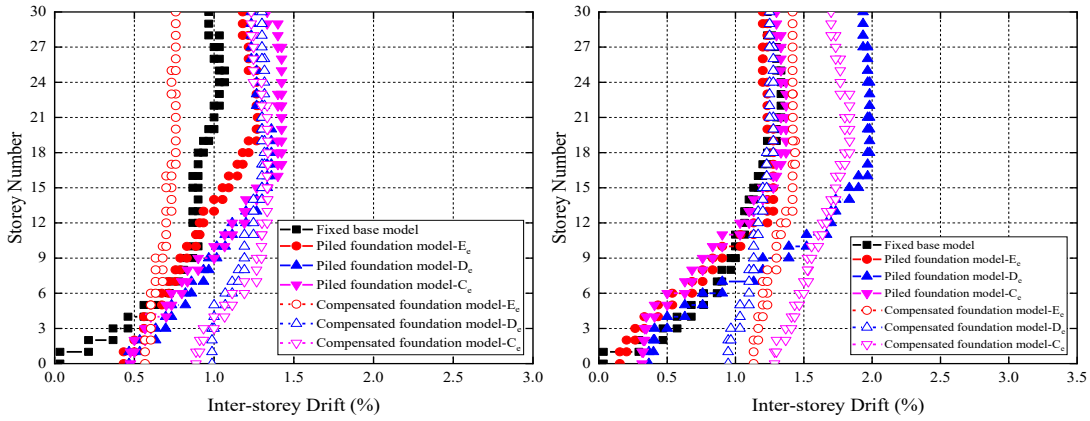

(c) Kobe (d) Northridge

Figure 5.26 Inter-storey drifts of 30-storey structure (HWR=6, BD=10) under the four seismic records

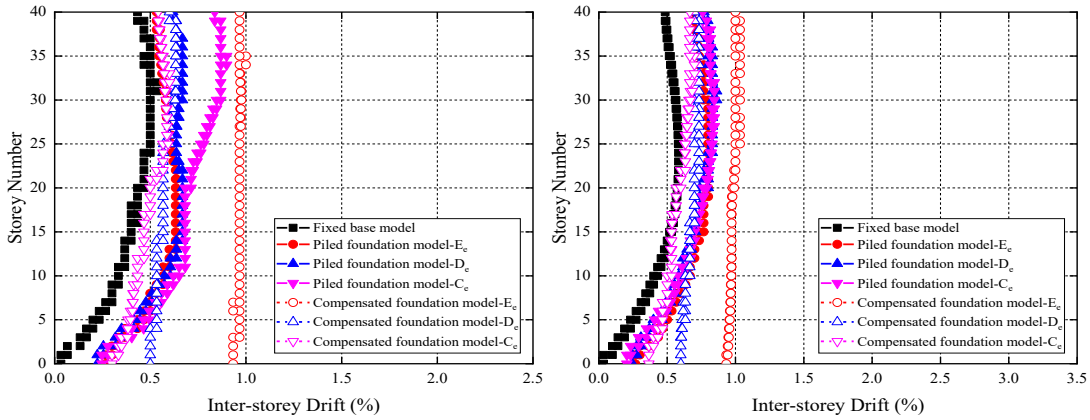

(a) El Centro (b) Hachinohe

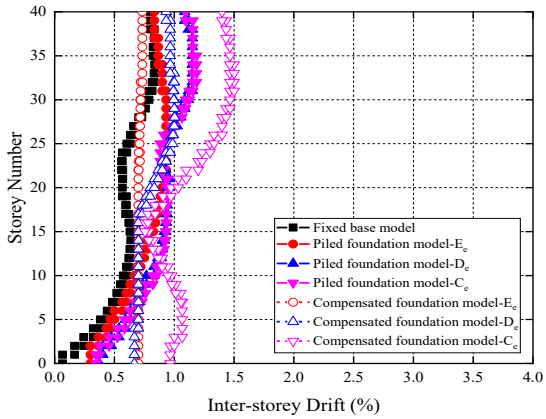

(c) Kobe

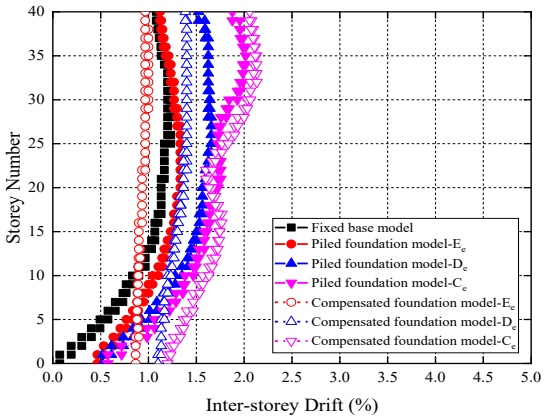

(d) Northridge

Figure 5.27 Inter-storey drifts of 40-storey structure (HWR=6, BD=30) under the four seismic records

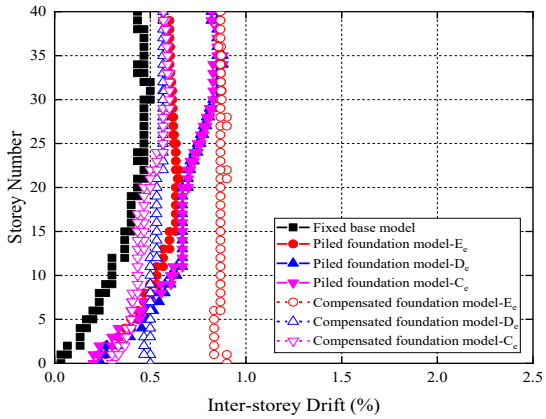

(a) El Centro

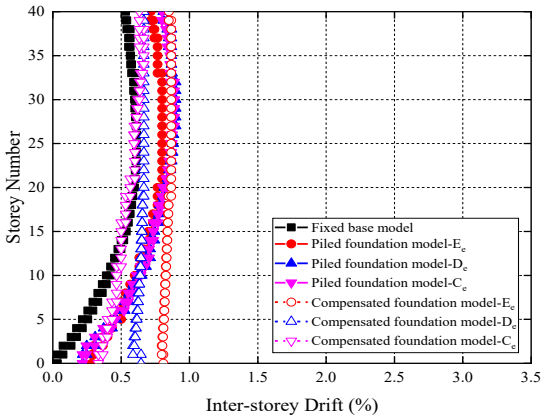

(b) Hachinohe

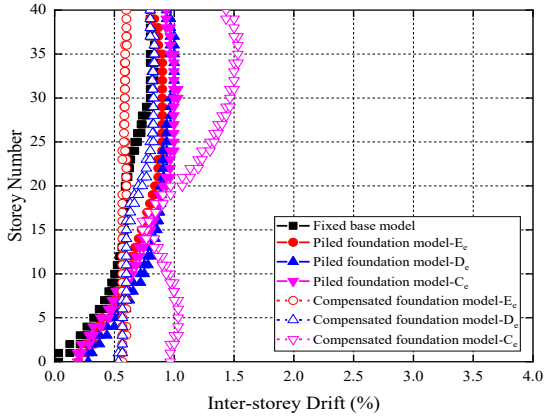

(c) Kobe

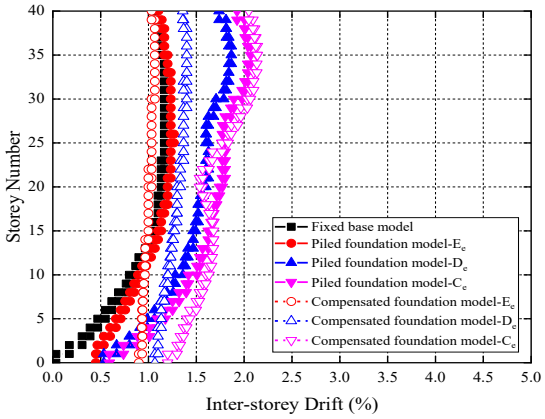

(d) Northridge

Figure 5.28 Inter-storey drifts of 40-storey structure (HWR=5, BD=30) under the four seismic records

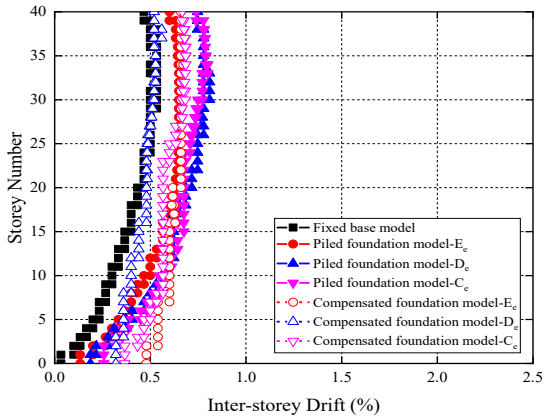

(a) El Centro

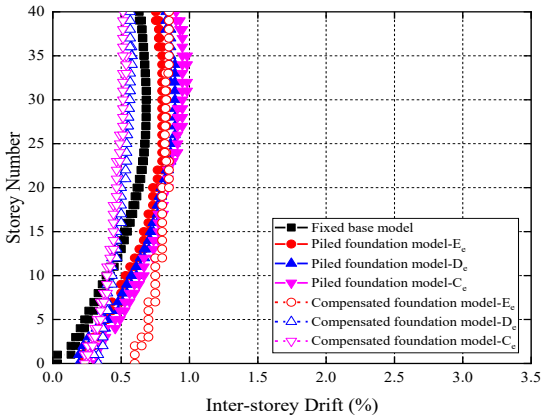

(b) Hachinohe

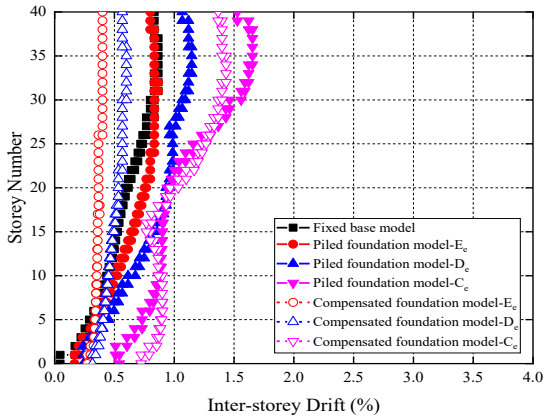

(c) Kobe

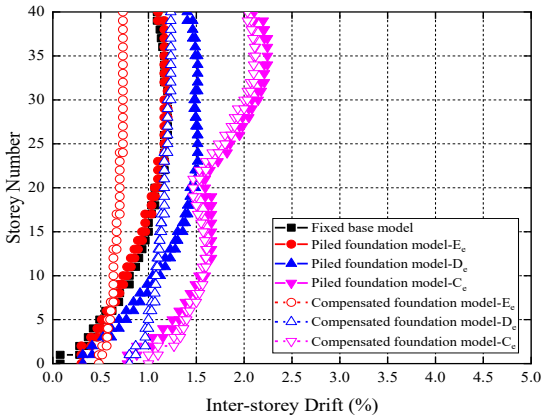

(d) Northridge

Figure 5.29 Inter-storey drifts of 40-storey structure (HWR=4, BD=30) under the four seismic records

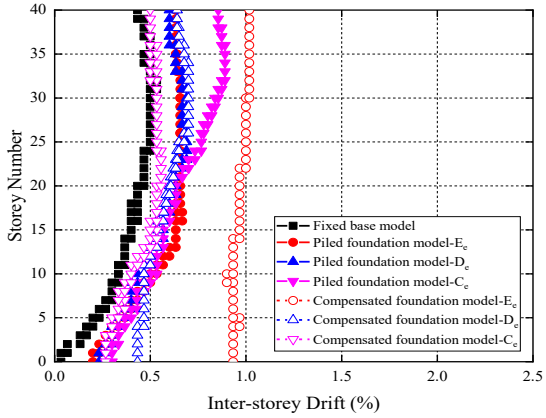

(a) El Centro

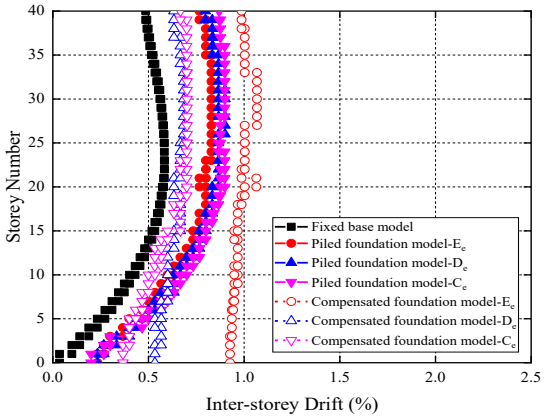

(b) Hachinohe

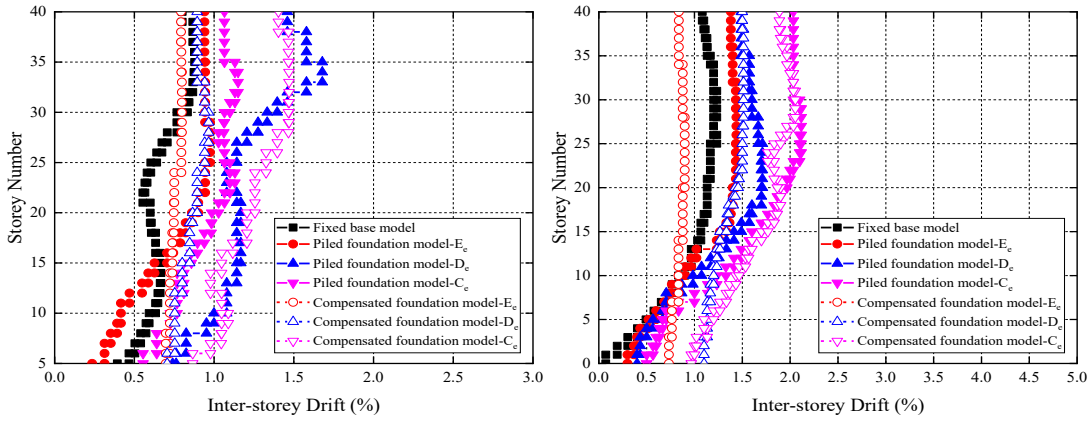

(c) Kobe (d) Northridge

Figure 5.30 Inter-storey drifts of 40-storey structure (HWR=6, BD=20) under the four seismic records

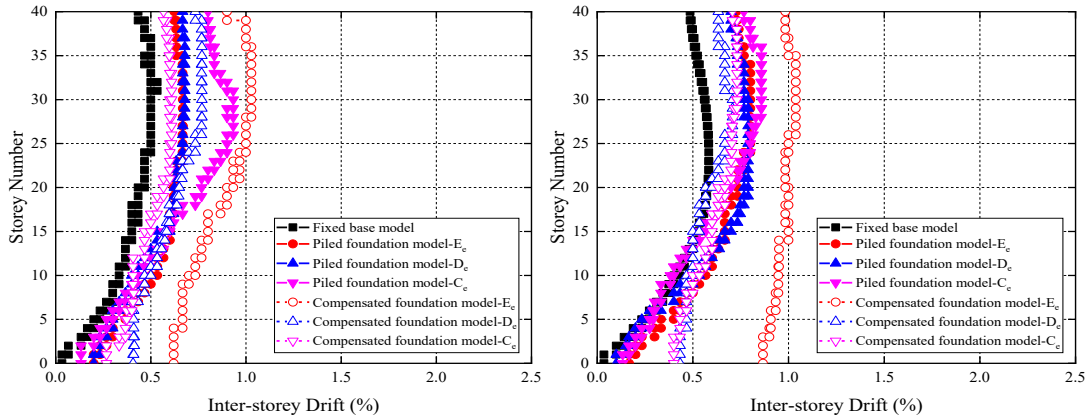

(a) El Centro (b) Hachinohe

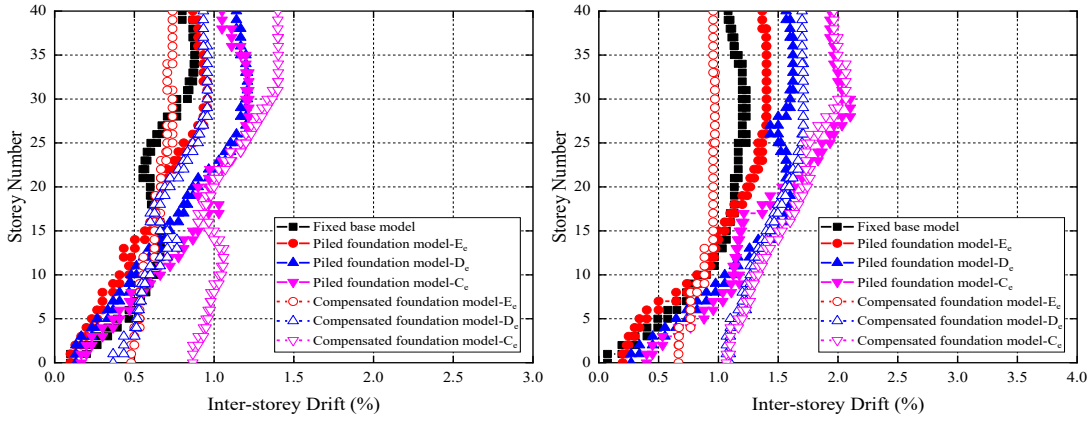

(c) Kobe (d) Northridge

Figure 5.31 Inter-storey drifts of 40-storey structure (HWR=6, BD=10) under the four seismic records

5.3.4 Shear Force

Figures 5.32-5.46 present a comparison of the storey shear forces of structures with various influencing factors. Upon considering SSI, the magnitude of the shear force in a structure can vary, either increasing or decreasing, based on the type of foundation and soil. For instance, the shear forces of structures with classical compensated foundations constructed on soft soils (type E_e and D_e) are typically lower than those of their fixed base counterparts. In contrast, the shear forces of classical compensated foundation and piled foundation structures resting on C_e soil are amplified. This suggests that increasing the stiffness of the substructure can absorb more seismic energy, rendering the traditional assumption that SSI always cuts down the seismic demand of a structure invalid. This finding aligns with that of Van Nguyen et al. (2017). Therefore, although a piled foundation can reduce foundation rocking, it may increase the seismic shear force and, subsequently, the lateral deflection of the structure. This also explains why the deformation of a piled foundation model may not necessarily be less than that of a classical compensated foundation model, as observed in Sections 5.3.1 and 5.3.3. Additionally, while the absolute value of the base shear increases with an increase in HWR, this change does not have a dramatic influence on the relative value of the base shear.

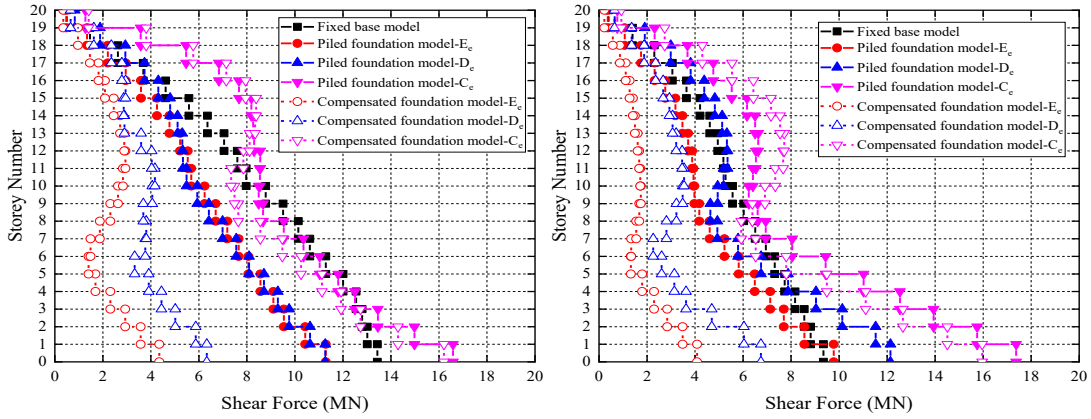

(a) El Centro (b) Hachinohe

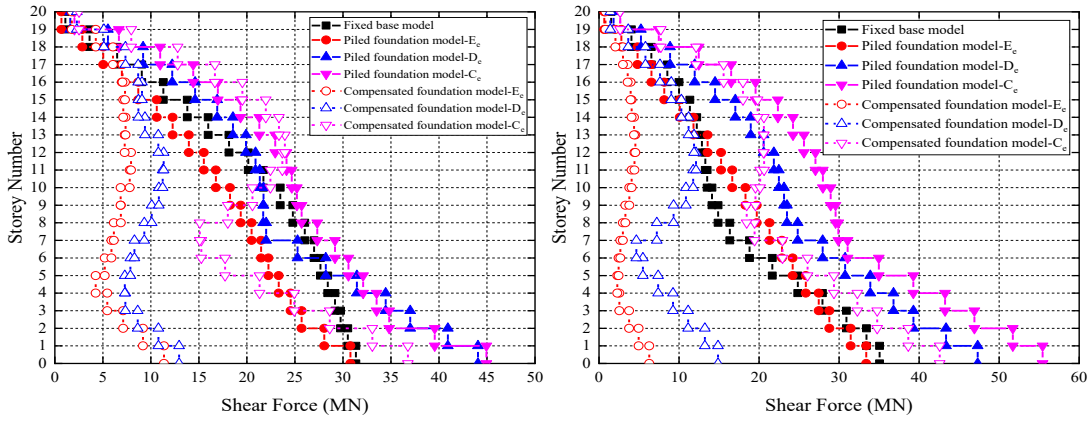

(c) Kobe (d) Northridge

Figure 5.32 Storey shear forces of 20-storey structure (HWR=6, BD=30) under the four seismic records

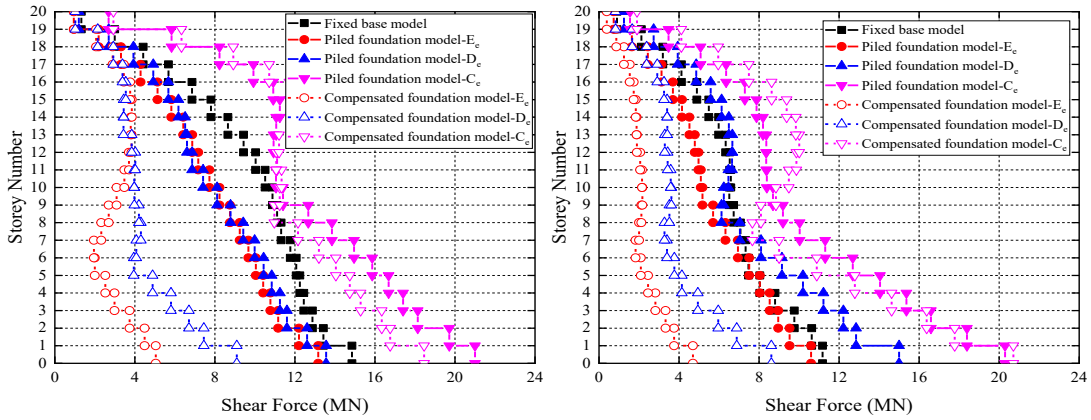

(a) El Centro (b) Hachinohe

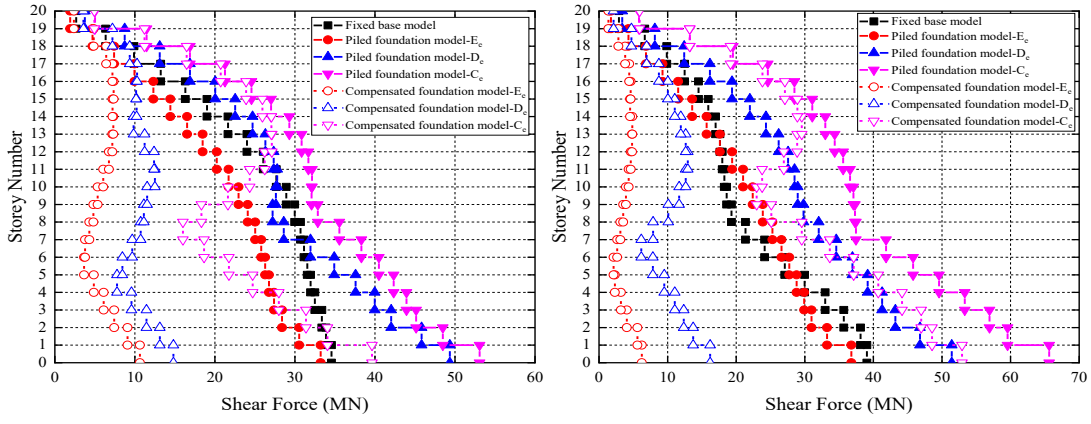

(c) Kobe (d) Northridge

Figure 5.33 Storey shear forces of 20-storey structure (HWR=5, BD=30) under the four seismic records

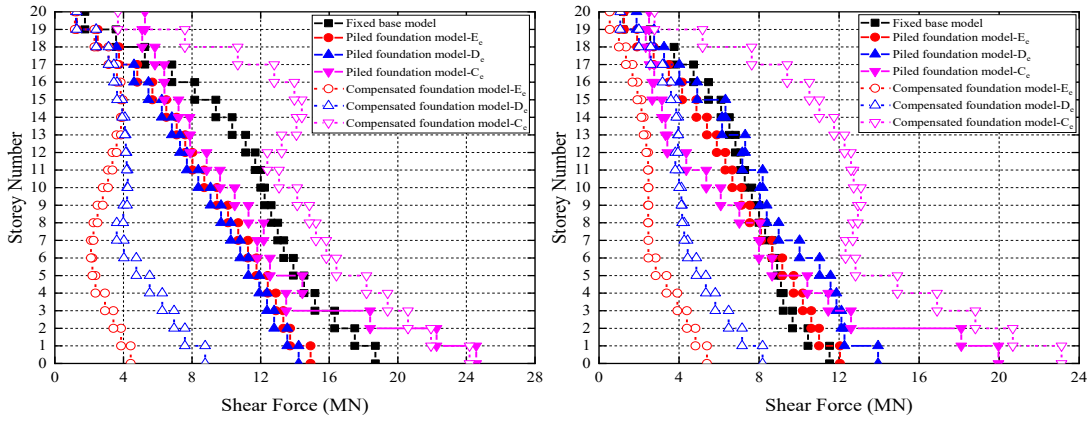

(a) El Centro (b) Hachinohe

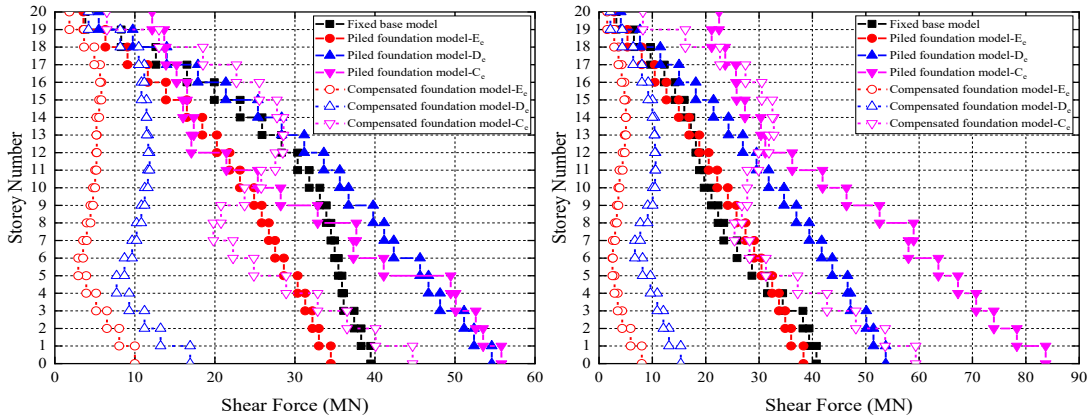

(c) Kobe (d) Northridge

Figure 5.34 Storey shear forces of 20-storey structure (HWR=4, BD=30) under the four seismic records

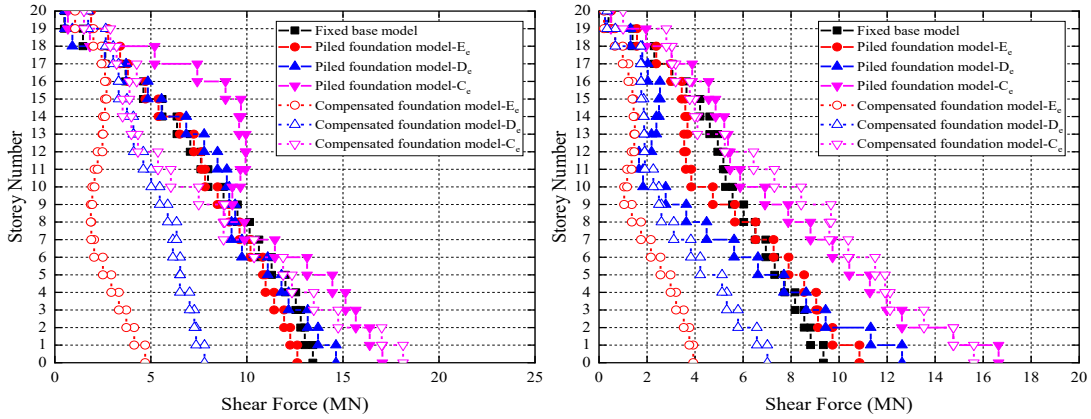

(a) El Centro (b) Hachinohe

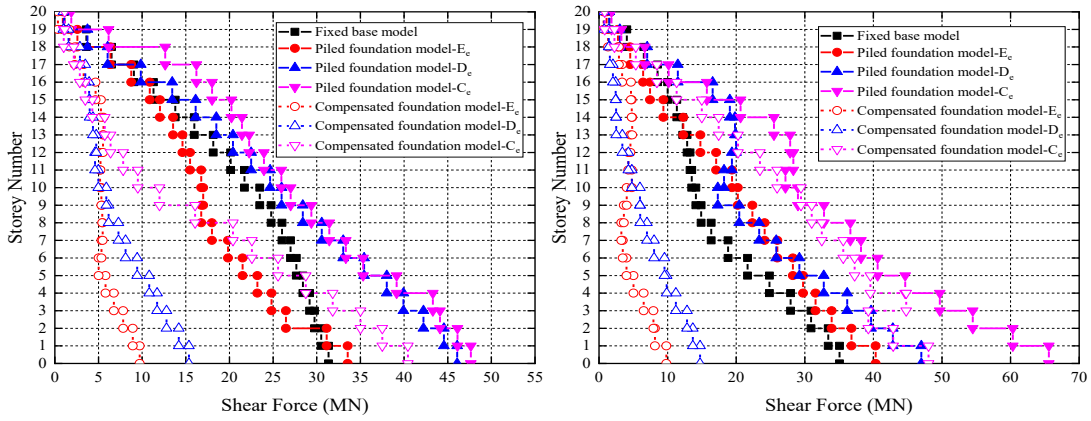

(c) Kobe (d) Northridge

Figure 5.35 Storey shear forces of 20-storey structure (HWR=6, BD=20) under the four seismic records

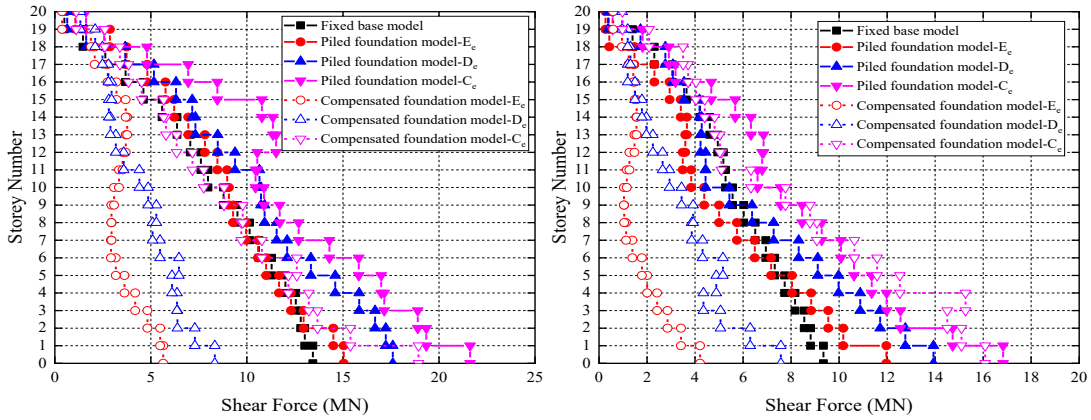

(a) El Centro (b) Hachinohe

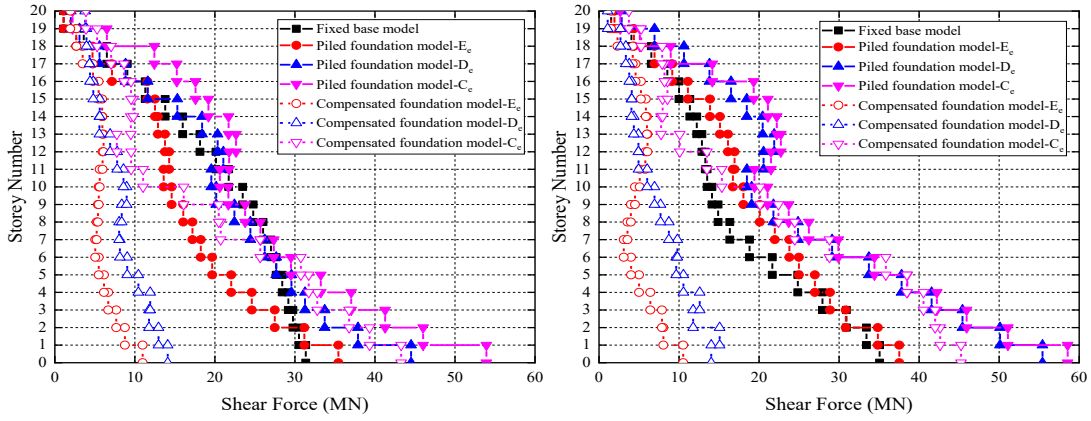

(c) Kobe (d) Northridge

Figure 5.36 Storey shear forces of 20-storey structure (HWR=6, BD=10) under the four seismic records

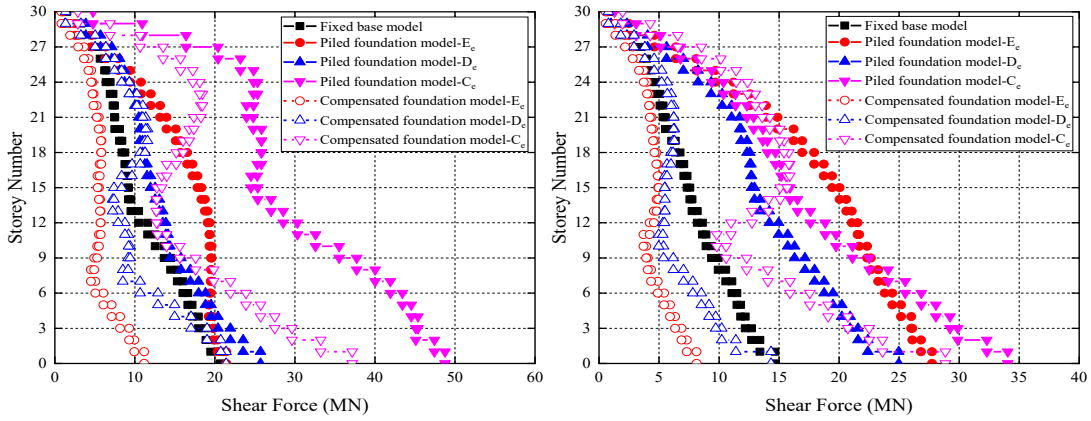

(a) El Centro (b) Hachinohe

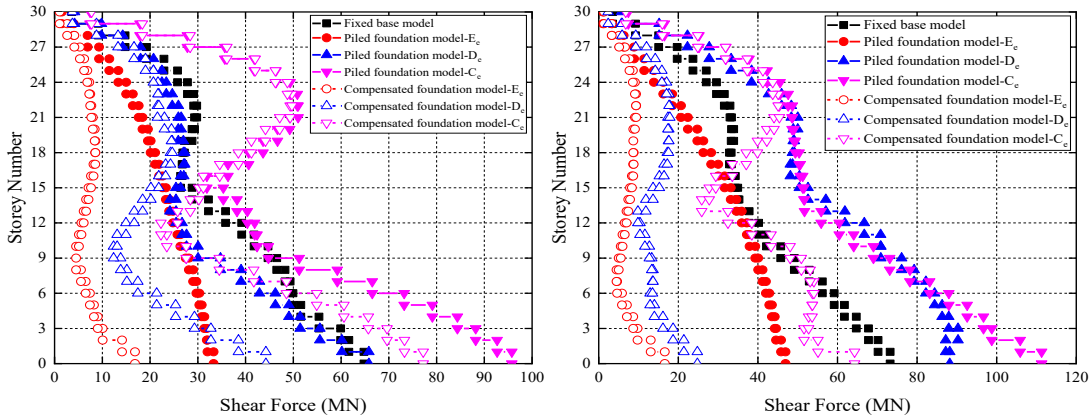

(c) Kobe (d) Northridge

Figure 5.37 Storey shear forces of 30-storey structure (HWR=6, BD=30) under the four seismic records

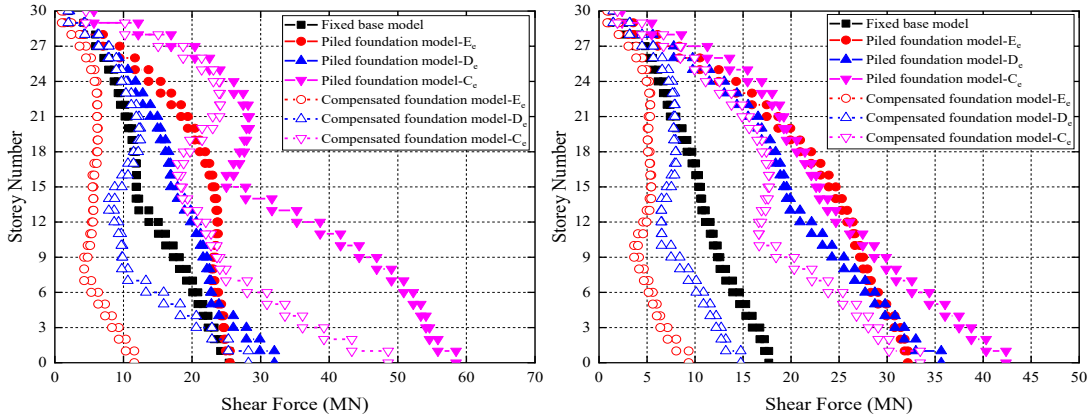

(a) El Centro (b) Hachinohe

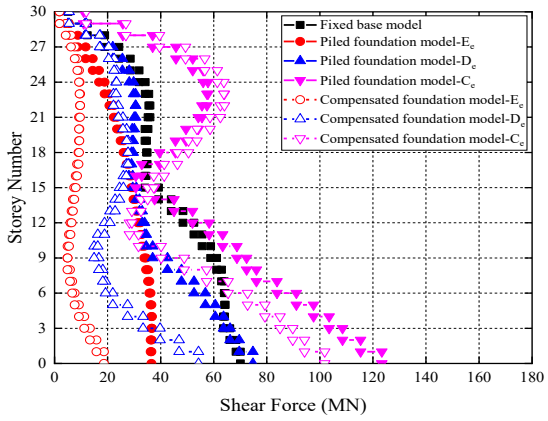

(c) Kobe

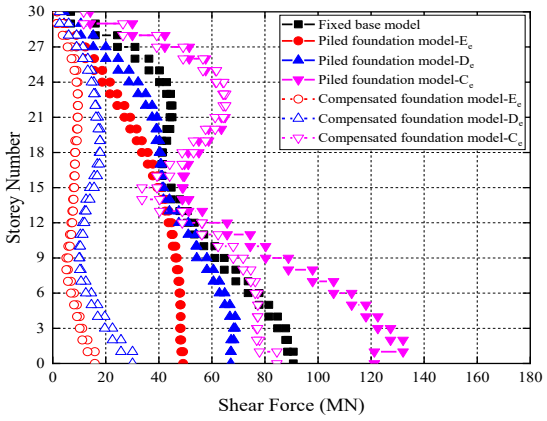

(d) Northridge

Figure 5.38 Storey shear forces of 30-storey structure (HWR=5, BD=30) under the four seismic records

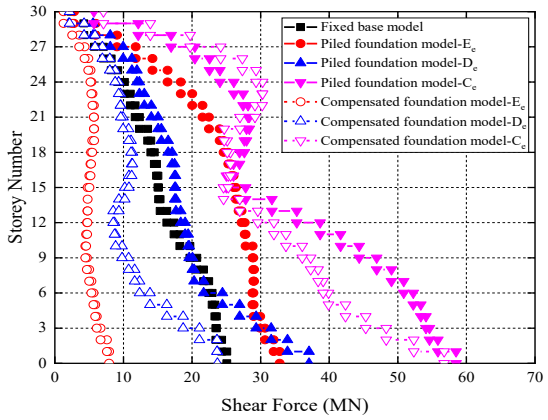

(a) El Centro

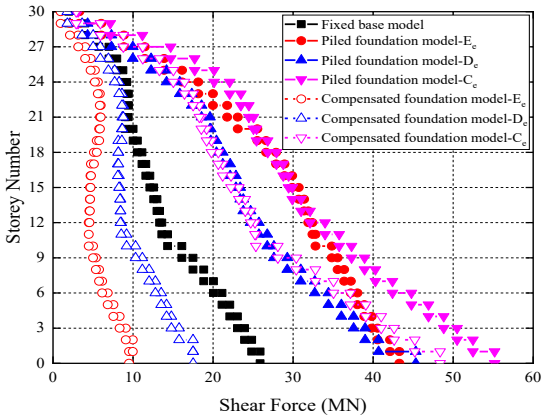

(b) Hachinohe

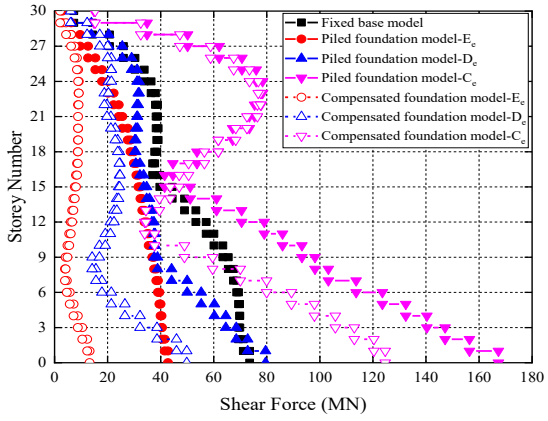

(c) Kobe

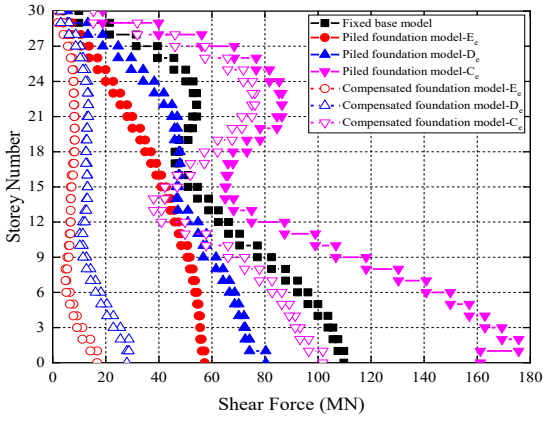

(d) Northridge

Figure 5.39 Storey shear forces of 30-storey structure (HWR=4, BD=30) under the four seismic records

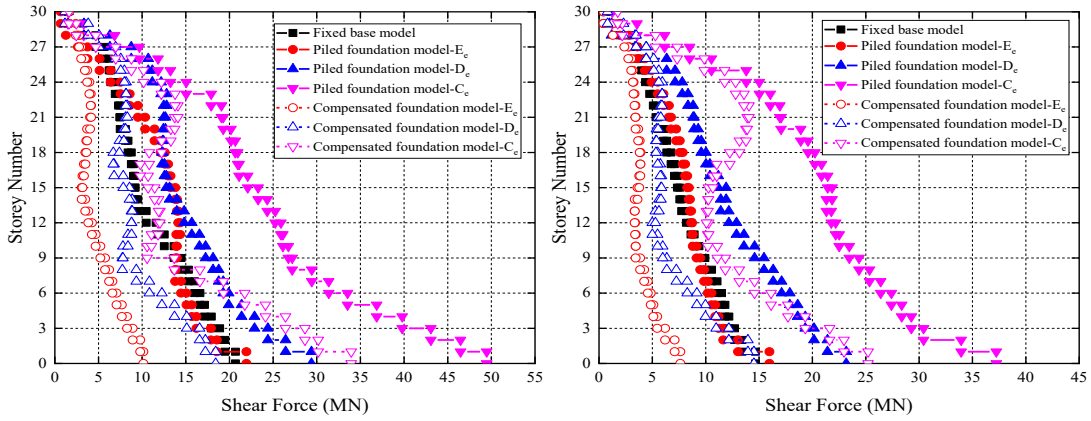

(a) El Centro (b) Hachinohe

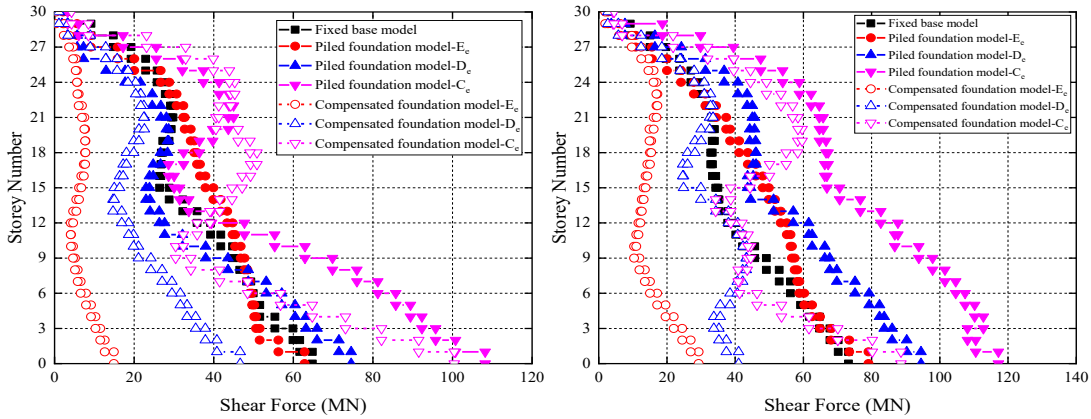

(c) Kobe (d) Northridge

Figure 5.40 Storey shear forces of 30-storey structure (HWR=6, BD=20) under the four seismic records

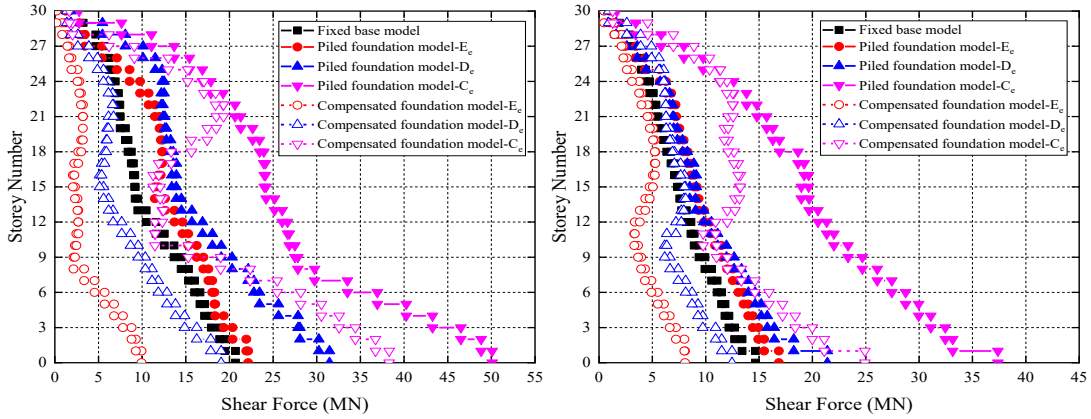

(a) El Centro (b) Hachinohe

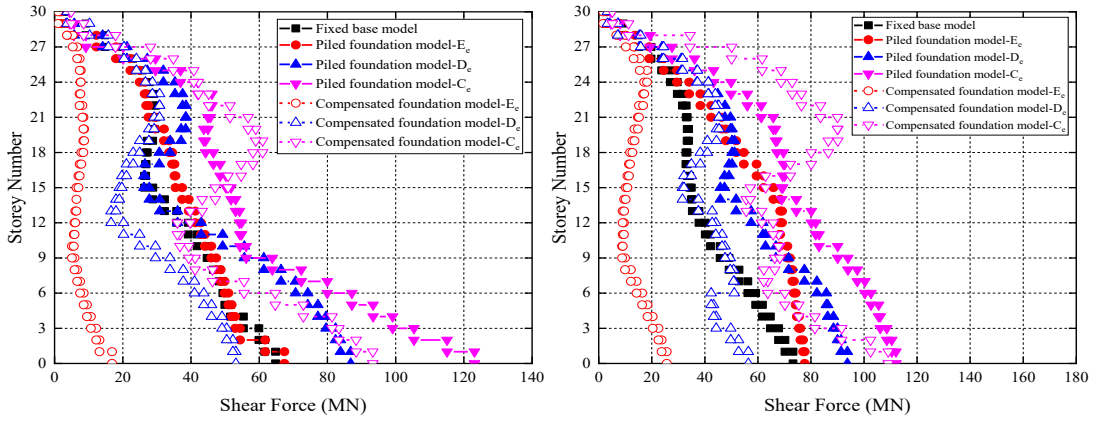

(c) Kobe (d) Northridge

Figure 5.41 Storey shear forces of 30-storey structure (HWR=6, BD=10) under the four seismic records

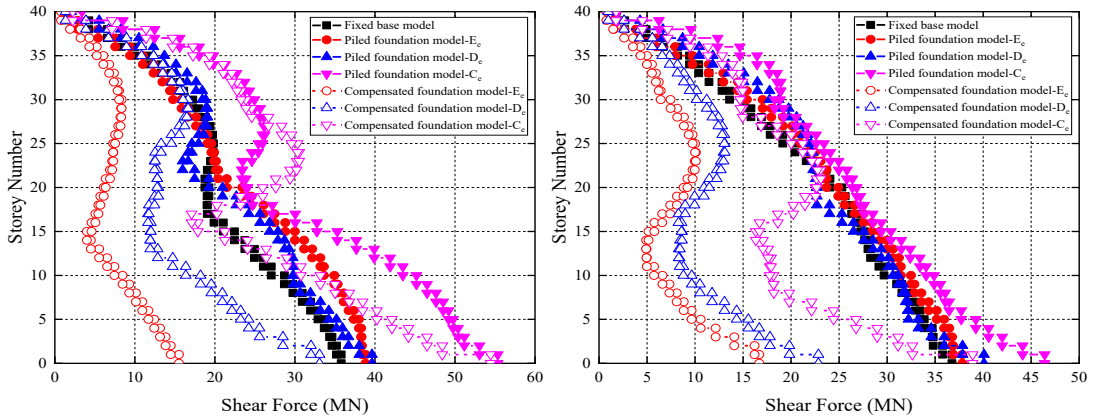

(a) El Centro (b) Hachinohe

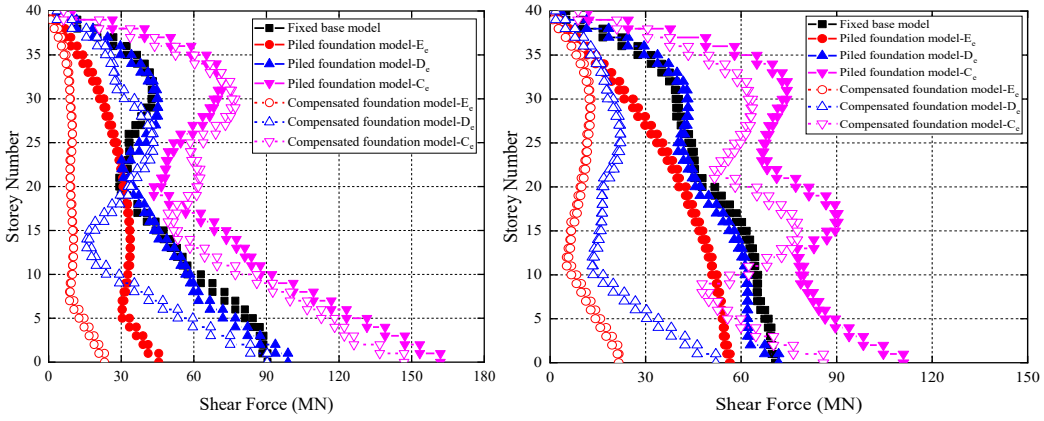

(c) Kobe (d) Northridge

Figure 5.42 Storey shear forces of 40-storey structure (HWR=6, BD=30) under the four seismic records

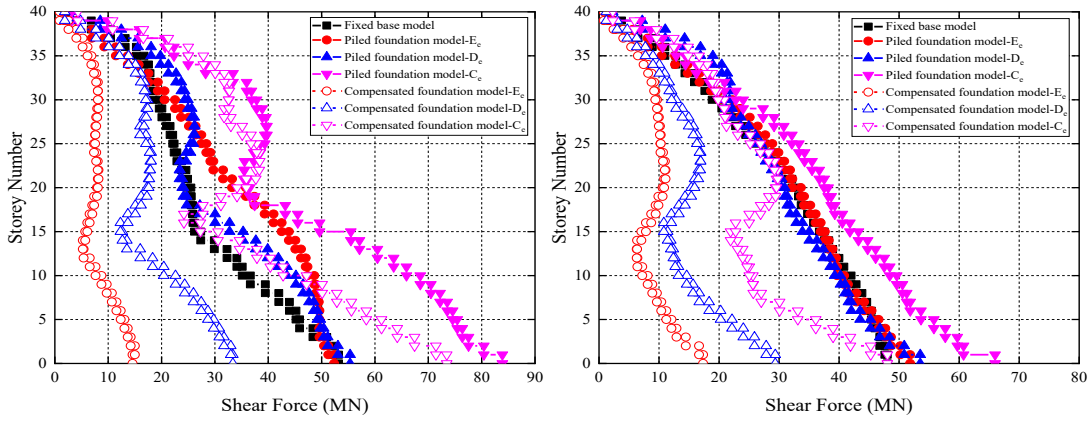

(a) El Centro (b) Hachinohe

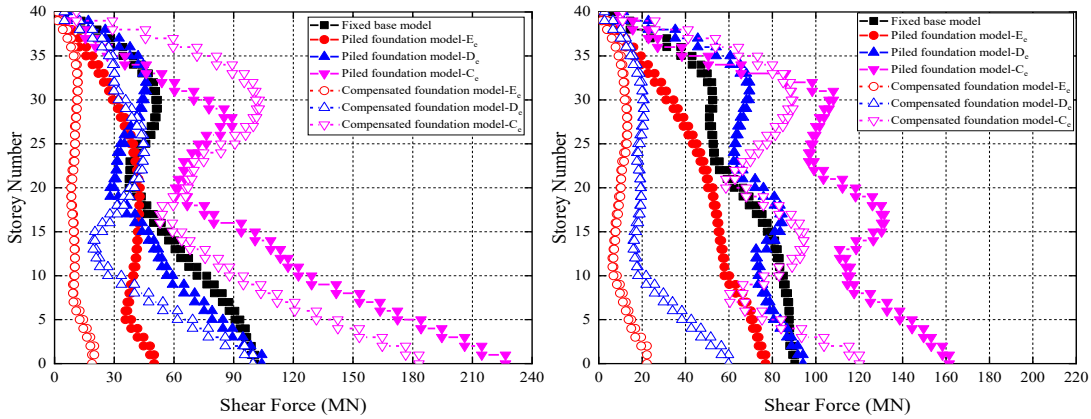

(c) Kobe (d) Northridge

Figure 5.43 Storey shear forces of 40-storey structure (HWR=5, BD=30) under the four seismic records

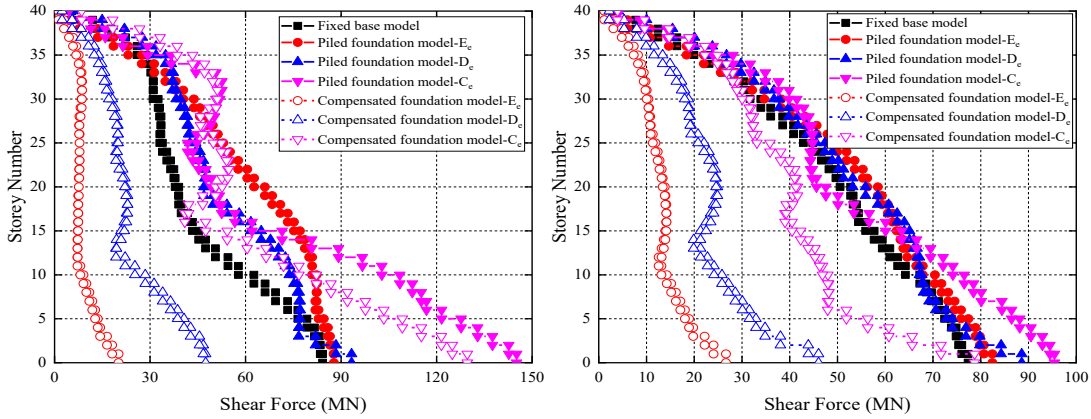

(a) El Centro (b) Hachinohe

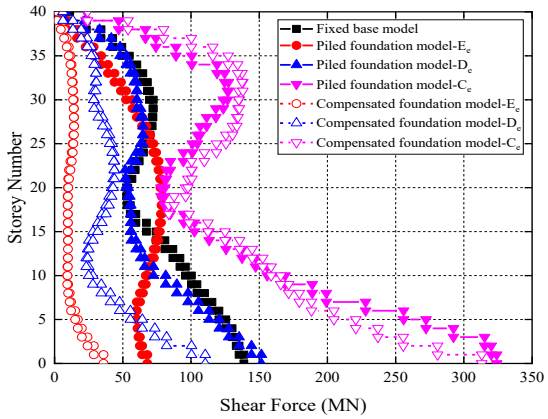

(c) Kobe

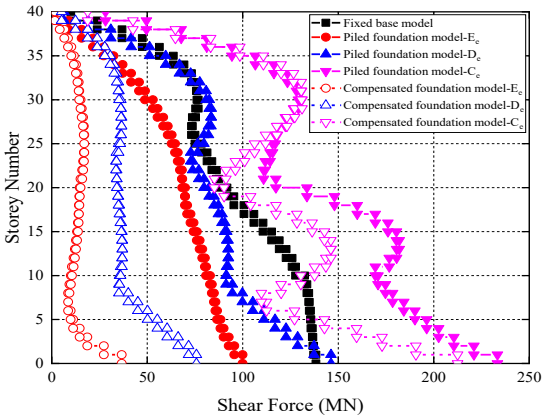

(d) Northridge

Figure 5.44 Storey shear forces of 40-storey structure (HWR=4, BD=30) under the four seismic records

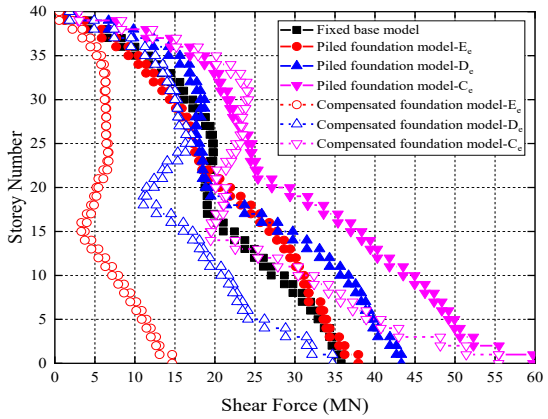

(a) El Centro

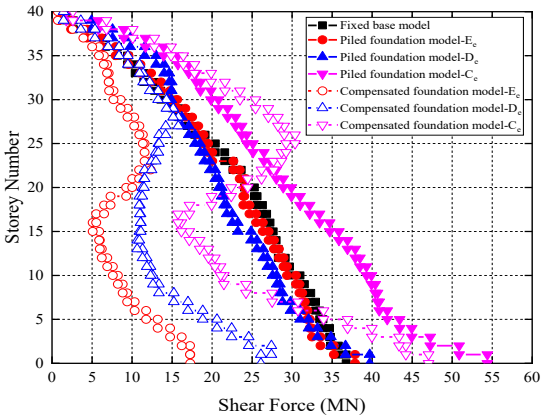

(b) Hachinohe

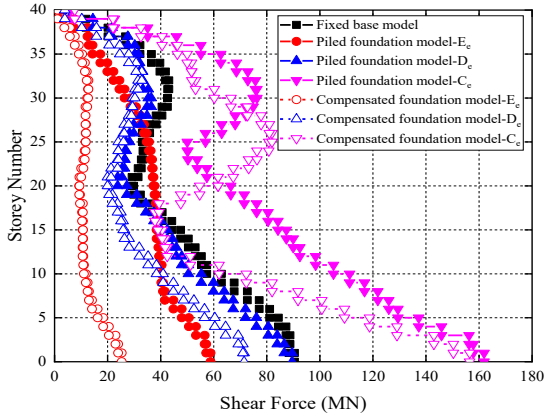

(c) Kobe

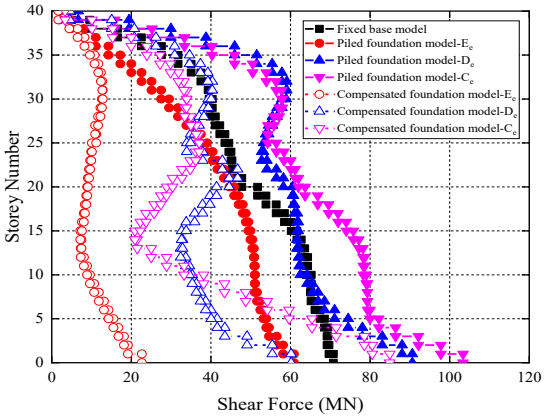

(d) Northridge

Figure 5.45 Storey shear forces of 40-storey structure (HWR=6, BD=20) under the four seismic records

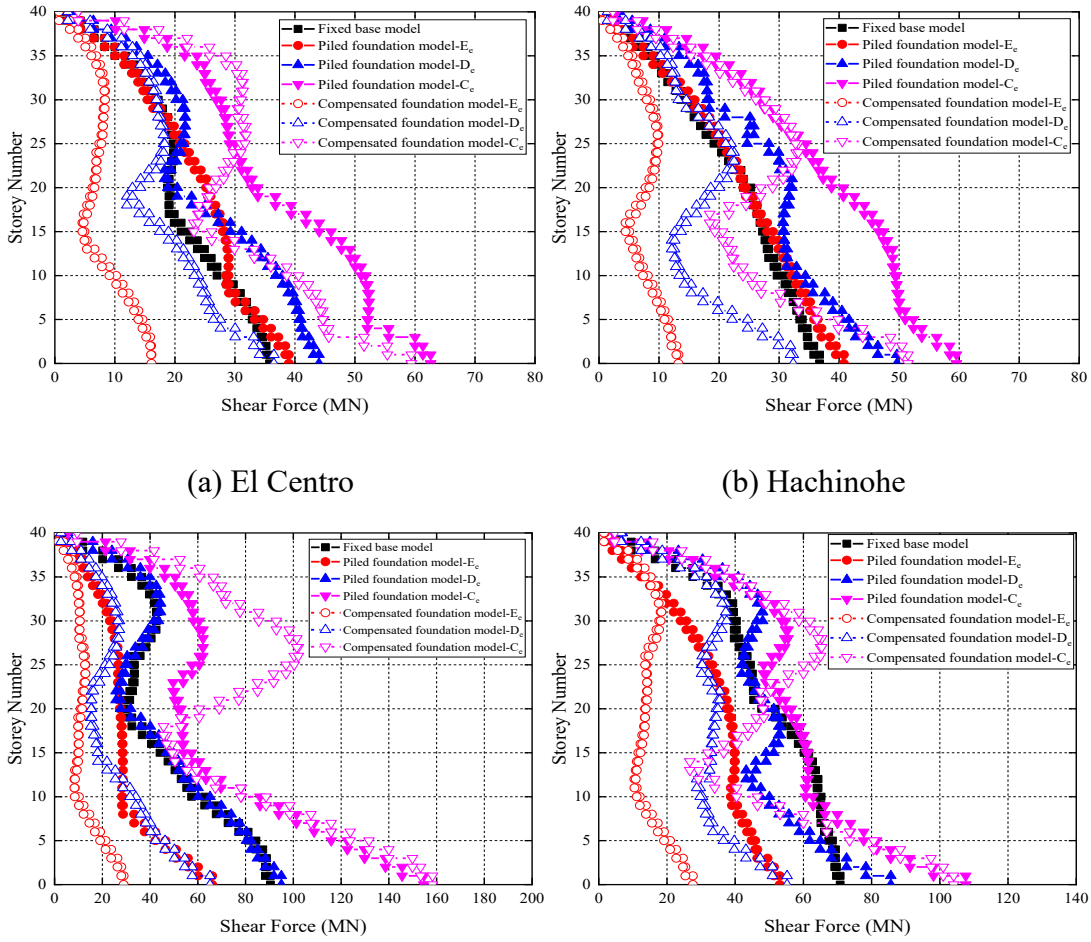

(a) El Centro (b) Hachinohe

(c) Kobe (d) Northridge

Figure 5.46 Storey shear forces of 40-storey structure (HWR=6, BD=10) under the four seismic records

5.3.5 The Effects of Parameters on V_{fle}/V_{fix}

To facilitate a comprehensive analysis and comparison of the positive and negative impacts of SSI on high-rise frame-shear wall buildings, two widely used parameters V_{fle} and δ_{fle} were normalised by those obtained from conventional fixed base models (V_{fix} and δ_{fix}) using numerical soil-structure models. Similar to frame-core tube models, this study averaged the values of the base shear ratio (V_{fle}/V_{fix}) and maximum inter-storey drifts ratio ($\delta_{fle}/\delta_{fix}$) under the action of four seismic records (Figure 4.2) to clearly demonstrate the effects of different parameters. Therefore, if the value of V_{fle}/V_{fix} or $\delta_{fle}/\delta_{fix}$ is greater than 1, it indicates that the SSI amplifies the base shear or

inter-storey drifts, indicating a detrimental effect. Figures 5.47, 5.48, 5.49, 5.50, 5.51, and 5.52 present the V_{fle}/V_{fix} values for classical compensated foundation structures and piled foundation structures with different superstructure and substructure parameters.

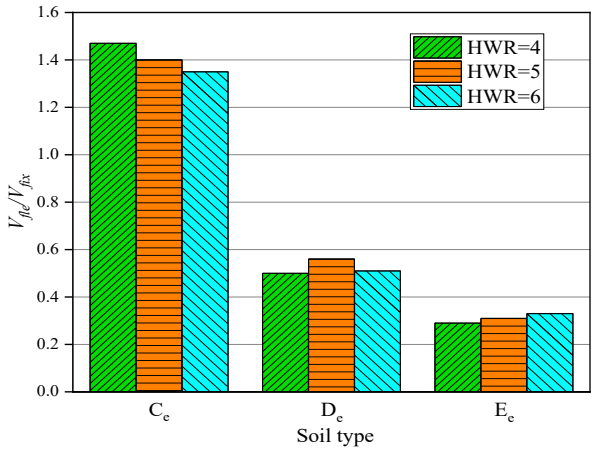

(a)

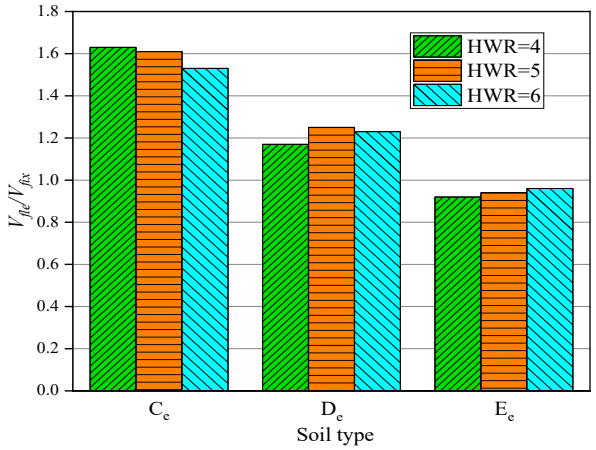

(b)

Figure 5.47 The value of V_{fle}/V_{fix} of 20-storey buildings with different HWRs (a) classical compensated foundation structure (b) piled foundation structure

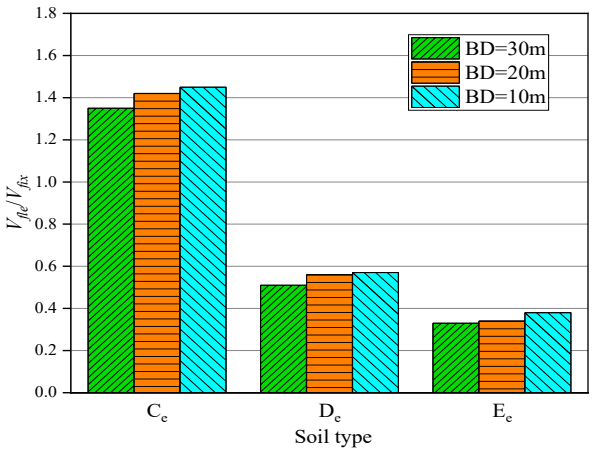

(a)

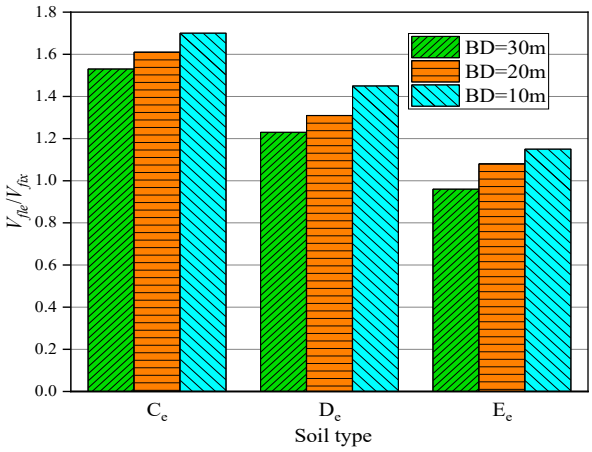

(b)

Figure 5.48 The value of V_{fle}/V_{fix} of 20-storey buildings with different BDs (a) classical compensated foundation structure (b) piled foundation structure

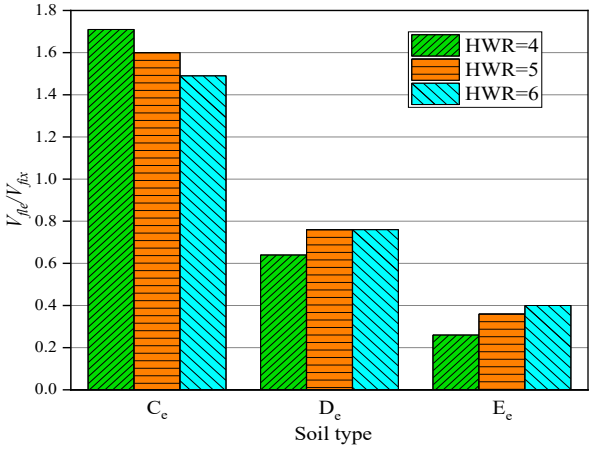

(a)

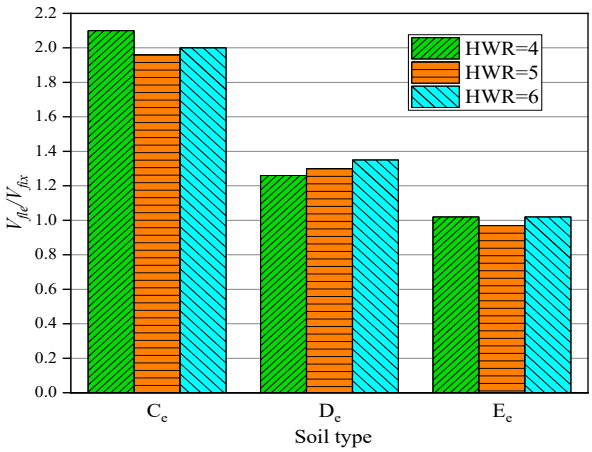

(b)

Figure 5.49 The value of V_{fle}/V_{fix} of 30-storey buildings with different HWRs (a) classical compensated foundation structure (b) piled foundation structure

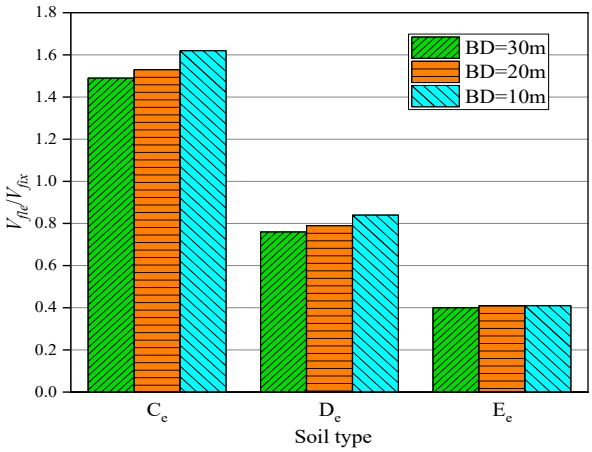

(a)

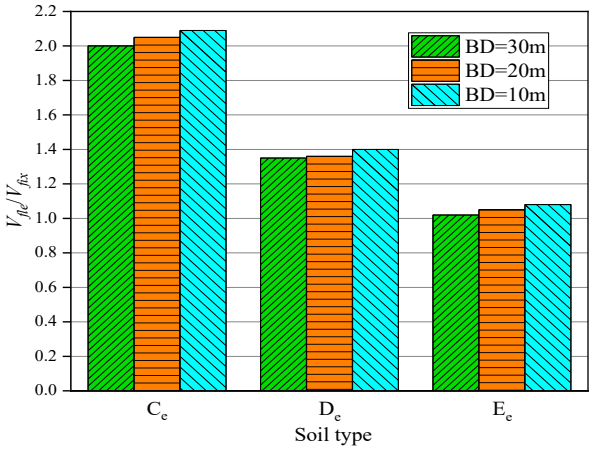

(b)

Figure 5.50 The value of V_{fle}/V_{fix} of 30-storey buildings with different BDs (a) classical compensated foundation structure (b) piled foundation structure

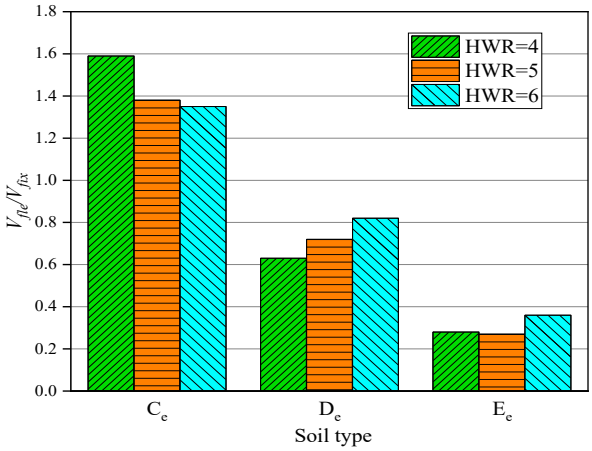

(a)

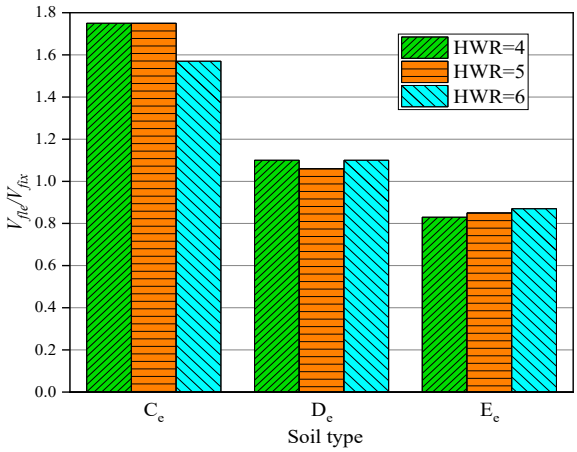

(b)

Figure 5.51 The value of V_{fle}/V_{fix} of 40-storey buildings with different HWRs (a) classical compensated foundation structure (b) piled foundation structure

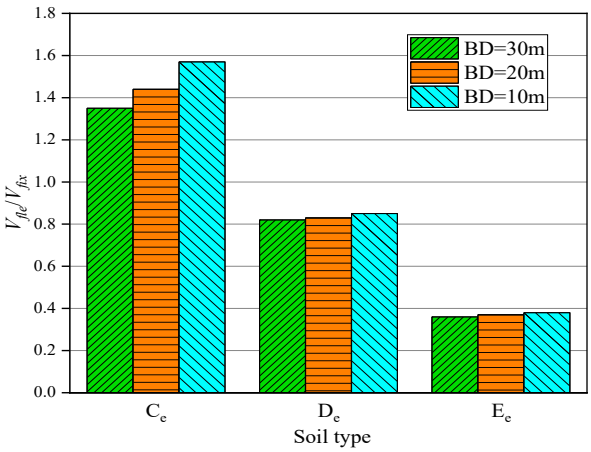

(a)

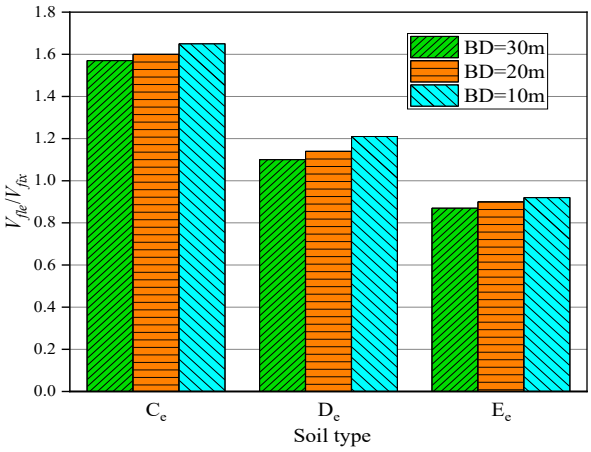

(b)

Figure 5.52 The value of V_{fle}/V_{fix} of 40-storey buildings with different BDs (a) classical compensated foundation structure (b) piled foundation structure

The results of the study indicate an increase in soil stiffness leads to a considerable amplification in the ratio of V_{fle}/V_{fix}. While the effects of variations in model characteristics such as HWR and BD on this ratio were found to be minor, the influence of soil type was found to be substantial. For classical compensated foundation structures, the ratio of V_{fle}/V_{fix} for those built on C_e soil was consistently found to be greater than 1, indicating an increase in base shear for frame-shear wall structures when SSI effects is incorporated. In contrast, the ratio of V_{fle}/V_{fix} for structures built on D_e and E_e soil types was less than 1, indicating a reduction in base

shear when structures are built on medium or soft soils. The findings imply that the stiffness of soil is a vital factor that impacts the increase or decrease of base shear caused by SSI. Hence, it should be given due attention in the design process of high-rise frame-shear wall structures.

In the case of high-rise frame-shear wall buildings with piled foundation, it has been observed that a higher amount of seismic energy can be attracted during an earthquake event. This is reflected in the values of V_{fle}/V_{fix}, which are consistently greater than 1 in almost all cases involving piled foundation. This indicates that SSI impacts on the seismic demand of such structures is detrimental, as it results in an amplification of the base shear.

5.3.6 The Effects of Parameters on $\delta_{fle}/\delta_{fix}$

Figures 5.53, 5.54, 5.55, 5.56, 5.57, and 5.58 illustrate the values of $\delta_{fle}/\delta_{fix}$. It is observed that SSI always amplifies the inter-storey drifts of the strcuture, as $\delta_{fle}/\delta_{fix}$ is greater than 1 in almost all cases. Consequently, SSI has the potential to alter the performance level of high-rise buildings. Moreover, the impact of SSI on the values of $\delta_{fle}/\delta_{fix}$ exhibit different trends when superstructure and substructure parameters are altered. This is because the HWR and substructure stiffness have intricate effects on the deformation of the building. On the one hand, stiffer ground soil and wider structure can limit the foundation rocking, thereby reducing the superstructure deformation. On the other hand, the increased structural weight and stiffness of the substructure system can attract more seismic energy to deform the superstructure. Hence, when investigating SSI effects on the superstructure deformation, the base shear, inter-storey drift, and foundation rocking should be comprehensively considered.

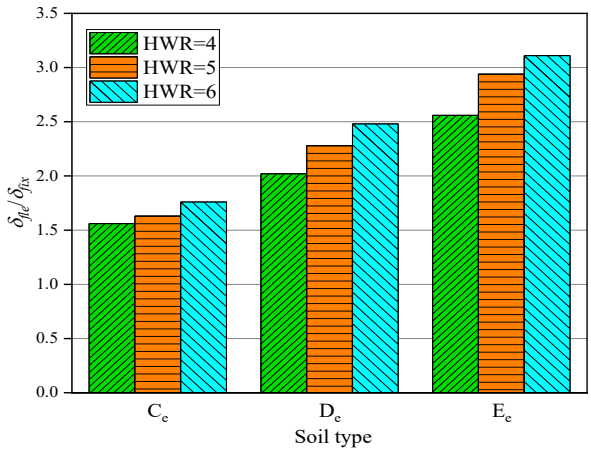

(a)

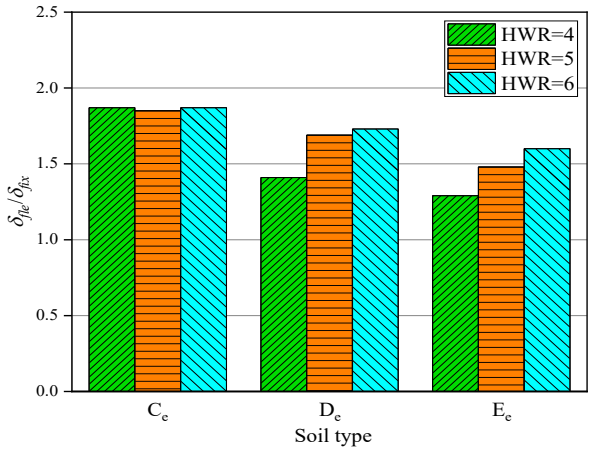

(b)

Figure 5.53 The value of $\delta_{fle}/\delta_{fix}$ of 20-storey buildings with different HWRs (a) classical compensated foundation structure (b) piled foundation structure

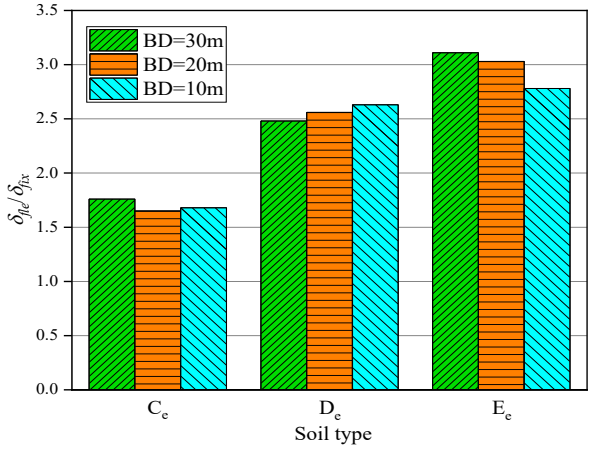

(a)

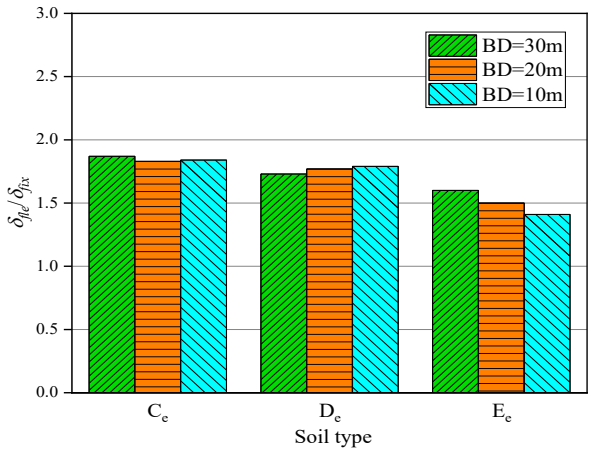

(b)

Figure 5.54 The value of $\delta_{fle}/\delta_{fix}$ of 20-storey buildings with different BDs (a) classical compensated foundation structure (b) piled foundation structure

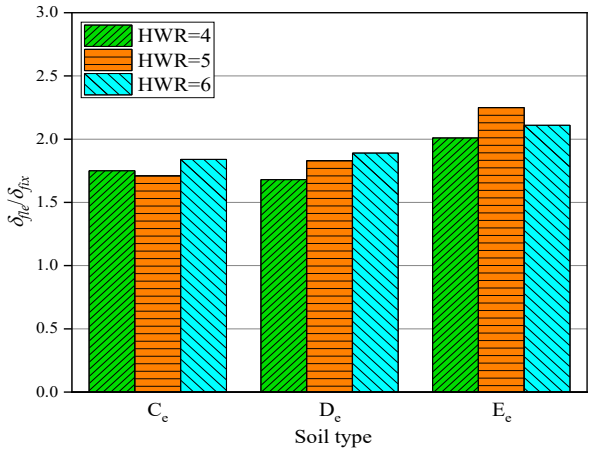

(a)

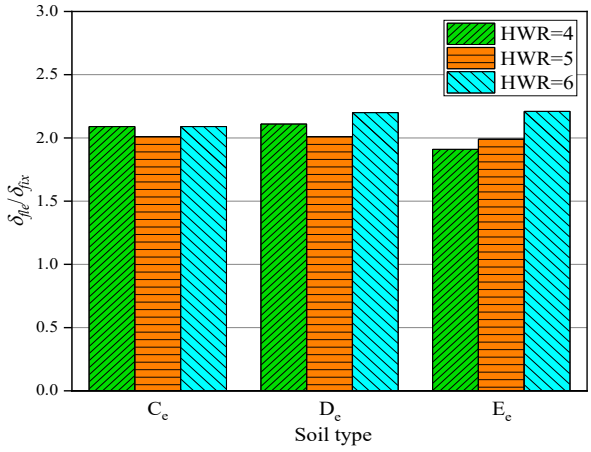

(b)

Figure 5.55 The value of $\delta_{fle}/\delta_{fix}$ of 30-storey buildings with different HWRs (a) classical compensated foundation structure (b) piled foundation structure

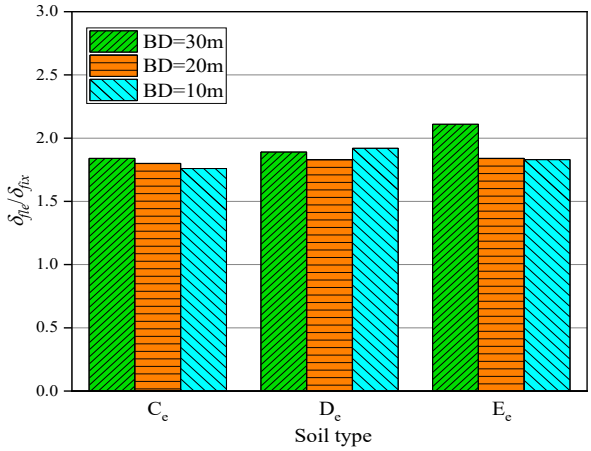

(a)

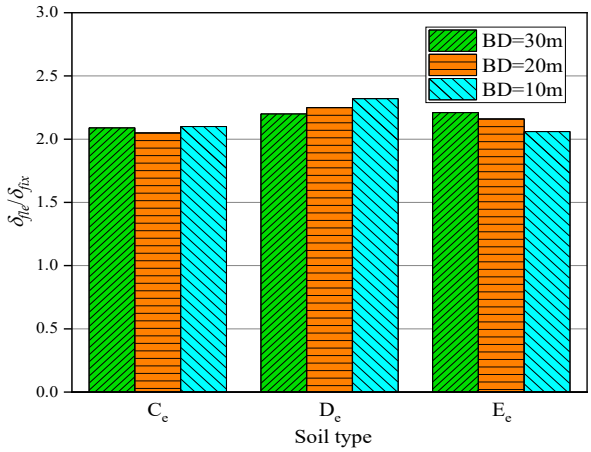

(b)

Figure 5.56 The value of $\delta_{fle}/\delta_{fix}$ of 30-storey buildings with different BDs (a) classical compensated foundation structure (b) piled foundation structure

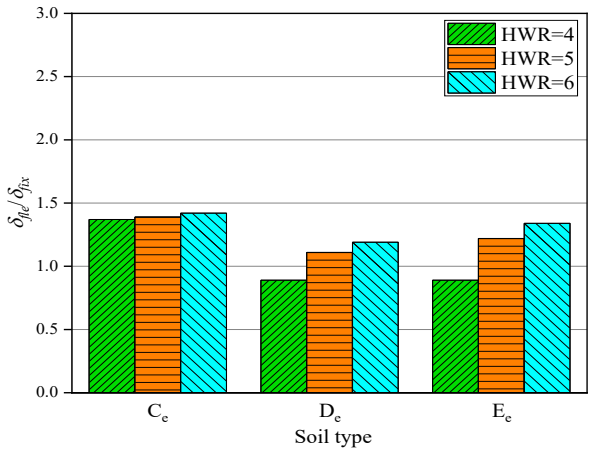

(a)

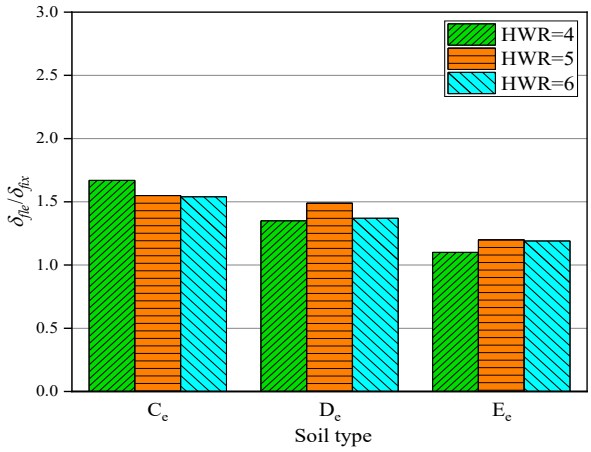

(b)

Figure 5.57 The value of $\delta_{fle}/\delta_{fix}$ of 40-storey buildings with different HWRs (a) classical compensated foundation structure (b) piled foundation structure

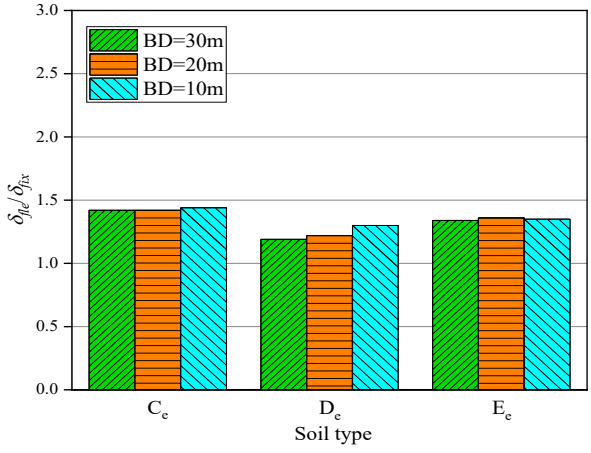

(a)

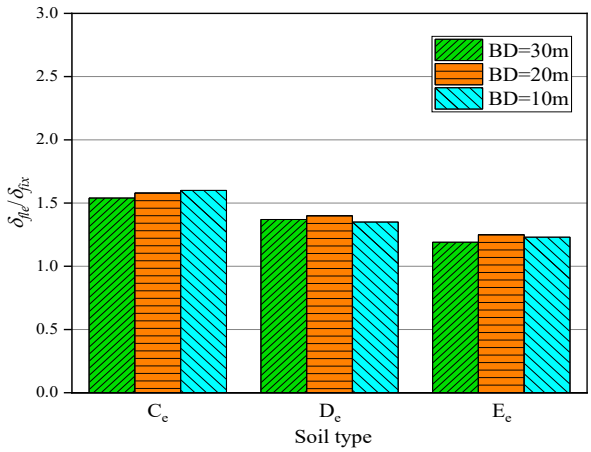

(b)

Figure 5.58 The value of $\delta_{fle}/\delta_{fix}$ of 40-storey buildings with different BDs (a) classical compensated foundation structure (b) piled foundation structure

Figure 5.59 presents the correlation among $\delta_{fle}/\delta_{fix}$, V_{fle}/V_{fix}, and Δ_θ/Δ_t for models with various HWRs and substructure parameters. The data points are plotted near the $y=x$ line when the subsoil is stiff enough, and the values of Δ_θ/Δ_t are small (less than 0.5 for classical compensated foundation structures and less than 0.15 for piled foundation structures). This observation implies that the amplification coefficients for the base shear and inter-storey drifts are nearly the same when SSI is considered. However, as soil stiffness decreases and the values of Δ_θ/Δ_t become larger, the data points gradually move away from the $y=x$ line and shift to the right and downward. This trend suggests that the increase in Δ_θ/Δ_t tends to amplify the inter-storey drifts and reduce the base shear of high-rise frame-shear wall structures. Therefore, when studying SSI effects on the seismic performance of high-rise buildings, it is necessary to comprehensively consider the base shear, inter-storey drifts, and foundation rocking while taking into account the complex interplay among soil stiffness, HWRs, and substructure parameters.

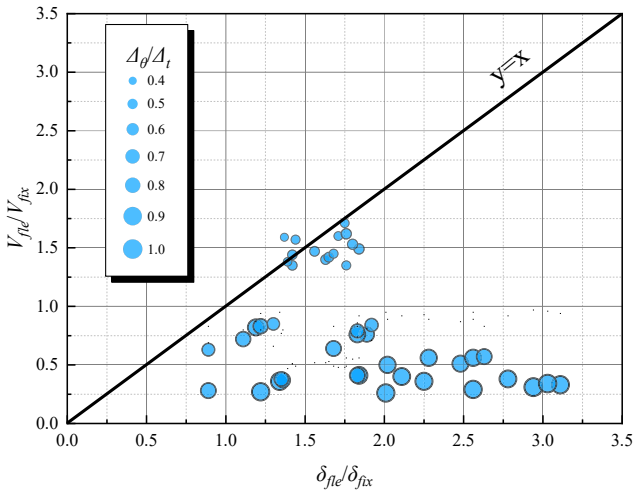

(a)

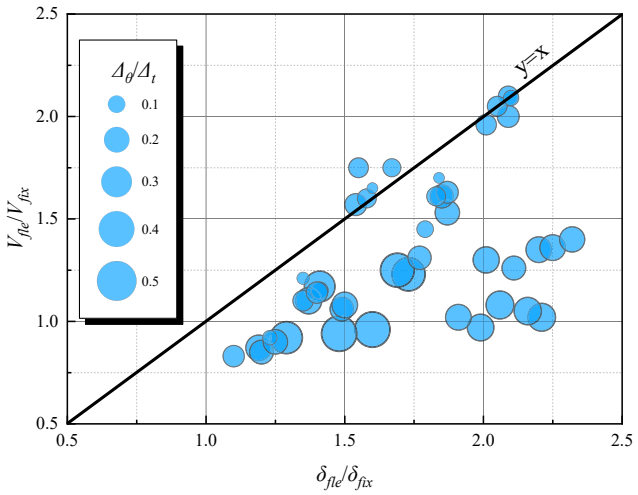

(b)

Figure 5.59 The relationship between $\delta_{fle}/\delta_{fix}$, V_{fle}/V_{fix} and Δ_θ/Δ (a) classical compensated foundation structure (b) piled foundation structure

It should be emphasised that the dominant factor affecting the lateral displacement of the classical compensated foundation model is Δ_θ, while the proportion of Δ_θ in the piled foundation model is relatively small (less than 50%). This is not surprising since end-bearing piles can effectively limit the foundation rotation. Furthermore, the difference in SSI effects on seismic responses of structures with different foundation types can be observed in Figure 5.59. Almost all data points of the pile foundation model fall within the range of $\delta_{fle}/\delta_{fix}>1$ and $V_{fle}/V_{fix}>1$, indicating that regardless of

how the model parameters are varied, SSI has adverse effects. However, for the classical compensated foundation model, structures with D_e and E_e soil types fall below the V_{fle}/V_{fix}=1 line, suggesting that SSI can have a beneficial effect by reducing the base shear of the superstructure, even though inter-storey drifts are still amplified.

5.3.7 The Relationship between T_{fle}/T_{fix} and V_{fle}/V_{fix}

Based on the analysis above, it is evident that SSI can have detrimental effects on the inter-storey drifts of high-rise frame-shear wall buildings, and its impact on the base shears is influenced by the type of foundation and the stiffness of the subsoil. However, previous research has primarily focused on the amplification of inter-storey drifts, neglecting the effect of SSI on the shear force. This is because most prior studies have concluded that SSI reduces the shear force of the superstructure. For instance, Tabatabaiefar et al. (2014a) developed an empirical relationship to predict the value of $\delta_{fle}/\delta_{fix}$ and evaluate the performance level of buildings. Accordingly, this study aims to summarise the influence of SSI on the base shear of high-rise frame-shear wall buildings and devise a straightforward and precise method to estimate the value of V_{fle}/V_{fix}.

Figure 5.60 depicts the correlation between the ratio of T_{fle}/T_{fix} and the ratio of V_{fle}/V_{fix}. As substructure stiffness decreases and T_{fle}/T_{fix} increases, V_{fle}/V_{fix} decreases linearly. However, once a certain threshold is reached, V_{fle}/V_{fix} remains relatively constant. For classical compensated foundation structures, V_{fle}/V_{fix} stabilises at 0.343, while for piled foundation structures, this value is 0.971. This implies that current seismic standards may need to consider the foundation type and specify different minimum values for the reduction of shear forces.

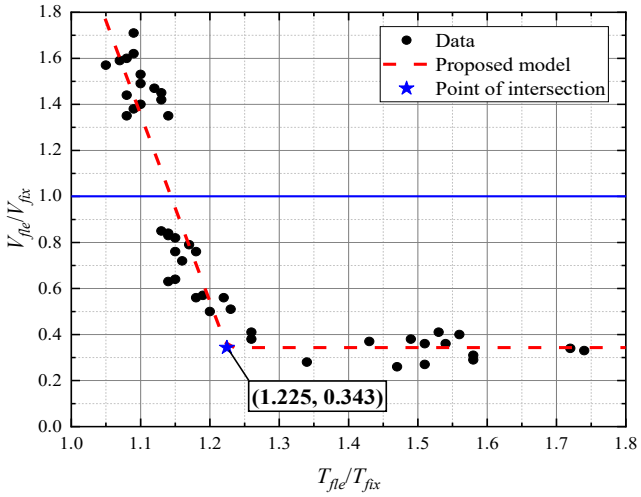

(a)

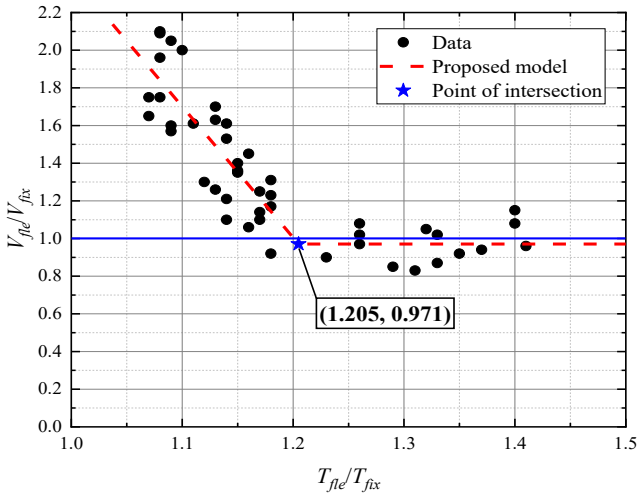

(b)

Figure 5.60 The relationship between T_{fle}/T_{fix} and V_{fle}/V_{fix} (a) classical compensated foundation structure (b) piled foundation structure

Moreover, straight line fittings were also performed on the descending sections in Figure 5.60. The fitting results of the classical compensated foundation structure (Equation 5.1) and piled foundation structure (Equation 5.2) are as follows, respectively:

$$V_{fle}/V_{fix}=10.3018-8.1326\ (T_{fle}/T_{fix}) \quad (5.1)$$

$$V_{fle}/V_{fix}=9.3358-6.9401\ (T_{fle}/T_{fix}) \quad (5.2)$$

The highly negative correlation between the two variables is indicated by the linear

correlation coefficients r = -0.8765 and -0.8078 for the classical compensated foundation structure and the piled foundation structure, respectively. As a result, designers can easily determine the value of V_{fle} for high-rise buildings by calculating V_{fix} and T_{fle}/T_{fix} during the structural design process, without performing time-consuming numerical calculations. Moreover, many empirical relationships have been proposed in previous studies to calculate T_{fle}, which can be found in Balkaya et al. (2012) and Renzi et al. (2013).

5.4 Summary

This chapter presents a discussion of the seismic behaviour of frame-shear wall structures with 20-, 30-, and 40-storeys, taking into account SSI and the influence of various superstructure and substructure parameters. Parameters such as HWR, BD, foundation type, and soil type are considered. Numerical simulations are conducted to obtain Δ, foundation rocking, inter-storey drifts, and base shear for both fixed base and flexible base structures. The results are compared to identify the positive and negative effects of SSI. Based on the numerical analysis, several conclusions can be drawn:

- Upon consideration of SSI, the numerical simulations indicate that the Δ of nearly all models are amplified, regardless of the parameters such as HWR, BD, foundation type, and soil type.
- The numerical simulations reveal that, for many cases, the δ have exceeded 1.5%, indicating that the seismic performance levels of the structures have been altered after considering SSI. Hence, traditional design methods that overlook SSI may not adequately guarantee the structural stability of high-rise frame-shear wall buildings.
- The use of piled foundation can effectively reduce the amount of foundation rocking as compared to classical compensated foundation. However, in many

cases, the numerical simulations indicate that the lateral deformation of the piled foundation models are the largest, particularly under the influence of near-field earthquakes.

- Considering SSI in structural analysis may increase or decrease the base shear of the structure, depending on the category of foundation and soil. Therefore, increasing the stiffness of the substructure without proper consideration of SSI effects may not necessarily enhance structural safety or economic efficiency.

- The numerical simulations show that regardless of the type of foundation used, an increase in the Vs of the subsoil can significantly increase the value of the V_{fle}/V_{fix} of the structures. Conversely, the HWR and BD have little effect on this ratio.

- The effect of substructure parameters on the $\delta_{fle}/\delta_{fix}$ is quite complex. Generally, an increase in Δ_θ/Δ_t can lead to amplified inter-storey drifts and reduced base shear of high-rise frame-shear wall structures.

- The numerical simulations conducted in this study reveal that SSI amplifies the δ for nearly all the cases analysed. As a result, the influence of SSI is found to be detrimental to the inter-storey drifts of high-rise frame-shear wall structures.

- The numerical simulations conducted in this study show that SSI amplifies the V_{fle}/V_{fix} for piled foundation structures and classical compensated foundation structures supported by C_e soil. However, for classical compensated foundation structures supported by D_e and E_e soil types, the SSI effects are found to be beneficial because the value of V_{fle}/V_{fix} is reduced.

- The numerical simulations conducted in this study indicate that, as the T_{fle}/T_{fix} increases, the V_{fle}/V_{fix} decreases linearly until it reaches 0.343 for classical compensated foundation structures or 0.971 for piled foundation structures. Beyond these values, the ratio V_{fle}/V_{fix} remains constant. Therefore, current

seismic standards may need to consider the type of foundation and determine whether shear forces should be reduced, and specify different minimum values of reduced shear force accordingly.

Chapter 6 CONCLUSIONS AND RECOMMENDATIONS

6.1 Conclusions

The conventional approach of structure design assumes a fixed superstructure at the base and neglects the effects of SSI. This approximation is valid when the subsoil is sufficiently rigid, allowing for an input motion at the structure base induced by an earthquake that is nearly identical to the free field motion. Nonetheless, when buildings located on soft ground, the inflexible foundation cannot adapt to the free field motion deformations and seismic activity from the superstructure may cause further soil ground deformation. This phenomenon, where the seismic response of the superstructure influences the soil behaviour and, reciprocally, the seismic response of the soil affects the superstructure behaviour, is referred to as SSI.

It is widely held SSI can enhance the seismic performance of buildings, as the ground's flexibility can extend the natural period of the soil-structure system and dissipate a significant portion of the seismic energy into the soil. However, recent earthquakes have demonstrated that disregarding the effects of SSI can be exceedingly detrimental. Furthermore, some investigations have revealed that SSI may augment the deformation of the superstructure. Consequently, conflicting viewpoints regarding SSI effects on the seismic behaviour of structures have arisen, leading some contemporary structural design codes to either disregard SSI or solely consider its advantageous effects. As a result, incorporating SSI into the design practice of the most prevalent building systems worldwide remains an infrequent occurrence. Additionally, prior research has primarily focused on low or mid-rise moment frames, and the SSI effects on commonly employed structural systems of high-rise buildings have received scant exploration.

The aim of this study is to assess the impact of SSI on high-rise frame-core tube and frame-shear wall structures, using a verified numerical model established with Abaqus

software. The seismic behaviour of high-rise buildings with different structural systems, heights, HWRs, foundation types, soil types, and BDs is studied. The numerical simulations evaluate the Δ, foundation rocking, inter-storey drifts, and storey shear forces of both rigidly and flexibly supported structures, and compare the results. The study identifies the governing factors, including the V_{fle}/V_{fix} and the $\delta_{fle}/\delta_{fix}$, to distinguish between beneficial and detrimental SSI scenarios. Based on these findings, code-based procedures are proposed to facilitate safe and cost-effective structural design practices. The results of the parametric study reveal several important conclusions.

When compared to structures modeled with a fixed base, those modeled with a flexible base that incorporate SSI effects demonstrate amplified Δ and inter-storey drifts to varying extents, regardless of factors such as HWR, foundation type, soil type, and BD. Moreover, the analysis of inter-storey drifts resulting from both near-field and far-field earthquakes has revealed that they often exceed 1.5%, indicating that SSI can significantly impact the seismic performance of structures. Therefore, relying solely on traditional design approaches that neglect SSI effects may not provide sufficient measures to ensure the safety of high-rise buildings. This highlights the importance of incorporating SSI considerations into the design process to accurately assess and mitigate seismic risks.

Piled foundations have been found to be an effective means of mitigating foundation rocking in comparison to classical compensated foundations. However, in many cases, the displacement response of piled foundation models is the largest, especially when subjected to near-field earthquakes. This can be attributed to the fact that the shear forces in piled foundation structures are typically higher than those in both compensated foundation and fixed base structures. Therefore, while piled foundations may provide certain advantages over classical compensated foundations, their performance under seismic loading conditions should be thoroughly evaluated, and

appropriate design measures should be implemented to ensure the safety of the structure. In addition, when the superstructure parameters are kept constant, the effect of soil type on the deformation of pile foundation structures is relatively insignificant compared to classical compensated foundation structures, particularly in response to far-field earthquakes. Hence, the seismic performance of pile foundation structures is less susceptible to changes in soil type as compared to classical compensated foundation structures. This finding implies that incorporating piled foundations into the design of structures in seismically active regions may offer advantages in terms of minimising the influence of the soil variability on the structural response.

The adoption of stiff soil can considerably reduce foundation rocking, and this impact is especially noticeable in classical compensated foundation-supported models. In scenarios where classical compensated foundations are constructed on soft soils, the horizontal deflection caused by foundation rocking represents a significant portion of the overall lateral deflection. Hence, the inter-storey drifts generally exhibited an almost vertical line, signifying that the inter-storey drifts remain relatively constant with increasing structural height. Therefore, while designing structures with classical compensated foundations, careful consideration should be given to soil properties to guarantee that adequate stiffness is maintained to minimise the influence of foundation rocking on structural response.

The consideration of SSI in structural analysis can lead to varied outcomes regarding the base shear of a structure, depending on the specific soil and foundation characteristics. Simply increasing the stiffness of the foundation and subsoil without proper consideration of SSI effects may not necessarily improve structural safety or economic efficiency, as it could result in excessive seismic energy absorption. Hence, careful evaluation of SSI is crucial during the design process to ensure that design measures are appropriately balanced, achieving an optimum balance between structural safety and economic efficiency.

Regardless of the type of foundation used, a significant increase in the V_s of the subsoil can lead to a substantial increase in the value of V_{fle}/V_{fix} of structures. On the other hand, the HWR and BD have a relatively minor impact on this ratio. Besides, the results of this study also demonstrate that SSI can significantly increase the V_{fle}/V_{fix} for both piled foundation structures and classical compensated foundation structures supported by C_e soil. In contrast, SSI has a beneficial effect on classical compensated foundation structures supported by D_e and E_e soil types, as it reduces the value of V_{fle}/V_{fix}. These findings underscore the importance of conducting a comprehensive assessment on various types of foundation and soil when the SSI effects are considered.

The analysis presented in this paper indicates that SSI generally increases the value of $\delta_{fle}/\delta_{fix}$ for almost all cases examined, which exerts a negative impact on the inter-storey drifts of high-rise buildings. Consequently, it is essential to evaluate the potential impact of SSI when designing high-rise structures to optimise their performance. Moreover, it should be noted that the influence of substructure parameters on the value of $\delta_{fle}/\delta_{fix}$ is intricate and multi-dimensional. When analysing the SSI effects on the deformation of the superstructure, it is important to consider the base shear, inter-storey drift, and foundation rocking comprehensively.

When the subsoil exhibits sufficient stiffness, and the values of Δ_θ/Δ_t are small, the amplification coefficient for base shear is nearly equivalent to the amplification coefficient for inter-storey drifts after accounting for SSI. However, as the soil stiffness decreases and the values of Δ_θ/Δ_t increase, the inter-storey drift is amplified, and the base shear is reduced.

As the ratio of T_{fle}/T_{fix} increases, the value of V_{fle}/V_{fix} decreases linearly until it reaches a minimum value. Beyond this point, the value of V_{fle}/V_{fix} remains constant. Based on these findings, current seismic codes may specify different minimum values of reduced shear force for different types of foundations to ensure adequate seismic

performance of structures. In addition, straight line fittings were also performed on the descending sections. Thus, designers can easily determine the V_{fle} value of high-rise buildings by calculating V_{fix} and T_{fle}/T_{fix}, without conducting laborious numerical computations during the design process.

6.2 Recommendations and Future Works

In this study, a numerical soil-foundation-structure model established in finite element software Abaqus and verified by shaking table tests is used to critically explore the effects of SSI on high-rise frame-core tube and frame-shear wall structures. The seismic behaviour of high-rise buildings with various structural heights, HWRs, foundation types, soil types and BDs are studied. Based on the content of current research, here are some recommendations for future studies:

Investigate the effects of different soil conditions on the seismic behaviour of high-rise buildings with SSI. In this study, different soil types and bedrock depths have been considered, but it would be interesting to investigate how different soil profiles, such as saturated soils, liquefiable soils, or layered soils affect the seismic response of high-rise buildings. In addition, the following future works are recommended:

- Exploring the effects of different structural systems on seismic behaviour of super high-rise buildings with SSI. In the current study, two commonly used high-rise building systems: frame-core tube and frame-shear wall structures, are considered. However, it would be interesting to investigate super high-rise buildings with the tube in tube structures and how they behave under SSI.
- Validating the code-based procedures developed in the current study by comparing them with experimental data or other numerical models. This would provide more confidence in the accuracy of the proposed design method.
- Investigating the economic feasibility of the proposed design method by comparing it with other existing design methods. This could help to evaluate the

practicality of the proposed method and its potential impact on the construction industry.

- Carrying out the numerical parametric study on SSSI, which is of great importance to the structural design in urban areas. This phenomenon occurs when two or more adjacent structures interact with each other through the soil or foundation on which they are built, and it can lead to increased stresses and deformation in the structures.

REFERENCES

Adhikary, S. and Deoda, V. R. 2022. "Seismic response of a tall tower on deep soil-A case study." Structures, 37, 1183-1199.

Akbari, A., Eslami, A. and Nikookar, M. 2021. "Influence of soil stiffness on the response of piled raft foundations under earthquake loading." Transportation Infrastructure Geotechnology, 8, 590-606.

Al Agha, W., Almorad, W. A., Umamaheswari, N. and Alhelwani, A. 2021. "Study the seismic response of reinforced concrete high-rise building with dual framed-shear wall system considering the effect of soil structure interaction." Materials Today: Proceedings, 43, 2182-2188.

Anand, V. and Satish Kumar, S. R. 2018. "Seismic soil-structure interaction: a state-of-the-art review." Structures, 16, 317-326.

Ansari, M., Nazari, M. and Panah, A. K. 2021. "Influence of foundation flexibility on seismic fragility of reinforced concrete high-rise buildings." Soil Dynamics and Earthquake Engineering, 142, 106521.

Arboleda-Monsalve, L. G., Mercado, J. A., Terzic, V. and Mackie, K. R. 2020. "Soil-structure interaction effects on seismic performance and earthquake-induced losses in tall buildings." Journal of Geotechnical and Geoenvironmental Engineering, 146 (5), 04020028.

AS1170.4. 2007. Structural Design Actions-Part 4: Earthquake Actions in Australia. Australian Standards, Sydney.

AS3600. 2018. Concrete Structures. Australian Standards, Sydney.

ASCE/SEI 7-10. 2010. Minimum Design Loads for Buildings and Other Structures. Virginia, American Society of Civil Engineers.

ASCE/SEI 7-16. 2016. Minimum Design Loads for Buildings and Other Structures. Virginia, American Society of Civil Engineers.

ATC40. 1996. Seismic Evaluation and Retrofit of Concrete Buildings. Applied Technology Council, Seismic Safety Commission, California, USA.

Ayala, F., Sáez, E. and Magna-Verdugo, C. 2022. "Computational modelling of dynamic soil-structure interaction in shear wall buildings with basements in medium stiffness sandy soils using a subdomain spectral element approach calibrated by micro-vibrations." Engineering Structures, 252, 113668.

Bagheri, M., Jamkhaneh, M. E. and Samali, B. 2018. "Effect of seismic soil-pile-structure interaction on mid-and high-rise steel buildings resting on a group of pile foundations." International Journal of Geomechanics, 18 (9), 04018103.

Balkaya, C., Yuksel, S. B. and Derinoz, O. 2012. "Soil-structure interaction effects on the fundamental periods of the shear-wall dominant buildings." The Structural Design of Tall and Special Buildings, 21 (6), 416-430.

Bariker, P. and Kolathayar, S. 2022. "Dynamic soil structure interaction of a high-rise building resting over a finned pile mat." Infrastructures, 7, 142.

Borja, R. I., Wu, W. H., Amies, A. P. and Smith, H. A. 1994. "Nonlinear lateral, rocking and torsional vibration of rigid foundations." Journal of Geotechnical Engineering, 120 (3), 491-513.

Bowles, J. E. 2001. Foundation Analysis and Design. 5th Ed., McGraw-Hill International, New York.

Building Seismic Safety Council (BSSC). 1997. NEHRP guidelines for the seismic rehabilitation of buildings. 1997 edition, Part 1: Provisions and Part 2: Commentary. FEMA 273/274, FEMA, Washington, DC.

Carbonari, S., Dezi, F. and Leoni, G. 2011. "Linear soil-structure interaction of

coupled wall-frame structures on pile foundations." Soil Dynamics and Earthquake Engineering, 31 (9), 1296-1309.

Carbonari, S., Dezi, F. and Leoni, G. 2012. "Nonlinear seismic behaviour of wall-frame dual systems accounting for soil-structure interaction." Earthquake Engineering and Structural Dynamics, 41 (12), 1651-1672.

Choinière, M., Paultre, P. and Léger, P. 2019. "Influence of soil-structure interaction on seismic demands in shear wall building gravity load frames." Engineering Structures, 198, 109259.

Darendeli, M. B. 2001. Development of a new family of normalized modulus reduction and material damping curves. Doctoral Dissertation, Texas, University of Texas at Austin.

Dassault Systèmes SIMULIA 2012. Abaqus analysis user's manual. Dassault Systèmes SIMULIA Corporation, Minneapolis.

El Ganainy, H. and El Naggar, M. H. 2009. "Seismic performance of three-dimensional frame structures with underground stories." Soil Dynamics and Earthquake Engineering, 29, 1249-1261.

EN 1998-5, Eurocode 8. 2004. Design of structures for earthquake resistance - part 5: foundations, retaining structures and geotechnical aspects, European Committee for Standardization, Brussels.

Far, H. 2019. "Advanced computation methods for soil structure interaction analysis of structures resting on soft soils." International Journal of Geotechnical Engineering, 13 (4), 352-359.

Far, H. and Flint, D. 2017. "Significance of using isolated footing technique for residential construction on expansive soils." Frontiers of Structural and Civil Engineering, 11 (1), 123-129.

Fardis, M. N. 2010. Advances in Performance-Based Earthquake Engineering. Springer.

Fatahi, B., Hokmabadi, A. S. and Samali, B. 2014. "Seismic performance based design for tall buildings considering soil-pile structure interaction." International Conference on Geotechnical Engineering, ASCE, Geoshanghai2014, Shanghai, China, 333-342.

Fatahi, B. and Tabatabaiefar, H. R. 2014. "Effects of soil plasticity on seismic performance of mid-rise building frames resting on soft soils." Advances in Structural Engineering, 17 (10), 1387-1402.

Fatahi, B., Tabatabaiefar, H. R., Ghabraie, K. and Zhou, W. H. 2015. "Evaluation of numerical procedures to determine seismic response of structures under influence of soil-structure interaction." Structural Engineering and Mechanics, 56 (1), 27-47.

Fatahi, B., Tabatabaiefar, H. R. and Samali, B. 2011. Performance based assessment of dynamic soil-structure interaction effects on seismic response of building frames. In: Juang CH, Phoon KK, Puppala AJ, Green RA, Fenton GA (eds), Proceedings of georisk 2011-geotechnical risk assessment & management (geotechnical special publication No. 224) (pp 344-351). USA: American Society of Civil Engineers (ASCE)

Fathi, A., Sadeghi, A., Azadi, M. R. E. and Hoveidae, N. 2020. "Assessing the soil-structure interaction effects by direct method on the out-of-plane behavior of masonry structures (case study: Arge-Tabriz)." Bulletin of Earthquake Engineering, 18 (14), 6429-6443.

FEMA. 1997. NEHRP guidelines for the seismic rehabilitation for buildings. FEMA 273/274, Washington, DC.

FEMA. 2015. NEHRP recommended seismic provisions for new buildings and other structures. FEMA P-1050. Washington DC, Federal Emergency Management Agency.

Galal, K. and Naimi, M. 2008. "Effect of soil conditions on the response of reinforced concrete tall structures to near-fault earthquakes." The Structural Design of Tall and Special Buildings, 17 (3), 541-562.

Ganjavi, B. and Hao, H. 2012. "A parametric study on the evaluation of ductility demand distribution in multi-degree-of-freedom systems considering soil-structure interaction effects." Engineering Structures, 43, 88-104.

Gao, L., Fang, E. and Qian, J. 2005. Conceptual Design of High-Rise Building Structure, Beijing, CHINA, China Planning Press.

Gazetas, G. 1983. "Analysis of machine foundation vibrations: state of the art." Soil Dynamics and Earthquake Engineering, 2 (1), 2-42.

Gazetas, G. 1991. "Formulas and charts for impedances of surface and embedded foundations." Journal of Geotechnical Engineering, 117 (9), 1363-1381.

GB50011. 2010. Code for Seismic Design of Buildings. China Architecture and Building Press, Beijing.

Ghandil, M. and Behnamfar, F. 2017. "Ductility demands of MRF structures on soft soils considering soil-structure interaction." Soil Dynamics and Earthquake Engineering, 92, 203-214.

Gu, Y., Liu, J. B. and Du, Y. X. 2007. "3D consistent viscous-spring artificial boundary and viscous-spring boundary element." Engineering Mechanics, 24 (12):31-37.

Guin, J. and Banerjee, P. K. 1998. "Coupled soil-pile-structure interaction analysis under seismic excitation." Journal of Structural Engineering, 124, 434-444.

Han, Y. 2002. "Seismic response of tall building considering soil-pile-structure interaction." Earthquake Engineering and Engineering Vibration, 1 (1), 57-64.

Hokmabadi, A. S., Fatahi, B. and Samali, B. 2012. "Recording inter-storey drifts of structures in time-history approach for seismic design of building frames." Australian Journal of Structural Engineering 13 (2), 175-179.

Hokmabadi, A. S., Fatahi, B. and Samali, B. 2014. "Assessment of soil-pile-structure interaction influencing seismic response of mid-rise buildings sitting on floating pile foundations." Computers and Geotechnics, 55, 172-186.

Hokmabadi, A. S., Fatahi, B. and Samali, B. 2015. "Physical modeling of seismic soil-pile-structure interaction for buildings on soft soils." International Journal of Geomechanics, 15 (2), 04014046.

Hradilek, P. J. and Luco, J. E. 1970. Dynamic soil-structure interaction. IDIEM Technical Report No. 14, University of Chile, Santiago, Chile.

IBC 2012. International Building Code. International Code Council (ICC).

IS 1893-3. 2014. Criteria for earthquake resistant design of structures-part 3: bridges and retaining walls. IS 1893-3. New Delhi, Bureau of Indian Standards.

IS 1893-4. 2015. Criteria for earthquake resistant design of structures - part 4: industrial structures including stack-like structures. IS 1893-4. New Delhi, Bureau of Indian Standards.

JSCE 15. 2007. Standard specifications for concrete structures-design. JSCE 15. Tokyo: Japan Society of Civil Engineers.

Kamal, M. and Inel, M. 2021. "Correlation between ground motion parameters and displacement demands of mid-rise RC buildings on soft soils considering soil-structure-interaction." Buildings, 11 (3), 11030125.

Kamal, M., Inel, M. and Cayci, B. T. 2022. "Seismic behavior of mid-rise reinforced concrete adjacent buildings considering soil-structure interaction." Journal of Building Engineering, 51, 104296.

Kausel, E. 2010. "Early history of soil-structure interaction." Soil Dynamics and Earthquake Engineering, 30 (9), 822-832.

Khazaei, J., Amiri, A. and Khalilpour, M. 2017. "Seismic evaluation of soil-foundation-structure interaction: Direct and Cone model." Earthquakes and Structures, 12 (2), 251-262.

Kramer, S. L. 1996. Geotechnical Earthquake Engineering, Prentice Hall, Upper Saddle River.

Kramer, S. L. 2008. Performance-based earthquake engineering: opportunities and implications for geotechnical engineering practice. Geotechnical Earthquake Engineering and Soil Dynamics IV.

Li, M., Lu, X., Lu, X. and Ye, L. 2014. "Influence of soil-structure interaction on seismic collapse resistance of super-tall buildings." Journal of Rock Mechanics and Geotechnical Engineering, 6, 477-485.

Liang, J., Zhang, G., Ba, Z., Liang, J. and Zhao, H. 2023. "Seismic response analysis of high-rise frame-core tube building on fluid-saturated soil considering soil-pile-structure interaction." Journal of Building Engineering, 63, 105563.

Liu, J. B., Du, Y. X., Du, X. L., Wang, Z. Y. and Wu, J. 2006. "3D viscous-spring artificial boundary in time domain." Earthquake Engineering and Engineering Vibration, 5 (1), 93-102.

Lu, Y. 2005. "Inelastic behaviour of RC wall-frame with a rocking wall and its analysis Incorporating 3-D effect." The Structural Design of Tall and Special Buildings, 14 (1), 15-35.

Luo, C., Yang, X., Zhan, C. B., Jin, X. L. and Ding, Z. K. 2016. "Nonlinear 3D finite element analysis of soil-pile-structure interaction system subjected to horizontal earthquake excitation." Soil Dynamics and Earthquake Engineering, 84, 145-156.

Ma, S. J., Chi, M. J., Chen, H. J. and Chen, S. 2020. "Implementation of viscous-spring boundary in ABAQUS and comparative study on seismic motion input methods." Chinese Journal of Rock Mechanics and Engineering, 39 (7), 1445-1457.

Maheshwari, B. K. and Sarkar, R. 2011. "Seismic behavior of soil-pile-structure interaction in liquefiable soils: Parametric study." International Journal of Geomechanics, 11 (4), 335-347.

Mercado, J. A., Mackie, K. R. and Arboleda-Monsalve, L. G. 2021. "Modeling nonlinear-inelastic seismic response of tall buildings with soil-structure interaction." Journal of Structural Engineering, 147 (7), 04021091.

Meymand, P. J. 1998. Shaking table scale model tests of nonlinear soil-pile superstructure interaction in soft clay. PhD thesis in Civil Engineering, University of California, Berkeley.

Mittal, V. and Samanta, M. 2021. "A critical review on design philosophies of different design standards on seismic soil-structure interaction." Seismic Design and Performance, 1-13.

Mukand, J., Padmanabhan, P., Arya, A. S., et al. 1973. National conference on tall buildings. New Delhi.

Mylonakis, G. and Gazetas, G. 2000. "Seismic soil-structure interaction: beneficial or detrimental?" Journal of Earthquake Engineering, 4, 377-401.

Nasab, M. S. E., Chun, S. and Kim, J. 2021. "Soil-structure interaction effect on seismic retrofit of a soft first-story structure." Structures, 32, 1553-1564.

NBCC 2010. National Building Code of Canada (NBCC). NRC Institute for Research in Construction, Canada.

NZS1170.5 2007. Structural Design Actions-Part 5: Earthquake Actions-New Zealand. New Zealand Standards, Wellington.

Park, D. and Hashash, Y. M. A. 2003. "Soil damping formulation in nonlinear time domain site response analysis." Journal of Earthquake Engineering, 8 (2), 249-274.

Qaftan, O. S., Toma-Sabbagh, T., Weekes, L. and Augusthus-Nelson, L. 2020. "Validation of a finite element modelling approach on soil-foundation-structure interaction of a multi-storey wall-frame structure under dynamic loadings." Soil Dynamics and Earthquake Engineering, 131, 106041.

Radkia, S., Rahnavard, R., Tuwair, H., Gandomkar, F. A. and Napolitano, R. 2020. "Investigating the effects of seismic isolators on steel asymmetric structures considering soil-structure interaction." Structures, 27, 1029-1040.

Rayhani, M. and Naggar, M. 2008. "Numerical modeling of seismic response of rigid foundation on soft soil." International Journal of Geomechanics 8 (6), 336-346.

Renzi, S., Madiai, C. and Vannucchi, G. 2013. "A simplified empirical method for assessing seismic soil-structure interaction effects on ordinary shear-type buildings." Soil Dynamics and Earthquake Engineering, 55, 100-107.

Roesset, J. M. 2013. "Soil structure interaction the early stages." Journal of Applied Science and Engineering, 16 (1), 1-8.

Saleh, A., Far, H. and Mok, L. 2018. "Effects of different support conditions on experimental bending strength of thin walled cold formed steel storage upright frames." Journal of Constructional Steel Research, 150, 1-6.

Samali, B., Fatahi, B. and Far, H. 2011. "Seismic behaviour of concrete moment

resisting buildings on soft soil considering soil-structure interaction." In: Proceedings of the 21st Australasian conference on the mechanics of structures and materials (ACMSM21), 407-412.

Scarfone, R., Morigi, M. and Conti, R. 2020. "Assessment of dynamic soil-structure interaction effects for tall buildings: A 3D numerical approach." Soil Dynamics and Earthquake Engineering, 128, 105864.

Seed, H. B., Murarka, R., Lysmer, J. and Idriss, I. M. 1976. "Relationships of maximum acceleration, maximum velocity, distance from source, and local site conditions for moderately strong earthquakes." Bulletin of the Seismological Society of America, 66 (4), 1323-1342.

Seed, H. B., Wong, R., Idriss, I. M. and Tokimatsu, K. 1986. "Moduli and damping factors for dynamic analysis of cohesionless soil." Journal of Geotechnical Engineering, 112 (11), 1016-1032.

Segaline, H., Sáez, E. and Ubilla, J. 2022. "Evaluation of dynamic soil-structure interaction effects in buildings with underground stories using 1 g physical experimentation in a transparent shear laminar box." Engineering Structures, 266, 114645.

Shabani, M. J., Shamsi, M. and Ghanbari, A. 2021. "Slope topography effect on the seismic response of mid-rise buildings considering topography-soil-structure interaction." Earthquakes and Structures, 20 (2), 187-200.

Sharma, N., Dasgupta, K. and Dey, A. 2018. "A state-of-the-art review on seismic SSI studies on building structures." Innovative Infrastructure Solutions, 3 (22), 1-16.

Shirzadi, M., Behnamfar, F. and Asadi, P. 2020. "Effects of soil-structure interaction on inelastic response of torsionally-coupled structures." Bulletin of Earthquake Engineering, 18 (4), 1213-1243.

Son, H., Park, J., Kim, H., Lee, Y. H. and Kim, D. J. 2017. "Generalized finite element analysis of high-rise wall-frame structural systems." Engineering Computations, 34 (1), 189-210.

Sun, J. I., Golesorkhi, R. and Seed, B. 1998. Dynamic module and damping ratios for cohesive soils. Earthquake Engineering Research Centre, Report No. UCB/EERC-88/15, University of California, Berkeley.

Tabatabaiefar, H. R. and Massumi, A. 2010. "A simplified method to determine seismic responses of reinforced concrete moment resisting building frames under influence of soil-structure interaction." Soil Dynamics and Earthquake Engineering, 30 (11), 1259-1267.

Tabatabaiefar, H. R. 2012. Determining Seismic Response of Mid-rise Building Frames Considering Dynamic Soil-Structure Interaction. PhD. Thesis. University of Technology Sydney.

Tabatabaiefar, H. R., Fatahi, B. and Samali, B. 2012. "Finite difference modelling of soil-structure interaction for seismic design of moment resisting building frames." Australian Geomechanics Journal, 47 (3), 113-119.

Tabatabaiefar, H. R., Fatahi, B. and Samali, B. 2013. "Seismic behaviour of building frames considering dynamic soil-structure interaction." International Journal of Geomechanics, 13 (4), 409-420.

Tabatabaiefar, H. R. and Fatahi, B. 2014. "Idealisation of soil-structure system to determine inelastic seismic response of mid-rise building frames." Soil Dynamics and Earthquake Engineering, 66 (11), 339-351.

Tabatabaiefar, H. R., Fatahi, B. and Samali, B. 2014(a). "An empirical relationship to determine lateral seismic response of mid-rise building frames under influence of soil-structure interaction." The Structural Design of Tall and Special Buildings,

23 (7), 526-548.

Tabatabaiefar, H. R., Fatahi, B. and Samali, B. 2014(b). "Numerical and experimental investigations on seismic response of building frames under influence of soil-structure interaction." Advances in Structural Engineering, 17 (1), 109-130.

Tabatabaiefar, H. R. 2016. "Detail design and construction procedure of laminar soil containers for experimental shaking table tests." International Journal of Geomechanics, 10 (4), 328-336.

Tabatabaiefar, H. R. and Clifton, T. 2016. "Significance of considering soil-structure interaction effects on seismic design of unbraced building frames resting on soft soils." Australian Geomechanics Journal, 51 (1), 55-64.

Tabatabaiefar, H. R. and Mansoury, B. 2016. "Detail design, building and commissioning of tall building structural models for experimental shaking table tests." The Structural Design of Tall and Special Buildings, 25 (8), 357-374.

Tabatabaiefar, H. R., Mansoury, B., Khadivi Zand, M. J. and Potter, D. 2017. "Mechanical properties of sandwich panels constructed from polystyrene/cement mixed cores and thin cement sheet facings." Journal of Sandwich Structures and Materials, 19 (4), 456-481.

Van Nguyen, Q., Fatahi, B. and Hokmabadi, A. S. 2016. "The effects of foundation size on the seismic performance of buildings considering the soil foundation-structure interaction." Structural Engineering and Mechanics, 58 (6), 1045-1075.

Van Nguyen, Q., Fatahi, B. and Hokmabadi, A. S. 2017. "Influence of size and load-bearing mechanism of piles on seismic performance of buildings considering soil-pile-structure interaction." International Journal of Geomechanics, 17 (7), 04017007.

Veletsos, A. S. and Meek, J. W. 1974. "Dynamic behaviour of building-foundation

systems." Earthquake Engineering and Structural Dynamics, 3, 121-138.

Vision 2000 Committee. 1995. Performance based seismic engineering of buildings. Proc., Structural Engineers Association of California (SEAOC), Structural Association of California, Sacramento, CA.

Wang, J. and Yang, J. 2022. "Parametric analysis on the effect of dynamic interaction between nonlinear soil and reinforced concrete frame." Applied Sciences, 12, 9876.

Wolf, J. P. 1985. Dynamic Soil-structure Interaction. Englewood Cliffs, New Jersey, Prentice-Hall.

Wolf, J. P. 1998. Soil-Structure Interaction Analysis in Time Domain. Upper Saddle River, NJ: Prentice Hall Co.

Wolf, J. P. and Deeks, A. J. 2004. Foundation Vibration Analysis: A Strength of-Materials Approach. Oxford, Elsevier.

Xu, R. and Fatahi, B. 2019. "Impact of in situ soil shear-wave velocity profile on the seismic design of tall buildings on end-bearing piles." Journal of Performance of Constructed Facilities, 33 (5), 04019053.

Yang, J. P., Lu, Z. and Li, P. Z. "Large-scale shaking table test on tall buildings with viscous dampers considering pile-soil-structure interaction." Engineering Structures, 220, 110960.

Yashinsky, M. 1998. The Loma Prieta, California, earthquake of October 17, 1989-highway systems. Professional paper 1552-B. U.S. Geological Survey.

Yeganeh, N., Bazaz, J. B. and Akhtarpour, A. 2015. "Seismic analysis of the soil-structure interaction for a high rise building adjacent to deep excavation." Soil Dynamics and Earthquake Engineering, 79, 149-170.

Zhang, W. Y., Liu, S. T., Shokrabadi, M., Dehghanpoor, A. and Taciroglu, E. 2022. "Nonlinear seismic fragility assessment of tall buildings equipped with tuned mass damper (TMD) and considering soil-structure interaction effects." Bulletin of Earthquake Engineering, 20 (7), 3469-3483.

Zomorodian, R., Soltani, F., Sivandi-Pour, A. and Noroozinejad Farsangi, E. 2021. "Effect of foundation flexibility on the seismic performance of a high-rise structure under far-field and near-field earthquakes." International Journal of Engineering, 34 (7), 1611-1622.